Photo-biomodulation of human skin fibroblast sub-populations: a systematic approach for the optimization of optical treatment parameters

Charles-Antoine Georges Marie MIGNON

Submitted for the Degree of Doctor of Philisophy

Centre for Skin Science

Faculty of Life Sciences

University of Bradford

2017

Abstract

Charles-Antoine Georges Marie Mignon

Photo-biomodulation of human skin fibroblast sub-populations: a systematic approach for the optimization of optical treatment parameters

Keywords: Photobiomodulation, skin, light, fibroblasts, sub-populations, monte-carlo, design of experiment

The thesis presents a rational path for the optimization of the selection of optical treatment parameters in photobiomodulation of human skin fibroblasts. The project begins with an extensive analysis of 90 bibliographic reports in photobiomodulation published between 1985 and 2015, and revealed major inconsistencies in optical parameters selected for clinical applications. Seeking greater clarity for optimal parameter choice, a systematic approach to disentangle the multiple factors underpinning the response of human dermal fibroblasts *in vitro* to visible and near-infra red (NIR) light was employed. Light-based devices were constructed to specifically and systematically screen the optical parameter window (i.e. wavelength, irradiance and dose) observed in literature. Additionally, critical culture and treatment conditions that have dramatic impact on the outcome of specific light treatment of these human skin dermal cells were identified. In particular, environmental oxygen concentration, cell confluency and serum concentration were all found to have a great effect on the response of dermal fibroblasts to light. In parallel, the induction of reactive oxygen species (ROS) by short visible wavelengths on two dermal fibroblast sub-populations or lineage, reticular and papillary, was monitored by live-cell imaging. The ROS species were found to be created in or close to mitochondria. Lastly, gene expression studies revealed a strong impact of short visible wavelengths, as compared to long and NIR wavelengths on both subpopulations of human dermal fibroblasts. In particular, blue light (450 nm) specifically down-regulated proliferation, metabolism and protein synthesis molecular pathways. At the protein level, 450-nm light inhibited the

production of procollagen I in human reticular and papillary fibroblasts in a dose-dependent manner. Gene expression results were in agreement i.e., the same light parameter down-regulated collagen fiber genes, integrins and up-regulated collagenase MMP1. This thesis concludes with a chapter presenting a characterization of the accuracy of a potential translation tool for the prediction of optical photon density inside human skin.

Acknowledgements

I would first like to thank my thesis advisors Prof. Desmond Tobin of the Center for Skin Sciences at the University of Bradford and Dr. Natallia Uzunbajakava of Philips Research Eindhoven. Both provided tremendous help for the development and writing of this thesis. In particular, I thank them for their expertise, passion and commitment in the project CLaSSiC in which this thesis is included.

I would also like to thank the additional advisors Dr. Natalia Botchkareva of the Center for Skin Sciences at the University of Bradford and Dr. Mounir Zeitouny of Philips Research. Even though they were less involved in this thesis, they helped when it was required with important advice.

I would like to specifically thank several key contributors to this PhD study: Bianca Raafs for all her support in the laboratory and contribution to the biological work of this thesis, Irene Castellano and Serena Buscone for their friendship and constant support during the course of this PhD, Dr. Jim Coombs head of department Personal Care and Wellness at Philips Research Eindhoven for welcoming me in the department at Philips Research, and Ms. Carolina de la Torre and Prof. Norbert Gretz from the University of Mannheim for granting me with the opportunity to perform a gene expression analysis with their help. I am grateful to them as they provided critical help at diverse levels of my PhD studies.

I would also like to acknowledge experts who were involved in many of the parts of this research project. They include all the other team members of the CLaSSiC project, namely Dr. Julie Thornton, Dr. Andrei Mardaryev, and Dr. Gill Westgate of the Center of Skin Sciences at the University of Bradford, and Dr. Marijke van Vlimmeren, Dr. Tom Nuijs of Philips Research Eindhoven. Without their participation and input, this PhD thesis could not have been successfully conducted. I am also truly grateful for the contribution of Rene Kragt, Michel Bruyninckx, Theo Loring and Frank Jaartsveld of PiNS (Philips Innovation Services), and Peter Jutte and Arno Ras of Philips Research in the manufacture, development and safety assessment of the light-based prototypes.

A long list of persons would have to complete these acknowledgements including Dr. Frank van Abeelen, Dr. Gerrit Oversluizen, Dr. Joerg Liebmann, Dr. Roland Vulders, Ms. Christa Dam, Mr. Tom van Gijsel, Ms. Evelyn Simons, Mr. Erik van Buijtenen, Ms. Naomi Weertman, Mr. Mitchel Moolenaar, Mr. Freek van Hemert, Mr. Lucas Scheffers, Mr. Martijn van Zelst, Mr. Dirk Ross, Mr. Frans Engelsen, Dr. Gerry van Someren from Philips Research Eindhoven, and Dr. Stephen Sikkink, Ms. Rachael Sedman, Ms. Andrea, Mr. Emtiaz Aziz from the University of Bradford.

Here should also be mentioned the funding support by the European Marie-Curie Actions for which I am really grateful (Grant agreement no. 607886).

Last but not least, I must express my very profound gratitude to my parents, all my friends and to my girlfriend Joana for providing me with great support and continuous encouragement through the process of researching and writing this thesis. Thank you.

Contents

List of Figures

List of Tables

Glossary

ATP Adenosine Triphosphate

Coherence Degree of similarity between the phase and frequency of the optical wave

DMEM Dulbecco's Modified Eagle Medium

ERK Extracellular signal regulated kinases

IR Infrared radiation, [700 1e6] nm

Irradiance Optical power impinging over a defined area ($mW\,m^{-2}$)

NADPH Nicotinamide adenine dinucleotide phosphate

NIR Near infrared radiation, restricted part of the IR [700 2500] nm

NO Nitric oxide

Optical energy Energy emitted by a light source in the form of photons (J)

Optical power Optical energy emitted per unit time by a light source (W)

Optical Transport Propagation of light photon in a defined medium

Phase Fraction of a complete cycle corresponding to an offset (degree or radian)

Polarisation Direction of variation of the electro-magnetic field

Pulsing Emission of light characterised by successive emission and stop period

Radiant Exposure Optical energy received by a defined area ($J.m^{-2}$)

ROS Reactive Oxygen Species

TRPA1 Transient receptor potential cation channel, subfamily A, member 1

UV Ultra-Violet radiation, 10 to 400 nm

Vis Visible radiation, 400 to 800 nm

Chapter 1: Introduction

The uptake of energy-based home-use devices for medical treatment and personal care is increasing rapidly, due to the appeal of their practicality, simplicity of use, and efficacy (Metelitsa and Green, 2011). Within this trend, skin health attracts particular interest, underlined by a large burden of skin and hair diseases (Hay et al., 2014).

The non-invasive nature of light, free of potential systemic side-effects, is a very attractive treatment modality, where skin interaction with light in the ultraviolet (UV) to infrared (IR) range with subsequent photochemical, photothermal, and photomechanical effects, drives the therapeutic effects.

Professionals have already successfully exploited the benefits of photothermal, photomechanical and photochemical light-based treatment (Jacques, 1992; Stern, 2007). Some examples include: photothermal effects for skin rejuvenation (Rinaldi, 2008) and for removal of hair and vascular lesions (Babilas et al., 2010); photomechanical skin rejuvenation using laser-induced optical breakdown (Habbema et al., 2012; Habbema et al., 2013); PUVA-, UVB-, and blue-light-based photochemical treatment of psoriasis (Lim et al., 2015; Pfaff et al., 2015).

Photobiomodulation is formally defined as the use of visible (Vis) to NIR light absorbed by endogenous chromophores, triggering non-thermal, non-cytotoxic, biological reactions through photochemical events (Anders, Lanzafame, and Arany, 2015). In November 2015 the term “Photobiomodulation Therapy” was formally adopted as an official NIH U.S. National Library of Medicine (MeSH) term (Carroll, 2015).

The field of photobiomodulation of skin and its appendages, kick-started by a landmark study on hair regrowth in the late 1960s (Mester, Szende, and Gart-

ner, 1968), has now expanded to include applications for hair cycle modulation (Sheen et al., 2015), hair re-growth (Lanzafame et al., 2013), wound healing (Kajagar et al., 2012; Hopkins et al., 2004; Gupta et al., 1998), psoriasis (Weinstabl et al., 2011), skin barrier recovery (Denda and Fuziwara, 2008), stem cell regenerative therapy (Arany et al., 2014), where several books were published on the topic summarizing experimental studies and basic mechanisms (Hamblin, Waynant, and Anders, 2010; Waynant and Tata, 2008; Smith, 2007).

As of today, more than thirty light-based devices based on photobiomodulation have been cleared to market by the FDA for the management of hair regrowth (Lanzafame et al., 2013; Lanzafame et al., 2014; Jimenez et al., 2014; Administration and Drugs, 2016), and this number is constantly increasing. The translation of photobiomodulation to human applications has therefore already started.

However, we are very much in the dark in many fundamental mechanistic features behind the therapy. First, the very first point of reception of light in so-called non-photosensitive tissues (i.e. extra-ocular) is unknown. We have reason to believe that this light reception may involve a growing list of cellular components including cytochrome c oxidase (Karu, 2014), nitrosated proteins regulating nitric oxide (NO) bioactivity (Liebmann, Born, and Kolb-Bachofen, 2010; Keszler et al., 2014), ion-gated channel (Wang et al., 2016), circadian rhythm regulator flavoprotein cryptochrome (Bouly et al., 2007) and the more recently-considered opsin family photoreceptors (Denda and Fuziwara, 2008; Haltaufderhyde et al., 2015; Kim et al., 2013a; Sikka et al., 2014; Wicks et al., 2011; Buscone et al., 2017).

Second, the selection of optical settings is not based on systematic studies but rather on empirical observations (Chung et al., 2012). The main criterion for the selection of wavelength is its penetration depth in the skin. The lack of rationality in the selection of optical settings may be partly responsible for the mix of positive, negative and neutral outcomes of photobiomodulation reported by many reviews of the literature, wound healing (Woodruff et al., 2004) for example.

Third, the selection of optical settings is further complicated by the propagation of light in human skin. *In vivo* targets, particularly those lying deep in the skin,

will receive very different photon density than the one applied on top of the skin. Therefore, parameters that were found effective *in vitro* on selected human skin cells, will need adaptation for correct translation to the skin surface in order to deliver similar optical settings to the same skin cell population *in vivo*. Additionally, as light will be randomly scattered in the skin, there will be a large number of targets that will be simultaneously irradiated by the same light treatment. A modelling tool is critical to understand which skin components are affected by which amount of light.

The objectives of this thesis were thus defined according to the gaps of the literature mentioned above:

- Investigate the molecular mechanisms involved in the action of visible and NIR light on skin cells in photobiomodulation
- Optimize the selection of optical treatment parameters in photobiomodulation of human skin cells
- Characterize a numerical model of light propagation in the skin and evaluate its potential use for the translation of photobiomodulation research

In response to these objectives, the results of the thesis are divided in 4 chapters. The first results chapter presents a detailed literature review of the current state of knowledge in photobiomodulation as it pertains in dermatology and the current use of optical treatment parameters in studies involved in wound healing and hair regrowth. The second results chapter employs a systematic approach to optimize the selection of effective optical treatment settings in photobiomodulation using normal human primary dermal fibroblast subpopulations as a target. A third chapter provides mechanistic insights and a functional analysis of the effect of some selected optical treatment parameters on both lineages of human dermal fibroblasts based on the expression of genes after light treatment. Finally, the last chapter presents a characterization of the accuracy of a potential translation tool for the prediction of the propagation of optical photon density inside human skin. Before entering in the topic, the reader is advised to read the annex A for

the basics and essentials in photobiology.

Chapter 2: Materials and Methods

2.1 Cell biology

2.1.1 Isolation of normal primary human dermal fibroblasts

Human dermal fibroblasts were isolated from fresh human facial skin within 8 hours of surgery. Human skin was obtained as excess tissue after facelift surgery from healthy donors adhering to the Declaration of Helsinki principles under Tissue Transfer Agreement, where clinics were responsible for having a full written consent from all patients. All experimental protocols were carried out in accordance with relevant guidelines and regulations of the Internal Committee of Biological Experiments both at the University of Bradford and Philips Research (Eindhoven). All skin cells used within this PhD thesis were isolated from Caucasian skin samples.

Papillary and reticular fibroblasts lineages were extracted from superficial dermis just below the epidermis and deep dermis above the hypodermis, respectively as previously described (Mine et al., 2008; Sorrell and Caplan, 2004). Cells were initially cultured in DMEM supplemented with penicillin/streptomycin (1%), Glutamax (1%) and fetal bovine serum (FBS) (10%). The concentration of FBS was later very gradually reduced to 2% to bring the *in vitro* model closer to the normal *in vivo* environment of the dermal fibroblasts where it was associated with a significant reduction in proliferation rate. Pairs of reticular and papillary were donor sample-matched, unless otherwise indicated.

In figure 2.1 it is possible to see that the extracted dermal fibroblast lineages show expected morphological features. Indeed, the reticular fibroblasts are more fried-

egg-shaped and spread on the plastic disk while papillary fibroblasts exhibit a spindle, thin and thicker shape (Driskell et al., 2011; Mine et al., 2008; Sorrell and Caplan, 2004).

At the University of Bradford and Philips Research, primary human papillary fibroblasts were obtained from frozen vials directly from the cell bank of the laboratory.

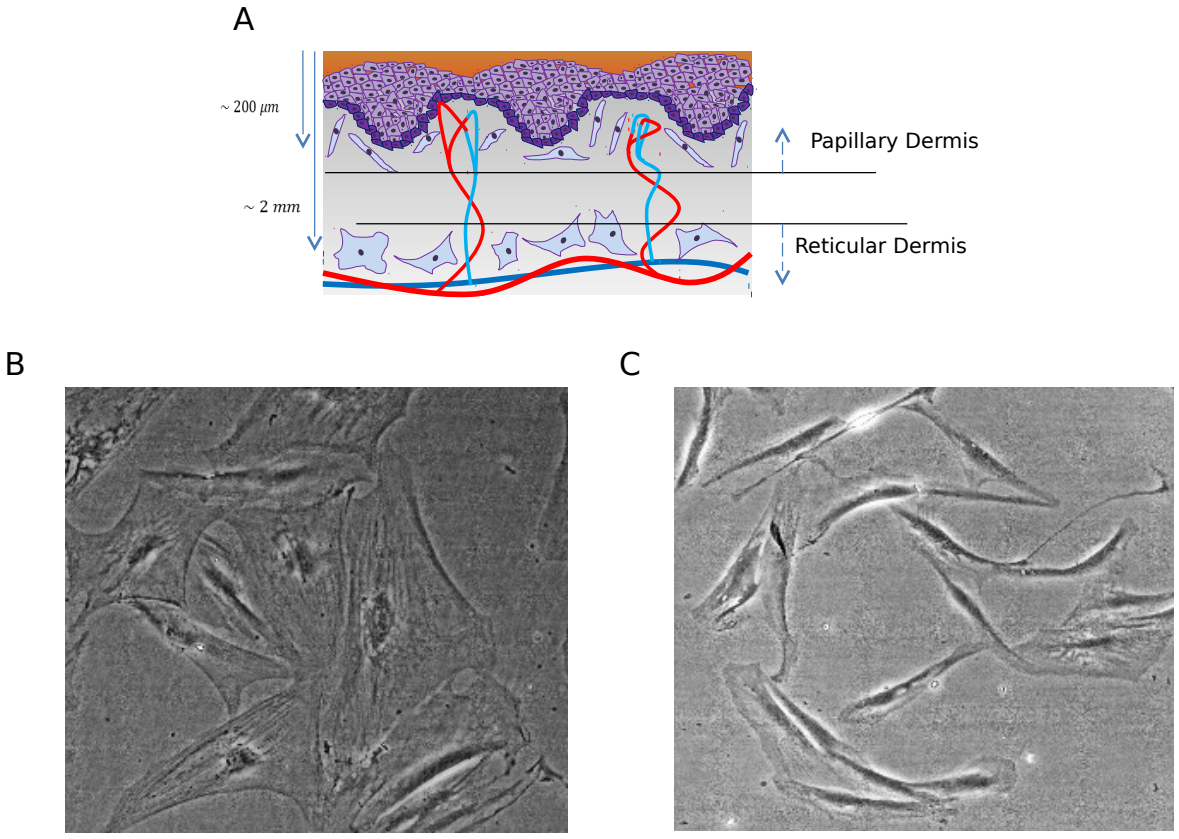

Figure 2.1: A: Explanation scheme of the skin cross-section showing the locations of the papillary and reticular dermis. Phase-contrast pictures of the reticular (B) and Papillary (C) fibroblasts where their morphology is clearly different (Original magnification x10). Donor shown is donor F64 (facelift, female, 64yo)

2.1.2 Culture of primary human dermal fibroblasts

The dermal fibroblasts populations were typically started in T-75 flasks from frozen vials. The starting culture medium was DMEM supplemented with 1% Pen/Strep, 1% Glutamax and variable concentration of FBS. The passage of the cells was always kept under passage 8 for all experiments. The limit (passage 8) was se-

lected in order to ensure that the cells will conserve as much as is practical their lineage-specific traits when used in experiments. Indeed, the conversion of papillary to reticular phenotype was observed *in vitro* at much higher passage (10-15) (Janson et al., 2013).

The sources of the chemicals used to supplement the culture medium are provided here:

- Penicillin-Streptomycin (P/S) , 15140122, Gibco (ThermoFisher)
- Fetal Bovine Serum (FBS), 10270106, Gibco (ThermoFisher)
- GlutaMAX™ (100X), 35050038, Gibco (ThermoFisher)
- Dulbecco's Modified Eagle's Medium - low glucose, with and without phenol red D5921 and D5546, Sigma-Aldrich

Trypsin-EDTA was used to detach adherent cell culture (passage, seeding). The reagent reference is: 0.25% Trypsin-EDTA (1X),25200056, Gibco (ThermoFisher).

2.1.3 Biological assays

Cell counting and viability

The counting of cells were performed using automatic cell counters. The following machines were used depending on the location where the work was carried out: TC20™ Automated Cell Counter (Bio-Rad) at the University of Bradford, Vi-CELL XR (Beckman Coulter Life Sciences) at Philips Research.

Cell morphology

All photographs were performed using a Leica microscope (TCS SP5) with a 10x objective unless otherwise indicated. Phase-contrast configuration was usually used to provide the best resolution of the cell morphology.

Assessment of cell metabolic activity: Alamar Blue assay

The metabolic activity of the dermal fibroblasts was assessed using the Alamar Blue® assay (Thermofisher, DAL1100) (Tonder et al., 2015). This assay was selected for its lower variability across the different cell lineages, compared to MTT assay, often considered as the gold standard for determination of cell viability and proliferation (Mosmann, 1983). MTT assay measures cell viability in terms of reductive activity as the enzymatic conversion of the tetrazolium compound to water insoluble formazan crystals by dehydrogenases occurring in the mitochondria of living cells, although reducing agents and enzymes located in other organelles such as the endoplasmic reticulum can also be involved.

In contrast to MTT assay, the Alamar Blue kit involves the conversion of its active component, resazurin, to fluorescent resorufin occurs, which mostly in the mitochondria. The quantity of resorufin generated can therefore be used as indicator of metabolic activity (Zhang et al., 1990). On the day of assessment Alamar Blue® was added to fresh DMEM (10% by volume). The solution was then incubated in contact with the cells for 3 to 5 hours depending on the confluency of cells. The fluorescence generated was read using a plate reader FLUOstar Omega II (ex: 544 nm, em: 590 nm). The experimental outcome of the light-based treatments was expressed in terms of relative metabolic activity, defined as a ratio between the means of the treated groups and the control group.

Reactive Oxygen Species (ROS) detection, fluorescence dye

Evidence of the induction of ROS in human cell culture by short visible wavelengths exist (Consentino et al., 2015; Kuse et al., 2014; Becker et al., 2016). Therefore, detection of ROS under light treatment was performed in culture of human dermal fibroblasts. On the day of measurement, a solution of 10 μM of either CellROX Orange or CellROX Deep Red (ThermoFisher, C10443 & C10422) in PBS was prepared. Adherent fibroblasts were incubated in contact with the solution for 30 minutes at 37 $^{\circ}$C. After incubation, the fibroblasts were washed three

times with PBS and put back in supplemented DMEM. Excitation and emission wavelengths are provided by the manufacturer: Ex: 644 nm, Em: 655 nm.

Mitochondria tracker, fluorescence dye

MitoTracker® Red CMXRos (ThermoFisher M7512) was used to track mitochondria inside the cells. On the day of measurement, a solution of 400 nM of MitoTracker in PBS was prepared. Adherent fibroblasts were incubated in contact with the solution for 30 minutes at 37 °C. After incubation, the fibroblasts were washed once with PBS and put back in supplemented DMEM. Excitation and emission wavelengths are provided by the manufacturer: Ex: 579 nm, Em: 599 nm.

Treatment of human dermal fibroblasts with antioxidants

Quercetin and Vitamin E were selected for their antioxidant properties. The following concentrations were prepared in supplemented DMEM: 1 μM quercetin and 100 μM vitamin E. Quercetin (Sigma-Aldrich Q4951-10G) was dissolved in DMSO. Vitamin E (258024-5G) was added to sterile water and vortexed to force miscibility. Evidence in the literature showed that the antioxidant action of quercetin was improved when used in combination with vitamins (Milton Prabu, Shagirtha, and Renugadevi, 2010). Thus, both antioxidants were always used in combination and not separately.

RNA isolation and purification

Cell lysis and RNA isolation was performed using the RNeasy Mini Kit from Quiagen (74106). The procedure was followed according to the manufacturer instructions. The cell lysis was performed using 350 μL of buffer RLT (Qiagen proprietary lysis buffer) supplemented with 10 µL of β-mercaptoethanol per mL of buffer. The lysis was performed at RT and collected samples were immediately put in -80 °C freezer for storage before extraction. The RNA isolation protocol was followed from the Quick-Start Protocol and the optional step of DNase digestion was performed.

Human dermal fibroblasts were cultured in low serum DMEM (2% FBS, 1% P/S,

1% Glutamax) at a low confluency (40-60%) in 35-mm dish. They were treated once a day for three consecutive days with selected light parameters. The cells lysates were collected 24 hours after the last light treatment. For each replicated 8 individual 35-mm dishes were pooled together to reach sufficient material.

Gene expression and gene set enrichment analysis (GSEA)

The high quality of the RNA samples was confirmed by capillary electrophoresis on an Agilent 2100 bioanalyzer (Agilent). Arrays of GeneChipTM Human Transcriptome Array 2.0 from Affymetrix were used to quantify the transcriptome of the samples. The Affymetrix standard labelling protocol was followed to prepare the biotinylated antisense cDNA using the GeneChip® WT Plus Reagent Kit and the GeneChip® Hybridization, Wash and Stain Kit (both from Affymetrix, Santa Clara, USA). The following steps: hybridization on the chip, dying and scanning were performed on a GeneChip Hybridization oven 640, a GeneChip Fluidics Station 450 and a GeneChip Scanner 3000 respectively. The equipment and machines performing the steps were manufactured by the Affymetrix-Company (Affymetrix, High Wycombe, UK).

Following the experimental protocol the analysis of the transcriptome was performed, in particular annotations, data processing and Gene Set Enrichment Analysis (GSEA). Annotations were made based on the Custom CDF Version 20 with Entrez based gene definitions (Dai et al., 2005). The raw fluorescence intensity values were normalized applying quantile normalization. Differential gene expression was analyzed using a commercial software package: SAS JMP10 Genomics, version 6, from SAS based on OneWay-ANOVA. GSEA method was applied to our dataset. This method extracts defined lists (or sets) of genes showing a statistically significant bias in their distribution in the treated group versus a control group within a ranked gene list (Subramanian et al., 2005). A threshold on the false positive rate was used to select significant pathways ($FDR < 0.1$). The public pathway database KEGG was used.

cDNA synthesis

The synthesis of cDNA was performed from $100\ ng$ of purified RNA using the High-Capacity cDNA Reverse Transcription Kit (Thermofisher, 4368814). The reverse transcription reaction was performed via a thermocycler according to the manufacturers instructions. The temperature steps were: $25\ °C$ for 10 minutes, $37\ °C$ for 120 minutes and $85\ °C$ for minutes. Immediately after reaction, the samples were stored at $-20\ °C$.

Real-time qPCR

In order to validate the results of gene expression analysis, qPCR (quantitative polymerase chain reaction) was used to measured the expression of relevant genes in the treated and control groups. Results obtained with microarray and qPCR were then compared. Quantitative real-time PCR of *MMP1*, *TGFB2*, *GJA1*, *CDH2*, *NR1D1*, *GPRC5A* and *PDE5A* was performed, where primers sequences are shown in table 2.1. Annealing temperatures were optimized and selected as follows: $59.8\ °C$ for *GPRC5A*, *TGFB2*, *PDE5A*, *NR1D1* and *GJA1*, and $63.1\ °C$ for *CDH2* and *MMP1*. A standard RT-PCR thermal sequence was programmed: $95\ °C$ for 2 minutes, followed by 35 three-step cycles ($95\ °C$ for 20 seconds, 20 seconds at the corresponding annealing temperature, and at $72\ °C$ for 30 minutes), a final step at $72\ °C$ for 2 minutes. Quantification was carried out using SYBR green (SYBR® Green PCR Master Mix, Thermofisher 4344463). Thermal cycler was from Bio-Rad (C1000 Thermal Cycler, CFX96 Real-Time System).

Quantification of human procollagen-I in supernatant

An ELISA kit from Takara (MK101, Procollagen Type I C-Peptide (PIP) EIA Kit) was used to quantify the concentration of procollagen-I in the supernatant of fibroblast culture. Human dermal fibroblasts were treated three times once per day on three consecutive days by selected light parameters. After each light treatment, the culture medium was replenished to avoid any cytotoxic effects due to the interaction of light with the culture medium. The supernatants were collected

Table 2.1: qPCR: primer sequences

Primer	Sequence
MMP1-F	GGGGCTTTGATGTACCCTAGC
MMP1-R	TGTCACACGCTTTTGGGGTTT
TGFB2-F	CCATCCCGCCCACTTTCTAC
TGFB2-R	AGCTCAATCCGTTGTTCAGGC
GJA1-F	TGGTAAGGTGAAAATGCGAGG
GJA1-R	GCACTCAAGCTGAATCCATAGAT
CDH2-F	ATGTGCCGGATAGCGGGAGC
CDH2-R	ACAGACGCCTGAAGCAGGGC
NR1D1-F	ATCGTCCGCATCAATCGCAA
NR1D1-R	CTGCTTCTCTCGTTTGGGGAT
GPRC5A-F	GCTGCTCACAAAGCAACGAA
GPRC5A-R	ATAGAGCGTGTCCCCTGTCT
PDE5A-F	GATCCTCGGTTCAATGCAGAA
PDE5A-R	ACAAAATGCCAAATAAGCAGCAA

72 hours after the last light treatment and immediately frozen (-80$^{\circ}C$). Later, samples were thawed and the protocol of the manufacturer was carefully followed to quantify the procollagen I content. The samples were not diluted before quantification except the supernatants coming from the experiments performed on from donor female 64 years old papillary subtype (dilution 1/2).

2.2 Characterization of tissue donors and cell culture conditions

2.2.1 Clinical details of donors of isolated fibroblasts

The cell lines used to perform the experiments will be introduced here. They were associated with the three time periods of the PhD studies: a first period at Philips Research Eindhoven, a second at the University of Bradford and a last period again at Philips Research. The cells used in the three time periods were not from the same donors (see table 2.2). The following notation was used to designate individually the donors (independently of the lineage): gender-age. By extension, the reticular and papillary subtypes of a donor will be referred as follow: first letter of subtype-age. For example, a 64 year-old skin donor is referred to as: F64, the reticular subtype to as: R64 and the papillary subtype to as: P64. No two

donors were of the same age, therefore when the age number is the same the population are originated from the same donor. When the age was not available due to patient data protection, the notation was simply reduced to gender/subtype and increment number starting from 1. All donor and cell population notation are shown in table 2.2.

Donor	Age	Gender	Origin	Lineage	Period
R1	Unknown	Female	Facelift	Reticular	1
R2	67	Female	Facelift	Reticular	1
P1	Unknown	Female	Facelift	Papillary	1
P2	43	Female	Facelift	Papillary	1
R3	Unknown	Female	Facelift	Reticular	1
P3	Unknown	Female	Facelift	Papillary	1
P51	51	Male	Browlift	Papillary	2
P57	57	Female	Arm Skin	Papillary	2
P67	67	Female	Facelift	Papillary	2
P72	72	Female	Facelift	Papillary	2
R53	53	Female	Facelift	Reticular	3
P53	53	Female	Facelift	Papillary	3
R59	59	Male	Facelift	Reticular	3
P59	59	Male	Facelift	Papillary	3
R62	62	Female	Facelift	Reticular	3
P62	62	Female	Facelift	Papillary	3
R64	64	Female	Facelift	Reticular	3
P64	64	Female	Facelift	Papillary	3

Table 2.2: Age, gender, body location for isolation and lineage for each donor used throughout the project. The skin type of all the donors was Caucasian. No two donors were of the same age, therefore the age identifies the donor. Mean age of the donors: 59.5 ± 8.7 yo.

The extent of morphological distinctiveness between papillary and reticular fibroblasts are variable accross different skin donors (Figs. 2.2 and 2.3). Cells from donors F64 and M53 showed the stereotypical morphologies, whereby reticular cells were flat and spread over the plastic substratum while the papillary cells were thin and elongated (2.3, B/E,C/F).

The associated metabolic activity of the reticular and papillary cells from donors F53, M59 and F64 are also showing significant differences (Fig. 2.4). Indeed, reticular cells exhibited a higher metabolic activity as compared to the corresponding papillary cells (the seeding density of each population being the same). This is in agreement with previously reported results where cell quiescence was asso-

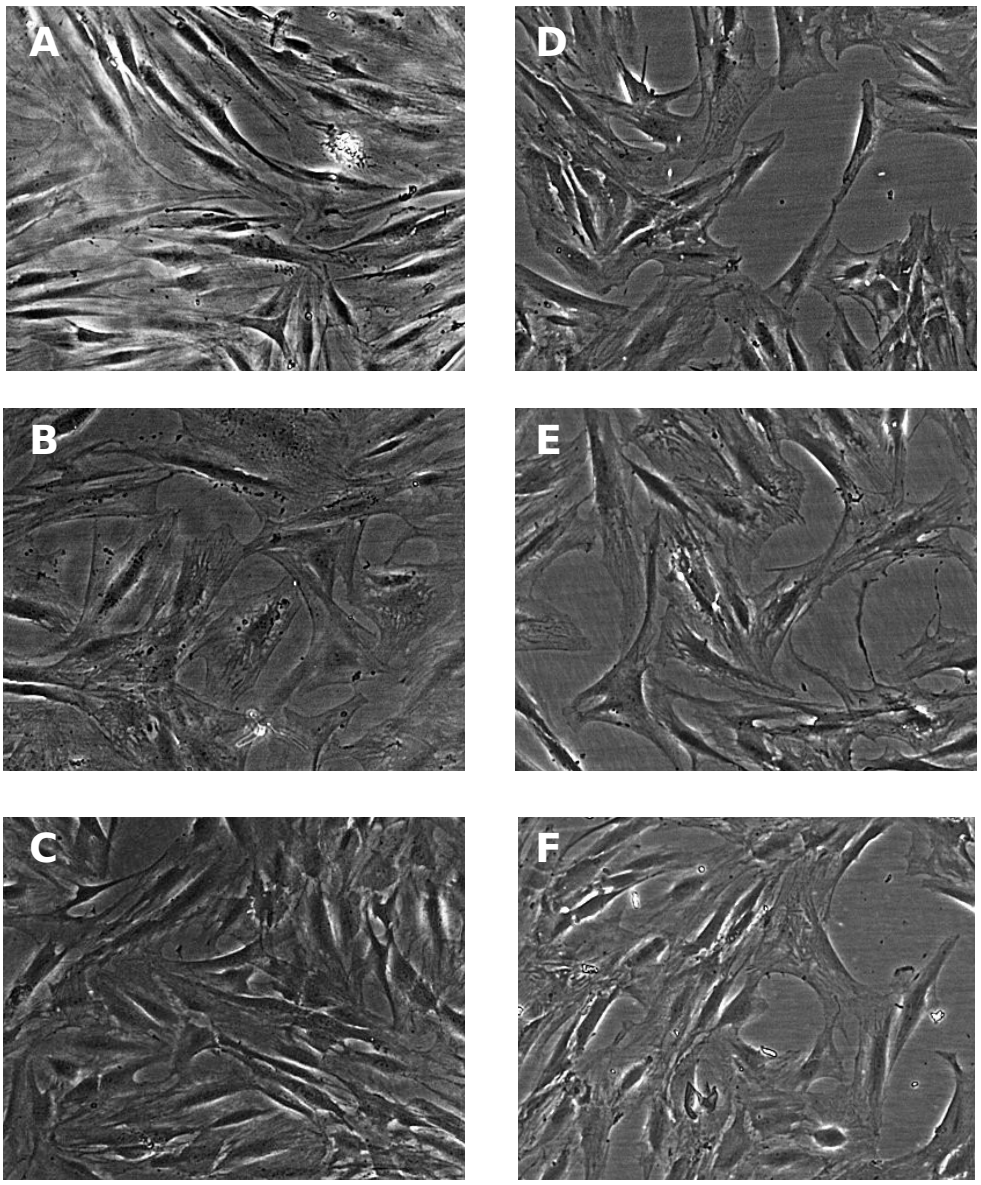

Figure 2.2: Phase-contrast microscopy pictures of human dermal reticular (A,B,C) and papillary (D,E,F) fibroblasts from the donors (R1,R2,R3) and (P1,P2,P3), original magnification was x10.

ciated to high metabolic activity (Lemons et al., 2010; Driskell et al., 2015).

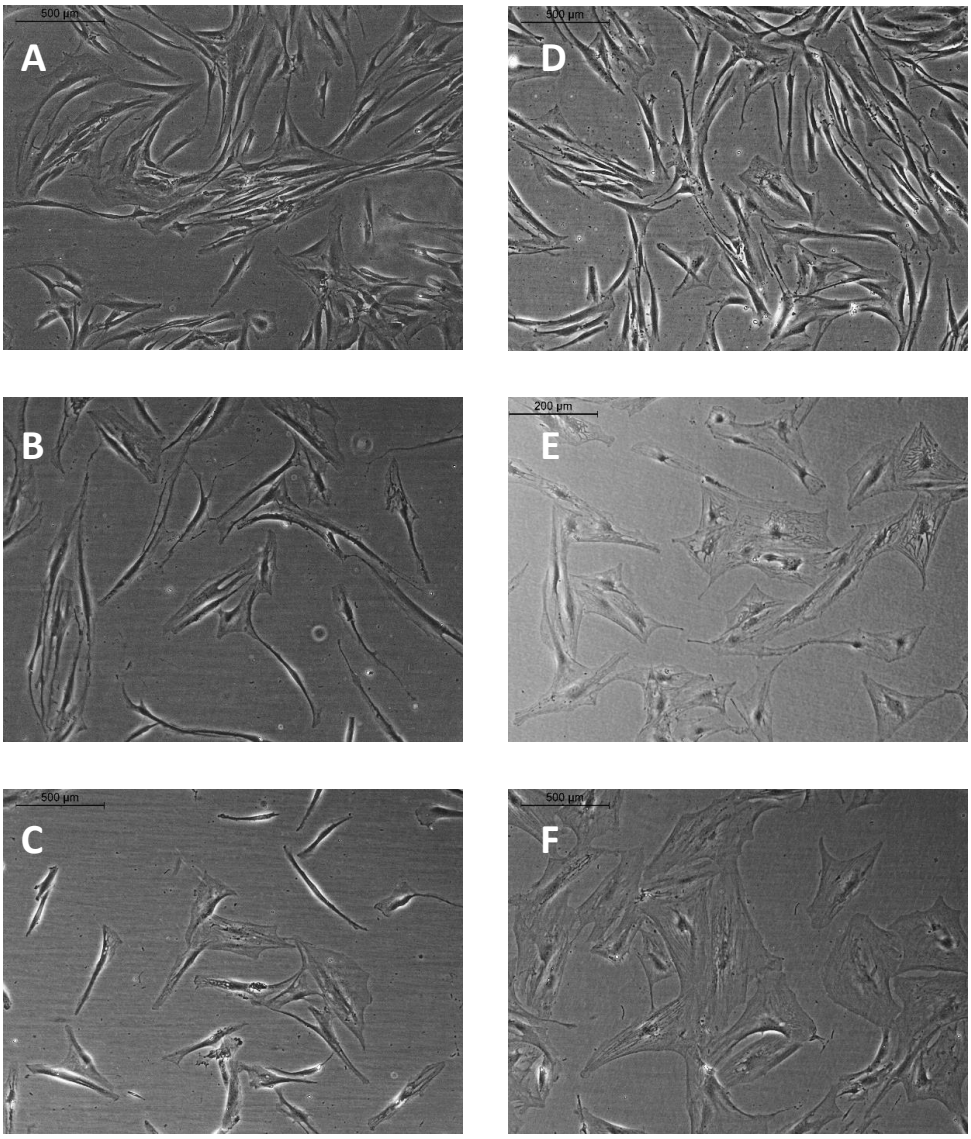

Figure 2.3: Phase-contrast microscopy pictures of human dermal reticular (A,B,C) and papillary (D,E,F) fibroblasts from the donors used in the third period, respectively (R53,R59,R64) and (P53,P59,P64), original magnification was x10.

2.2.2 Range of serum concentration, cell density and environmental oxygen concentration used in this study

Serum concentration

Serum concentration was varied in the range [2 10]% volume of the culture medium. The serum concentration in the culture medium had a strong effect on the proliferation of human dermal fibroblasts (Fig. 2.5). Under the microscope, a much higher

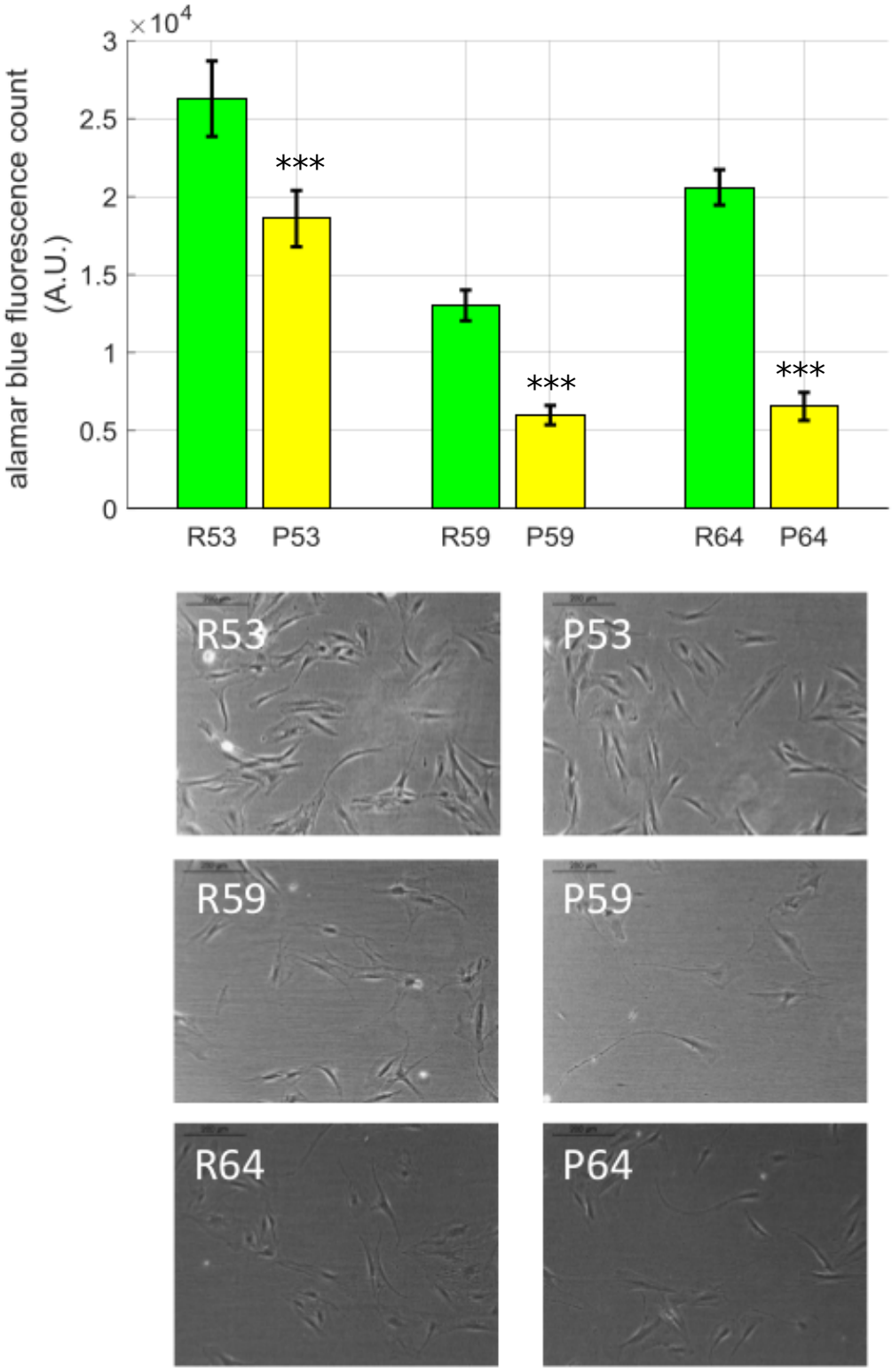

Figure 2.4: Metabolic activity of the matching reticular and papillary couples respectively R53/P53, R59/P59 and R64/P64, together with the phase-contrast microscopy pictures of both lineages for each donor. Each population was seeded at the same density. Original magnification was x10. Differences are statistically significant ($p < 0.001$) for all three comparisons reticular/papillary (3 replicates, 4 repeats per donor and sub-population). Standard deviations are shown in error-bars.

growth rate of the cells cultured was observed in 10% FBS than when cultured in 2% FBS (Fig. 2.5, A). This was quantitatively confirmed by the metabolic activity of cells cultured in 10% and 2% FBS (Fig. 2.5, B). Interestingly, fibroblast proliferation in 2% FBS is slow. Over 4 days, there was negligible change (Fig. 2.5, C).

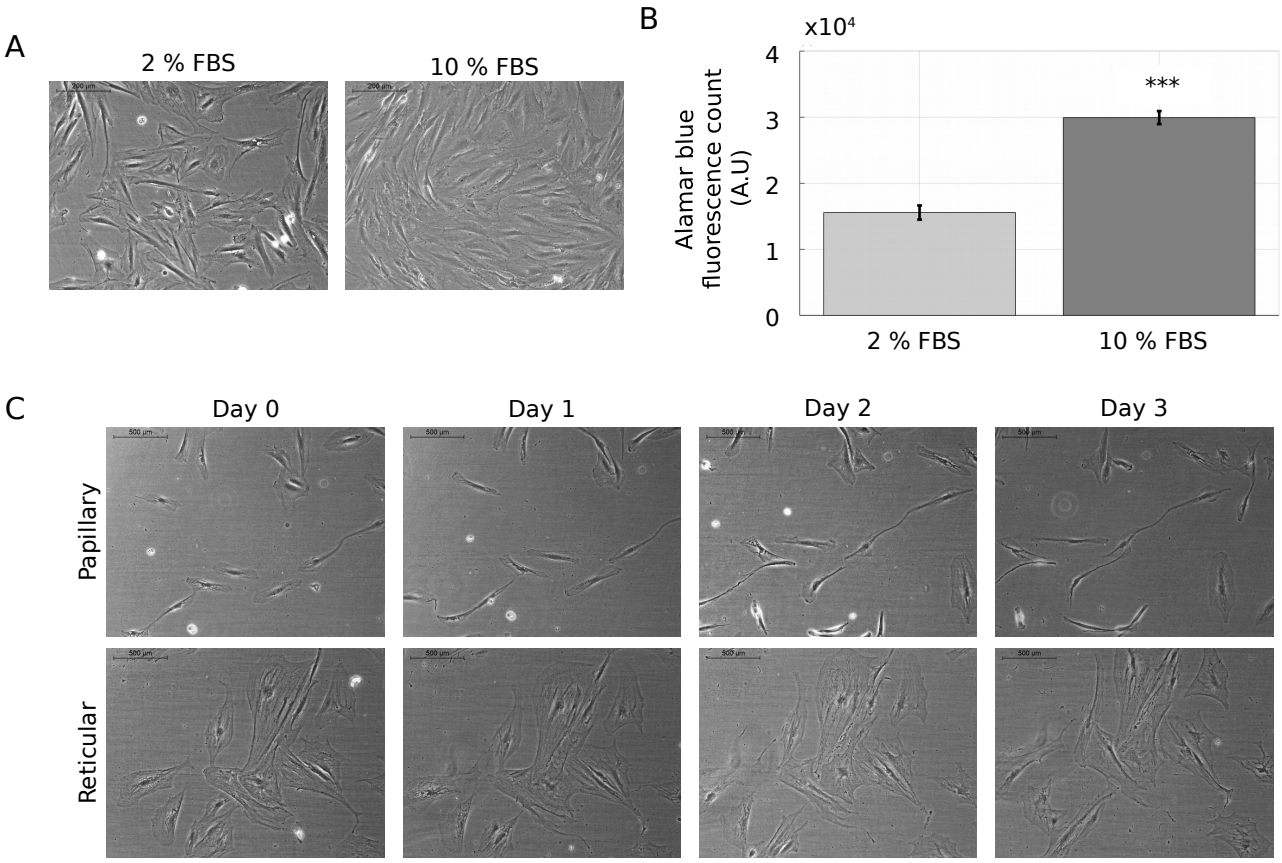

Figure 2.5: A: Phase-contrast microscopy pictures of normal human papillary fibroblasts cultured in 10% (right) and 2% (left) FBS 8 days after seeding starting from the same initial density. Original magnification was x10. B: Metabolic activity of the same human papillary fibroblasts measured via the Alamar Blue assay 4 days later, C: Phase-contrast microscopy pictures of normal human reticular and papillary fibroblasts cultured in 2% FBS followed over 4 days, original magnification was x10. The data shown here was measured on cells from donor F64 (facelift, female, 64yo). Standard deviations are shown in errorbars.

Cell density

Cell confluency was varied from 10% to over 100% (i.e. where cells begin to multi-layer). The confluency levels correspond to different cell number depending on the format of culture plate used. In 24-well plate, 10% and 90% confluency

levels corresponded to 2,500 and 30,000 cells per well respectively. In a 35-mm dish, another format which was used commonly in experiments, these levels correspond to 5,000 and 60,000 cells per well. In this thesis, to 'low' confluency as confluency levels which are under 60% confluency and 'high' confluency to confluency levels which are over 80% confluency. Phase-contrast microscopy pictures are shown to illustrate ´low´ and ´high´ confluency levels, together with the corresponding Alamar Blue (metabolic activity) absolute reading (Fig. 2.6).

Environmental oxygen

Environmental oxygen level experienced by the cells *in vitro* was also varied directly via the incubator settings (Forma™ Steri-Cycle™ i160 Tri-Gas CO2 Incubators). Indeed, recent evidence suggests the existence of gradients of physiological oxygen levels throughout the different layers of human skin layers, where oxygen level in dermis (outside capillary loops) can be as low as 1-5%, compared to 20% atmospheric level (Wang, 2005; Upton et al., 2015). Phase-contrast microscopy pictures are shown to illustrate the morphology of the cells in hypoxia (2% partial oxygen pressure) and normoxia (20% partial oxygen pressure), together with the corresponding Alamar Blue absolute reading (Fig. 2.7).

The standard culture conditions of human dermal fibroblasts use high confluency, high serum concentration and high environmental oxygen concentration (i.e. 20% oxygen). However, the *in vivo* environment of the dermal fibroblasts would rather correlate with lower values: low cell density, low to no serum and low environmental oxygen concentration.

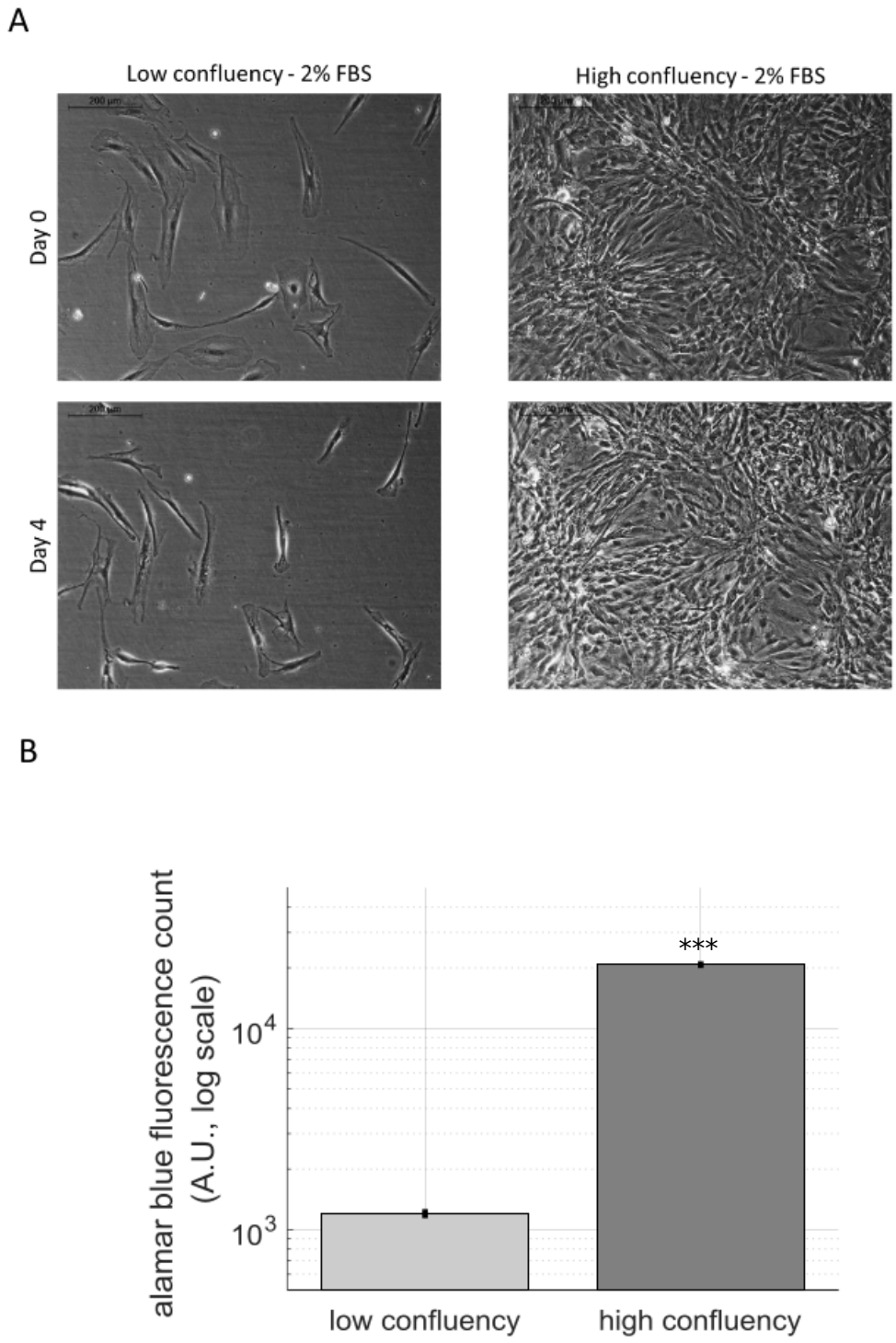

Figure 2.6: A: Phase-contrast microscopy pictures of normal human papillary fibroblasts cultured at ´low´ and ´high´ confluency levels at day 0 and day 4, original magnification was x10. B: Metabolic activity of the same human papilary fibroblasts measured via the Alamar Blue assay on day 4 (log scale). The data shown here was measured on cells from donor F64 (facelift, female, 64 yo). Standard deviations are shown in errorbars.

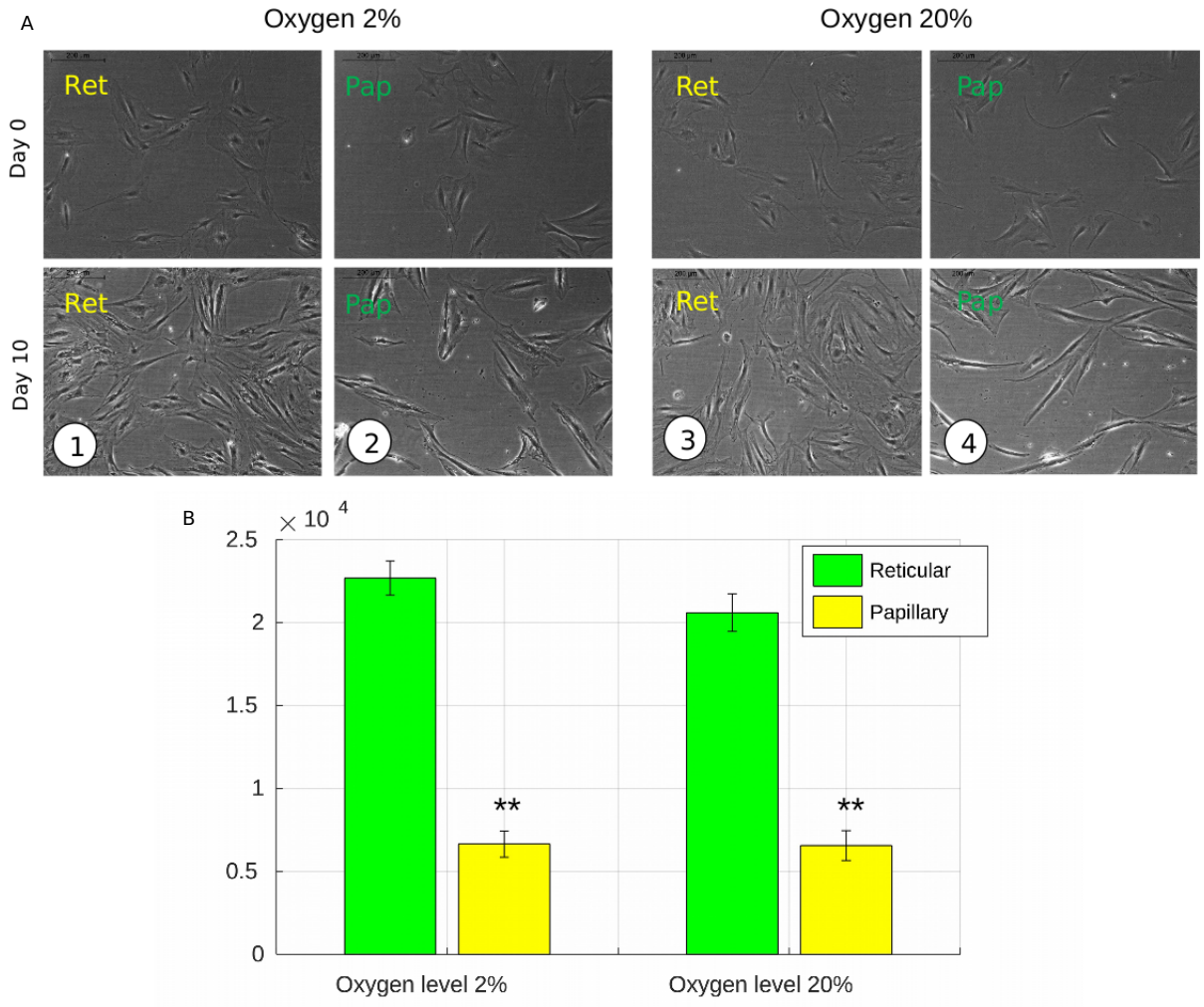

Figure 2.7: A: Phase-contrast microscopy pictures of normal human reticular and papillary fibroblasts cultured at ´low´ and ´high´ environmental oxygen levels, original magnification was x10. Human papillary and reticular fibroblasts from the same donors were cultured in both 2% and 20% oxygen incubators for 10 days. B: Metabolic activity of the same human papillary and reticular fibroblasts measured via the Alamar Blue assay on day 10. The data shown here was measured on cells from donor F64 (facelift, female, 64yo). Differences are statistically significant ($p < 0.001$) for the comparisons reticular/papillary (3 replicates, 4 repeats per donor and sub-population). Standard deviations are shown in errorbars.

2.3 Literature review

A review of studies in Photobiomodulation involving wound healing and hair regrowth, was performed where the literature search included several selected keywords. Examples of included keywords are shown in Figure 2.8.

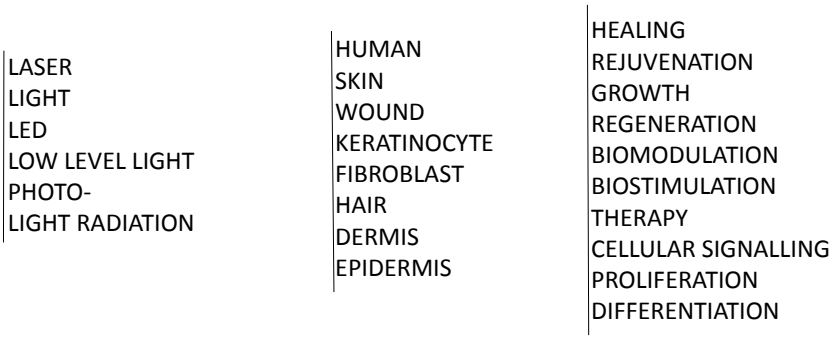

Figure 2.8: Combinations of keywords used for the systematic literature search. Treatment methods, targets and readouts are shown in the first, second and third column, respectively. The systematic search was performed in such a way that a combination of several words from the columns was included in the title or abstract of bibliographic references.

The selection was based on several criteria. First, core subjects of the selected studies were wound healing and hair regrowth. Second, the studies were directed to humans or material derived from humans e.g., human skin cells culture. While diverse skin cells types are used throughout the studies reported in literature, this review was focused on the most commonly studied (and thus the most statistically interesting) i.e., fibroblasts and keratinocytes. As the goal is the selection optical parameters for treatment, the third inclusion criterion was the disclosure of the optical parameters. Finally, the presence or absence of a sham/control group was monitored. Both *in vivo* and *in vitro* studies were included. In total 60 separate articles published between 1985 and 2015 were included. Twenty *in vivo* clinical

studies on wound healing (Kajagar et al., 2012; Gupta et al., 1998; Hopkins et al., 2004; Minatel et al., 2009; Zhou, Luo, and Xie, 2008; Malm, 1991; Whelan and Turner, 2001; Schindl et al., 2002; Schindl, Schindl, and Schindl, 1997; Schindl et al., 1998; Kopera et al., 2005) and hair regrowth (Lanzafame et al., 2013; Lanzafame et al., 2014; Jimenez et al., 2014; Leavitt et al., 2009; Satino and Markou, 2003; Blum et al., 2014; Kim et al., 2013a; Waiz et al., 2006; Abdelhalim, 2014) were included. Regarding the *in vitro* studies, in total 11 studies on fibroblasts cell lines (Hawkins and Abrahamse, 2006; Esmaeelinejad et al., 2014; Evans and Abrahamse, 2008; Webb, Dyson, and Lewis, 1998; Zhang et al., 2003; Houreld et al., 2008; Azevedo et al., 2006; Abergel et al., 1987; Houreld; et al., 2014; Danno et al., 2001; Damante et al., 2009), 7 on fibroblasts primary cells (Oplander et al., 2011; Poon, Huang, and Burd, 2005; Rigau et al., 1994; Webb and Dyson, 2003; Fushimi et al., 2012; Barolet et al., 2009; Mamalis, Garcha, and Jagdeo, 2015), 7 on keratinocytes cell lines (Kim et al., 2013a; Basso et al., 2013; Pellicioli et al., 2014; Becker et al., 2015; Danno et al., 2001; Fushimi et al., 2012; Gavish et al., 2004) and 5 on keratinocytes primary cells (Liebmann, Born, and Kolb-Bachofen, 2010; Grossman et al., 1998; Ejiri et al., 2014; Yu et al., 1996; Haas et al., 1990) were found, respectively.

2.4 Characterization of light-based devices for hair regrowth

As presented in the introduction of this thesis, more than 20 light-based devices are already cleared by the FDA for hair regrowth and are currently sold on the market. One of the objective of this PhD study is to optimize the selection of optical treatment parameters in photobiomodulation in dermatology. Therefore, the use of photobiomodulation in commercial light-based products was also evaluated. Three commercial home-use devices for hair regrowth were characterized in terms of their optical performance. The spectral output was measured using an integrating sphere (Labsphere, model AS-02478-000 LMS 200, 50 cm)

and their spatial distribution using a digital camera (RadiantImaging, Laser2000, PM1403E-1) and a diffuser. Optical power was measured at the recommended working distance (i.e. at the assumed position of the scalp) of the devices using a powermeter (Ophir Nova II, its sensor PD300-3W-V1, calibrated in October 2014).

2.5 Design of light-based prototypes for the illumination of biological material: Sirius-24 and Sirius-8

The present project aims to gain knowledge on the photo-chemical actions of light on skin components, and to design experiments that will allow controlled illumination of multiple skin components and cells. This approach will require the development of a robust and rigorous practical light-based solution.

Although commercial solutions exist, they generally do not accommodate the large ranges in optical parameters found in literature (Mignon et al., 2016b). In order to proceed with this project experimental design, customized prototypes were needed. Two light-based prototypes were designed and manufactured by PiNS (Philips Innovation Services). These devices were named Sirius-8 and Sirius-24. They are shown in figure 2.9. Both work on the same concept: Light-emitting diode (LED) illumination underneath the target. Requirements associated with the devices as well as their designs and characterizations will be presented here.

Within the photobiomodulation (i.e. low-level light therapy (LLLT)) literature, researchers have used various ways to illuminate biological systems. Lasers, laser diodes, LED and lamps as light sources mounted within mechanical structures and sometimes with optical elements form a high variety of home-made illumination solutions which are available. There is a considerable difference between pointing a laser beam at a cell culture, and, homogeneously illuminating the same cell culture without providing other stimuli (such as thermal increase), thus design considerations are important. Overall a review of the literature has indicated that the solutions typically chosen are not rational in the majority of cases, with wavelength alone appearing as the major criterion for treatment parameter selection. Additionally, a lack of optical metrology knowledge has brought confusion in the reporting of optical parameters in the literature (Hadis et al., 2016).

A plurality of properties needs to be taken into account when designing and characterizing a light-based illumination source including:

Sirius-24

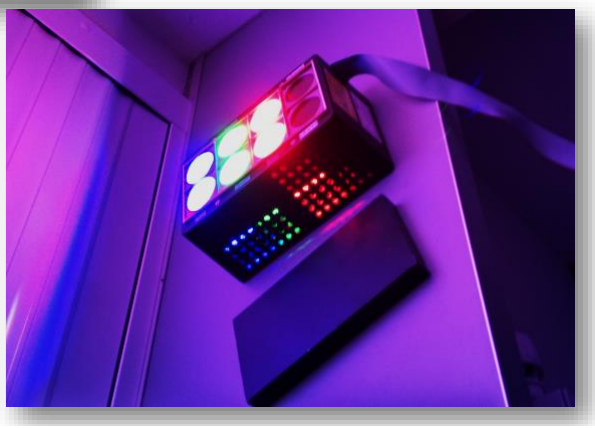

Sirius-8

Figure 2.9: Photographs of light-based prototypes Sirius-24 and Sirius-8.

- Direct light properties; wavelength, irradiance range, light regime (pulsed and continuous),beam geometry and homogeneity.

- Indirect practical properties; heating of the structure and cooling configuration, compatibility with biological system and requirements, automation and software control.

2.5.1 Requirements when targeting biological systems with light

A rational choice of illumination characteristics will be explored here; laying out the requirements first. In the current project, the first series of prototypes were aimed at illumination of a cell culture with cells seeded in two different formats; a 24-well plate and a series of individual $35\ mm$ dishes, in order to interrogate the ranges of optical parameters found in literature (Mignon et al., 2016c). The aforementioned formats were chosen to meet two needs. The first (Sirius-24) was aimed at screening a large range of optical parameters (wavelength, irradiance and radiant exposure) that also enabled robust statistical power. The second (Sirius-8)

allowed for an in-depth study of the biological response to light stimuli, where a large amount of biological material is needed, i.e. via larger culture dish size. Thus two devices, which were designed and manufactured, are named Sirius-24 and Sirius-8, referring to the number of component wells which can be illuminated in parallel.

It is important to keep two undesirable features in mind while designing a light-based prototype: unwanted exposure and heating. These will result in two drawbacks: color-mixing, ie. unwanted reflection or direct exposure from a different wavelength reaching the target of a primary wavelength, and, heating, due to exposure of components other than the target resulting in absorbed light heating up of the system. The latter triggers the potential thermal stimulation of the target. Thus as much as possible, heat and light effects should be separated.

2.5.2 Design solution for illumination of skin cells and tissue

Properties of light source

In terms of the properties of light, LEDs were chosen to be the component emitting the light. Wavelengths were chosen so that they were equally distributed around the absorption peaks of potential cellular photoreceptors as seen in figure 2.10. Sirius-24 has a lower available irradiance range compared to Sirius-8 due to the limited size of their illuminated area. Optional pulsing structure of the light stimuli was made available via the electronic control.

When targeting skin fibroblasts in cell culture, the target is around $100\ \mu m$ thick (thickness of a cell layer). Light propagation in such a structure, characterized with low scattering and absorption properties, will be negligible i.e. provide the same illumination for the whole system. When targeting 3D organs, the propagation of light in turbid media becomes significant and should be considered. The spatial coherence of the light source will not play a significant role (Karu, 2003) *in vitro*, and therefore the low spatial and temporal coherence of the LEDs is not expected to be problematic.

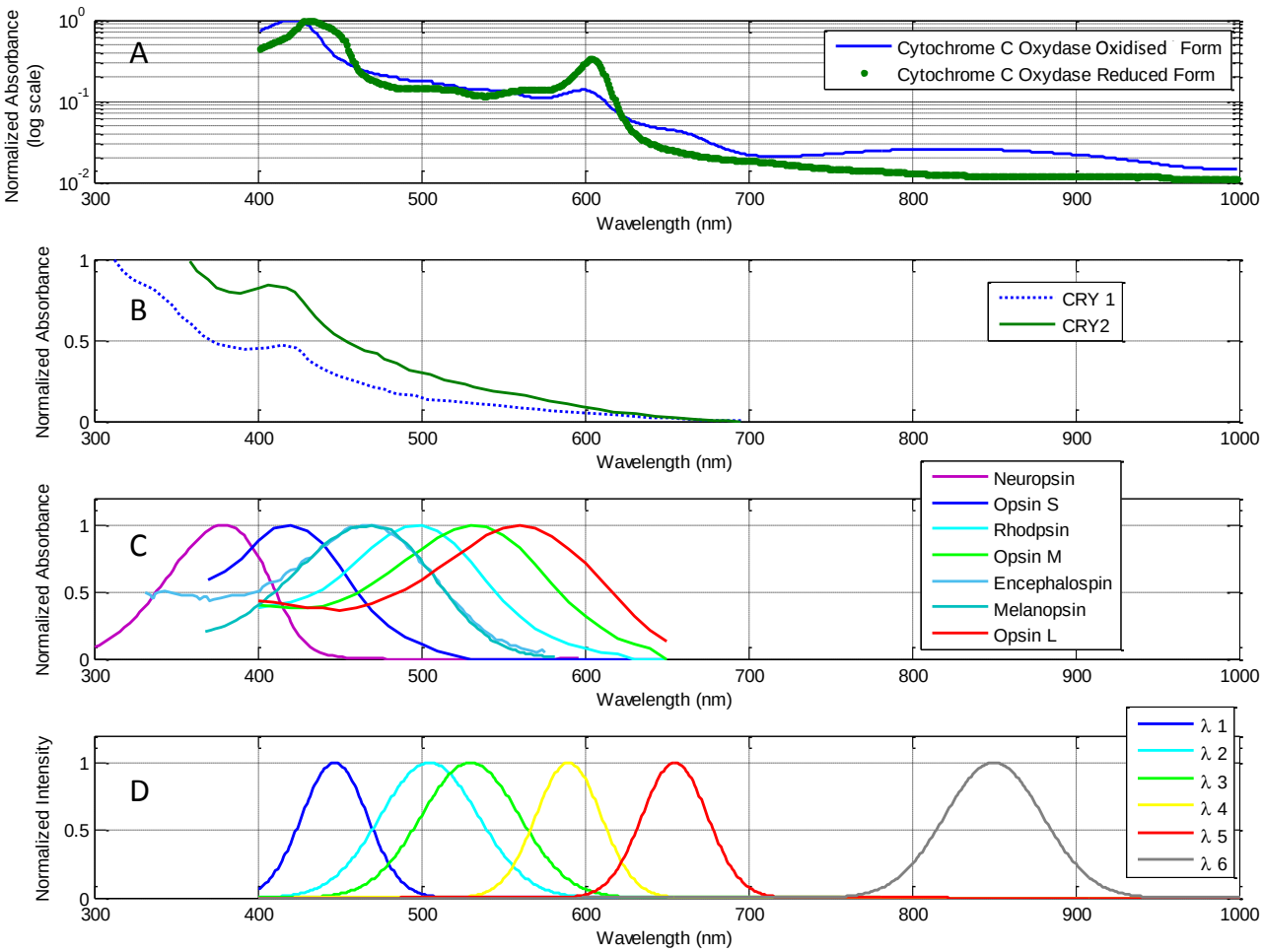

Figure 2.10: Absorption Spectra of relevant potential photoreceptors (panels A, B and C), and Emission Spectra of the LED contained in the prototypes (panel D)

Mechanical structure of the prototypes

The mechanical structure of the Sirius devices is designed for two functions, apart from its obvious container function: (a) implementing the desired illumination while blocking undesired exposures, and, (b) ensuring suitable cooling of the device itself and target. To that end, both devices exhibit a similar design: where the illumination is from under the target as seen in figure 2.11. Its design was inspired by Barolet et al. (Barolet et al., 2010), where researchers illuminated fibroblasts seeded in 24-well plate from the bottom. It provides several interesting features: multiple, polychromatic and physically-separated illuminations in a restricted space, while having a heating and cooling advantageous structure. It is a

pragmatic solution, where all the energy emitted by the source is directed to the target and not reflected nor absorbed by the support as that could result in unpredictable exposure and heating respectively. Indeed, illuminating the target from underneath and directed to the top of the instrument is a smart design to evacuate the remaining light which has already crossed the target. In that way, it is not reflected back to the target, nor absorbed by the support creating unnecessary heating.

Additionally, the internal design supports the directionality of the beam, meaning that light exiting the LED (over $2\pi str$) is restricted to an angle limit through a physical aperture and/or wall within the device itself. This prevents unwanted illumination of part of the target, as well as reducing the heating of the cell substratum. In the case of Sirius-8, small reflectors were added on top of the LED to focus the energy on the desired area.

Cooling of the devices, necessary for the LED and for the target, works by mechanical fans with directive flow, as shown in figure 2.11, C. This is key so as not to burn out the LEDs that inevitably heat up by the high electrical current (e.g. $1\ A$) going through them, and consequently heating up of the target closeby.

Sirius-24 used 6 different wavelengths in this project: 447, 501, 530, 591, 655 and 850 nm. These LEDs are grouped in two different physical boxes: 447, 501 and 530 nm representing the ”blue” light box and 591, 655 and 850 nm in the ”red” light box. These boxes are designed to fit under a 24-well culture plate, so that only one LED illuminates each of the well of a 24-well culture plate. The illuminated areas are organised as following: a 24-well culture plate has 4 rows of 6 wells, each of these rows is illuminated with a different wavelength (See figure 2.11 A). In the red box: two rows are illuminated with red LEDs (655 nm), while the remaining two rows are illuminated with yellow (590 nm) and infrared (850 nm) LEDs. On the blue box, two rows are illuminated with blue LEDs (450 nm) and the two remaining rows with green (530 nm) and cyan (500 nm) LEDs. The distance between the LED chip and the illuminated plane was $13\ mm$.

Sirius-8 uses 4 different wavelengths: 447, 530, 655 and 850 nm. Overall the light

box have 8 plastic windows corresponding to 8 optical outputs, 2 of each color, each with 9 LEDs as a source. Every LED (except Infrared LEDs) was covered by a small reflector allowing better collimation of the light (Reflector OPC1-2-COL from Dialight ”Wide” Model). The distance between the LED chip and the surface was $50\ mm$. The resulting beam created at $50\ mm$ by the LED array is homogeneous.

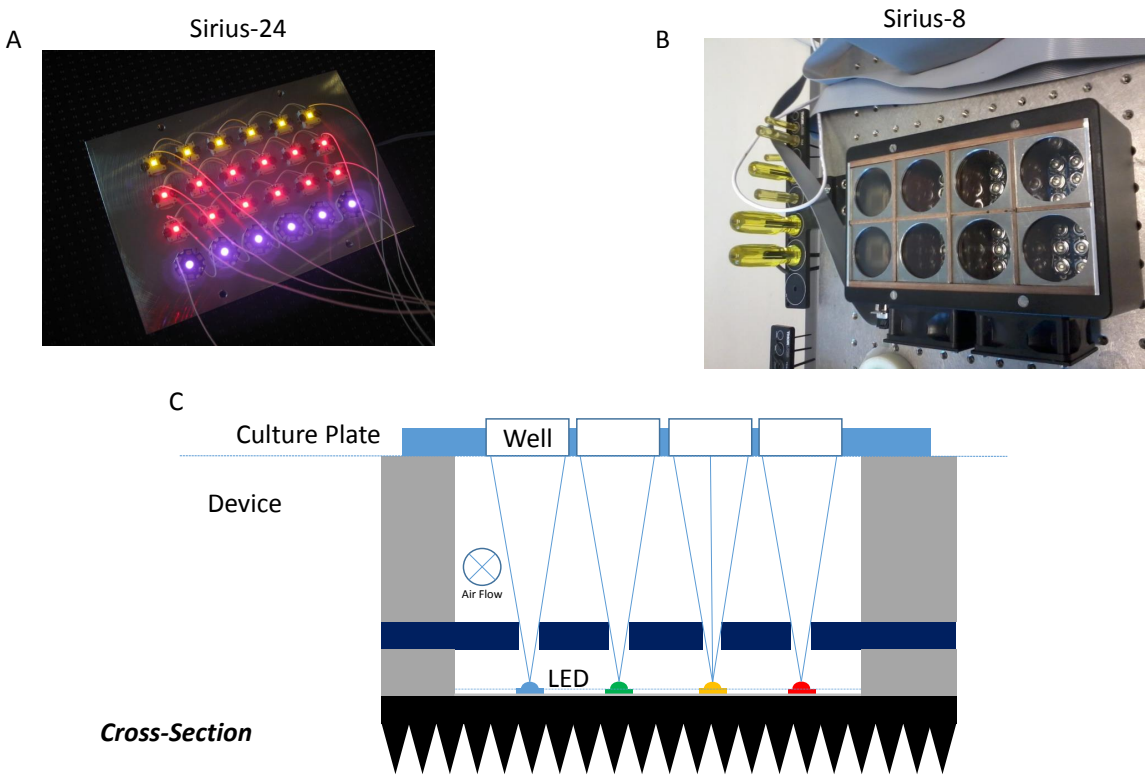

Figure 2.11: Device Principle: Illumination from the bottom of the well/dish; A: Photograph of the LED structure of Sirius-24 Box ’Red’ where the yellow, red and infrared (appears in purple) LEDs are visible; there are 24 LEDs in total, one under each well of a 24-well plate B: Photograph of the LED structure of Sirius-8 where 9 LEDs are positioned under each well and C: Cross-section diagram applicable to both devices

Over this thesis work, the maximum of the emission spectrum of the LED will be taken as the reference wavelength of the LED. As all physical light emitters, LEDs have a non-zero bandwidth (typically around 20 nm) and, by definition, they are thus not monochromatic. However, this will be omitted in the text and in the interpretation of the results, mainly for simplicity reasons. The effect observed will be attributed to the central wavelength of the LEDs. This represents a limitation in the notation only. The effect of the bandwidth of the light source is most probably not null, however the study of its impact is not included in the scope of this work. A second limitation of the mechanical design of the devices is the inter-wavelength contamination. Indeed, the Sirius devices have been designed to allow the irradiation of multiple cell culture dishes at the same time, side by side, with one single wavelength per target. The mechanical structure has therefore been designed to limit the light contamination of irradiation by a neighboring irradiation, potentially at a different wavelength. However, it is certain that a small amount of inter-wavelength contamination will occur due to always-existing reflections and misalignment. This amount was non measurable with a powermeter (Ophir Nova II, its sensor PD300-3W-V1, calibrated in October 2014), and therefore assumed to be small enough in front of the primary irradiation. The effect is thus assumed to be of low significance.

Beam homogeneity

LEDs have a high numerical aperture allowing homogeneous illumination of objects of larger sizes. The angular distribution of the intensity of the LED beam is not homogeneous over $2\pi sr$, and more energy is generally directed toward the front direction. It was therefore needed to select an homogeneous angular cone. The forward restricted cone of the emission beam of one LED (up to 30° off axis) is quasi-homogeneous and powerful enough to irradiate areas of several square centimetres (See Figure 2.12). This is enough to irradiate one single well of a 24-well plate using one single LED (i.e. design of Sirius-24). When the area to illuminate is larger, in the $35\ mm$ dish for example, it is possible to combine the beams of several LED to create a larger homogeneous area. If the target is placed

far away enough, the combined beam will provide a highly homogeneous illumination with a powerful beam. In the Sirius-8 design, 9 LEDs are combined under each well allowing a higher irradiance range, as can be seen in the description of the technical characteristics in section 2.5.4.

The homogeneity of Sirius-24 and Sirius-8 were both estimated to be within 10% (Fig. 2.12).

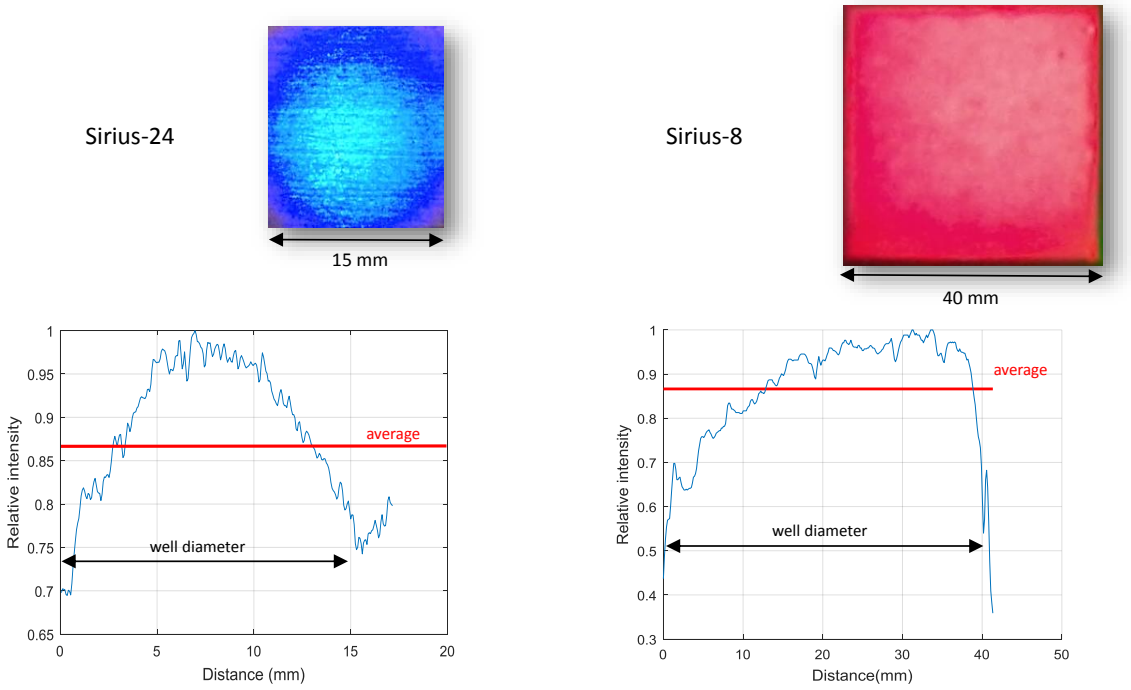

Figure 2.12: Typical profiles of one single light beam in the axial x-y direction (at 450 nm) in Sirius-24 and in Sirius-8 measured using a standard camera (shown for 450 nm in Sirius-24 and 655 nm in Sirius-8, all wavelengths behave similarly).

2.5.3 Assessment of the thermal increase in target when treating with visible light (FLIR Infrared Camera)

An important consideration of the design of any study in photobiology is the characterization of the light-associated thermal increase. Indeed, most objects absorbs light, including the cell culture plates and support. It is therefore necessary to verify that light is not influencing too much the thermal equilibrium of the cells' environment *in vitro*. Thermal measurements during light treatment on a black

24-well plate were made using the Sirius-24 device for light irradiation and a FLIR Infrared camera as a thermometer. Tests were performed outside the incubator. The optical settings tested were the same as the ones tested in the parameter screening experiments (Tab.2.7).

At the end of treatment, the images obtained from the FLIR camera revealed small differences in temperature between the control and treated wells (Fig. 2.13). Specifically, irradiation with all the wavelengths (except yellow, 590 nm) were associated with a slight increase of the temperature (up to 2 $^{\circ}C$) compared to control. However, the impact of blue, cyan, green, red and infrared wavelengths on the dermal fibroblasts metabolic activity was not similarly impacted, and even sometimes triggered an opposed response (See results, chapters 3 or 4). Indeed, short visible wavelengths have been shown to inhibit the metabolic activity of dermal fibroblasts while long visible and NIR wavelengths treatment results in neutral to stimulatory effects on dermal fibroblasts in similar dose range (Chapter 3).

Next, the temperature of the cells' environment never exceeded $37^{\circ}C$ and was always included in the skin temperature range (Olesen, 1982) which suggests that no significant effect would be expected to occur.

Additionally, this difference in temperature between treated and control wells is assumed to have an insignificant effect due to the limited time of treatment and the fact that immediately after treatment each well was replenished with fresh culture medium and the culture plate was put back in the incubator.

Finally, *in vivo*, it is important to note that the skin chromophores such as melanin and haemoglobin will be highly optically absorbing and will induce a strong heating effect in response to light treatment. Therefore, *in vivo* it will be impossible to separate the direct effect of light from an increased temperature. Chasing the strict equality of temperature between control and treated wells would thus appear as artificial.

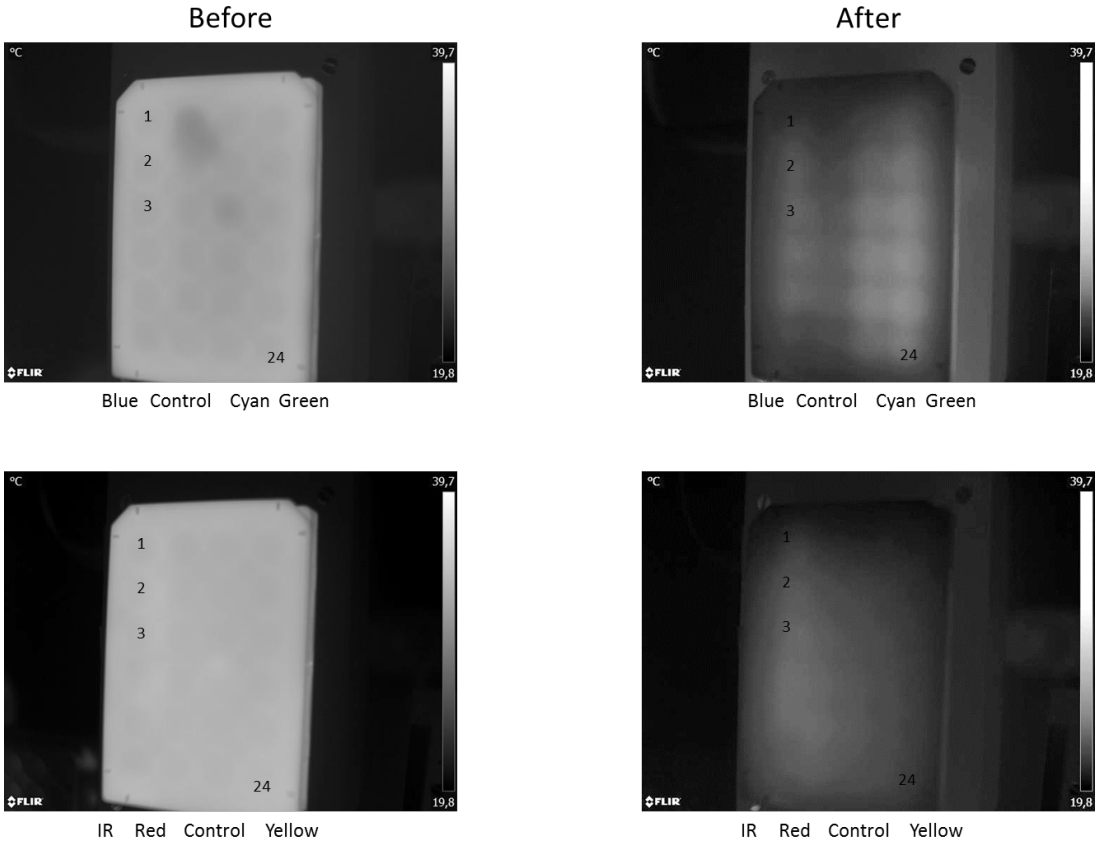

Figure 2.13: Temperature profiles before and after light treatment using the DoE light parameters (high irradiance and high radiant exposure). Top (blue 450 nm, cyan 500 nm and green 530 nm), bottom (yellow 590 nm, red 650 nm and IR 850nm). Maximum differences recorded after treatment were 1.5 and 2 $^{\circ}C$ for green and infrared treatments respectively. The culture plate was a black 24-well plate and was imaged from above. The focus of the camera was made on the lid of the culture plate. The localization of wells 1,2,3 and 2 were indicated in images for better understanding.

2.5.4 Technical specifications of the LEDs present in both prototypes: Sirius-24 & Sirius-8

All LEDs included in the prototypes are manufactured by Luxeon Lumileds Color Series except the infrared LED which is from OSRAM Oslon Black Series. Datasheets were available from the manufacturer and describe the spectral and power properties of the corresponding LEDs. Key specifications of the LEDs used in the devices Sirius-24 and Sirius-8 are extracted and shown in tables 2.3 and 2.4 re-

spectively.

Box	Color	Wavelength (nm)	Reference	Radiometric Flux (mW)	Radiometric Flux (lm)
”Blue”	Blue	447	LXML-PR01-0500	910	N.A.
	Cyan	505	LXML-PE01-0070	N.A.	122
	Green	530	LXML-PM01-0090	N.A.	150
”Red”	Yellow	591	LXML-PL01-0040	N.A.	77
	Deep Red	655	LXM3-PD01-0300	640	N.A.
	Infrared	850	OSLON Black Series	1070	N.A.

Table 2.3: Specifications of LED used in Sirius-24 (no reflectors are used in Sirius-24)

Box	Color	Wavelength (nm)	Reference	Radiometric Flux (mW)	Radiometric Flux (lm)
Sirius-8	Blue	447	LXML-PR02-1000	1030	N.A.
	Green	530	LXML-PM01-0100	N.A.	161
	Red	655	LXM3-PD01-0300	640	N.A.
	Infrared	850	OSLON Black Series	1070	N.A.

Table 2.4: Specifications of LED used in Sirius-8 (LED 447, 530 and 655 are used in combination of a reflector OPC1-2-COL on top reducing the FWHM of the angular distribution to 26 degrees.)

2.5.5 Software control of the light-based devices

The software was programmed under LabView, environment controlling the different electrical components via the PC.

The control allows the variation of the current going through the LEDs, as well as of the ’on’ and ’off’ times of the LED. Irradiance levels were measured at specific positions for both devices. The devices have working distances of $13\ mm$ and $50\ mm$ for Sirius-24 and Sirius-8 respectively. The irradiance was then measured at the heights corresponding to the working distances using a Powermeter Ophir Nova II with its sensor PD300-3W-V1 (recently calibrated, October 2014). They were measured at the maximum current under which these LED can be driven according to the datasheet i.e., $700\ mA$. These are thus the highest irradiances reachable on the device since getting closer to the LED is mechanically impossible (less than a working distance). Irradiances are summarized in tables 2.5 and 2.6.

Box	Wavelength (nm)	Measured Irradiance ($mW.cm^{-2}$) @ 13 mm
”Blue” Box	447	50
	505	40
	530	30
”Red” Box	591	10
	655	65
	850	80

Table 2.5: Sirius-24: Irradiances at $13\ mm$ distance from the LED chip, measured under the maximum (software) current of $700\ mA$ using Ophir Powermeter Nova II and sensor PD300-3W-V1 calibrated Oct-2014

Box	Wavelength (nm)	Measured Irradiance ($mW.cm^{-2}$) @ 50 mm
Sirius-8 Box	447	225
	530	73
	655	163
	850	125

Table 2.6: Sirius-8: Irradiances at $50\ mm$ distance from the LED chip, measured under the maximum (software) current of $700\ mA$ using Ophir Powermeter Nova II and sensor PD300-3W-V1 calibrated Oct-2014

2.6 Design of flexible monochromatic light-based illumination devices

In total four monochromatic prototypes were designed and built in order to perform experiments that required more flexibility than the restricted working formats offered by Sirius-24 and Sirius-8. The following wavelengths were selected: 450, 530, 655 and 850 nm. The light source component were LEDs mounted on Star PCB (Printed Circuit Board) as shown in figure 2.14. The components references were: LUXEON Rebel LEDs on SkinPAD-II at 450 nm, 530 nm, 655 nm (Luxeon StarLEDs) and OSLON IR 4 PowerStar LEDs at 850 nm (RS components). The visible Luxeon StarLEDs were completed with optics in order to make the beam more convergent (Khatod 30° 25 mm Circular Beam Optic - Integrated Legs). These devices were used for various experiments such as: irradiation of cell-free media and real-time light treatment on confocal microscope.

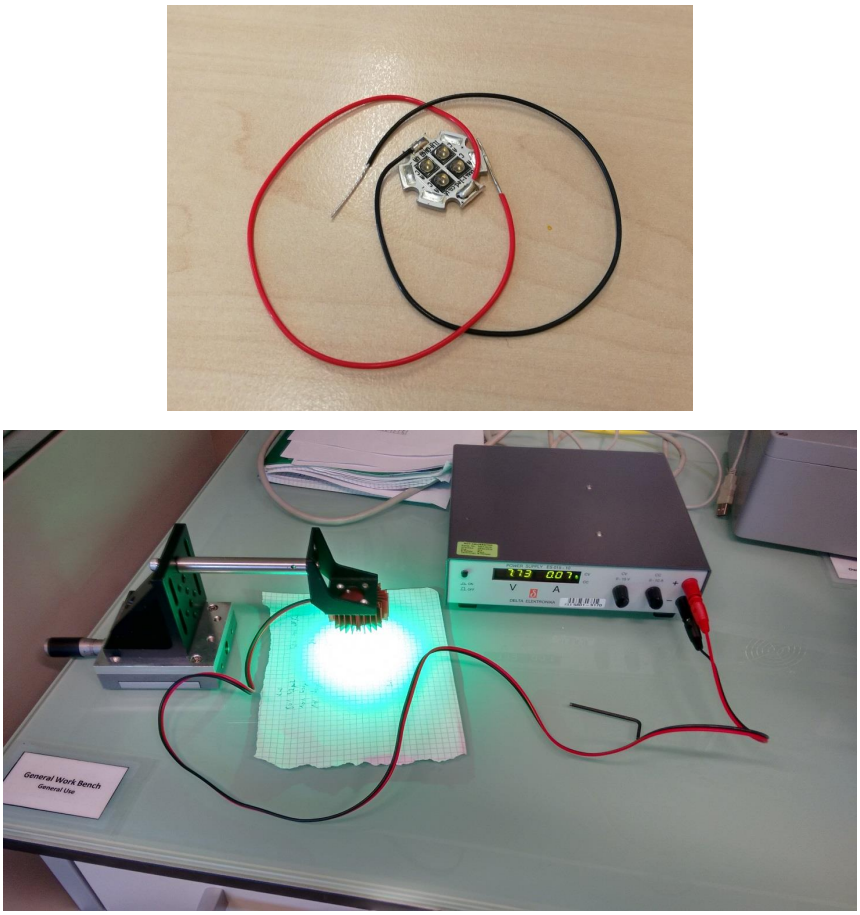

Figure 2.14: Photographs of the light source component: LEDs mounted on a Star PCB (above) and the complete setup including power supply, heat tank and mechanical support (below)

2.7 Experimental methods involving light treatment

2.7.1 Measurement of the optical absorbance of common cell culture media

When treating cultured cells with light, the absorption of the media in which the cells are cultured is of primary importance. Usually the medium of culture for primary fibroblasts is DMEM (Dulbecco's Modified Eagle Medium) with serum (commonly 10%). The specific composition of DMEM can be found online and includes: inorganic salts, amino acids, other components such as phenol red and some additives such as glucose. The full composition includes a few tens of components and some of them are known to have light absorbing properties: amino acids such as tryptophan can have strong UV absorbance (Edelhoch, 1967), flavoproteins such as riboflavin and all FAD- or FMN- containing molecules have strong UV properties, and large tails in the visible spectra till almost $550\ nm$ (Massey and Ganther, 1965). Serum also contains Vitamin A (at least three forms retinol, retinal and retinoic acid) which will also have absorption properties depending on which molecule it is coupled to (Dartnall, Bowmaker, and Mollon, 1983). All three are present in the culture medium as well as *in vivo* in skin (Lee, Lerner, and Halberg, 1953; Vahlquist et al., 1982).

The visible absorption spectra of DMEM was measured with and without phenol red (Fig. 2.15 A), as well as the fine UV/visible absorption spectra of DMEM (without phenol red) and serum (Fig. 2.15 B). DMEM appears to have no visible absorbing properties itself perhaps expected, since it looks highly transparent. However it is known that DMEM contains components such as riboflavin with known absorbing properties. Their quantity may just be too small and so cannot absorb enough light to be detected by the spectrophotometer. Serum exhibits an intrinsic yellowish color and this is reflected in the absorption spectra. Components in serum absorbs light at around $420\ nm$, attributed to haemoglobin present in serum (Lamola et al., 2013).

However, in general, no components of the medium appear to have strong absorb-

ing properties (apart from phenol red), which will significantly change the level of light reaching the cells or increase the temperature of the medium. Most of the species previously mentioned will absorb light but will not significantly reduce its intensity as their concentration in the culture medium are very small. Still, it is clear that components contained in the medium may be triggered by light through photo-chemical reactions. These components of the DMEM and serum will also be present *in vivo* as suggested by Liebel et al. (Liebel et al., 2012). Their study showed similar effects of UV and visible light regarding the induction of reactive oxygen species following irradiation *in vivo* (Liebel et al., 2012); and *in vitro* in the study by Sato et al. which showed UV photo-chemical reaction on riboflavin (Sato et al., 1995).

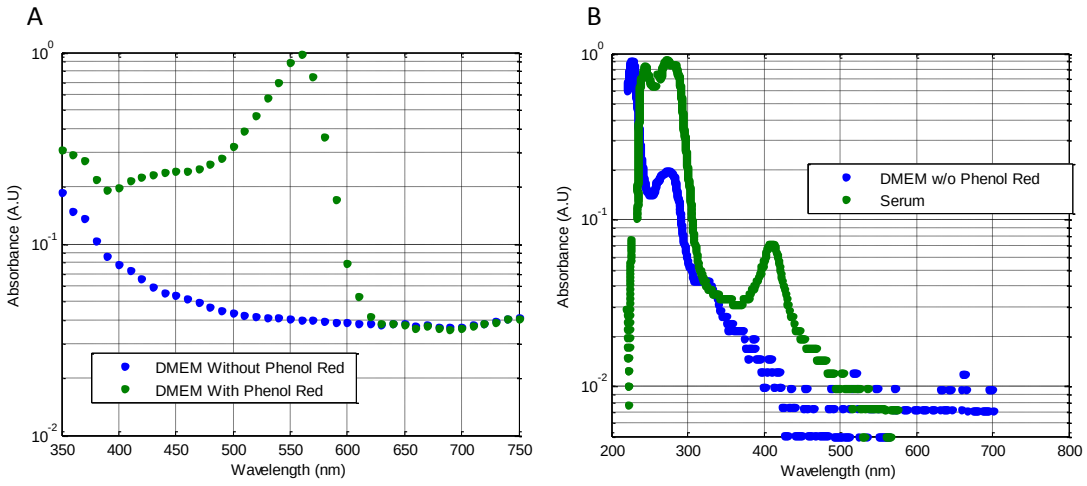

Figure 2.15: Absorption spectra of biological media, panel (A) DMEM with and w/o phenol red and panel (B) DMEM w/o pheneol red and serum (pure), measured with NanoDrop 1000 Spectrophotometer

2.7.2 Light treatment protocols

In order to separate direct and indirect effects of the light treatment on the cells, several protocols were used:

Treatment in PBS

To prevent any interaction between light and the culture medium, treatment was performed in PBS with $[Ca^{2+}, Mg^{2+}]$ during light treatment. After treatment the

PBS was removed and fresh medium was replenished. Two washes were performed during this procedure.

Treatment followed by replenishement of the culture media

In order to take into account the interaction of light and culture medium, cells were also irradiated in culture medium. Right after light treatment, the culture medium of each treated wells was replenished. This prevented prolonged contact of irradiated culture medium with the cells.

Treatment by ´irradiated cell-free media´

To assess any potential indirect impact of light on dermal fibroblasts via possible interactions with irradiated DMEM culture medium, a cell-free DMEM medium was similarly irradiated using the same wavelengths and doses of light and immediately brought in contact with the test cells. The time of cell 'exposure' to light-irradiated cell-free medium was equal to that of treatment when light was applied directly on the cells.

2.7.3 Live cell imaging setup with side irradiation

Confocal microscopy was used to image live cells during irradiation with visible and NIR light. The aim was to assess the direct light effect on cellular properties such as redox homeostasis. After the loading of the cell culture with a fluorescence dye, the dermal fibroblasts were imaged using a confocal microscope (Leica TCS SP5). In order to image the effect of the irradiation of the cells in real-time, a side light source was fixed in the close surroundings of the culture plate and pointed in the direction of the cells (See fig. 2.16). The irradiance of the light treatment reaching the cells was measured using a powermeter Ophir Nova II and sensor PD0130 inserted at the location of the culture dish. The irradiances were fixed at 30 $mW.cm^{-2}$ at 450 nm and 30 $mW.cm^{-2}$ at 850 nm. The wavelength of the irradiation and excitation/emission were carefully selected in order to avoid any color overlap.

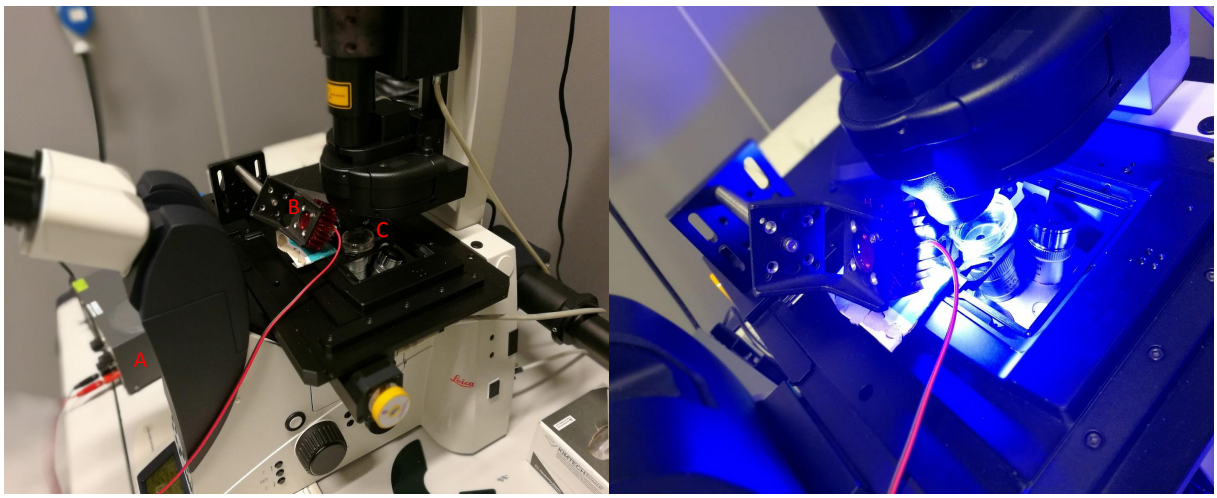

Figure 2.16: Photographs of the setup used to measure/image real-time response of *in vitro* cell culture to visible and NIR light. A: Power supply for the light source, B: LED light source and its heat tank mounted on a mechanical support, C: microscope stage and culture dish.

2.8 Design Of Experiment (DoE)

A statistical approach was used for a systematic assessment of the impact of optical and biological factors on the response of human dermal fibroblasts to light. It is based on a factorial design of experiment, allowing identification of the factors having a significant impact on the variation of a variable under investigation, i.e., Alamar Blue® reading for metabolic activity in case of this study. Such factors span a multidimensional space and are related to light treatment (i.e., optical variables) and the target and its environment (biological variables). Optical variables investigated in this project: wavelength (nm), irradiance ($mW.cm^{-2}$), radiant exposure or dose ($J.cm^{-2}$). Biological variables included: serum concentration (% FBS), confluency (cells per units of surface), oxygen level (%) and treatment protocols (with or without replenishment of media after treatment, treatment with irradiated cell-free media).

Each factor was then varied along pre-defined levels; in the present case this was 2, except for wavelength where 6 discrete wavelengths were used. The level intervals were chosen to be large enough to show impact, if present, on the variable of interest. The selected levels for optical parameters are given in the next section, while the levels of the biological factors are mentioned in the associated experimental results.

The pre-defined factors were then varied within the same experiment in a full factorial design mode. This allowed for a fair estimation of the effect of each factor independently, as well as any interaction between them. As a consequence, the number of experiments performed was equal to the number of levels to the power of the number of factors. This provided statistical power when assessing the effect of one factor on variation of the readout, as the variation of response due to each level was weighted by the same combinations of all the other factors and levels. The resulting variation is therefore most probably due to the variation of this single factor itself. Visually two data representations were adopted here, namely a) main effects plot and b) interaction plot. While the first shows the effects of each factor

separately, the second shows the interaction between the factors and how this impacts the variable of interest, e.g., metabolic activity. The statistical analysis was performed using ANOVA.

Our measurement method and setup were analyzed through a gage R&R approach. Operator, measuring instrument and method (plate reader, etc.), microplate type (black/white), illumination system and technical repeatability were all tested. The results of the ANOVA analysis directly determined the selection of optical treatment parameter and method to reduce the variability and reach an acceptable level of reproducibility and repeatability ([Editorial], 2016).

2.8.1 Selection of the light parameters to be tested on the dermal fibroblast subpopulations

In order to assess the influence of the optical factors on the responses of fibroblasts sub-populations, three optical factors were varied within 2 or 6 (in case of wavelength) levels. The following levels are shown in table 2.7. In this thesis, these will be often referred to as level 1 and 2 or level low and high (i.e. and not with the actual numerical value of the factor). While a DoE assesses a large number of very different combination of parameters, its advantage also relies on its ability to reveal the trends resulting from varying a factor.

2.8.2 Experimental details on the implementation of the DoE

The design of experiment approach was carefully followed to reveal the impact of optical treatment parameters on the dermal fibroblasts subpopulations. Typically, 24-well plates were used to assess the change in the metabolic activity of fibroblasts after light treatment. The cells were treated daily over 3 consecutive days, during which the culture medium was refreshed after each light treatment, unless stated. Light treatment was conducted outside the culture incubator but never extended beyond a maximum of 45 minutes at room temperature. Any increase in temperature of the cell substratum due to the light treatment was assessed using a FLIR infrared camera (SC600). Thermal increase never exceeded 37 $^{\circ}C$ (i.e.,

Wavelength (nm)	Irradiance ($mW.cm^{-2}$)	Rad. Exposure ($J.cm^{-2}$)	Exposure Time (s)
453	10	2	200
453	50	2	40
453	10	30	3000
453	50	30	600
500	10	2	200
500	40	2	50
500	10	30	3000
500	40	30	750
530	10	2	200
530	30	2	67
530	10	30	3000
530	30	30	1000
590	3	2	667
590	7	2	286
590	3	8	2667
590	7	8	1140
655	10	2	200
655	65	2	30
655	10	30	3000
655	65	30	460
850	10	2	200
850	80	2	25
850	10	30	3000
850	80	30	375

Table 2.7: List of the 24 Light Parameters Combinations used in a typical DoE

body and culture incubator temperature) for all tested wavelengths and at all treatment time intervals. In a typical experiment the same 24-well plate contained both control and treated groups, as one row of the 24-well plate was always kept as control, i.e. not irradiated. This helped to control for any effect due to the treatment being performed outside the incubator. Indeed, both control and treated groups were always under the same ambient conditions. Light treatment was performed using transparent DMEM medium without phenol red (Sigma, D5921). A typical protocol is shown as a scheme in figure 2.17.

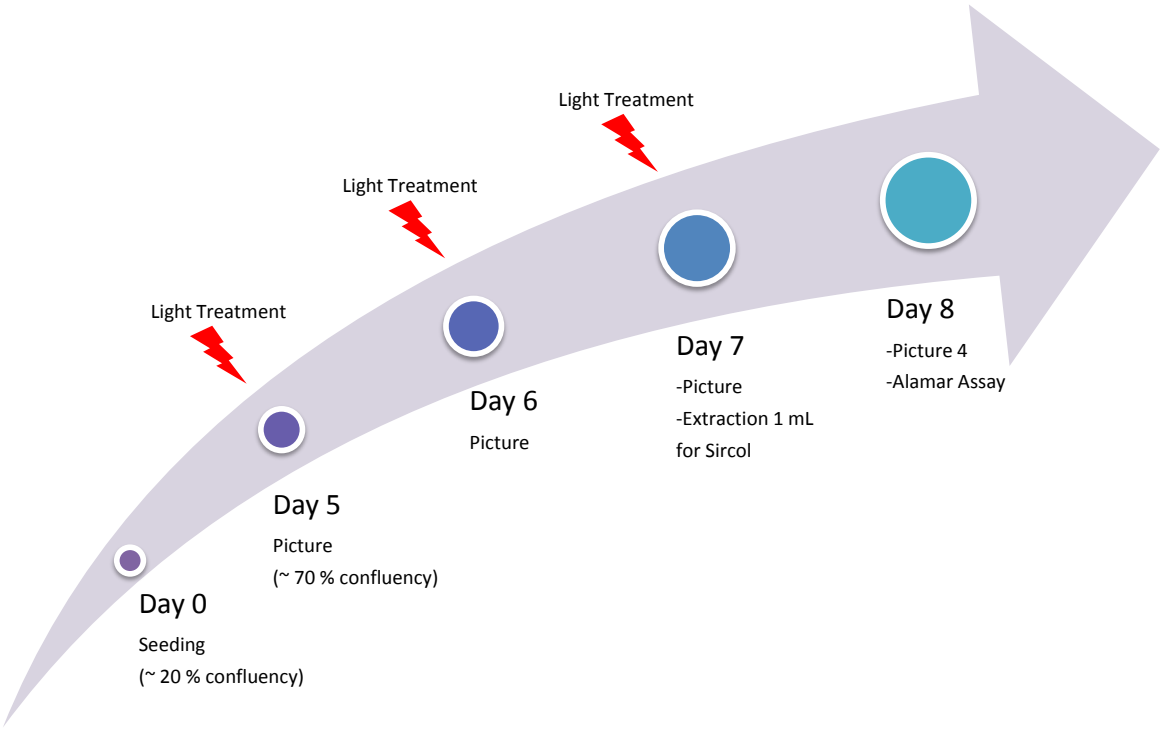

Figure 2.17: Protocol of a typical experiment following the design of experiment approach.

2.8.3 Optical and biological factors included in the design of experiment

The impact of several optical and biological factors have been systematically investigated over the course of this thesis. Their impact was generally studied in accordance with a design of experiment methodology. The included factors are listed in table 2.8.

Optical	Biological
wavelength, irradiance, radiant exposure	serum concentration, confluency, lineage, environmental oxygen concentration

Table 2.8: Optical and biological factors included in the study

2.9 Image processing and time-series analysis

The impact of visible and NIR light on dermal fibroblast behavior and morphology was observed in real-time using confocal fluorescence microscopy. Time-series images were recorded over short time (30 minutes at maximum). In order to analyze the time series data, a 2-step procedure was used. First, the images were processed to remove the background intensity, i.e. the fluorescence background intensity present in the images acquired on the confocal microscope. Second, the ImageJ plugin Time Series Analyzer (Balaji J, Dept. of Neurobiology, UCLA) was used to record the intensity of selected ROIs (cells) in the image over the time sequence.

2.9.1 Fluorescence background removal algorithm

A simple algorithm was built in order to remove the background of the images. For each image, the average intensity of 3 separated areas of the images (area of the image without objects) were recorded. The spatial locations and the average intensity of the selected background areas were used to interpolate a map of the background level. This map was simply subtracted to all the images of the time series. This was repeated for each image sequence which was analyzed.

2.9.2 Analysis of time series

The image sequences were analyzed over time using the Time Series Analyzer. For each image sequence 10 ROIs were selected from around 10 individual cells. Each ROI was drawn by hand, via the mouse, to surround the individual cell as illustrated on figure 2.18. Each ROI average intensity was automatically recorded for each time frame.

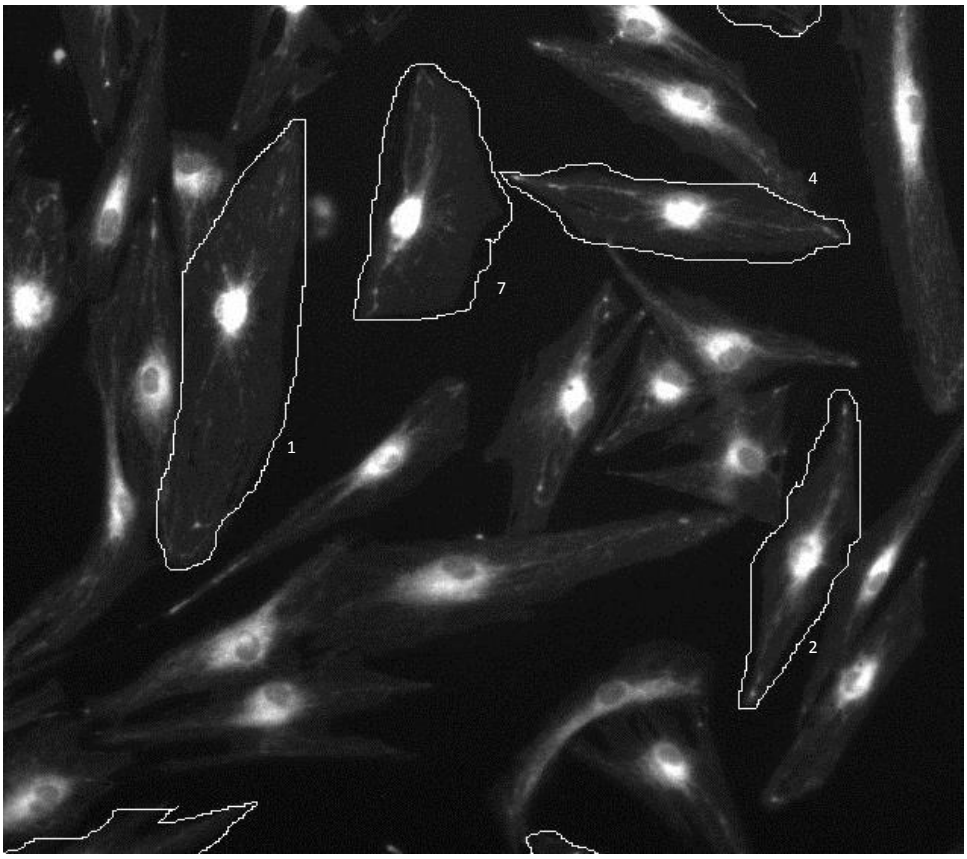

Figure 2.18: Selection of region of interest (ROI) in a typical fluorescence image via ImageJ. The ROI contours were drawn by hand.

2.10 Statistical Analysis

Statistical analysis was used throughout this project to compare populations. *Student t-test* and ANOVA analysis were the two main tests used (Seltman, 2015).

2.10.1 Significance difference between two statistical populations

A significant difference between two populations is reached when the mathematical means of each population is different and their distributions are statistically different. While the first criterion is trivial and just an application of the mean μ formula, the second one requires a test giving a binary response true or false depending on a limit. The result of the test will be true if the probability of false falls below the limit. Typically, in this thesis, the levels of significance are indicated with the results presented. When not specified the statistical significance levels will be taken as shown in table 2.9. Several tests exists to assess the difference between two independent Gaussian variables although, the *student t-test* is broadly used though and will be described in this section. A second statistical tool of interest is the ANOVA (Analysis of Variances) assessing the effect and interaction of a group of two or several variables on a readout. ANOVA analysis were routinely performed in this project.

Several generic formulae are included here:

The mean of a variable X:

$$\mu_X = \frac{1}{N} \sum_{n=1}^{N} X_n \tag{2.1}$$

The standard deviation of a variable X:

$$\sigma_X = \sqrt{\frac{1}{N-1} * \sum_{n=1}^{N} (X_n - \mu_X)^2} \tag{2.2}$$

2.10.2 Student t-test

The *student t-test* relies on the application of the formula shown in equation 2.3, it calculates the probability that two independent Gaussian variables X_1 and X_2

p-value upper limit	Significance	Star
0.05	Low	*
0.01	Medium	**
0.001	High	***

Table 2.9: Significance levels used when assessing the statistical differences between two populations

have the same mean. If the test is negative, and the two variables do not have the same mean, it computes from a table of values a p-value reflecting the 'chance' that this result is due chance i.e., randomness. In order to be confident that both variables have indeed a different mean and are significantly different, the p-value must be under limits of confidence as the one shown in table 2.9.

$$t = \frac{\mu_{X_1} - \mu_{X2}}{\sqrt{\frac{\sigma^2_{X_1}}{N_1} + \frac{\sigma^2_{X_2}}{N_2}}} \tag{2.3}$$

2.10.3 ANOVA

Analysis of variance allows a statistical comparison of 2 or more populations. In its basic form, this method returns a binary response of whether or not the different tested populations belong to the same statistical population.

Assumptions and Hypothesis

Analysis of variance relies on three assumptions:

- Normal Distribution of the statistical populations
- Homogeneity of their variances.
- Statistical independence of the errors.

The hypothesis tested is called the null hypothesis, meaning that all the tested groups have been randomly picked from the same statistical population. The rejection of the hull hypothesis leads to statistical differences between the groups.

Principle of the method

In this project, a one-way analysis of variance was performed. It considered one variable and evaluate the influence of several factors. The variable was the fibroblast metabolic activity M, and the factors were the wavelength W, irradiance I and radiant exposure R. The analysis evaluated the separate influence of each of the factors at the first order, i.e. linearly dependant on the value of the factor itself, and while will also look at the interactions between the factors at the second order, i.e. dependant on the combined variation of 2 factors.

2.11 Prediction of the optical transport in turbid medium: Monte Carlo Optical Model (MCOM)

2.11.1 General Description of the Monte Carlo method

A Monte Carlo method is a numerical evaluation of a quantity using random processes. It has numerous applications, and one of them is optical transport in a turbid medium. While an analytical solution of the light propagation in any medium could theoretically be obtained by solving the Radiative Transfer Equation, the complexity of biological tissue in non-flat layers and sub-layers makes it a very difficult problem to solve. Monte Carlo methods applied to optical propagation can be used to derive a numerical solution of the radiative transfer equation in complex media. The first use of Monte Carlo methods for optical transport can be attributed to Wang & Jacques (Wang, Jacques, and Zheng, 1995), where the method is fully described.

The process relies on two major light-matter interactions: absorption, where light energy is absorbed by component in the medium (typically melanin and haemoglobin in the skin) and scattering, where light bounces off a component and changes direction (typically collagen fibers and components in the dermis). A medium has at the same time absorbing and scattering properties, characterized by two coefficients absorption and scattering coefficients μ_a μ_s respectively. Two other optical properties are involved in a Monte Carlo transport simulation: the index of refraction and the anisotropy factor. The first describes how light propagates inside a medium, while the second is linked to its scattering property. Indeed the anisotropy factor, usually noted g, is a numerical value related to the 'way' the medium scatters. It takes values from 0, fully isotropic scattering where light is randomly scattered in all the possible directions, to 1, fully anisotropic situation where light is scattered in one direction. Skin has typically a value of 0.8, describing an almost straightforward propagation. A typical function to get the actual angular probability of a scattering event is the Henvey-Greenstein function, equa-

tion 2.4.

$$p(\theta) = \frac{1}{4\pi} \frac{1 - g^2}{(1 + g^2 - 2g\,\mathrm{cos}(\theta))^{\frac{3}{2}}} \tag{2.4}$$

This Greenstein function is not null for back-scattering angles, therefore it is worth mentioning that a photon packet can be back-scattered.

Using a mathematical modeling both interactions and a high number of iterations, it is possible to evaluate the photon density spatial distribution resulting of the illumination of a medium.

2.11.2 Input parameters of the model

The evaluation of the propagation of light photons in a turbid medium is highly dependent on the geometrical and optical properties of the medium. The skin itself is generally modeled in parallel layers including stratum corneum, viable epidermis, dermis and subcutaneous layer. Geometric parameters include the general physical size and thickness of the skin layers, while optical properties describe the variation of the absorption and scattering coefficients of each layer with respect to the wavelength applied.

Next, the wavelength and the beam geometry will strongly impact the spatial distribution. Indeed most of the optical properties of the medium depends on the wavelength, and the geometry will directly impact the propagation of photon as it defines the entry of the photons in the skin.

2.11.3 Output parameters of the model

The main output of Monte Carlo optical simulations is the amount of deposited photon energy in skin compartments versus spatial coordinates.

A grid has thus to be defined in order to register photon energy deposition versus spatial coordinates. It represents a 3D-cut of the virtual skin labeled (x, y, z) with a pre-chosen spatial resolution $(\delta_x, \delta_y, \delta_z)$.

A large number of virtual photons N typically 1×10^8, with energy W, will be launched throughout the virtual skin, and will propagate in incremental steps de-

fined by the scattering length, $L_{scattering}$ as defined in equation 2.5, giving the pace at which absorption and scattering events occur. While each time an absorption event occurs the photon will drop a part of its energy δW as shown in equation 2.6 depending on the absorption and scattering coefficient of the layer, it will also be bounced in another direction randomly chosen according to the angular distribution chosen. A photon will virtually lose weight throughout its trajectory until its remaining weight goes under the threshold limit, after which it will be terminated. At each coordinate where the photon stopped, it is possible to register at the same time the weight δW of photon energy dropped at this specific location (eg. the absorption A) and the remaining weight $W - \delta W$ (eg. the density T) of each photon. Combining the trajectories and weights of all the simulated photons will create a photon absorption and density maps. A global principle is shown in figure 2.19. The mathematical expressions of the quantities, absorption A and photon density T are shown in equations 2.7.

$$\langle L_{scattering} \rangle = \frac{1}{\mu_A + \mu_S} \tag{2.5}$$

$$\delta W = \frac{\mu_A}{\mu_A + \mu_S} * W \tag{2.6}$$

$$T_{grid,element_i}[x_i, y_i, z_i] = \sum\nolimits_{x-x_i<\delta_x, y-y_i<\delta_y, z-z_i<\delta_z} W_{photons}[x, y, z] \tag{2.7}$$

$$A_{grid,element_i}[x_i, y_i, z_i] = \sum\nolimits_{x-x_i<\delta_x, y-y_i<\delta_y, z-z_i<\delta_z} \delta W_{photons}[x, y, z] \tag{2.8}$$

2.11.4 Variability study: skin model

In this project, the impact of the variation of the optical properties of the skin layers on the prediction of the optical properties of the skin layers was studied. An in-house Monte Carlo optical model was thus used to calculate the map of photon density inside the skin. The input beam was selected as a collimated beam, homogeneous and square. The Monte Carlo model used was based on the algorithm published by Wang (Wang, Jacques, and Zheng, 1995). The geometry of the virtual skin was fixed as three infinite layers of defined thickness, and optical

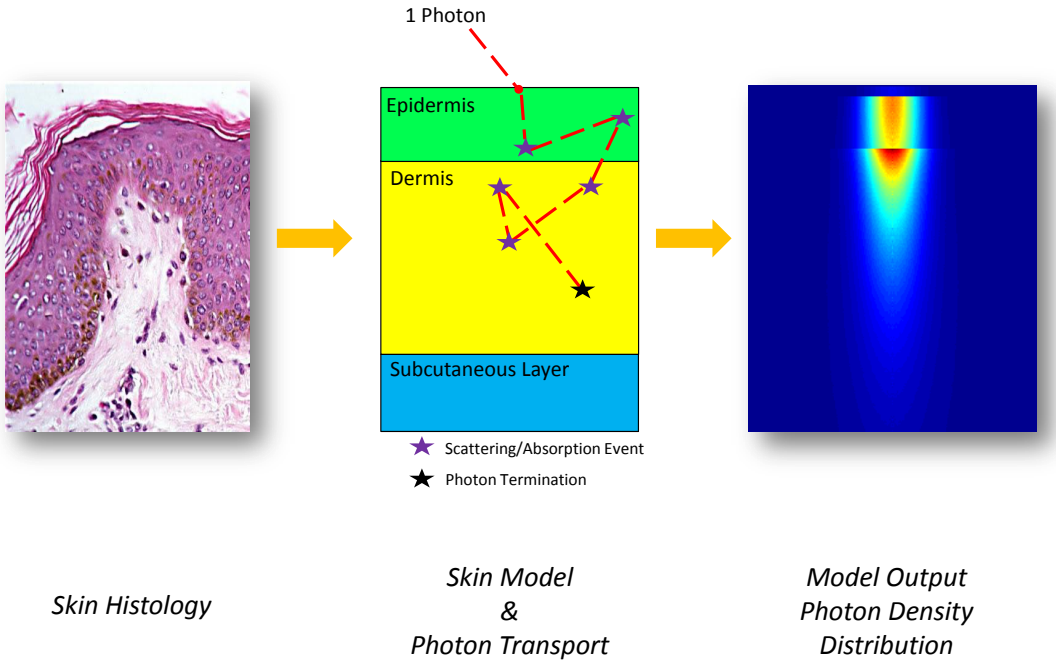

Figure 2.19: Principle of the Monte Carlo Model for Optical Transport in Skin

properties were assumed uniform within the layers and non-variant. The number of photon packets sent per simulation was 100×10^6, while the grid resolution was 20 μm in X and Y axes and 16.5 μm in the Z axis. The skin had an overall size of 2 by 2 cm^2 in surface and 3.5 cm in depth (Fig. 2.20). Thicknesses were taken in accordance to references; epidermis thickness was set to 100 μm (Gambichler et al., 2006); dermal thickness to 1.4 mm (Dykes, Marks, and Marks, 1977) and subcutaneous fat layer to 2 mm (Booth, Goddard, and Paton, 1966). The diameter of the input beam was 3000 μm.

2.11.5 Literature review of the optical properties of the skin layers

The quantitative values of the optical properties of the skin layers were extracted from the literature (epidermis, dermis, subcutaneous fat layer). The optical properties include the absorption and scattering coefficients (μ_A and μ_S), the anisotropy factor (g) and the refractive index (n). For simplicity the most common skin structure was adopted, that is to say a three-layer skin model (epidermis, dermis, sub-

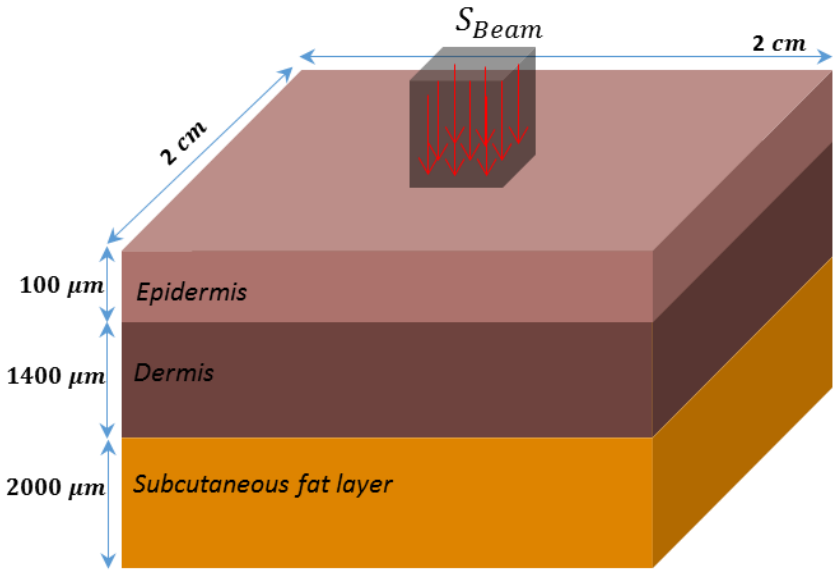

Figure 2.20: Geometry of the three-layer skin model

cutaneous fat layer). However, reports in the literature report the optical properties of the layers of a more complex skin structure including for example the separation of vascularized and non-vascularized dermis (Meglinski and Matcher, 2002; Altshuler, Smirnov, and Yaroslavsky, 2005). When the literature report did not evaluate a 3-layered skin model, the average of multi-skin component complexity was evaluated e.g., the average of the coefficients for vascularized and non-vascularized dermis was taken as the representative dermis coefficient.

When not available, the anisotropy factor of the subcutaneous fat layer was taken to 0.75 from Meglinski et al. (Meglinski and Matcher, 2002) in all references and assumed independent of wavelength, while the index of refraction of both layers epidermis and dermis was extracted from Ding et al. (Ding et al., 2006) and assumed non-variant; the refractive index of the subcutaneous fat layer was taken to 1.44 from Meglinski et al. (Meglinski and Matcher, 2002) and assumed independent of wavelength.

Chapter 3: Overview of optical treatment parameters, photoreceptors and mechanisms of action involved in photobiomodulation of human skin cells

The following literature review evaluates the last 30 years of photobiomodulation research to get a global picture of the theoretical knowledge that underpins the use of photobiomodulation for hair regrowth and wound healing, particularly around the optical settings used by the researchers. Here four key elements of current knowledge are discussed including; rationality of selected optical parameters; potential photoreceptors; downstream reactions; and the strategies used by industry to translate photobiomodulation science into effective commercial devices.

3.1 Inconsistencies in reported optical parameters applied during in vitro studies in the literature

Typically, optical parameters for light therapy such as wavelength, irradiance, and radiant exposure are obtained from *in vitro* and *ex vivo* studies. Translation to *in vivo* conditions is therefore needed before the implementation of associated devices in clinical settings. *In vitro* studies focusing on skin and hair health are most often performed on isolated cells including fibroblasts (Oplander et al., 2011), keratinocytes (Liebmann, Born, and Kolb-Bachofen, 2010), melanocytes (Bellono et

al., 2013), mesenchymal stem cells (Lipovsky et al., 2013), hair follicle dermal papilla cells (Sheen et al., 2015) and others (Guffey et al., 2014; Anders et al., 2010).

In the context of the heterogeneity of wavelengths of light reported in 60 studies here, one can see that the associated data span the entire Vis to near-IR range (see Fig. 3.1). There is some clustering around 420, 630, and 800 nm, with wavelengths close to 600 nm predominating. Moreover, variation of up to 2 orders of magnitude in irradiances (1 $mW.cm^{-2}$ to 100 $mW.cm^{-2}$) and radiant exposure (1 $J.cm^{-2}$ to 100 $J.cm^{-2}$) is reported in 30 *in vitro* studies that use primary or immortalized keratinocyte and dermal fibroblasts, where the 'working window' ranges from 1 $mW.cm^{-2}$ to 100 $mW.cm^{-2}$ for irradiance and from 1 $J.cm^{-2}$ to 100 $J.cm^{-2}$ for radiant exposure (see Fig. 3.2).

Other perplexing, if not abstruse, features of the current photobiomodulation

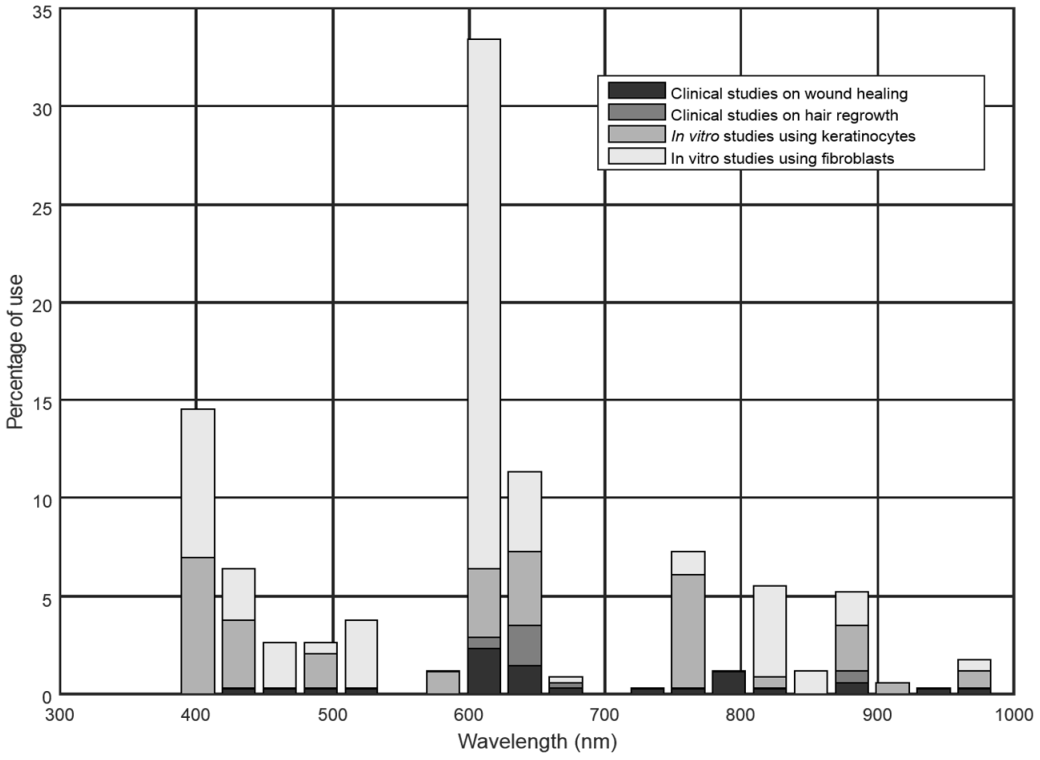

Figure 3.1: Histogram representation of the wavelength of the light sources used across the 60 clinical and in vitro studies on wound healing and hair regrowth included in this review. The percentage of use is calculated by counting the number of times that a particular wavelength was used within all the parameter combinations (wavelength, irradiance and exposure) reported for a particular observed effect available in the studies included in the analysis.

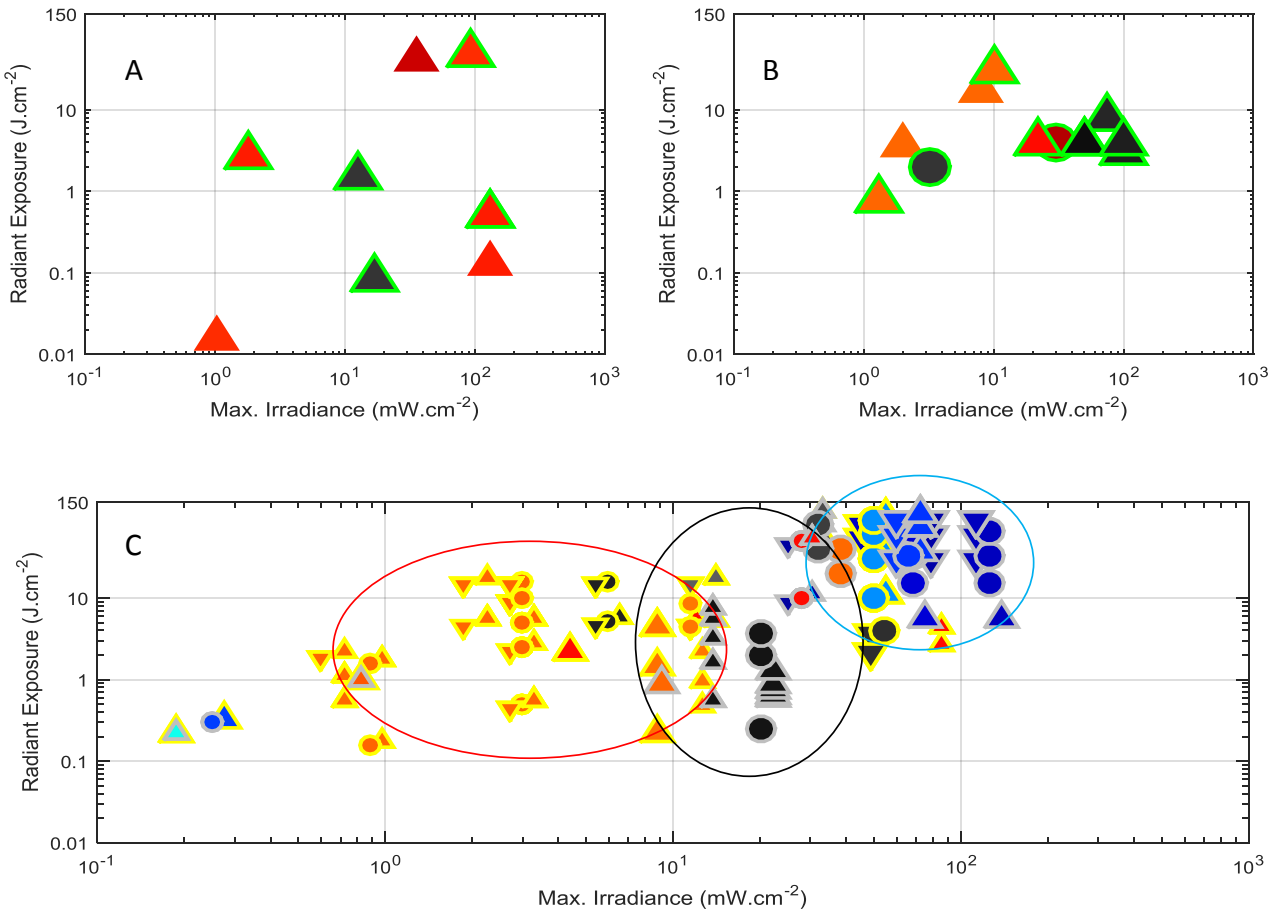

Figure 3.2: Scatter diagrams of the optical parameters and experimental outcomes of the clinical trials for hair regrowth (a), of the clinical trials for wound healing (b) of the *in vitro* studies on human dermal fibroblasts and epidermal keratinocytes (c). The filling color of the symbols indicates the wavelength range: blue – 400 nm, red – 600 nm, black – 1000 nm. The shape of the symbol represents the observed effect: stimulatory (up triangle), inhibitory (down triangle) or neutral (round). In (a) and (b) symbols outlined with green are studies where control group was present. In (c) the outline color of the symbols codes the cell type: yellow - fibroblast and grey – keratinocytes; the size of the triangle/dot indicate the cell line type: large – primary and small – cell line.

literature pertain to myriad biological effects associated with the applied optical parameters. For example, a single light parameter can be reported as effecting alternately stimulatory, inhibitory and neutral change for any given phenotypic readout (see Fig. 3.2). Some studies are associated with experimental designs that use very similar but non-identical parameters. For example, studies looking at the effects of blue light on human epidermal keratinocytes (Liebmann, Born, and Kolb-Bachofen, 2010; Kim et al., 2013a) have used similar but not identical wavelengths (i.e., 453 nm versus 410 nm) and still reported opposite effects on

the expression of the keratinocyte differentiation markers such as keratin-1 and -10. While this finding may suggest the existence of rather narrow wavelength 'windows', it also reflects the importance of defining the model target and culture conditions under study as they can impact the action of light. This point is clearly illustrated by the effect of light treatment of human melanocytes and mouse skin melanoma cells in the presence of retinal and riboflavin, respectively (Wicks et al., 2011; Ohara, Fujikura, and Fujiwara, 2003).

The effect of other light parameters such as pulsing (Barolet et al., 2010; Brondon, Stadler, and Lanzafame, 2009), coherence (Karu, 2003) and polarization (Ribeiro et al., 2004) have less commonly appeared in studies on photobiomodulation.

3.2 Diverse chromophores and photoreceptors mediating responses to light

The first point of a photon perception in the cell is unknown. There is a wide choice however, and one can readily list numerous chromophores and photoreceptors that could potentially mediate the physiological and ultimately, therapeutic effects of photobiomodulation. For example, relevant receptor molecules include photoactive pigments or chromophores like the flavins (Lewis and Escalante-Semerena, 2006; Ghisla, 1980), pterins (Johnson et al., 1988; Hsu et al., 1996), retinal (Brown and Wald, 1964; Merbs and Nathans, 1992), carotenoids (Sancar, 2000) and several metal-containing centres such as hemes and cupredoxins (Caughey et al., 1975; North, Rein, and Tappel, 1996). These photoactive pigments represent the photoreactive site of larger molecules called photoreceptors. An extensive, though inexhaustive, list of photoreceptors includes cytochrome c oxidase (Karu, 2014), cryptochromes 1 and 2 (Bouly et al., 2007), and opsin family proteins (I, II, III, IV, V) (Denda and Fuziwara, 2008; Haltaufderhyde et al., 2015; Kim et al., 2013a; Tsutsumi et al., 2009).

Current opinion in the photobiomodulation research community contends that light

is absorbed by mitochondrial cytochrome c oxidase around 420 nm, 600 nm and 850 nm (Moody, 2005; Mason, Nicholls, and Cooper, 2014; Wharton and Tzagoloff, 1964). Photons interacting with this enzyme's metal centres are thought to trigger the increase of ATP via the generation of a proton gradient. The process involves the release of nitric oxide NO either via photodissociation from the complex cytochrome c oxidase or via the catalysis of the reduction of nitrite to NO. The balance results in direct production of ATP and NO as well as ROS as by-product of the respiration metabolism. All are assumed to be responsible for the observed biological and therapeutic effects of light (Chung et al., 2012). This view is principally based on the work of Karu (Karu, 2014) and is widely though not universally accepted (Lanzafame et al., 2013; Jimenez et al., 2014; Karu, 2014; Khan, Tang, and Arany, 2015; Blum et al., 2014). This is perhaps because we still do not fully understand the structure, optical properties, and function of this enzyme nor of its intermediate products formed during electron transport (Wong-Riley et al., 2005; Karu and Kolyakov, 2005).

The human cryptochromes (Bouly et al., 2007), reported to be involved in circadian rhythm entrainment (Vieira et al., 2012; Hoang et al., 2008), contain two key photoactive pigments, pterin and flavin, which define their absorption spectrum in the UV-blue spectral range (Rajagopalan and Handler, 1964; Cashmore et al., 1999) with two prominent bands around 350 nm and 420 nm. Their analogues in plants have a clear light-sensitive function (Cashmore et al., 1999). As gene transcription regulators, cryptochromes could potentially be very interesting targets in photobiomodulation. Indeed, they have been found to be one of the main circadian clock effectors in mammals (Cashmore et al., 1999; Nakao, 2014) and to participate in the regulation of metabolism and immune responses (Narasimamurthy et al., 2012; Hashiramoto et al., 2010). It is currently hypothesized that light interaction with flavin in cryptochrome leads to its conformational change, permitting transcription factors to bind to the C-terminus. Also, redox reaction of flavins and therefore cryptochromes can be accompanied by ROS generation and signalling, indicating the cryptochromes may participate also in ROS signalling (Consentino

et al., 2015; Arthaut et al., 2017).

More recently, the opsin-family of G-protein coupled receptors, well-known as photoreceptors responsible for light sensing by retinal cones and rods (Dartnall, Bowmaker, and Mollon, 1983), have come to the attention of photobiomodulation researchers. They includes OPN 1 (Short, Middle and Long wavelengths) in cones, OPN 2 (or Rhodopsin) (Stenkamp, Teller, and Palczewski, 2002) in rods, as well as non-visual opsins, such as OPN 3 or encephalopsin (Koyanagi et al., 2013), OPN 4 or melanopsin (Melyan et al., 2005; Matsuyama et al., 2012; Panda et al., 2005) and OPN 5 or neuropsin (Kojima et al., 2011). Peaks of OPN1 to OPN 5 absorption spectra span 380 nm to 570 nm (Dartnall, Bowmaker, and Mollon, 1983; Koyanagi et al., 2013; Matsuyama et al., 2012; Kojima et al., 2011). Recently, expression of these selected opsin receptors was demonstrated in non-visual tissues, such as mouse aorta (Sikka et al., 2014) and even in the human skin (Tsutsumi et al., 2009), melanocytes and keratinocytes (Haltaufderhyde et al., 2015; Kim et al., 2013a; Bellono et al., 2013; Tsutsumi et al., 2009), and human hair follicle (Buscone et al., 2017) making this family an intriguing target for photobiomodulation for skin and hair. More specifically, they were shown to have functional effects, Oancea et al. showed that human epidermal melanocytes were expressing rhodopsin, and that this last was regulating melanin production under UVA radiation (315 to 400 nm) (Haltaufderhyde et al., 2015; Bellono et al., 2013), Berkowitz et al. demonstrated that the vaso-relaxation of *ex vivo* mouse artery is regulated via blue light interaction with OPN 4 (Sikka et al., 2014), Kim et al. revealed that specific human epidermal keratinocytes differentiation markers were down-regulated by violet light (410 nm) irradiation via rhodopsin mediated pathways (Kim et al., 2013b), and, Buscone et al. showed that blue light (453 nm) exerted a positive effect on hair growth *ex vivo*.

3.2.1 Absorption spectra of photoreceptors relevant for skin photobiomodulation

The presence of peaks and position of maxima in absorption spectra of both chromophores and the chromophore-protein complex depend on many variables. As an instructive example Brooks et al. (Brooks, Sucheta, and Einarsdóttir, 1997) showed the evolution of the cytochrome c oxidase spectrum as a function of pH as an instructive example. Environmental factors include the influence of surronding molecules, pH, solvent, and more. Yet, typically, there are one or more absorption bands that will be specific for each of the chromophores and photoreceptors.

The absorption spectra of the afore-mentioned photoreceptors can be found in the literature. Cytochrome c oxidase absorption spectra in both fully-reduced and fully oxidised forms are available online from the Biomedical Optics Department of the University of Central London(Moody, 2005). Classical opsin-like photoreceptor spectra were obtained from spectroscopy measurements of human eye proteins by Dartnall et al. (Dartnall, Bowmaker, and Mollon, 1983); while spectra of novel opsin-like proteins were taken from Koyanagi et al. (Koyanagi et al., 2013), Matsuyama et al. (Matsuyama et al., 2012) and Kojima et al. (Kojima et al., 2011) for OPN3, OPN4 and OPN5 respectively. Finally, human cryptochromes spectra were published in 1996 by Hsu et al. (Hsu et al., 1996).

Limiting ourselves at the visible and near-IR parts of the radiation spectrum, it was possible to note maximum absorption peaks that could be characteristic of different photoreceptors. It must be said here that most of the latter have broad spectra, strong absorption in the UV range and strong environmental dependence.

Cytochrome c oxidase absorption extends over the whole visible, UV and near-IR spectrum. Its absorption decreases at the first order with wavelength from UV to IR. Some local peaks, in the visible/near-IR parts, can be found around $420\ nm$, $600\ nm$ and $850\ nm$.

Cryptochromes appear to have strong absorption in UV. Although they also absorb visible light up to around $700\ nm$ in an almost a linear way, inversely proportional

to the wavelength. One local peak in the far blue region can be found for both form CRY1 and CRY2, at around $420\ nm$.

Opsins spectra are mostly bell-shaped curves allowing a net determination of a peak and a computation of a FWHM (full-width at half maximum) giving information on the spectral extension of the absorption. Peaks are observable around $420\ nm$, $530\ nm$, $570\ nm$, $500\ nm$, $480\ nm$, $470\ nm$ and $380\ nm$ for OPN1 (S, M and L), OPN2, OPN3, OPN4, OPN5 respectively. Typical FWHM average around $100\ nm$. A summary is showed below in table 3.1.

Table 3.1: Absorption Peaks of photoreceptors relevant for photobiomodulation in the visible and near-IR spectrum (Dartnall, Bowmaker, and Mollon, 1983; Koyanagi et al., 2013; Matsuyama et al., 2012; Kojima et al., 2011; Hsu et al., 1996) and online data from the Biomedical Optics Department of the University of Central London.

Photoreceptor	Abs. Peak Position (nm)	Area,FWHM (nm)
Cyt. Ox.	420, 600, 850	[400 1000]
CRY1	420	[400 700]
OPN1S	420	100
OPN1M	530	120
OPN1L	570	130
OPN2	500	110
OPN3	480	115
OPN4	470	105
OPN5	380	70

3.3 Multiple downstream biomolecular reactions explaining physiological effects

In addition to understanding the role of existing versatile potential photoreceptors present in human skin, the next challenge of the growing field of photobiomodulation is to unravel the exact molecular reaction cascades that mediate the physiological effects of light.

Given the considerable existing complexity, one has to start somewhere. For example, the absorption of red light by cytochrome c oxidase is traditionally accepted to trigger numerous reaction cascades that alter cellular homeostasis (e.g., fluxes in pH, [Ca], cAMP, ATP, NO) (Karu, 2014). Blue light is often reported to photolytically generate NO and ROS from nitrosated proteins and NADPH oxidase, respectively. These can then modulate cell metabolic activity, vasodilatation and improve wound healing (Liebmann, Born, and Kolb-Bachofen, 2010; Opländer et al., 2013). IR light has been shown to activate epidermal keratinocytes *in vitro* (Basso et al., 2013; Grossman et al., 1998) and to induce ROS production in mouse skin (Khan, Tang, and Arany, 2015).

In addition to these more 'traditional' downstream cascades, that follow the interaction of photons with chromophores or photoreceptors and leading to physiologically-relevant effects, new intriguing insights are emerging in the literature. Interestingly, red light has been reported to induce rhodopsin-mediated, phosphodiesterase-dependent recovery of skin barrier function (Denda and Fuziwara, 2008; Goto et al., 2011). In contrast, violet light of 410 nm suppresses human epidermal keratinocyte differentiation by the activation of rhodopsin, probably involving specific signalling pathways via G_{α_i} (Kim et al., 2013a). Expression of rhodopsin was also detected in human epidermal melanocytes, where it can be activated by violet-blue, 315 to 400 nm light. This leads to the activation of a transduction pathway involving G_{aq}-protein and TRPA1 eventually leading to intracellular calcium influxes and melanogenesis (Haltaufderhyde et al., 2015; Bellono et al., 2013).

The diversity of molecular reactions potentially stimulated by light, and the paucity of information about the specific pathways underpinning the observed phenotypic change(s) makes it difficult to rationally choose appropriate readouts for assessment of light effects. Currently, multiple cellular readouts have been evaluated where the impact is typically assessed via cell viability (Hawkins and Abrahamse, 2006; Poon, Huang, and Burd, 2005; Esmaeelinejad et al., 2014; Evans and Abrahamse, 2008), proliferation (Oplander et al., 2011; Grossman et al., 1998; Hawkins and Abrahamse, 2006; Poon, Huang, and Burd, 2005; Evans and Abra-

hamse, 2008; Webb, Dyson, and Lewis, 1998; Zhang et al., 2003; Houreld et al., 2008; Rigau et al., 1994; Webb and Dyson, 2003; Pellicioli et al., 2014; Azevedo et al., 2006), differentiation (Liebmann, Born, and Kolb-Bachofen, 2010; Kim et al., 2013a; Taflinski et al., 2014), morphology (Esmaeelinejad et al., 2014; Evans and Abrahamse, 2008; Rigau et al., 1994), and apoptosis (Liebmann, Born, and Kolb-Bachofen, 2010; Houreld et al., 2008). However, more specific methods are now needed to elucidate the stimulated pathways, including the assessment of changes in expression of specific genes expression in particular skin cell subpopulations for selected application (Zhang et al., 2003; McDaniel et al., 2010; Becker et al., 2015).

3.4 Pitfalls of translational research

Despite significant difficulties in interpreting the available published data derived from laboratory-based studies, there appears to be no doubt that photobiomodulation is indeed a real phenomenon, and one that has already begun to be translated for the management of a variety of dermatological conditions. Examples of associated claims range from healthier and thicker hair or improved hair counts 3 to 6 months after light treatment (red light, 650 nm) in cases of male and female age-associated hair loss (Lanzafame et al., 2013; Lanzafame et al., 2014; Leavitt et al., 2009), to acceleration of healing due to improved contraction after treatment of abrasions with red and infrared light (broadband, 600 to 1000 nm) (Hopkins et al., 2004) and improvement of psoriasis in two clinical trials (Weinstabl et al., 2011; Pfaff et al., 2015) where blue light (450 nm) reduced the severity of psoriasis vulgaris via downregulation of keratinocyte proliferation.

One of the aspirations of this project, during this detailed examination of the associated literature, was to see how to achieve greater consistency in optical parameters for *in vivo* studies. Indeed, the ‘optical window’ as reported for hair regrowth and wound healing appears slightly narrower than for other applications (Fig. 3.2, A and B), although in many cases reported irradiance and radiant exposure levels

vary by as much as 2 orders of magnitude.

A key question here is how (and if) high levels of inter- and intra-study variability in the devices', optical performance affect their reported therapeutic efficacy. To tackle this, the examination of photobiomodulation in hair growth is relevant, as the hair follicle is an excellent model to interrogate how light may influence complex biological tissues in health and disease. Also there are now at least twenty FDA-cleared (i.e., for safety, rather than efficacy) light-based devices for the treatment of androgenic alopecia in male and female, where reported efficacy was similar to that of existing drugs for hair regrowth (e.g., minoxidil and finasteride) (Mysore, 2012). Long-term data is required however, before definitive comparisons can be made between these light-based therapies for hair regrowth and current approved drug treatments. Here the focus was placed on three of the better known devices, a comb (device A), and two helmets, (devices B and C), which all use red light, albeit with somewhat different wavelengths: 660 nm (device A), 670 nm (device B) and 650 nm (device C) and emit beams of 5mW power in a continuous wave mode (with exception of device C, which has has extra pulsing LEDs).

However, the devices differ significantly in the number of beams per device (comb A emits 9 beams, helmet B emits 80, and helmet C emits 51 beams) and application duration to cover the area of treatment (helmets B and C directly treat a significant area of the scalp, while the comb (A) must be moved each 4 seconds to cover the same area as the helmets). As such, treatment time per spot is longer for the devices B and C (see Table 3.2).

Furthermore, the devices differ in their beam size and profile at the skin surface (Fig. 3.3 a-to c). Thus, having equal emitted optical power, the corresponding maxima of irradiances are 130, 35 and 2 mW/cm^{-2} and maxima of radiant exposures at the skin surface, 0.5, 42, and 2.7 J/cm^{-2} for devices A, B, and C, respectively.

Calculated photon densities inside the skin at the assumed level of the terminal scalp anagen hair bulbs (e.g., around 3-4 mm) for devices A and C differ by 10-fold (see Fig. 3.3 d-f, where Monte Carlo methods of light propagation in tissue were

Device	A	B	C
Name	HairMax	Theradome	iGrow
Wavelength (nm)	655	678	655
Power per source (mW)	5	5	5
Exposure (s)	4	1200	1500
Dose (J)	0.02	6	7.5
Treatment frequency (per week)	3	2	3
Efficacy	+20 terminal hairs per cm^{-2} after 6 months	Thicker and healthier hair after 4 to 6 months	35% increase in hair growth in 4 months
FDA clearance	Androgenetic alopecia in both adult males and females (2014)	Androgenic Alopecia in adult females (2013)	Androgenetic alopecia in both adult males and females (2013)

Table 3.2: Specification of devices as given on manufacturer website and in publications and in clinical trial publications.

used). Given the reported exposure times per treatment session, these devices will therefore have as much as 40-fold variability in radiant exposure at the level of the target.

These are very significant differences in irradiances and radiant exposures (per treatment session and per total treatment period). From this perspective it is rather astounding and perplexing that these devices offer comparable clinical hair growth-stimulating efficacy. In particular, for devices A and C the results of published clinical trials report a maximal increase of around 20 hairs per unit area (cm^{-2}) compared to a sham-control group in male and female cohorts (Lanzafame et al., 2013; Lanzafame et al., 2014; Jimenez et al., 2014) (see Table 3.2). Moreover, at least a report exists stating that there was no statistically-significant difference between the treated and untreated sides when using a device A (Rushton, Gilkes, and Van Neste, 2012). This uncanny inter-device reported similarity suggest that they may be stimulating entry of kenogen hair follicles into anagen rather than having any effect on reversing miniaturised hair follicles per se (Hugh Rushton, Norris, and Van Neste, 2016; Chu, Santos, and McElwee, 2015). One perhaps could be excused for concluding, at least for applications of photobiomodulation in hair growth studies, that there is a pitiful lack of rationality for the choice

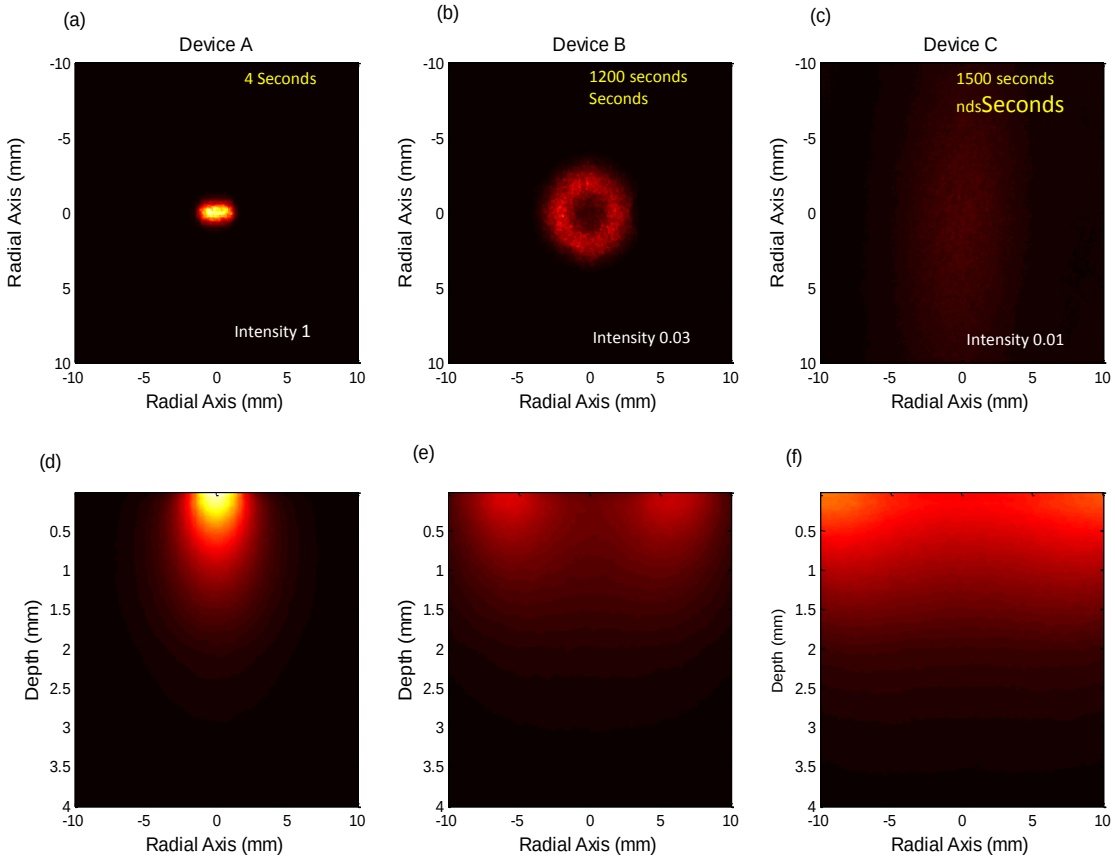

Figure 3.3: Beam profile and irradiance at the skin surface based on the measured optical output and beam profile (from a to c) and irradiance inside the skin as estimated using Monte Carlo method of light propagation in turbid medium (from d to f) for three commercial FDA-approved light-based devices for hair regrowth, noted as Device A, Device B and Device C, respectively. The recommended treatment durations and the relative maximum intensity are also shown in the upper right and the lower left corner, respectively. The relative maximum intensity was obtained by normalizing the photon density of each of the device on that of the Device A.

of selected treatment optical parameters.

3.5 Concluding remarks and recommendations

Here I have surveyed the last 30 years of published literature pertaining to skin photobiomodulation, and have focused on some of the unresolved complexity that retards rational development of this field. First, optical parameters remain poorly characterized and ill-defined. The range in wavelengths, irradiance and radiant exposures used for stimulating skin cells remain very wide and indeed I struggled

Device	Name	Wavelength (nm)	Maximum irradiance ($mW.cm^{-2}$)	Exposure (s)	Maximum Dose ($J.cm^{-2}$)
A	HairMax	660	130	4	0.52
B	Theradome	670	35	1200	42
C	iGrow	650	2	1500	2.7

Table 3.3: Measured beam profiles and powers.

to find evidence of any reported rational path for choosing light parameters for skin and hair follicle photobiomodulation, i.e. studies that could convincingly show the effect of particular optical parameters in any systematic way.

Second, skin cells express several potential photoreceptors covering the entire visible and infrared parts of the spectrum. The fact that most are reported to be involved in a particular photobiomodulation process, suggests that light, even at a particular wavelength, may trigger several photoreceptors simultaneously. This highlights the need for much greater sophistication in our research approach, in order to examine the presence and action spectrum of different photoreceptors as well as their physiological significance for specific applications.

Third, the mechanisms of action of light 'treatments' are currently very poorly understood. Few if any of the assumptions made on their behalf have been proven. Two potential mechanisms, however, are widely investigated. Red and NIR light, absorbed by cytochrome c oxidase, may trigger reaction cascades that alter cellular homeostasis (e.g., via changes to pH, [Ca^{+2}], cAMP, ATP). Blue light photolytically generates NO and ROS from nitrosated proteins and NADPH oxidase, respectively. These effectors can initiate physiological effects in cells (e.g., effects like proliferation, vasodilatation or wound healing). While neither of the mechanisms are accepted as being part of the photobiomodulation processes, they do not provide a convincing explanation for all the physiological effects observed. Thus, there remains a pressing need to identify the potential molecular mediators of these processes, and look for their mode of action.

While our understanding of photobiomodulation still has numerous gaps, its translation to commercial and therapeutic solutions continues apace against this backdrop of suboptimal characterization. This indicates premature translation with

consequent suboptimal efficacy. Further translation should ideally follow a more rational route, both by identifying the key targets of light, *in vitro* or *in vivo*, and involving the application of light stimuli in a controlled way. The latter is likely to require the use of optical modeling tools for light propagation in tissue as was successfully done for light-based hair removal (Ross et al., 1999), where melanin, haemoglobin, and purulent discharge would be strongly affecting light transport. To conclude I found a lack of consistency in experimental and translational approaches in photobiomodulation studies both *in vitro* and *in vivo* including experimental conditions, treatment methods, clear translation between *in vitro* study and *in vivo* study. Not only should the optical parameters be rationally selected, but so also should the biological models under study. Most *in vitro* studies do not even closely approximate *in vivo* conditions. Thus, coupling both approaches (i.e., unravelling the photochemical reaction cascades involved as well as controlling the amount of light delivered to a selected target *in vivo*) will be required to improve the efficacy of existing devices and identify new light-based treatment opportunities for skin and hair health. Similar unresolved challenges are applicable to the entire field of photobiomodulation-based therapies, where a large leap forward in basic understanding is required before it finds itself in the mainstream of therapies.

3.6 Summary

The literature review of this chapter provides a detailed overview of the inconsistencies surrounding the current knowledge in the fundamentals of photobiomodulation in dermatology. The main results are:

- The investigation of 90 reports published between 1985 and 2015 in photobiomodulation for wound healing and hair regrowth revealed major inconsistencies in the selection of optical treatment parameters for clinical applications spanning 2 orders of magnitude in irradiance and radiant exposure.

- Commercial light-based devices for hair regrowth were based on inconsis-

tent optical treatment parameters, however. leading to similar clinical outcomes. It is recommended to aim for double-blind, placebo-controlled randomized clinical trials as the gold standard for quantifying hair growth when conducting studies for hair regrowth.

- Many photoreceptors expressed in human skin such as cytochrome c oxidase, cryptochromes, opsins, ion-gated channel etc. may trigger different molecular mechanisms simultaneously in skin cells.

Chapter 4: A systematic approach for the optimization of the selection of optical treatment settings in photobiomodulation of human dermal fibroblasts

As mentioned in the discussion of the previous chapter, photobiomodulation in dermatology is lacking rationality in the selection of optical settings and understanding of the response of biological model, and this is valid for diverse applications such as hair regrowth and wound healing. This chapter thus aims at answering some of the questions raised in our literature review: finding the rationality in the selection of optical parameters and unravel the impact of experimental factors in photobiomodulation in order to design more robust studies.

One of the results of the previous chapter was that a remarkably wide range of optical parameters has been applied to both *in vitro* and *ex vivo* model systems (variable across 2 orders of magnitude), where negative, positive and neutral outcomes are reported for visible and near-infrared (NIR) light despite very similar optical settings (Mignon et al., 2016b; Afifi et al., 2016; Woodruff et al., 2004; Avci et al., 2014). For example, exposure of human epidermal keratinocytes to similar doses of short wavelength visible light (i.e., 420 and 450 nm) were reported to alternately induce and reduce expression of differentiation markers (Liebmann, Born, and Kolb-Bachofen, 2010; Kim et al., 2013a).

Clarity on how one particular optical setting truly impacts on cell behavior is compromised in published reports that don't even disclose parameters applied or if they do sadly report them incorrectly (Mignon et al., 2016b; Hadis et al., 2016).

Here an hypothesis can be formulated that *in vitro* cell response to light is not exclusively defined by optical parameters and regimes, but rather also depends on treatment protocols. Variations in the latter may account for the myriad inconsistencies in the PBM literature (Mignon et al., 2016b).

Indeed, a number of factors can potentially affect PBM experimental outcomes such as cell confluency, passage, donor, donor age, body site, as well as differences in gene expression programs between primary cells and cell lines and many others even more difficult to apprehend such as the lack of standardization of the composition of bioactive compounds in FBS batch (Seo et al., 2012; Baker, 2016).

Additional factors will also involve the biological diversity of any one histologically-distinct cell type e.g., different subtypes of skin dermal fibroblast (DF) (Driskell et al., 2013; Driskell et al., 2015). These include the reticular and papillary fibroblasts as well as the hair follicle fibroblast subpopulations (dermal sheath and dermal papilla) (Sorrell and Caplan, 2004), all having strikingly different morphology, metabolism and gene expression. It is expected that these different cutaneous fibroblast subtypes will respond differently to light (Janson et al., 2012; Janson et al., 2013).

Therefore robust assessment of the therapeutic value of PBM requires multi-dimensional investigations, where optical (wavelength, radiant exposure, irradiance) and biological factors (cell type, subtype), as well as treatment protocols (environment of the cells during culture and treatment, supplements/components in growth medium, treatment iteration etc.) all need to be evaluated.

The aim of this study was to investigate the impact of several key factors such as wavelength, irradiance, radiant exposure, serum concentration, cell culture confluency, environmental oxygen concentration, light-based treatment regime and cell culture protocols on the response to light of human dermal fibroblasts *in vitro*.

4.1 Impact of optical parameters on the response of human dermal fibroblasts to light treatment

Accordingly to a body of research on PBM, the wavelength of light and the radiant exposure exert the most profound effect on cell response to optical radiation. Moreover, reports indicating importance of irradiance in defining cell behavior upon irradiation can also be found in literature (Chung et al., 2012; Karu, 2014). Indeed, results demonstrated that wavelength ($p < 0.001$) and radiant exposure ($p < 0.001$) of light had the strongest impact on the metabolic activity of human DF. At the same time, irradiance showed no or little effect ($p = 0.6$) (Fig. 4.1, A B C). On average, shorter wavelengths (450, 500 and 530 nm) had a strong inhibitory impact on fibroblast metabolic activity, while long wavelengths ($> 550nm$) showed negligible effects within the tested radiant exposures when cells were cultured at 20% environmental oxygen (atmospheric level).

Wavelength and radiant exposure of light were strongly linked (Fig. 4.2, A $p < 0.001$), whereby a radiant exposure-dependent cell behavior was seen with the short visible wavelengths ($< 550nm$). Low light exposure (2 $J.cm^{-2}$) exhibited essentially neutral effects on fibroblast metabolic activity at all wavelengths, while cell inhibitory effects were seen at high exposures of light at 450, 500 and 530 nm (Fig. 4.2).

By contrast, no interaction was observed between irradiance levels and any of the optical factors (i.e. wavelength and radiant exposure, Fig. 4.2, B C) in terms of cell metabolic activity, specifically meaning that a choice of irradiance at a fixed dose and a wavelength did not impact cell response.

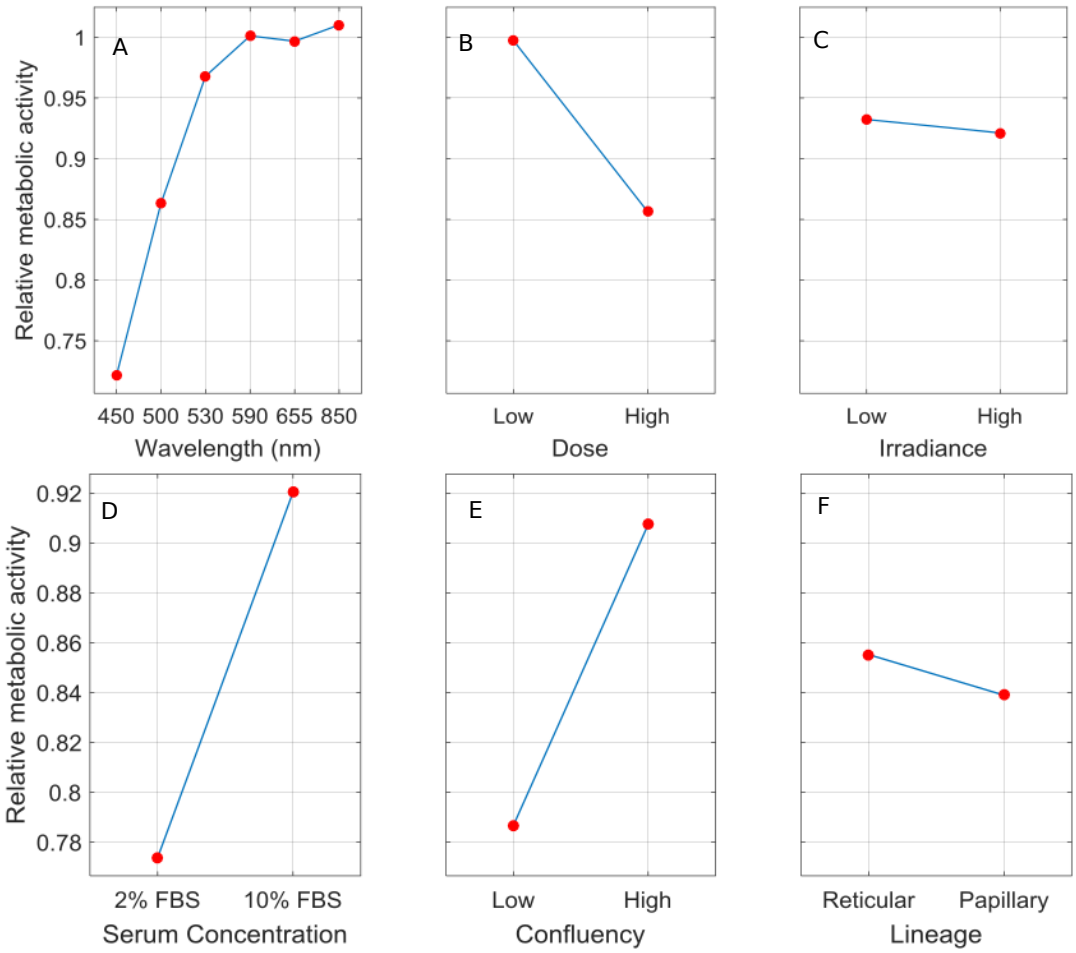

Figure 4.1: Main effects plot of the wavelength (A), radiant exposure (B) and irradiance (C) on the relative metabolic activity of human dermal fibroblasts (reticular and papillary). Statistical significance was evaluated using ANOVA (N = 3, 2 lineages and 3 replicates). The levels of radiant exposure correspond to 2 $J.cm^{-2}$ (low) and 30 $J.cm^{-2}$ (high), the levels of irradiance depended on wavelength and are reported in table 1 in the Materials and Methods Section. Main effects plot of serum concentration (D), initial confluency (E) and lineage (F) on the relative response of the metabolic activity of human dermal fibroblasts after light treatment (450 nm, 2 to 60 $J.cm^{-2}$). Statistical significance was evaluated using ANOVA (N = 2, 2 lineages and 3 replicates), wavelength ($p < 0.001$), radiant exposure($p < 0.001$) and irradiance ($p > 0.05$); serum concentration ($p < 0.001$), confluency ($p < 0.001$) and lineage ($p > 0.05$). The initial ratio at the moment of seeding between 'high' and 'low' confluency groups is 5. The control group is has an average relative metabolic activity of 1.

4.2 Impact of biological factors on the response of human dermal fibroblasts to light treatment

To assess the impact of several biological factors on the response of DFs to light a single wavelength (450 nm) was selected as it exerted the strongest effect on

the relative metabolic activity of the target cells, and varied radiant exposure from 2 $J.cm^{-2}$ to high 60 $J.cm^{-2}$ (Fig. 4.1, D E F).

Fibroblast confluency and serum concentration strongly influence how specific light parameters affect cell behavior (Fig. 4.1, D E). In particular, lower cell confluency or lower serum concentration resulted in stronger light-associated inhibition of cell metabolic activity (Fig. 4.2, D E). Both lineages of fibroblasts (i.e., reticular and papillary) responded similarly to test light parameters (Fig. 4.1, F).

As expected, serum concentration and confluency were related. High serum concentrations drove higher fibroblast proliferation and so confluency, given equal initial seeding density (Fig. 4.3, A B control bars).

In order to isolate the effect of serum concentration alone on the impact of light treatment, cells both at low and high confluency were treated using the same light parameter and protocol at the two culture conditions, 2% FBS and 10% FBS. At 60 $J.cm^{-2}$ (Fig. 4.3, B) the reduction of the metabolic activity of the fibroblasts grown in low serum was much stronger than at high serum, (60% versus 40%, respectively). This effect was also reflected in changes in cell morphology. Light treatment (450 nm, 60 $J.cm^{-2}$) in low serum and low confluency fibroblasts triggered cytotoxic effects (Fig 4.3, A), while cells in high serum and low confluency (Fig 4.3, A) and in combinations of high confluency/low serum and high confluency/high serum (data not shown) exhibited no cytotoxic effects.

To further investigate the effect of defined light parameters on DF metabolic activity, experiments were carried out at two different cell confluency levels: low (20%, 5,000 cells per 1.77 cm^2 well area at seeding) and a very high (90%, 30,000 cells per 1.77 cm^2 well area at seeding) (Fig. 4.4, A). Thus remarkably, the same light parameter applied to what is typically assumed in the PBM literature as 'identical' cells, albeit at different confluencies, resulted in opposite effects (Fig. 4.4, B). This was clearly different at two dose levels used, i.e., 2 and 30 $J.cm^{-2}$ (only the higher dose is shown). It appears that DF at high confluencies ($> 90\%$) may

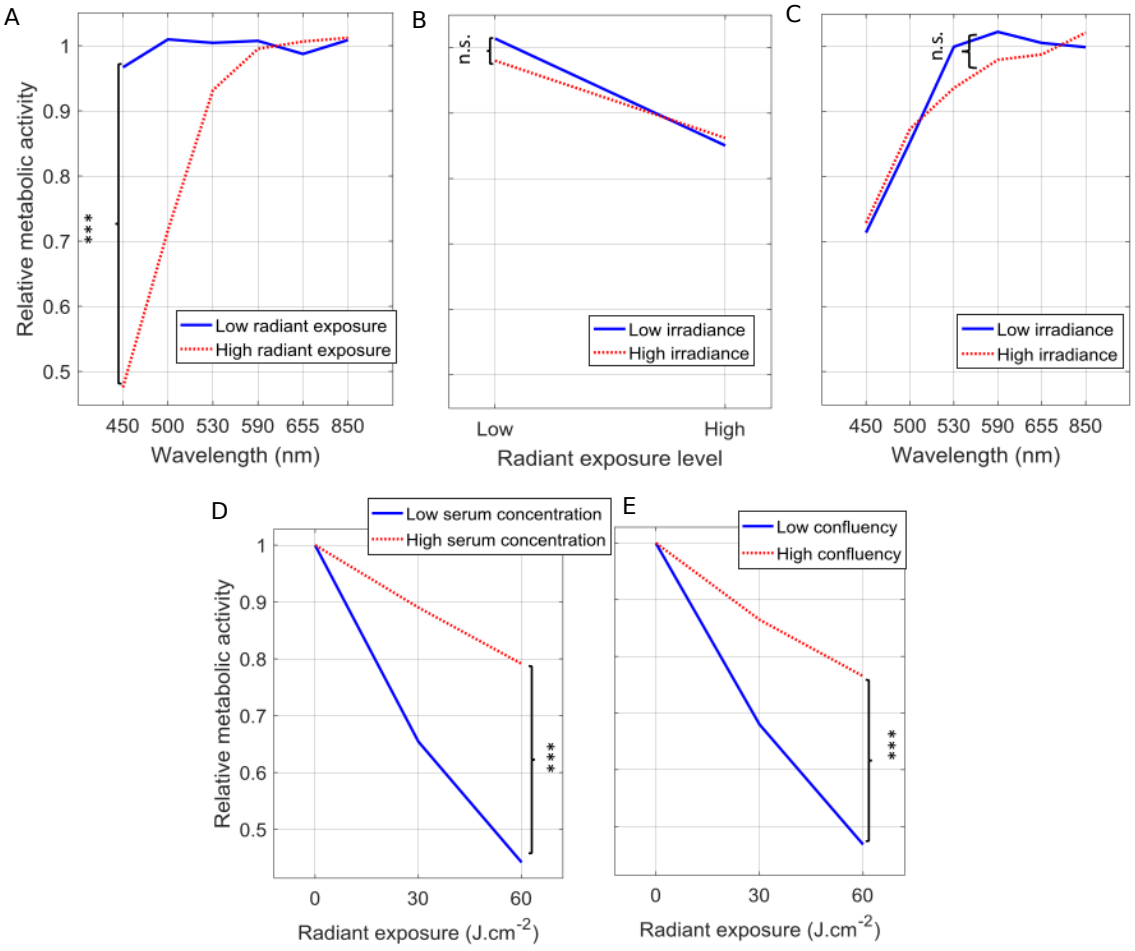

Figure 4.2: Interactions between wavelength and radiant exposure (A), irradiance and radiant exposure (B) and irradiance and wavelength (C) and their relative impact on human dermal fibroblasts metabolic activity (reticular and papillary). Statistical significance was evaluated using ANOVA (N = 3, 2 lineages and 3 replicates). The levels of radiant exposure correspond to 2 $J.cm^{-2}$ (low) and 30 $J.cm^{-2}$ (high), the levels of irradiance depended on wavelength and are reported in table 1 in the Materials and Methods Section. Interactions between levels of radiant exposure of 450 nm light and serum concentration (D), and initial confluency (E) and their impact on the relative response of the metabolic activity of human dermal fibroblasts. Statistical significance was evaluated using ANOVA (N = 2, 2 lineages and 3 replicates), *** ($p < 0.001$) and n.s. ($p > 0.05$). The initial ratio at the moment of seeding between 'high' and 'low' confluency groups is 5. The control group had an average relative metabolic activity of 1.

be more 'protected' in response to 450 nm light, at least in context of metabolic activity.

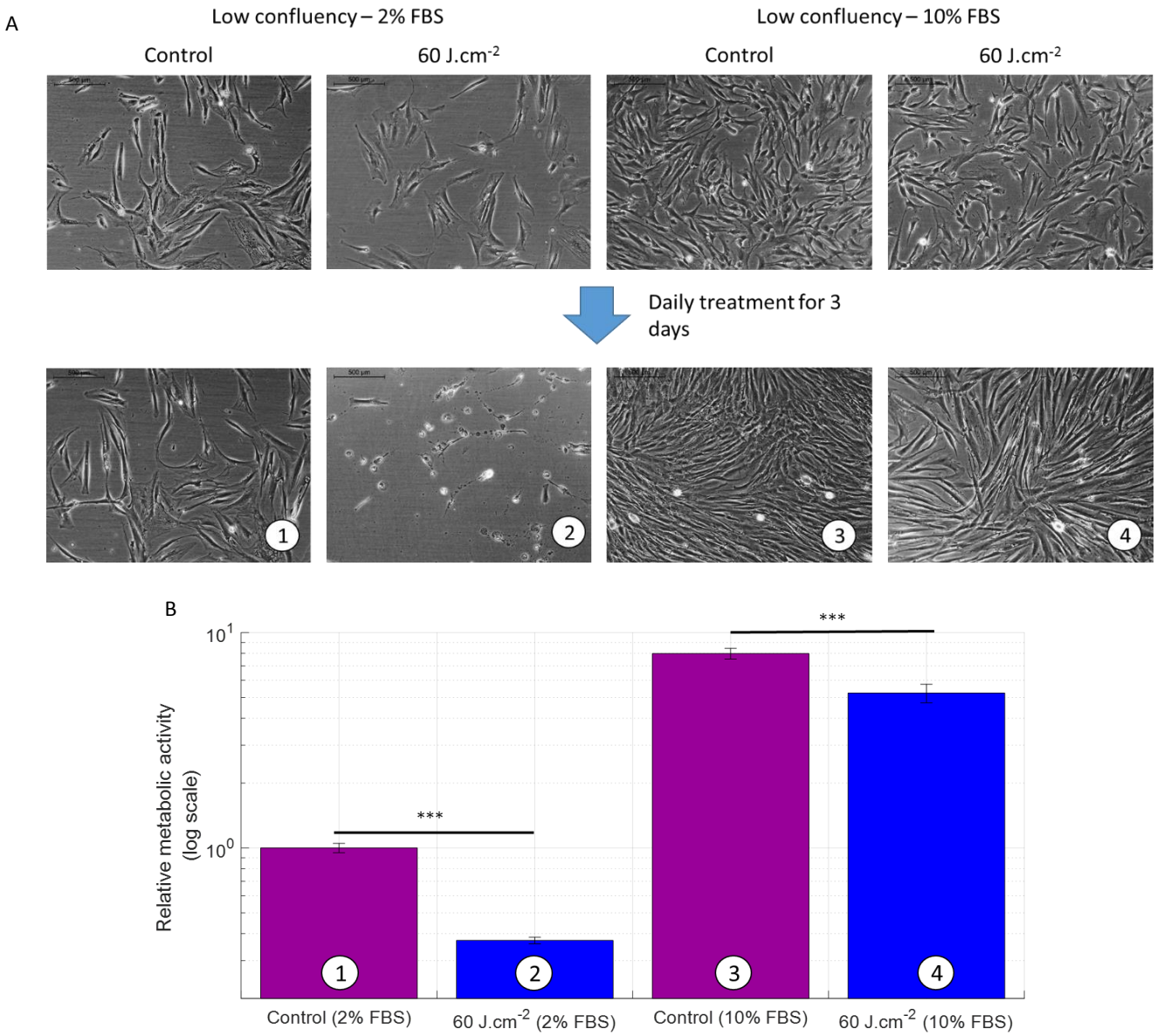

Figure 4.3: A: Phase-contrast images of human reticular fibroblasts on day 0 (8 days after seeding) at low initial confluency and cultured in DMEM with two serum concentrations 2% and 10% (upper line), and after three daily light treatments on day 4 at a low initial confluency (lower line). Papillary fibroblasts were found to behave similarly (not shown). A second donor responded similarly (not shown). B: Relative metabolic activity of human reticular fibroblasts after light treatment at 450 nm, 50 $mW.cm^{-2}$ with 60 $J.cm^{-2}$ (log scale). The high confluency level showed similar variation as a function of the change in FBS concentration (not shown), except for the cytotoxic effects observed in low serum/low confluency only. Statistical significance was evaluated using ANOVA. A second donor responded similarly (not shown as the scale is absolute). The control group has an average relative metabolic activity of 1. (N = 2, 2 lineages and 3 replicates). Standard deviations are shown in errorbars.

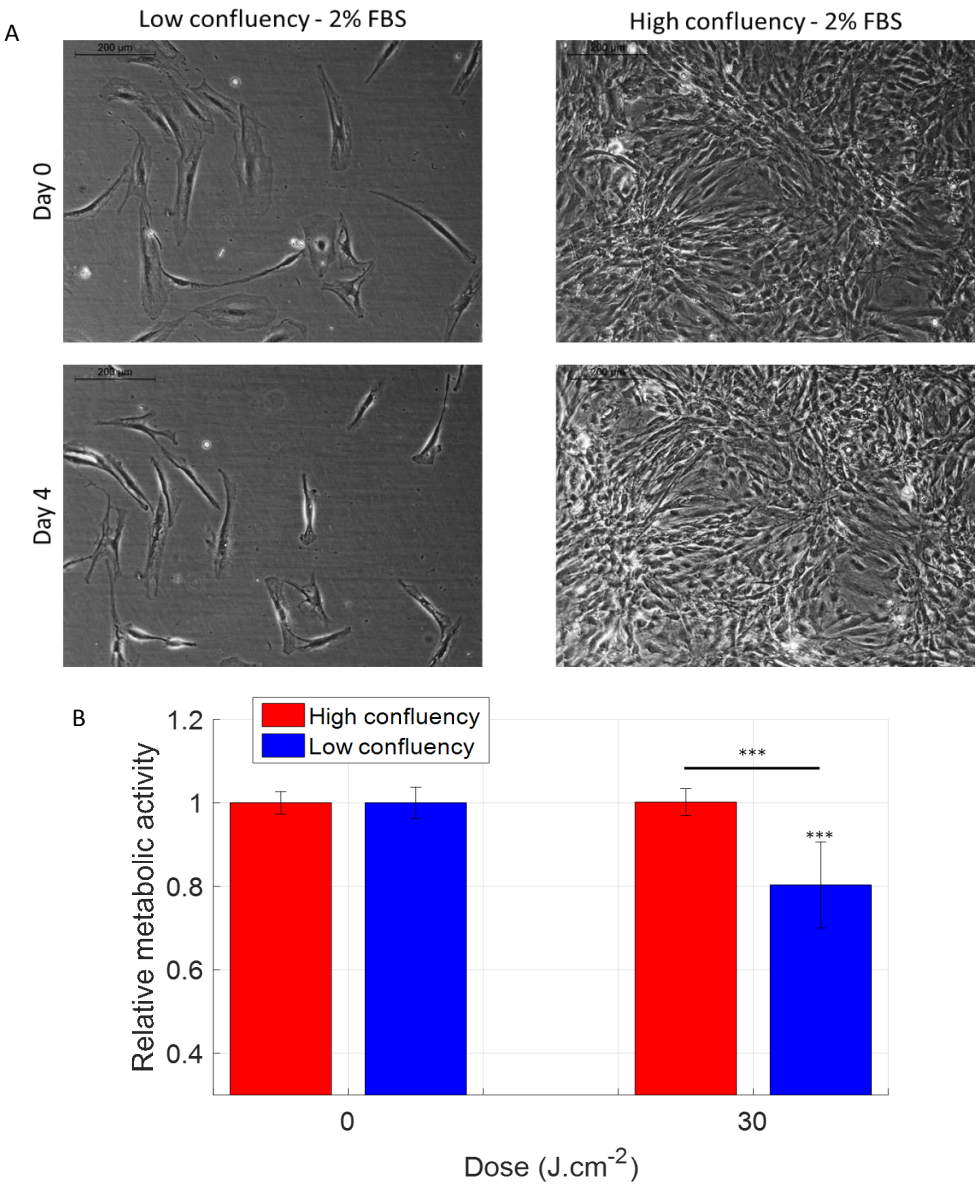

Figure 4.4: A: Phase-contrast images of human papillary fibroblasts on day 0 (8 days after seeding) at a low initial confluency (upper left) and high initial confluency (upper right), and after three light treatments on day 4 at a low initial confluency (lower left) and high initial confluency (lower right). Reticular fibroblasts were found to behave similarly (not shown). B: Relative metabolic activity of human papillary fibroblasts after light treatment at 450 nm, 50 $mW.cm^{-2}$ with 30 $J.cm^{-2}$ in function of the confluency level. Statistical analysis was evaluated using student t-tests between the control group and the treated group (N=3, 2 lineages and 3 replicates), with following thresholds $p < 0.05$ *, $p < 0.01$ **, $p < 0.001$ ***. The control group had an average relative metabolic activity of 1. The significance of the interaction between the radiant exposure and the confluency level was much lower than 0.001. Standard deviations are shown in errorbars.

4.3 Impact of the treatment regimes and protocols on dermal fibroblast metabolic activity

The choice of treatment regime, in particular, the number of consecutive treatments, impacts on the cell response to light, reflected in both cell metabolic activity and cell morphology. More specifically, a single exposure to 2 $J.cm^{-2}$ and 30 $J.cm^{-2}$ of 450 nm light resulted in an increase in metabolic activity, while 2, 3 or 4 consecutive treatments (Fig. 4.5, B) reversed the effect, leading to decrease in cell metabolism.

Observed changes in metabolic activity were accompanied by morphological alterations (Fig 4.5, A), such as shrinkage of cells, which became more pronounced with an increase in the number of exposures. After 4 treatments, cells were significantly smaller than the corresponding control cells. This observed steady shrinking of cell volume could reflect the observed decrease in cell metabolic activity. A similar effect was also present in cells grown at low confluency (Fig. 4.4, A).

Reducing light treatment frequency, from daily, every 24 hours, to every-other-day, every 48 hours, did not change the observed drop in metabolic activity or effect of cell morphology (Fig. 4.5, B), suggesting that the initial exposure triggers a chain of molecular reactions lasting longer than 24 hours.

Secondly, the treatment protocol used, in particular the interaction of light with the components of the culture medium exerted a significant impact on the outcome of the light exposure to short visible wavelengths (Fig. 4.6, A).

Exposure of DF to blue light of 450 nm (30 $J.cm^{-2}$) in culture media (DMEM), without its subsequent refreshment, resulted in cytotoxic effects 24 hours after treatment (Fig. 4.6). A similar effect at the wavelength up to 530 nm was observed, suggesting that a wide range of short visible wavelengths are absorbed by components of the cell culture media, leading to generation of molecules further impacting cell physiology (Fig 4.7, A).

Next I assessed whether this effect was dependent on cell-free elements of the

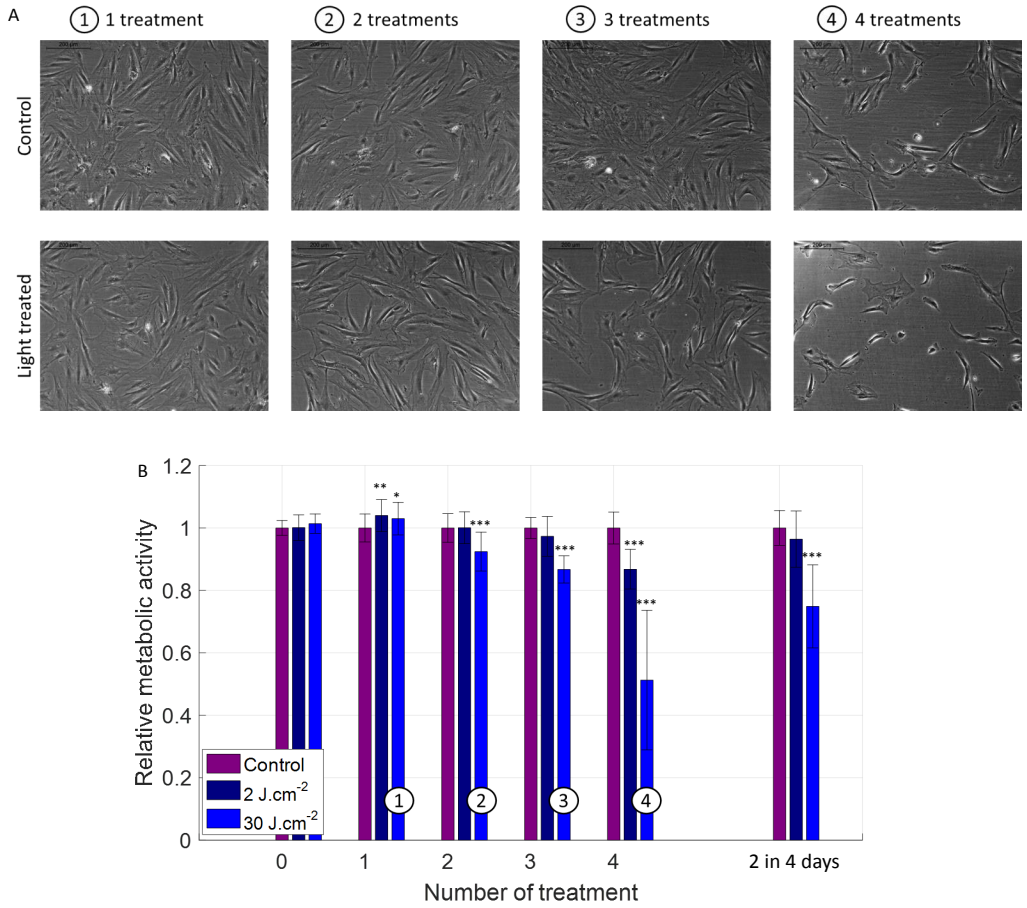

Figure 4.5: A: Phase-contrast images of human reticular fibroblasts 24h after the last treatment, when 1, 2, 3 or 4 daily treatments (30 $J.cm^{-2}$) were performed (lower line), together with the images of the control group (upper line). B: Relative metabolic activity of human papillary and reticular fibroblasts (merged) after light treatment for 2 radiant exposures of 450 nm light (at a fixed 50 $mW.cm^{-2}$ irradiance) and with variable number of treatments occurring on consecutive days. An irradiance of 50 $mW.cm^{-2}$ was used. Statistical analysis was evaluated using student t-tests between the control group and treated group (N=2, 2 lineages and 3 replicates), with following thresholds $p < 0.05$ *, $p < 0.01$ **, $p < 0.001$ ***. The control group had an average relative metabolic activity of 1. The significance of the interaction between the radiant exposure and the number of iterative treatment was much lower than 0.001. Standard deviations are shown in errorbars.

culture conditions, and found that DF exposure to cell-free media, irradiated using 30 $J.cm^{-2}$ and 60 $J.cm^{-2}$, resulted in reduced metabolic activity of the cells. The magnitude of this affect however, was lower than when cells in culture were directly irradiated (Fig 4.7, B), though fibroblast morphology was impaired only at 60 $J.cm^{-2}$ (Fig 4.7, C).

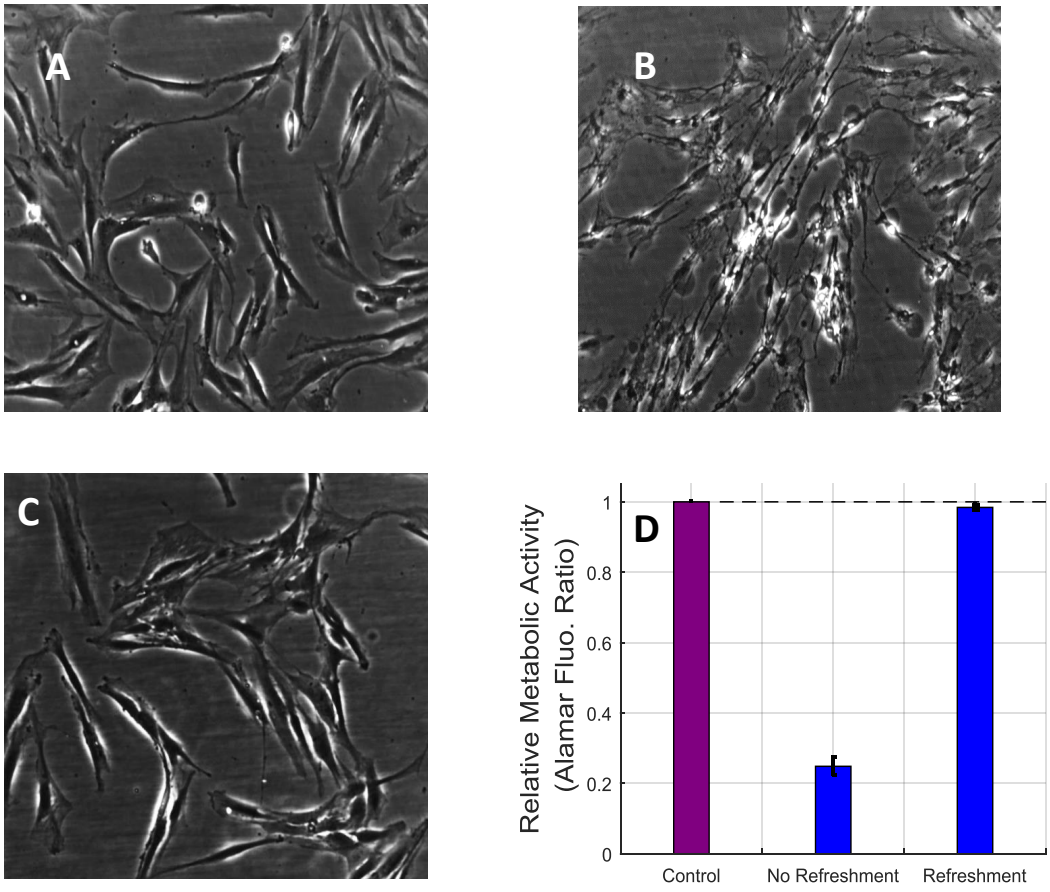

Figure 4.6: Representative light microscopy images of papillary fibroblasts taken after a single exposure to low- (A) and high dose (B) blue light versus the unirradiated control (C), and relative metabolic activity of human dermal fibroblasts after high dose of blue light (30 J/cm2) in two treatment conditions, with and without refreshment of the culture medium after light treatment (D). Cell detachment and cellular cytopathic effects reflected the cytotoxic effect in the treated sample without refreshment of the medium after exposure (B) and reduced Alamar Blue® fluorescence (D). Standard deviations are shown in errorbars.

4.4 Impact of the oxygen level in cell culture medium on cellular response to light

Recent evidence suggests the existence of gradients of physiological oxygen levels throughout the different layers of human skin layers, where oxygen level in dermis (outside capillary loops) can be as low as 1-5%, compared to 20% atmospheric level (Wang, 2005; Upton et al., 2015). I therefore studied the effects of lowering oxygen concentration from 20% to 2% in fibroblast cultures; i.e., to a physiologically-relevant concentration of oxygen in terms of DF interaction with

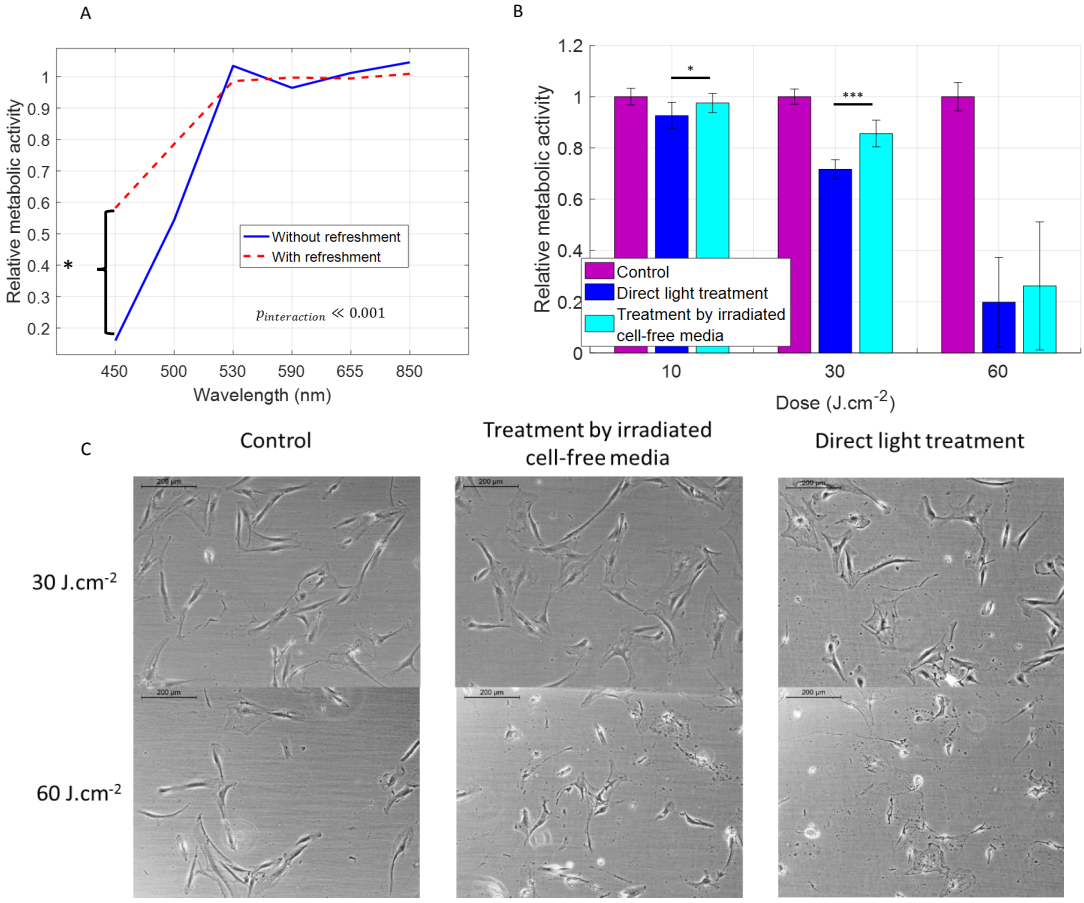

Figure 4.7: A: Relative metabolic activity of fibroblasts after light treatment as a function of the wavelength and the treatment regime (one or more consecutive irradiations) and protocol (direct light exposure or contact with pre-exposed culture medium). Metabolic activity after treatment was normalized to that of the control sample (Number of donors N=3, number of technical replicates n=3, data on papillary and reticular pools were merged together.) The significance of the interaction between wavelength and treatment method was evaluated with ANOVA ($p << 0.001$). (B) Relative metabolic activity of the fibroblasts after light treatment for two treatment protocols: direct light exposure (blue) and pre-exposure of DMEM alone followed by pouring on top of the cells (cyan). Standard deviations are shown in errorbars. C: Phase-contrast pictures of human reticular fibroblasts 24h after the last treatment, in control group, treated group (30 $J.cm^{-2}$ and 60 $J.cm^{-2}$) and treated by irradiated cell-free media. An irradiance of 50 $mW.cm^{-2}$ was used. Statistical analysis was evaluated using student t-tests between the control group and treated group (N=3, reticular and 3 replicates), with following thresholds $p < 0.05$ *, $p < 0.01$ **, $p < 0.001$ ***. The control group is has an average relative metabolic activity of 1.

visible light *in vivo*.

The reduction from 20% to 2% oxygen concentration did not result in noticeable changes in the metabolic activity or morphology in control fibroblast (papillary and reticular) cultures, (Fig. 4.8, A).

By contrast, lowering oxygen concentration resulted in dramatic differences in fibroblast response to light. In particular, blue light (450 nm) at 30 $J.cm^{-2}$ resulted in even stronger inhibition of metabolic activity of papillary fibroblasts than when grown in 20% oxygen. Remarkably, NIR light (850nm) at 20 $J.cm^{-2}$ stimulated metabolic activity of human reticular fibroblasts at physiological levels of oxygen (i.e. 2%), the effect that was not observed at 20% oxygen level. These effects were not associated with any significant change on the relative cell number (Fig. 4.8, B).

4.5 Discussion and Conclusions:

The goal of this study was to investigate the impact of optical parameters, cell culture protocols and treatment regimes on the metabolic activity of primary human dermal fibroblasts *in vitro* culture in response to visible and near-infrared radiation.

To achieve this I systematically studied the impact of wavelength, irradiance, dose, number of consecutive irradiations, serum- and oxygen concentration, cell confluency, medium refreshment and indirect treatment with irradiated medium alone in a design-of-experiment approach. The latter was specifically chosen in order to disentangle the effects caused by a direct interaction of photons of light with cells from the potential contribution of multiple 'environmental' factors.

This project also aimed to explore whether the response of DF to identical optical parameters would change when cultured at conditions that more closely resemble those *in vivo*, i.e. low proliferation, cell confluency, serum and oxygen levels, as this is crucial when considering application of new technologies to *in vivo* clinical settings.

Several interesting and unexpected findings resulted from the approach, new to the world of photobiomodulation, which cause one to step back and re-assess how we interpret PBM data derived from *in vitro* studies.

Firstly, all investigated parameters in this study, with the exception of irradiance, significantly impacted skin fibroblast metabolic responses to light.

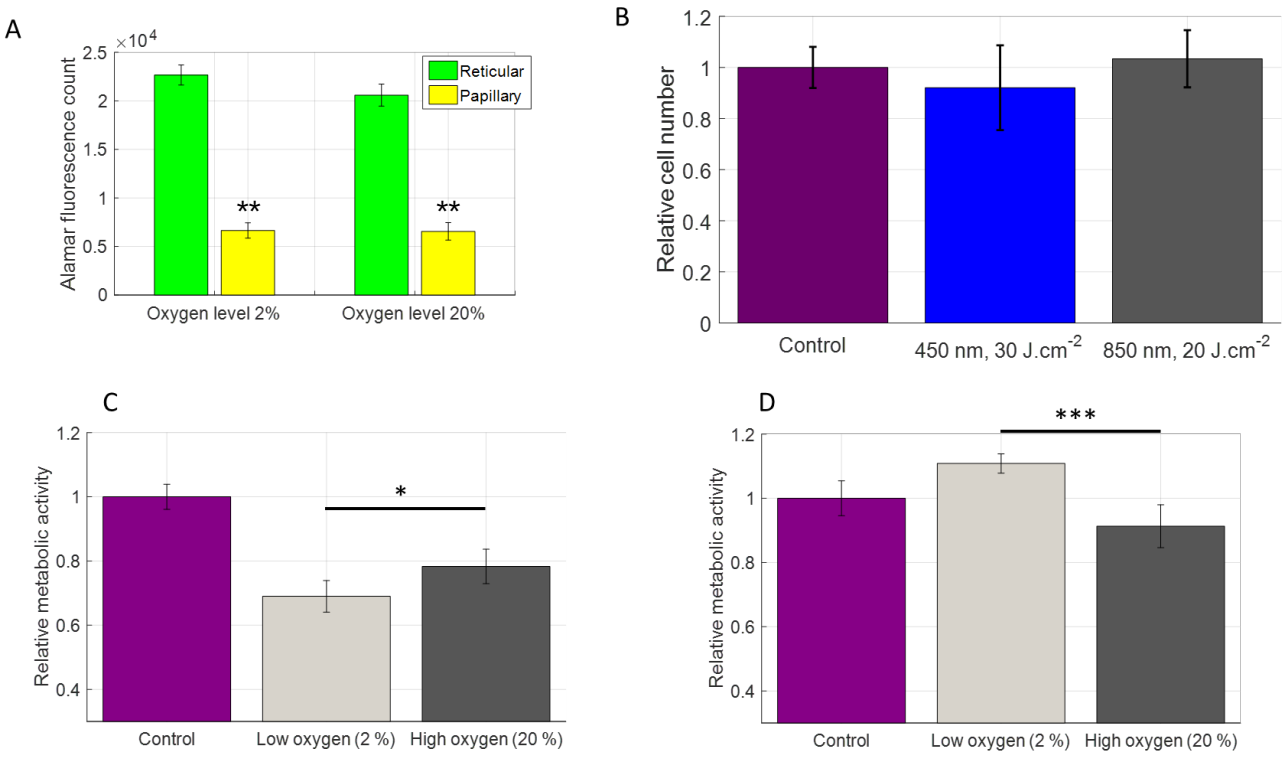

Figure 4.8: A:Fluorescence counts (Alamar Blue) measured in reticular and papillary fibroblasts (facelift, female, 64 yo) in low (2 %) and high (20 %) oxygen levels, together with the phase-contrast microscopy pictures of the reticular type in low (left) and high (right) oxygen levels. No strong change in Alamar fluorescence count nor in morphology is apparent. B: Relative cell counts of human dermal fibroblasts (reticular and papillary merged numerically) after light treatment in hypoxic conditions (2% oxygen). Cells were grown in 35-mm individual dishes and treated daily with light during three consecutive days. The cell were counted 24 h after last treatment. Material originating from two different donors was included in the experiment (N=2, reticular and papillary, 3 repeats, 12 counts per bar). C: Relative metabolic activity of human papillary fibroblasts in response to $30\ J.cm^{-2}$ at 450 nm in low and high environmental oxygen levels (N=2, papillary and 3 replicates). D: Relative metabolic activity of human reticular fibroblasts in response to $20\ J.cm^{-2}$ at 850 nm in low and high environmental oxygen levels (N=2, reticular and 3 replicates). Irradiance levels were $50\ mW.cm^{-2}$ (450 nm) and 80 mW.cm-2 (850 nm). Standard deviations are shown in errorbars.

Secondly, cell culture and treatment conditions (including confluency, serum- and environmental oxygen concentrations and treatment protocols) all significantly influence cellular responses to optical radiation, even when the identical wavelength, irradiance and dose were applied.

While medium-to-high confluency scenario is convention cell culture practice worldwide, *in vivo* DF are sparsely distributed throughout papillary and reticular dermal compartments. In an attempt to observe cells in a more natural situation, cultured at low confluency, I noticed that three consecutive daily treatments using short-wavelength visible light (450nm at 30 $J.cm^{-2}$) reduced their metabolic activity to a greater extent than when maintained at medium-to-high confluency.

Similarly, I observed that DF grown in lower FBS concentration 2%, though still higher than a fibroblast in a non-wounded skin environment would experience, coped less efficiently with induced stress, and were more inhibited by several consecutive exposures to 450 nm light at 30 $J.cm^{-2}$. This response was clearly different from that of fibroblasts cultured at 10% FBS who were less inhibited and even protected from light-associated reactive oxygen species (ROS), as evidenced by normal metabolic activity and morphology. Similarly to low confluency, lower serum exposure may be more physiologically relevant.

The latter two findings may suggest that 'non-physiological' highly confluent cell cultures of DF in 10% FBS may be 'more protected' from potential stressors induced by light, such as ROS (Stoppiglia et al., 2002; Ling, Hannaert, and Pipeleers, 1994), than the cells *in vivo*. Two factors could potentially play a role here. First, lower proliferative activity and thus lower number of mitotic cells, known to be more vulnerable to noxious factors (Rieder and Maiato, 2004; Chan, Koh, and Li, 2012), of highly confluent cell cultures of DF. Secondly, I also hypothesize that the higher the number of cells exposed to the light treatment event the stronger the antioxidant defense may be against any ROS created by irradiation of the cell medium constituents, as the latter was kept constant in all experiments regarding of cell number per well.

In addition to cell confluency and serum concentration, I assessed whether continuing to expose fibroblasts to their irradiated medium post-treatment negatively impacted on their viability. Specifically, I have shown that high radiant exposures of short visible wavelengths (450 and 500 nm, at 30 and 60 $J.cm^{-2}$) suppressed fibroblast metabolic activity, and even resulted in some cytotoxicity when

the medium was not refreshed after irradiation. Importantly, irradiation of cell-free culture medium that was then exposed to the cells resulted in an inhibitory effect, suggesting that ROS released after light absorption by riboflavin known to be present in the culture medium may have been at least in part responsible for this observed inhibitory effect. Previously it was shown that riboflavin mediated cytotoxic effects in human skin melanoma cells after irradiation by blue light (470 nm) (Ohara, Fujikura, and Fujiwara, 2003). However, it may not be completely artefactual to the *in vitro* situation, as it is also known that flavins are naturally present in normal human skin dermis (Olsen et al., 2016) where they are likely to respond to clinical PBM modalities. However, I observed greater effects with the irradiated cell plus medium combination (than with the irradiated medium treatment alone), suggesting that there is a distinct cellular-derived component to the light response, indicating that photons of visible light can indeed directly interact with DF cells. Previously, interesting effects were observed in cells irradiated by ionizing radiation where oxidative stress was transferred from the irradiated cell to non-irradiated cells, via the release of components in the medium and even via the irradiated supernatant alone, which received a name 'bystander effect' (Azzam, Jay-Gerin, and Pain, 2012; Narayanan et al., 1999). Several signaling molecules mediate transfer of oxidative stress. Small molecules, such as Ca2+ or peptides, were transmitted via gap junction intercellular communication to neighboring cells. Larger molecules, which could also be released by the irradiated cells, could propagate damage and include lipid peroxide products and cytokines and reach neighboring cells by diffusion (Prise and O'Sullivan, 2009; Klammer et al., 2015). Similar processes could occur after treatment with visible and NIR light.

Next to cell culture conditions, what is less clear in PBM literature is if and how the experimental outcome depends on a number of consecutive treatments. An observation of this project is that the effect of shorter wavelengths (450 nm- 590 nm) is accumulated over increasing number of consecutive daily and every-other-day treatments, suggests that the light can have prolonged effects on dermal fibrob-

lasts, beyond cessation of irradiation, via the initiation of downstream cascade of cell signaling.

A key finding of this PhD project was the observation that oxygen concentration markedly impacted on the response of dermal fibroblasts to both short visible- and to near-infrared light. Lowering oxygen to physiological level (i.e. 2%) resulted in fibroblast stimulation by near-infrared wavelengths: an observation not seen when cells were exposed to conventional cell culture oxygen levels (i.e. 20%), and so our protocol may allow researchers to appropriately investigate the photobiomodulation effects on skin and hair health. Indeed, researchers have shown the importance of environmental oxygen concentration at the genomic and proteomic levels in cells from various body locations. Physiological levels of oxygen in the body are organ-dependent and generally different from the standard oxygen concentration not only in human skin compartments but also in brain, lungs, liver and other body organs (Carreau et al., 2011). This therefore raises the need to distinguish between 'normoxia' and 'physioxia', and how this could impact PBM studies conducted using *in vitro* cell culture.

Skin temperature in itself could represent another condition to optimize in the pursuit of *in vivo* approximation. In the case of skin, the temperature is commonly assumed to be around $34°C$ (Olesen, 1982). However, finding the right skin temperature might be complex for at least two reasons. First, there is evidence showing that skin temperature is highly variable within the body and dependent on the ambient temperature (Olesen, 1982). Second, related to light treatment *in vivo*, there will be thermal effects involved due to the strong optical absorption of visible and NIR radiations by skin chromophores (melanin, blood). Similarly, our data suggests that *in vitro* protocols may be more physiological if irradiation is done with cells in culture medium rather than in a buffer such as PBS, given that *in vivo* (both steady state and during wounding/wound-healing) interstitial fluids and extracellular matrix will contain a complex mixture of essential minerals, ions, growth factors, and other nutrients and ligands', which likely contribute to the total cellular response to light. However, the lack of *in vivo* 'flow' conditions in our

static *in vitro* setup suggests that refreshment of medium after light treatment may be advisable. The downside being the loss of important autocrine cytokines and growth factors. In particular, it is known that it may be important in the context of photobiomodulation, where latent growth factors have been shown to be activable via infrared radiation (Arany et al., 2014).

Interestingly, some of this project findings differ from those previously reported in the literature. First, the results did not show any strong effect of long visible and NIR radiation under environmental partial oxygen pressure. This observation is not surprising by itself, as the literature contains large discrepancies between the optical parameters and experimental outcomes used hitherto, impeding progress of PBM modality as previously reported (Mignon et al., 2016b). More specifically, the majority of previous studies showed a measurable effect of red and NIR wavelengths *in vitro* and on *ex vivo* systems (Arany et al., 2014; Anders, Geuna, and Rochkind, 2004; Hashmi et al., 2011; Wang et al., 2016; Anders et al., 2008). Other studies, however, found no effect of long visible and NIR wavelengths on skin cells (Liebmann, Born, and Kolb-Bachofen, 2010; Oplander et al., 2011). While not excluding the impact of cell culture conditions and oxygen levels on these, often opposite, experimental outcomes, human dermal fibroblasts, positioned deeper than epidermal melanocytes and keratinocytes, might be more shielded from the blue part of the electromagnetic spectrum but much are more exposed to red and NIR components, and therefore could have adapted to them. Therefore one could suspect a stronger resistance of dermal fibroblasts to visible and NIR radiation, particularly in the long wavelength range, due to evolutionary reasons. The same reasoning may suggest that fibroblast originating from more deeply located tissues are more sensitive to light photons. Second, no irradiance effect was observable *in vitro* despite some existing evidence in the literature both for *in vitro* and *in vivo* cases (Anders et al., 2010; Holanda et al., 2017). However, irradiance effects have not been yet very clearly established *in vitro* in photobiomodulation. Although it might be expected *in vivo*, as light will be absorbed by skin chromophores (melanin, blood) and create bulk heat, it is less straight-

forward to expect irradiance effect *in vitro*. It might also have been that that our irradiance levels are not separated 'well enough' (only a factor 2 to 8 depending on the wavelength).

Third, this project did not reveal any strong effect on the relative cell number after light treatment. However, the literature does contain evidence that short visible wavelengths exert anti-proliferative effects (Liebmann, Born, and Kolb-Bachofen, 2010; Oplander et al., 2011). The underlying reason of observed differences is that our biological model (low confluency, low serum and low oxygen) was tailored to resemble *in vivo* conditions of the dermal fibroblasts, where their proliferative activity is very low under non-wounded conditions. Combined with the replenishment of the media after light treatment, a very slow proliferation was barely observable for the duration of the experiments with light. Therefore, it was not expected to be able to detect an effect on the relative cell number after treatment with light.

The conclusion from this chapter is that *in vitro* experimental design factors including cell confluency, serum concentration, culture conditions like oxygen level, impact cell behavior (Upton et al., 2015; McFarland et al., 2011) and so are critical to how we best define cell reactions to light i.e., either inhibitory, neutral or stimulatory, even when responding to light of the identical characteristics. Therefore, this emphasizes a recommendation that for all *in vitro* and *ex vivo* investigations on photobiomodulation researchers should not only carefully select their experimental conditions as close to the physiological *in vivo* setting as possible but in any event report these together with their experimental findings. Additionally, these findings emphatize the recommendation that confluency, serum- and environmental oxygen concentration should ideally be much lower than those currently used and reported worldwide in conventional dermal fibroblast culture protocols.

4.6 Summary

In this chapter the appropriateness of a range of previously-reported treatment parameters, including light wavelength, irradiance and radiant exposure, as well

as cell culture conditions (e.g., serum concentration, cell confluency, medium refreshment, direct/indirect treatment, oxygen concentration, etc.), in primary cultures of normal human dermal fibroblasts exposed to visible and near infra-red (NIR) light was investigated. The main results are:

- Apart from irradiance, all study parameters impacted significantly on fibroblast metabolic activity.

- When cells were grown at atmospheric O2 levels (i.e. 20%) short wavelength light inhibited cell metabolism, while negligible effects were seen with long visible and NIR wavelength. By contrast, NIR stimulated cells when exposed to dermal tissue oxygen levels (approx. 2%).

- The impact of culture conditions was further seen when inhibitory effects of short wavelength light were reduced with increasing serum concentration and cell confluency.

Chapter 5: Reticular and papillary fibroblasts exhibit a differential response to visible and NIR light

A second gap revealed from the literature review is the lack of knowledge of the mechanism(s) of action and therapeutic effects of visible and NIR light in photobiomodulation in dermatology (see chapter 3).

After wounding, human dermal fibroblasts are involved in the wound healing response of the skin. Besides, they are directly attainable for a potential light treatment. This fact makes them a first target in wound healing. Additionally, in aging, human papillary fibroblasts tend to disappear from the human dermis and are replaced by reticular fibroblasts. This emphasizes their importance in the process of aging. With those examples in mind, the focus of this chapter was set on human dermal fibroblasts because of their significant involvement in ageing and wound healing. In this chapter, the effects of selected optical settings on human dermal fibroblast subpopulations will be investigated in-depth.

While the exact molecular mechanisms of visible and NIR light on human skin cells are unknown, the number and variety of photoreceptors reported in the literature suggest that most probably there are many different molecular mechanisms which potentially occur simultaneously (Chung et al., 2012; Mignon et al., 2016b). The downstream mechanisms are dependent on wavelength and dose of the light treatment (Chung et al., 2012). The effect of red and NIR light are commonly attributed to cytochrome c oxidase where ROS signaling and ATP are the main actors (Chung et al., 2012). Other evidence demonstrate that NIR may activate latent growth factors in the extracellular space (Arany et al., 2014). Short visi-

ble wavelengths are most commonly assumed to induce ROS (reactive oxygen species) from flavoproteins or nitrosated proteins (Opländer et al., 2013; Becker et al., 2016; Lockwood et al., 2005), which leads to cascade of molecular reactions. Last but not least, recent evidence demonstrate the presence of opsins and cryptochrome photoreceptors in the skin and hair follicle suggesting a potential role for them in response to visible and NIR light treatment including via ROS (Buscone et al., 2017; Haltaufderhyde et al., 2015).

Despite the lack of knowledge regarding the mechanism(s) of actions, visible and NIR light treatment have been associated with a very large range of effects including inhibition of cell proliferation, induction of differentiation, stimulation of collagen production and changes in gene expression patterns (Mamalis, Garcha, and Jagdeo, 2015; Becker et al., 2016; Liebmann, Born, and Kolb-Bachofen, 2010). As of today the entire extent of the action of light on skin cells remains unknown. Gene expression studies represent an unavoidable path needed to understand the full potential range of impact of visible and NIR light on human skin cell populations.

Human skin contains different cell populations, each with their specific function in the skin. While most of them would be worthy to be studied with regards to their response to light, human dermal fibroblasts were chosen here as they represent a major cell type with important role in wound healing, ageing and scar formation. Human dermal fibroblasts exist in four different subtypes: the reticular and papillary fibroblasts which are located in the dermis, and the dermal papilla and dermal sheath fibroblasts which are part of the hair follicle. These populations play different and complementary roles in the skin (Jenkins and Carroll, 2011; Driskell et al., 2013).

Notably reticular and papillary fibroblasts have been shown to be involved in wound healing and ageing (Janson et al., 2013; Izumi, Tajima, and Nishikawa, 1995; Driskell et al., 2013). Photobiomodulation might readily have a differential effect on both of these cell subpopulations, and so provide potential treatment strategies for skin conditions which involve reticular and papillary fibroblasts differently. For

example some evidence suggests that scarring is due to the predominant action of the reticular fibroblasts, in the lower dermis, and the inaction of the papillary fibroblasts, in the upper dermis, during the first wave of wound healing (Woodley, 2017).

In the present study, the impact of visible and NIR light on both subpopulations of human skin fibroblasts, based on their metabolic activity, transcriptome and collagen production was investigated.

5.1 Action spectrum and dose responses of human dermal fibroblasts

Human dermal fibroblasts were treated with light once per day on three consecutive days using one of 6 different visible and NIR wavelengths. The metabolic activity of the fibroblasts was measured 24 hours after the last light treatment. No significant biologically-relevant effect of long visible wavelengths on the metabolic activity of the human dermal fibroblasts over $[0 - 250]\ J.cm^{-2}$ was observed when treated at atmospheric standard oxygen concentration (Fig. 5.1 A). The morphology of the dermal fibroblasts observed via a light microscope was not impacted (not shown). A slight decrease of the metabolic activity was observed at high dose levels of red and infrared wavelengths (655 nm and 850 nm at doses $> 100\ J.cm^{-2}$).

On the contrary short visible wavelengths showed significant inhibitory effects on the metabolic activity of human dermal fibroblasts (Fig. 5.1 A). The shorter the wavelength, the higher was the reduction of the metabolic activity at the same dose level. The dose responses at 450, 500 and 530 nm shared remarkably a similar shape: consisting of a inhibitory phase where the metabolic activity is reduced at low- to mid- dose levels ($<= 30\ J.cm^{-2}$), and a steep decrease of the metabolic activity associated with cytotoxic effects at higher dose levels ($> 30\ J.cm^{-2}$).

The dose response curve at 450 nm was compared with classical dose-response curve models traditionally used to model the response of cells to chemical drugs

(Di Veroli et al., 2015). The dose response curve at 450 nm was numerically associated with a biphasic dose-response model with two inflection points (Fig. 5.1 B). The two phases were associated with two effect types: non-cytotoxic inhibitory effect and cytotoxic effect observed via light microscopy (Fig. 5.1 C).
The impact of the wavelength of irradiation is in coherence with the observations of chapter 4. Indeed, short visible wavelength exerted strong inhibitory effects on human dermal fibroblasts while long visible wavelengths had neutral effects.
Both lineages responded similarly and there were no significant differences in their response at this stage.

5.2 Blue light (450 nm) induces intracellular ROS formation

Many studies in photobiomodulation research report the involvement of ROS in the mechanism of action of light in cells (Becker et al., 2016; Arany et al., 2014; Chung et al., 2012). Blue light (450 nm) induced ROS in a dose-dependent manner in reticular and papillary fibroblasts (Fig. 5.2 A). The induction of ROS was recorded in live cells versus time using a ROS dye. The intensity of the dye (cellROX deep red) varies proportionally to the intracellular ROS concentration. During the light treatment, the intensity of the ROS indicator increased linearly with the light dose (Fig. 5.2 A). Additionally, the increase of ROS per unit of time was clearly stronger during the irradiation than in baseline and/or post-treatment periods.
The induction of ROS by light was efficiently quenched with the addition of antioxidants in the culture medium (Fig. 5.2 A). However, there was an increase of the dye intensity under light treatment in the presence of antioxidants. It seems that antioxidants rather delayed the light-induced increase of the dye intensity rather than completely suppressed it. Representative images of the ROS distribution in dermal fibroblasts at the end of light treatment revealed a predominantly perinuclear localization (Fig. 5.2 B). The intracellular intensity of the dye was significantly lower in both subpopulations in presence of antioxidants at the same time point.

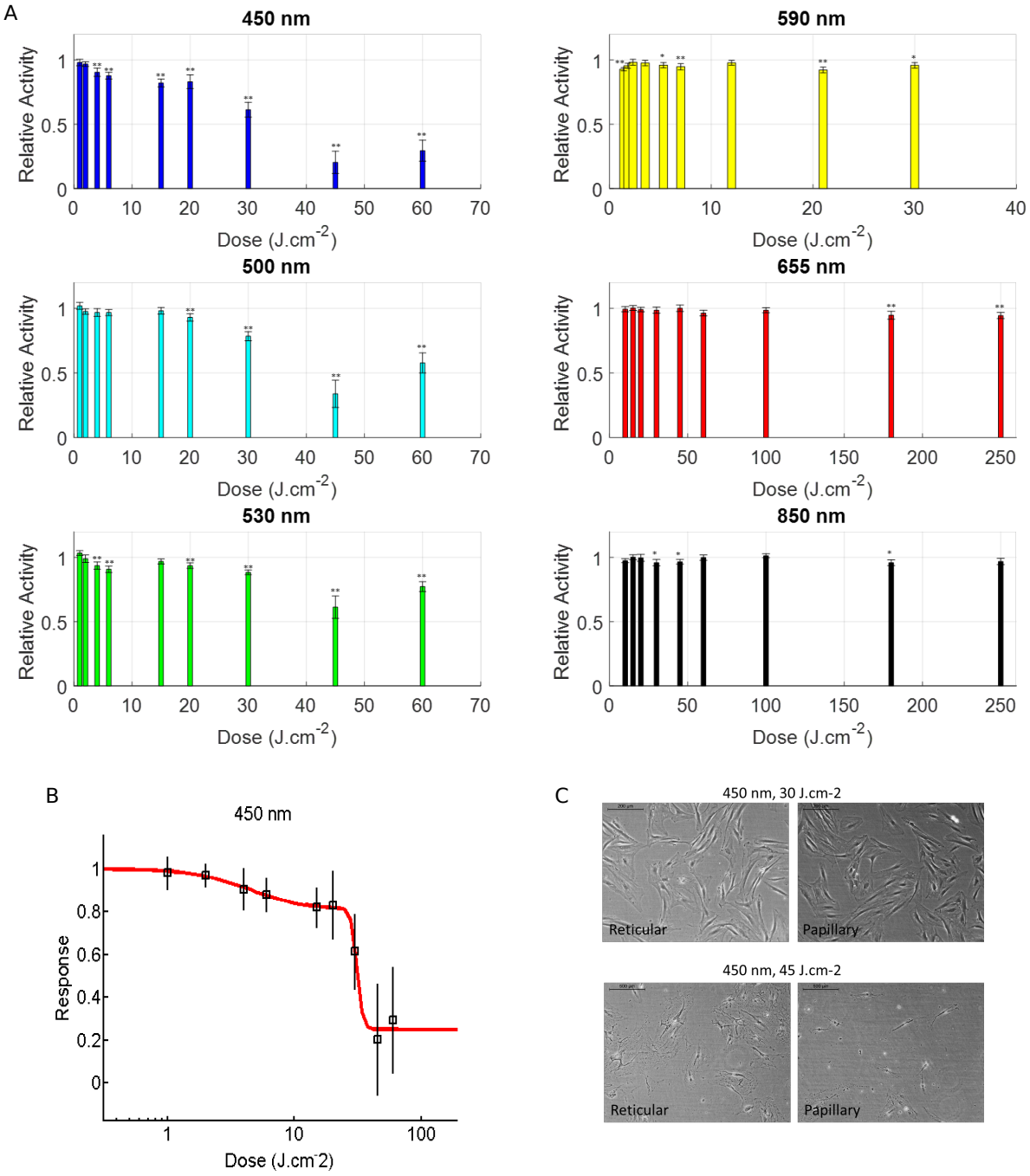

Figure 5.1: (A) Dose-response curves of human dermal fibroblasts to six visible and NIR wavelengths (450, 500, 530, 590, 655 and 850 nm) based on the relative change of their metabolic activity after irradiation. Human dermal fibroblasts were treated once per day on three consecutive days. Their metabolic activity was measured 24h after the last treatment. Cell culture medium was replenished immediately after each light treatment. Statistical significance was evaluated using student t-tests (N = 3, 2 lineages and 3 replicates). The responses of both lineages were merged. Standard deviations are shown in errorbars. (B) Dose-response curve of human dermal fibroblasts after irradiation with blue light (450 nm) together with the best-fit (biphasic, two inflection points, best fit: lowest BIC and AIC via Dr Fit software (Di Veroli et al., 2015)). Standard deviations are shown in errorbars. (C) Phase-contrast microscopy pictures of human dermal fibroblasts (female 64 yo) after three light treatment at 450 nm, $30 J.cm^{-2}$ and $45 J.cm^{-2}$.

Similar experiments were repeated using infrared light (850 nm). By contrast to blue light (450 nm), NIR radiation did not induce any measurable intracellular ROS formation in both lineages within the range 0-30 $J.cm^{-2}$.

The same set of experiments were repeated using a mitochondria tracker in combination with the cellROX dye. A high correlation of the localization of the ROS dye and the mitochondria tracker was observed (Fig. 5.2 C), the average Pearson correlation coefficient evaluated at 15 mins after start was 0.88 averaged over the replicates (N=2, reticular and papillary, 2 replicates).

5.3 Papillary and reticular fibroblasts express highly different transcriptome

As suggested by recent articles and reviews, the dermal tissue oxygen level (2-5 %) is significantly lower than standard oxygen concentration (20 %) used in conventional cell culture (Wang, 2005; Upton et al., 2015). Therefore, the response of both fibroblasts subpopulations to relevant dose levels at one of the 6 different visible and NIR wavelengths (2 % incubator oxygen concentration) was also evaluated. Fibroblasts were treated with light every day for three days in both hypoxic and standard oxygen conditions in parallel. Metabolic activity was assessed after the last treatment. Transcriptome analysis of both sub-populations was performed in hypoxic conditions only, as it represents conditions closer to the *in vivo* environment.

Almost 4000 genes were significantly differentially expressed between both subpopulations in control groups (i.e. without light treatment). A keyword analysis of the function of the 1000 most differentially expressed genes (DAVID Database (Huang, Sherman, and Lempicki, 2009)) revealed that those are mainly involved in: extracellular matrix (ECM), membrane proteins, cell adhesion, growth factors and others (Tab. 5.1). Additionally, the large difference in baseline gene expression between the two sub-populations is much higher than any change in gene expression due to light treatment (Fig. 5.3 A).

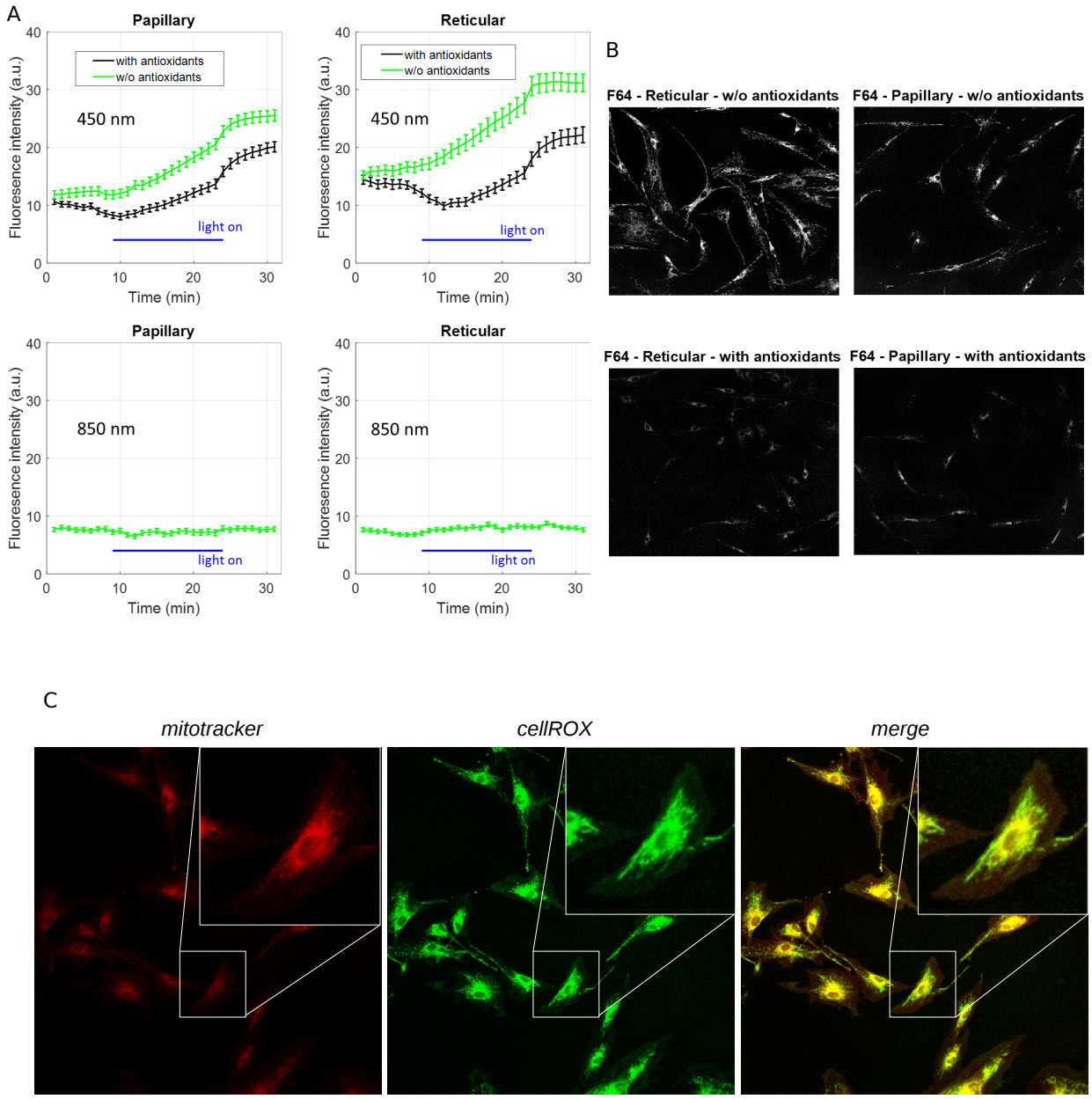

Figure 5.2: (A) Intracellular cellROX intensity before, during and after light treatment in reticular and papillary fibroblasts versus time. Light irradiation was performed with blue (450 nm) and infrared (850 nm) light in presence or absence of antioxidants (vitamin E 10 μM and quercetin 1 μM) in the culture media (N = 2, 3 replicates). Intracellular cellROX intensity was based on the fluorescence intensity of the cellROX dye, and averaged over 10 cells in the field of view using ImageJ Time Series Analyzer plugin. Standard errors are shown in errorbars. Irradiance at 450 nm and 850 nm was set to $30\ mW.cm^{-2}$ (B) Selected fluorescence intensity pictures of cellROX dye in human papillary and reticular fibroblasts at the end of light treatment at 450 nm (t=24 mins) in presence or absence of antioxidants. (C) Selected fluorescence intensity pictures of human papillary fibroblasts (male, 59 yo) with cellROX and Mitotracker in the middle of light treatment (450-nm) time point t=15 mins.

Table 5.1: Keyword analysis of the function of the 1000 most differentially expressed genes in reticular versus papillary fibroblasts populations using DAVID database (Huang, Sherman, and Lempicki, 2009). (N=1, reticular and papillary, 3 replicates)

Keywords	$Number_{gene}$	$Number_{gene}(\%)$	p-value
Phosphoprotein	499	50.3	3.4E-12
Glycoprotein	309	31.1	1.8E-11
Alternative splicing	593	59.7	1.7E-9
Membrane	442	44.5	1.7E-8
Signal	273	27.5	2.2E-8
Angiogenesis	021	02.1	1E-4
Transmembrane helix	324	32.6	2.7E-4
LIM domain	015	01.5	2.6E-4
Secreted	134	13.5	2.5E-4
Transmembrane	324	32.6	2.5E-4
Disease mutation	165	16.6	2.7E-4
Cell adhesion	045	04.5	5E-4
Endoplasmic reticulum	080	08.1	9.1E-4
Disulfide bond	206	20.7	1.6E-3
Actin-binding	029	02.9	2.4E-3
Cardiomyopathy	013	01.3	9.5E-3
Transferase	110	11.1	1E-2
Polymorphism	610	61.4	9.5E-2
Kinase	055	05.5	1.4E-2
Golgi apparatus	059	05.9	1.7E-2
Developmental protein	066	06.6	2.3E-2
Differentiation	049	04.9	3.5E-2
ATP-binding	089	09.0	3.4E-2
Vitamin C	006	00.6	3.4E-2
Extracellular matrix	024	02.4	3.8E-2
Heparin-binding	012	01.2	4.1E-2
Growth factor	015	01.5	5.0E-2
Cell projection	051	05.1	4.8E-2

5.4 Papillary and reticular fibroblasts respond differentially to visible and NIR light

Papillary and reticular fibroblasts' metabolic activity were differentially affected by light treatment, in particular at short visible and NIR wavelengths light, both in hypoxic (2 % oxygen) and and standard oxygen conditions (Fig. 5.3 B). At 450 and 500 nm, the same behavior was observed: the metabolic activity of the reticular

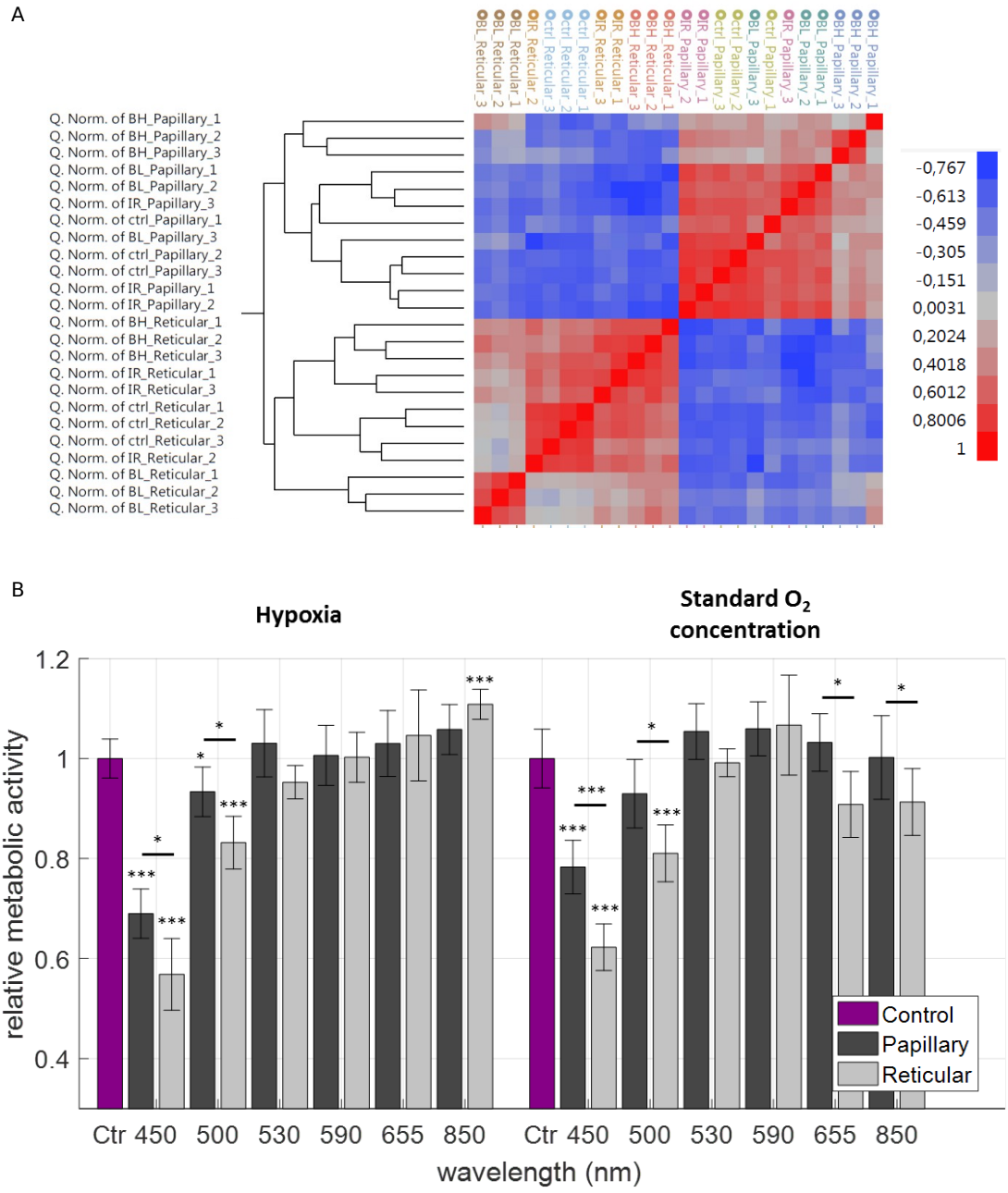

Figure 5.3: (A) Heatmaps of the transcriptome of the light treated samples. Human dermal fibroblasts were treated once per day for three days using blue light at two dose levels (450 nm, low: 2 $J.cm^{-2}$ and high: 30 $J.cm^{-2}$) and NIR light at a single dose level (850 nm, 20 $J.cm^{-2}$). RNA was collected and purified 24 hours after last treatment. Transcriptome analysis was performed (N=1, reticular and papillary, 3 replicates). BH, BL, IR stand for Blue High, Blue Low, NIR. Correlation is evaluated on the signal coming from the gene expression chips. (B) Metabolic activity of human reticular and papillary fibroblasts after light treatment when culture in hypoxia (2%) and standard oxygen concentration (20%). Human dermal fibroblasts were treated once per day for three days using blue light at two dose levels (450/500/530 nm, 30 $J.cm^{-2}$) and 590/655/850 nm, 20 $J.cm^{-2}$). Metabolic activity was measured 24 hours after last treatment (N=2, reticular and papillary, 3 replicates). Standard deviations are shown in errorbars.

subtype was more inhibited by 30 $J.cm^{-2}$ as compared to the papillary subtype. In standard oxygen concentrations there were subpopulation-dependant effects in dermal fibroblasts in response to 655 and 850 nm, where only the reticular subtype was (slightly) inhibited. In hypoxia, the response of the reticular subtype to 655 and 850 nm was reversed as compared to its response in standard oxygen conditions, where the reticular subtype was significantly stimulated by $20J.cm^{-2}$ of 850 nm light. The response of the papillary fibroblasts was however similar at both oxygen level conditions.

Interestingly, a differential response of reticular and papillary was also observed in the results of gene expression and Gene Set Enrichment Analysis using KEGG database (Tab. 5.2). Indeed, light affected a higher number of genes in the reticular subtype than in the papillary subtype for all tested parameters, concurring with the observation of a higher sensitivity of reticular subtype to light (Tab. 5.2).

No strong correlation was found in between the lists of the genes significantly regulated in the three light treated groups in a given sub-population (Fig. 5.4 A B). The highest correlation exists between the human reticular fibroblasts treated with a low dose ($2\ J.cm^{-2}$) and a high dose ($30\ J.cm^{-2}$) of blue light (450-nm), with 441 genes commonly significantly affected in both groups. This could suggest that both dose levels of blue light affect human reticular fibroblasts similarly, yet with a dose-dependant impact.

Additionally, it can be noted that there is a very low correlation between the genes significantly regulated by light in human papillary and reticular fibroblasts for all three tested light parameters. At a given light parameter, the number of genes which are significantly regulated both in the papillary and the reticular groups is less than 10% (Fig. 5.4 C D E).

The GSEA (Gene Set Enrichment Analysis) was performed on the results of the gene expression experiments. GSEA uses as input the list of the fold changes (treated vs. control) of all the genes analyzed, whether they show a significant change or not, and look for their significant collaboration or their common involvement in a pathway according to a pathway database. GSEA then outputs a list of

Table 5.2: Number of genes significantly expressed in light treated groups versus control in both dermal fibroblast subpopulations (N=1, reticular and papillary, 3 replicates). Human dermal fibroblasts were treated once per day for three days using blue light at two dose levels (450 nm, low: 2 $J.cm^{-2}$ and high: 30 $J.cm^{-2}$) and NIR light at a single dose level (850 nm, 20 $J.cm^{-2}$). BHP, BHR, BLP, BLR, IRP and IRR stand for Blue High - Papillary, Blue High - Reticular, Blue Low - Papillary, Blue Low - Reticular, NIR - Papillary, NIR - Reticular.)

Treatment group	Gene up-regulated	Gene down-regulated
BHP	243	371
BHR	314	584
BLP	20	17
BLR	565	1493
IRP	1	9
IRP	44	131

regulated pathway, up- or down, due to each light treatment. Each pathway of the database is associated with a list of genes. First, the pathways significantly regulated by blue light treatment were supported by many more of the genes which are part of the significant gene list (Tabs. Appendix C, 1-9) as compared to the pathway regulated of the NIR light treated groups (Tab. Appendix C, 10-14). It may indicate a stronger confidence in the results of the GSEA after blue light treatment. The GSEA analysis also revealed that more than 15 pathways were regulated in opposed direction in papillary and reticular (Tabs. Appendix C) in particular in response to NIR light (Tabs. Appendix C, 10-14). In particular, the pathways 'Valine, leucine and Isoleucine degradation', ´Butanoate matabolism' and ´Tryptophan metabolism' were up-regulated in papillary fibroblasts and down-regulated in reticular fibroblasts after treatment with NIR light (850 nm, $20\ J.cm^{-2}$).

The pathways regulated by light were clustered to functional groups. As observed before on the metabolic activity (Fig. 5.3 B), the pathways are similarly impacted by blue light parameters in both subpopulations (Tab. 5.4). On the other hand, the response to NIR light is most often opposite for both fibroblast subpopulations (Tab. 5.3).

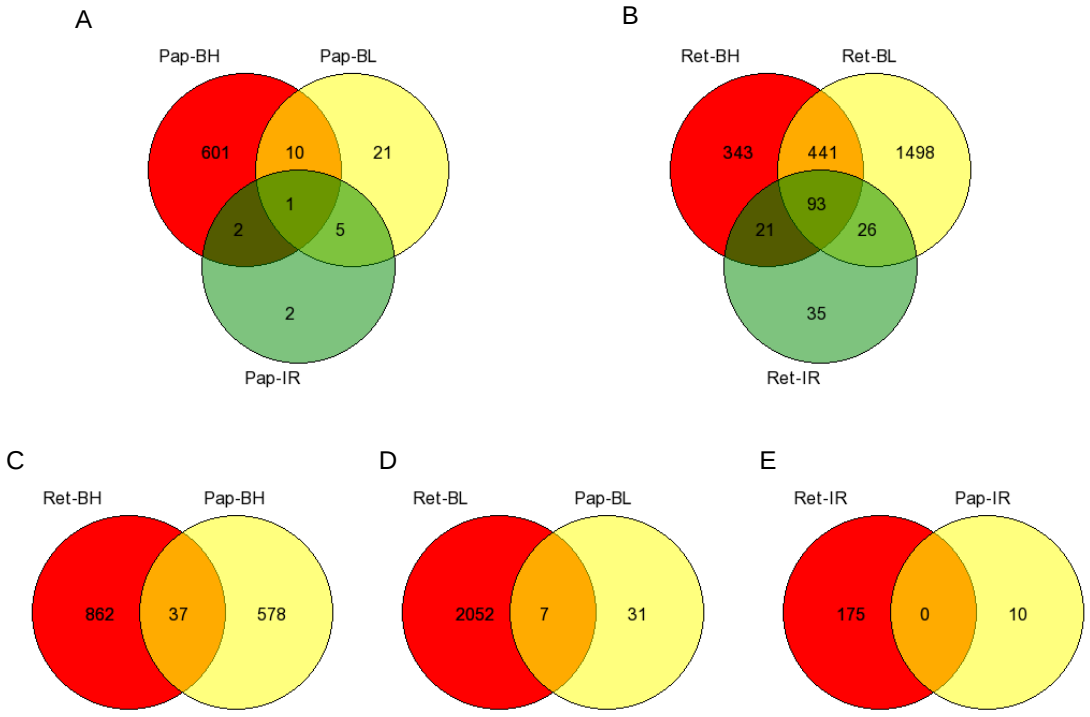

Figure 5.4: Venn diagrams of the significant gene lists treated with $2\ J.cm^{-2}$ and $30\ J.cm^{-2}$ of blue (450 nm) light and $20\ J.cm^{-2}$ of NIR (850 nm) light in (A) human reticular fibroblasts and (B) human papillary fibroblasts. Comparison (Venn diagram) of the significant gene lists of the reticular and papillary fibroblasts treated with (C) $2\ J.cm^{-2}$ of 450-nm light, $30\ J.cm^{-2}$ of 450-nm light and $20\ J.cm^{-2}$ of 850-nm light (N=1, reticular and papillary, 3 replicates). Generated using http://genevenn.sourceforge.net/.

Table 5.3: Clusters of pathways significantly regulated by NIR light treated groups versus control in both dermal fibroblast subpopulations, as obtained from the gene set enrichment analysis, together with the direction of regulation and the number of pathways regulated printed inside parenthesis (N=1, reticular and papillary, 3 replicates). Human dermal fibroblasts were treated once per day for three days using blue light at a single dose level (850 nm, 20 $J.cm^{-2}$).

Cluster	Papillary	Reticular
Metabolism	$\uparrow(9)$	$\downarrow(1)$
ECM proteins, adherence	$\downarrow(7)$	$\downarrow(1)$
Xenobiotics metabolism	$\uparrow(3)$	$\downarrow(3)$
Proteostasis	$\uparrow(3)$	$\downarrow(2)$
Signalling	$\downarrow(20)$	
Hormone biosynthesis	$\downarrow(4)$	
Protein machinery	$\uparrow(3)$	$\downarrow(3)$

5.5 450-nm light downregulates proliferation, metabolism and protein synthesis in papillary and reticular fibroblasts

The cell cycle pathway was downregulated after treatment with 450-nm light at two dose levels 2 and 30 $J.cm^{-2}$ in both reticular and papillary fibroblasts (Tab. 5.4). This corroborates with the inhibition of Alamar signal after blue light treatment observed above, also in both sub-populations (Fig. 5.3 B). Not only the cell cycle, but multiple pathways involved in metabolism, protein synthesis and ECM were downregulated by 450-nm light (Tab. 5.4, high dose). Pathways downregulated by blue light (450 nm) in reticular and papillary fibroblasts include the following: ´Aminoacyl-t-RNA biosynthesis´, ´N-glycan biosynthesis´, ´Butanoate metabolism´, ´Citrate cycle (TCA cycle)´ and others.

In comparison to the papillary fibroblasts' response, the reticular fibroblasts transcriptome showed a more pronounced alteration due to 450-nm light at high dose ($30\ J.cm^{-2}$) compared to low dose ($2\ J.cm^{-2}$). Indeed, the downregulation of three important pathways (Mismatch Repair, RNA degradation, Homologous recombination) was observed after treatment with a high dose of blue light only in the reticular subtype. This might indicate a damage effect of blue light for vital cell functions.

5.6 450-nm light downregulates the cell cycle and TGF-beta signalling pathway in reticular and papillary fibroblasts

450-nm light downregulated the cell cycle pathway in reticular and papillary fibroblasts at both tested dose level $2\ J.cm^{-2}$ and $30\ J.cm^{-2}$ (Tabs. Appendix C, 1-9). Many genes are involved in the cell cycle pathway, however the downregulation of

Table 5.4: Clusters of pathways significantly regulated by blue light treated groups versus control in both dermal fibroblast subpopulations as obtained from the gene set enrichment analysis together with the direction of regulation and the number of pathways regulated printed inside parenthesis (N=1, reticular and papillary, 3 replicates). Human dermal fibroblasts were treated once per day for three days using blue light at two dose levels (450 nm, low: 2 $J.cm^{-2}$ and high: 30 $J.cm^{-2}$).)

Dose	Cluster	Papillary	Reticular
High	Proliferation	$\downarrow (1)$	$\downarrow (1)$
	Steroid Hormone	$\uparrow (1)$	
	Signalling	$\downarrow (1)$	
	Proteostasis	$\uparrow (2)$	$\downarrow (2)$
	Protein machinery	$\downarrow (3)$	$\downarrow (7)$
	Xenobiotics metabolism	$\uparrow (3)$	$\downarrow (3)$
	Extracellular matrix proteins	$\uparrow (2)$	
	Metabolism	$\uparrow (2)/\downarrow (2)$	$\downarrow (10)$
	Repair		$\downarrow (3)$
Low	Proliferation	$\downarrow (1)$	$\downarrow (2)$
	Proteostasis	$\uparrow (3)$	
	Protein machinery	$\uparrow (4)$	$\downarrow (1)$
	Xenobiotics metabolism	$\uparrow (1)$	$\uparrow (1)$
	Metabolism	$\uparrow (2)$	
	ECM and adherence	$\downarrow (8)$	
	Hormone biosynthesis	$\downarrow (6)$	
	Signalling	$\downarrow (18)$	$\downarrow (1)$

CDK1, *CDC16*, *CDC20*, *CDKN2C*, *PLK1*, *CHEK2*, *BUB1*, *BUB1B*, *CCNH* as well as the up-regulation of *MAD1L1* was observed in more than one transcriptome of the treated groups.

The transcriptome of human reticular and papillary fibroblasts also revealed the downregulation of several genes involved in the TGF-beta signalling pathway after treatment by 450-nm light at $2\ J.cm^{-2}$ and $30\ J.cm^{-2}$ for papillary subtype and at $2\ J.cm^{-2}$ in reticular subtype (Tabs. S1, S2, S3 and S4). A high dose of blue light (450 nm) also downregulated the TGF-beta signalling pathway in reticular subtype (NES = -1.4), however the false discovery rate was slightly high (False Discovery Rate FDR = 0.12) and therefore it was not included in the reported pathways where a threshold was set to 0.1 for the FDR. While many genes are involved in the pathway, the downregulation of *TGFB2*, *NOG*, *INHBB*, *FST*, *SMURF2* and *ID4* was specifically noted.

5.7 450-nm light inhibits collagen biosynthesis at mRNA and protein levels

Additionally, the procollagen I content in the supernatant of the dermal fibroblasts was assessed 72 hours after the last light treatment. Light at 450 nm inhibited the procollagen production in human papillary and reticular fibroblasts in a dose-dependent manner (Fig. 5.5 B). This correlates with the transcriptome analysis of the corresponding treated groups. Indeed, several genes involved in the collagen biosynthesis were downregulated by 450-nm light (collagen chain, integrins), and importantly, collagenase *MMP1* was up-regulated in the same groups (Fig. 5.5 A).

5.8 Transcriptome analysis is validated by qPCR

The results obtained using microarray analysis were validated using qPCR on relevant genes (Fig. 5.6). The criteria for selection were the following: relevance for ageing and wound healing, statistical significance, high fold change and at least one gene from every treatment/subpopulation group.

5.9 Concluding remarks and discussion

This study revealed that the dose response of human dermal fibroblasts to light shows neutral, effective and cytotoxic dose ranges. These dose ranges have a clear dependence on the wavelength of irradiation. Particularly, the dose response curves showed a higher sensitivity of dermal fibroblasts to short visible wavelengths as compared to long visible wavelengths, based on the relative changes of their metabolic activity after light treatment. This might suggest a stronger absorption of short visible wavelength by the cells and might even correlate with the absorption spectrum of cytochrome c oxydase, where absorption is overall decreasing from UV to NIR with multiple local peaks (Mignon et al., 2016b).

This project confirmed the involvement of ROS as part of the immediate effect of

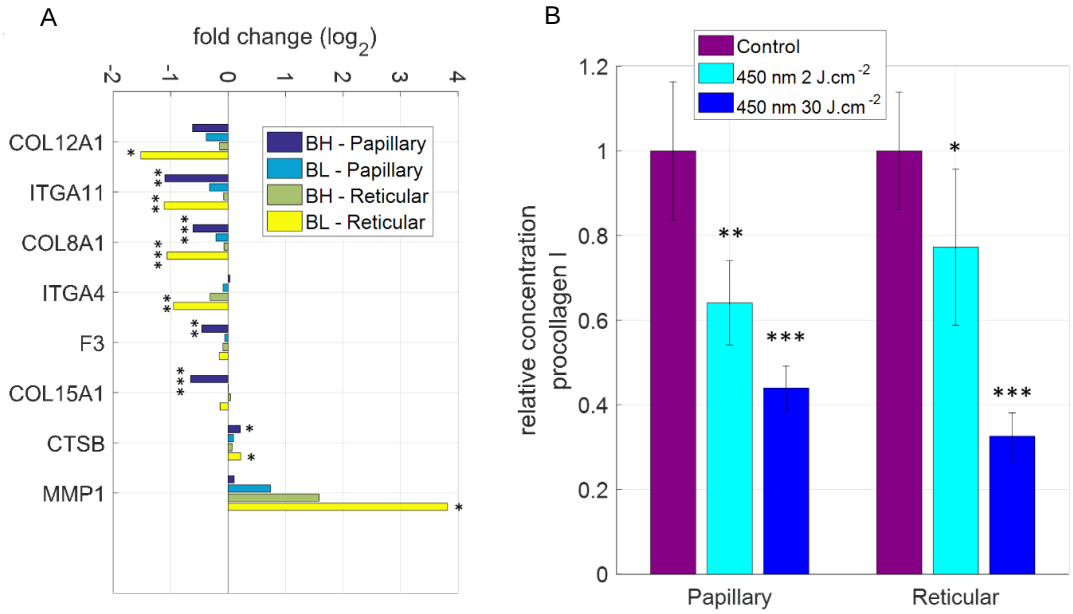

Figure 5.5: (A) Genes involved in collagen biosynthesis (Reactome R-HSA-1650814) significantly impact by blue light (450 nm) at two dose levels (2 $J.cm^{-2}$ and 30 $J.cm^{-2}$). Human dermal fibroblasts were treated once per day for three days using light. The RNA used for gene expression was collected 24 hours after the last light treatment (N=1, reticular and papillary, 3 replicates). (B) Human procollagen I content in the supernatants of human papillary and reticular fibroblasts after blue light treatment (450 nm, 2 $J.cm^{-2}$ and 30 $J.cm^{-2}$). Human dermal fibroblasts were treated once per day for three days using blue light. Fresh culture medium was replenished after each light treatment. Supernatants were collected 72 hours after the last light treatment (N=2, reticular and papillary, 3 replicates). Standard deviations are shown in errorbars.

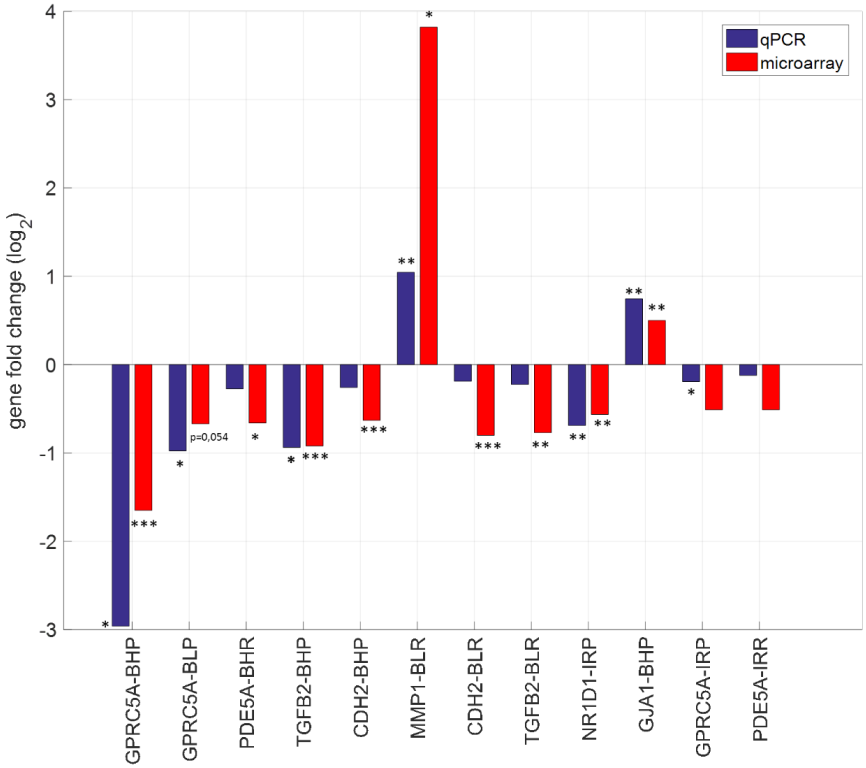

Figure 5.6: Comparison of the expression of relevant genes evaluated with microarray technique (Affymetrix Chips Human Transcriptome Array 2.0) and with qPCR technique (N=1, reticular and papillary, 3 replicates).

light on dermal fibroblasts. The direct induction of intracellular ROS due to blue light treatment was observed, and the induced ROS were highly colocalized (but not fully) with the mitochondria in the perinuclear area. This would also supports the involvement of mitochondria as one of the primary location of reception of light in human skin cells. Interestingly, NIR did not induce any measurable intracellular ROS.

The large production of intracellular ROS under blue light also corroborates with the higher impact of short visible wavelengths light on the cells' metabolic activity as compared to longer wavelengths. ROS are known to be harmful to cells when present in excess (Kawagishi and Finkel, 2014). The gene transcriptome analysis also showed that blue light negatively affects proliferation, metabolism and protein synthesis in human dermal fibroblasts. Similarly, a harmful impact was observed in the reticular subpopulation where important repair pathways were affected after a high dose of blue light. These negative effects are most probably due to excess ROS.

Overall it is now clear that the induction of ROS is one of the main actors of the negative action of blue light. The induction of ROS may have potentially been triggered by the flavoproteins (Ohara, Fujikura, and Fujiwara, 2003; Liebel et al., 2012) present in the intracellular and extracellular spaces. However, there is still a possibility that blue light is being absorbed by other photoacceptors in the cells (Mignon et al., 2016b), and that ROS induction is not the only downstream mechanism triggered by blue light. This leaves room for further experiment where antioxidants would be systematically added to the culture medium to avoid the negative impact of blue light.

The involvement of ROS in the action of blue light is somewhat reminiscent of the well-known action of UV radiation on human skin and skin cell populations (Rinnerthaler et al., 2015; Pillai, Oresajo, and Hayward, 2005; Hanson and Clegg, 2002; Han et al., 2005; Quan et al., 2002; Young, 2006). This project brings evidence that the action of UV-free blue light have some similarities with the action of UV in the skin. In particular, this project findings are in agreement with the conclu-

sions that Liebel et al. drew from their experiments (Liebel et al., 2012). Indeed, they also observed the induction of ROS and *MMP1* after irradiation with visible light in human skin equivalents. They concluded that visible light is therefore contributing to photoaging. Additionally, it has been reported that UV radiation has downregulated the TGF-beta signalling pathway, including the down-regulation of *TGFB2*, in human skin *in vivo* (Quan et al., 2002; Han et al., 2005). In this project, the significant down-regulation of *TGFB2* was noted after treatment with UV-free blue light (450 nm). Thus, it may be recommended to take care when using blue light as a PBM therapy in human as it may have potential harmful effect.

On the other end of the electromagnetic spectrum, NIR light had more positive effects. GSEA after NIR light treatment revealed positive regulation of protein synthesis and metabolism pathways without any indication of damage at the RNA level. At the cellular level, the reticular subpopulation was stimulated after NIR light treatment, in hypoxic conditions (i.e., tissue-similar) only. Furthermore, NIR light was not associated with a large amount of intracellular ROS.

Over the course of this project the fibroblasts of reticular subpopulation exhibited greater sensitivity to light treatment. At the gene expression level, there was a much higher number of genes significantly altered by all three tested light parameters in reticular versus papillary fibroblasts. At the pathway level, the presence of 'damage' pathways was noted only for the reticular subtype after treatment with $30\ J.cm^{-2}$ of blue light (450 nm). At the cellular level, short visible wavelengths exhibited a more inhibitory effect on the reticular subpopulation and a higher responsiveness to NIR light was observed on the reticular subtype as well. A possible explanation could be that the deeper localization of the reticular subtype in the skin might have evolved in an environment with lower light background as compared to the much more superficially located papillary subtype, explaining the former's higher sensitivity when stimulated by electromagnetic radiations.

This project is also an illustrative example of the complexity and specificity of biological models, even *in vitro*. Reticular and papillary fibroblasts would most probably be approximated as dermal fibroblasts or merged/pooled as a single dermal

fibroblast population by most research studies in photobiomodulation. However, the results presented in this chapter, in particular the gene expression in both lineages, clearly show that these are two very distinct cell subpopulations. This is already demonstrated further in the literature (Driskell et al., 2013; Janson et al., 2013).

One potential limitations of this thesis however, is in the gene expression interpretation. Indeed, some of the pathways which were highlighted as significantly altered as a gene set by the GSEA were associated with few changes that were significant at the gene level involved in the pathways. Thus, care is needed when interpreting individual gene expression results. Importantly, the latter revealed similar outcomes as the other assays. In particular, the impacts of light on collagen production at the RNA and protein level concur. While at the RNA level a significant down-regulation of genes involved in collagen biosynthesis and a up-regulation of collagenase was observed, at the protein level a down-regulation of the procollagen I content in the supernatants of the cells was measured. Blue light might therefore stimulate the expression of MMPs proteins leading to reduction of collagen production. Similarly the GSEA analysis revealed concurring results with the assessment of the metabolic activity at the cellular level. Indeed, the down-regulation of cell proliferation and metabolism pathways showed up in the GSEA results, and it is clear that both would be expected to result in a downregulation of the Alamar Blue signal.

5.10 Summary

In this chapter, the response of human dermal fibroblasts lineages (reticular and papillary) to visible and NIR light was investigated based on genetic expression, metabolic activity and collagen production. Additionally, the induction of ROS under light treatment was monitored live *in vitro*. The main results are:

- Irradiation with 450-nm light induced the production of ROS in live human dermal fibroblasts *in vitro*. The creation of ROS was proportional to the light

dose. The addition of anti-oxidants to the culture medium delayed the induction of ROS. The ROS were found to be created in the close vicinity of mitochondria in the cells.

- Short visible wavelength light exerted a bi-phasic dose response on human dermal fibroblasts based on their metabolic activity. Neutral, inhibitory and cytotoxic effects were observed with increasing light dose.

- 450-nm light down-regulated the procollagen I production in human dermal fibroblasts *in vitro*. This was associated with the down-regulation of integrins and up-regulation of MMP1 at the gene level.

- Gene expression study revealed a strong inhibitory effect of short visible wavelength light on human dermal fibroblasts. Metabolism and protein synthesis pathways were down-regulated after treatment with 450-nm light.

Chapter 6: Investigation into the origin of variability in the optical properties of different skin components for a more accurate prediction of light propagation in skin

The literature review presented in Chapter 3 revealed a need for modeling tools for the translation of photobiomodulation research to *in vivo* applications. A specific light parameter obtained *in vitro* will not be directly applied on top of the skin. Due to the strong absorption and scattering properties of the skin, light will have a disturbed path in the skin. The optical treatment parameter applied on top of the skin will thus be quantitatively different from what is received at different location within the skin. Roughly, the deeper inside the skin, the higher will be the reduction in irradiance and dose. This is illustrated in chapter 3 (Fig. 3.3) where it is possible to see that the three optical beams from the three light-based devices for hair regrowth are highly absorbed and scattered by their propagation in the skin. It was even demonstrated that the optical treatment parameters of the devices on top of the skin are quantitatively much higher than the corresponding amounts of light reaching the hair bulb. This translation issue between the input parameter on top of the skin and the actual treatment parameter reaching the desired location inside the skin remains to be addressed. Any optical treatment parameter obtained in a *in vitro* study would need to pass by a translation calculation before being able to apply the equivalent treatment parameter *ex vivo* or *in vivo*.

Therefore, there is a strong need for a predictive model allowing the direct understanding of how much light will reach for every location inside the skin. This may

be filled in by a Monte Carlo optical model.

Here a study aiming at characterizing the accuracy with which the prediction of light propagation in human skin is performed with a Monte Carlo optical model is presented at relevant wavelengths for Photobiomodulation. In particular this project improves the selection of datasets of optical properties of the skin components required for the proper functioning of the model.

In dermatology, optical energy has been used for decades both in diagnosis and in treatment. Application of light for therapeutic purposes covers both cosmetics and medical domains, and ranges from removal of vascular and pigmentary lesions, unwanted hair, (Svaasand et al., 1995) and tattoo (Kupermanbeade, Levine, and Ashinoff, 2001) to wound healing (Woodruff et al., 2004), scar resurfacing (Preissig, Hamilton, and Markus, 2012), skin rejuvenation (Mignon et al., 2016e; Varghese et al., 2016), and hair loss (Lanzafame et al., 2014) and more. There are already effective therapy regimes which rely on all three types of light-tissue interactions (photomechanical, photothermal and photochemical), which were very successfully translated in a large range of professional and home-use devices (Metelitsa and Green, 2011; Raulin, Greve, and Grema, 2003). Light interactions with tissue depend on the wavelength, the optical power density and the exposure time (Jacques, 1992). With ongoing quest in developing new light-based therapies and further mastering the parameters space of the existing ones towards even higher efficacy and safety, it is thus essential to assess the amount of light reaching the targets inside the tissue to provide accurate treatment. Several tools exist to predict the propagation of light in tissue. They include the solutions of the radiative transfer equation under strict approximation, the analytical application of the random walk theory to biological tissue (Gandjbakhche, Bonner, and Nossal, 1992), and the Monte Carlo methods (Wang, Jacques, and Zheng, 1995).

Monte Carlo methods gained most popularity and trust and are highly appreciated when there is a need in modeling light propagation in inhomogeneous tissues with complex geometry. They are commonly used in dermatological applications because the structure of the skin is complex, where the optical properties are rapidly

varying in lateral and axial spatial dimensions. The Monte Carlo method relies on the random sampling of the trajectories of photon packets propagating in the medium. The calculations of the trajectories are based on the random occurrence of scattering and absorbing events in the turbid medium. The basic requirement is thus the knowledge of the optical properties (absorption and scattering) associated with the tissue structure. The skin is generally approximated as a pile of infinite layers with homogeneous properties such as the epidermis, the dermis, the subcutaneous fat layer and sometime blood capillaries (Meglinski and Matcher, 2002). The successful functioning of the method in delivering value for clinical applications in dermatology (e.g. when selecting optical treatment parameters for *in vivo* studies on human based on extrapolation of settings shown effective using *in vitro* studies on cells) thus requires the accurate knowledge of the optical properties of the skin layers.

Although the literature contains numerous articles with the data on the optical properties of the skin layers and its appendages, they are unfortunately quantitatively inconsistent when comparing individual reports by different research investigators. It is known that the disparities between the quantitative values of the optical properties will create much variability in the quantitative predictions of photon density in tissue, while keeping all other parameter fixed (Mignon et al., 2016a). The explanation is straightforward as in the model the absorption of photon is, at the first order, proportional to the absorption coefficient (skin is a turbid media with absorption much smaller than scattering, $\mu_A << \mu_S$) (Wang, Jacques, and Zheng, 1995). Any large variability in the absorption coefficient of the layer will largely affect the calculated photon density. Therefore, the wide range of the optical properties of the skin layers reported in the literature (up to 100 fold (Mignon et al., 2016a)) not only poses a problem when selecting treatment parameters but also raises a question about the validity of the references reporting the optical properties of the skin layers. Therefore, a better understanding of the origin of the spread in the skin layers optical properties values could lead to a selection of a more narrow optical window, i.e., a set of the optical properties more closely

resembling the ‘true’ biological values resulting in stronger predicting power of the model and eventually delivering more reliable output for prediction of parameters for clinical applications.

In this project approach, a simple yet a very powerful fact (Jacques, 2013) was followed, stating that the absorption and scattering of any tissue, and particularly of any homogeneous skin layer, should simply find their origins in the biological composition of the layer. The components of the epidermis, dermis and subcutaneous fat layer are known,(Jacques, 2013; Raicu and Feldman, 2015) and they have known absorption spectrum with prominent absorption peaks (Jacques, 1996). This information should provide a critical help in order to select trust-worthy dataset(s) from the existing literature using objective arguments rather than trying to quantify the optical values *de novo*.

This idea was implemented on practice by, in the first instance, evaluating each of the reported dataset in terms of presence of the absorption bands of the strongest chromophores over visible to NIR range, specific for each of the skin layers: melanin - in epidermis, haemoglobin and water - in dermis, and water and lipids – in subcutaneous fat. Subsequently, the sample preparation and handling during optical measurements was also extracted trying to link differences in the reported value with variations in experimental lab protocol. Besides, coherence or clustering between the datasets originating from different research investigations was analyzed.

In the second instance, after the sets of the optical properties were narrowed down, Monte Carlo simulation of light propagation in the skin layers were performed and the impact of the remaining spread in the optical properties on the resulting photon densities was evaluated. As a final verification step towards recommending specific sets of the optical properties the diffuse reflectance estimated on the simulations was compared with an independent dataset of *in vivo* measurements of the diffuse reflectance performed in human subjects.

6.1 Optical properties of the skin layers

The methods used to quantify the optical properties of the skin layers are categorized in two groups: mathematical models based on molecular composition of a particular layer and experimental measurements (Table, 6.3 and 6.4).

6.1.1 Mathematical models

In the literature search 5 mathematical models were found (Jacques, 2013; Meglinski and Matcher, 2002; Altshuler, Smirnov, and Yaroslavsky, 2005; Svaasand et al., 1995; Douven and Lucassen, 2000) reporting analytical expressions to derive the optical properties of skin layers. Chronologically, the model of Svaasand (Svaasand et al., 1995) was the first one, where later on, Douven (Douven and Lucassen, 2000), Jacques (Jacques, 2013), Meglinski (Meglinski and Matcher, 2002) and Altshuler (Altshuler, Smirnov, and Yaroslavsky, 2005) brought further modifications and improvements.

All mathematical models considered here are built on a similar concept: quantification of the absorption coefficient of each of the skin layers is derived based on the baseline absorption i.e. the absorption of a skin layer without its major absorber(s), and, on the contribution of the major absorber(s) of the layer, which in their turn can be measured or modeled separately (Table 6.1). There are different degrees of complexity between the models. Indeed, the older models such as the ones of Jacques (Jacques, 2013) or Svaasand (Svaasand et al., 1995) have a lower number of factors taken into account as compared to the models of Altshuler (Altshuler, Smirnov, and Yaroslavsky, 2005) and Meglinski (Meglinski and Matcher, 2002). In this project the model of Douven (Douven and Lucassen, 2000) was omitted as in a nutshell it represents an intermediate state between the two more extreme models, the one by Svaasand (Svaasand et al., 1995) and the one by Altshuler (Altshuler, Smirnov, and Yaroslavsky, 2005). Logically and as expected, there are also many links between the models. In particular, the

background measurements of the baseline absorption or scattering of the skin proposed by Jacques (Jacques, 2013) are re-used in the models of Meglinski (Meglinski and Matcher, 2002) and Altshuler (Altshuler, Smirnov, and Yaroslavsky, 2005). Some of the mathematical models also made the choice to have (partly) an empirical quantification of the scattering coefficient such as Svaasand (Svaasand et al., 1995) or Altshuler (Altshuler, Smirnov, and Yaroslavsky, 2005). The similarity of the approach to quantify the optical properties of the skin layers between the models is directly visible based on on the consistency of the resulting values of the optical properties (Fig. 6.1 dashed-lines). In particular, the absorption coefficients of the epidermis and dermis are almost quantitatively agreeing.

6.1.2 Experimental measurements

In total 6 references (Anderson and Parrish, 1981; Bashkatov et al., 2005; Salomatina et al., 2006; Simpson et al., 1998; Wan et al., 1981; Marchesini et al., 1992) were found reporting the indirect measurements of the absorption and scattering coefficients of the skin layers (Tables 6.3 and 6.4). The skin type used in most studies was classified as Caucasian or fair skin, with the exception of the studies of Anderson (Anderson and Parrish, 1981) and Salomatina (Salomatina et al., 2006) where the skin type of the sample was not reported. The tissue samples were obtained either after surgery or post-mortem, where measurements were performed within different time frame, ranging from 1 hour post-surgery to 5 days after excision (Tables 6.3 and 6.4). The body location of the samples was also highly variable and included most of the body and face tissues such as abdominal, groin or breast. The handling of the skin before and during the measurement was also not consistent between the studies; the separation of layers was either performed via mechanical means with the help of a razor or thermally; the preparation of the sample included various steps such as rinsing or not with saline or the addition of mechanical elements to stabilize the sample.

All these differences are expected to have not only an impact on the actual bio-

logical state of the sample such as hydration, swelling, amount of blood, degree of cellular necrosis, but also introduce uncertainties about surface roughness and geometry of a tissue slab, parameters of crucial importance for optical measurements. As a result, not only the results of the optical measurements performed using tissue samples prepared under different conditions will differ but also the results of the back calculation, eventually impacting the estimated optical properties of the skin layers.

What was consistent in all bibliographic references is that the estimation of the optical properties was done based on the measurement of diffuse reflectance and transmittance of the sample. On the contrary, the back-calculation methods, performed to quantify the absorption and scattering coefficients, differed from one reference study to the other. They included the solution of the one dimensional diffusion approximation, the Kubelka-Munk model and the inverse Monte Carlo method.

These differences between the methods applied to estimate the optical properties of the skin layers, are reflected by the reported quantitative values (Fig. 6.1, full-lines), where there is little or, in a more strict sense, no quantitative agreement between the results (Fig. 6.1).

6.2 Origin of the spread in the optical properties

A large spread between the reported values of the optical absorption and scattering coefficient showed up (Fig. 6.1), which was extending up to 100-fold for the same skin layer between different literature sources.

6.2.1 Absorption coefficient of the epidermis

Two clusters in the reported quantitative values of the absorption coefficient of the epidermis are observable. The values obtained using mathematical models of Jacques (Jacques, 2013), Meglinski (Meglinski and Matcher, 2002) and Alt-

shuler (Altshuler, Smirnov, and Yaroslavsky, 2005) and those obtained based on the empirical measurement of Wan (Wan et al., 1981) form a first cluster, while that obtained using the model of Svaasand (Svaasand et al., 1995) and the measurements by Marchesini (Marchesini et al., 1992) and Salomatina (Salomatina et al., 2006) form another cluster, having in general a lower absorption (Fig. 6.1, A).

The absorption of the epidermis in the visible and NIR spectral range originates mainly due to the melanin. The human Caucasian epidermis (light-pigmented) will contain on average 5 % of melanosomes (Jacques, 1996), with large variabilities within individuals. Thus, theoretically, at least 5% of the absorption of melanin should be seen back in the absorption coefficient of the epidermis. The melanin absorption and the melanosome absorption spectrum were measured (Jacques and McAuliffe, 1991), and it shows absorption higher than $100\ cm^{-1}$ over the whole visible/NIR range. Using these data as a rational, one could logically set a limit equal to $5\ cm^{-1}$ for the value of the absorption coefficient of the epidermis. The epidermal absorption coefficients of the datasets of Salomatina (Salomatina et al., 2006), Svaasand (Svaasand et al., 1995) and Marchesini (Marchesini et al., 1992) are much lower (Fig. 6.1, A) than this ultimate limit.

Additionally, the epidermal absorption coefficient of the model of Svaasand (Svaasand et al., 1995) appeared quantitatively lower as compared to all the other mathematical models, despite showing a consistent trend for the variation of the coefficient with wavelength (Fig. 6.1, A, dashed lines).

Two reasons which could explain this shift towards a lower absorption level were identified. First, Svaasand (Svaasand et al., 1995) selected a single value $0.25\ cm^{-1}$ to model the background absorption of the epidermis (absorption without pigments present). It corresponds to the absorption of low-absorbing tissue (uterine, eye) in the wavelength range 600-900 nm and it is assumed to be independent of wavelength (Table 6.1). In contrast to that assumption, Jacques (Jacques, 2013), Altshuler (Altshuler, Smirnov, and Yaroslavsky, 2005) and Meglinski (Meglinski and Matcher, 2002) relied on the wavelength-dependent absorption of *ex vivo* neo-

natal skin sample, which showed much higher number as compared to a single value used by Svaasand, in particular in the low wavelength range (10 times higher at 450 nm).

Second, while Jacques (Jacques, 2013), Altshuler (Altshuler, Smirnov, and Yaroslavsky, 2005) and Meglinski (Meglinski and Matcher, 2002) were directly using the absorption of melanin, Svaasand (Svaasand et al., 1995) used the absorption of melanin at 694 nm and extrapolated this value over the spectral range using $1/^4$ law to represent the variation with wavelength. The overall absorption level is then strongly dependent on the empirical value of the absorption of melanin at 694 nm. Among the experimental datasets (Wan (Wan et al., 1981), Salomatina (Salomatina et al., 2006) and Marchesini (Marchesini et al., 1992)), the measurement of Marchesini (Marchesini et al., 1992) is standing out because of its low absorption level and the steep variation with wavelength (Fig. 6.1, A). This steep decrease in the NIR range is in contradiction with slowly decreasing absorption spectrum of melanin over the visible to NIR band (Jacques and McAuliffe, 1991; Jacques, 1996).

The sample handling reported by all three references (Wan (Wan et al., 1981), Salomatina (Salomatina et al., 2006) and Marchesini (Marchesini et al., 1992)) differ in one important aspect, the addition of saline to the sample before measurement. This step was present in the methods of Salomatina (Salomatina et al., 2006) and Marchesini (Marchesini et al., 1992) (Tables 6.3 and 6.4). It might be possible that the saline buffer has increased the volume of the epidermis sample and therefore reduced the absorption per unit of length as well as affected tissue scattering and surface roughness, therefore reducing the global absorption level of the coefficients of Salomatina (Salomatina et al., 2006) and Marchesini (Marchesini et al., 1992).

It appears that only the mathematical models of Jacques (Jacques, 2013), Meglinski (Meglinski and Matcher, 2002) and Altshuler (Altshuler, Smirnov, and Yaroslavsky, 2005) and the experimental dataset of Wan (Wan et al., 1981) are coherent in terms of both basic spectroscopic arguments and order of magnitude that one

can expect from the absorption of the epidermis.

6.2.2 Absorption coefficient of the dermis

The main absorbing components of the dermis are blood (dominating along visible spectrum) and water (which is becoming to be prominent in the NIR region). Therefore, one should expect that the estimated absorption spectrum of human blood containing dermis should show the characteristic absorption peaks of the haemoglobin, specifically at 420 nm and 540 nm in the short wavelength region of the visible spectrum (Roggan et al., 1999), and that of water in the NIR area with a specific absorption band at 970 nm (Hale and Querry, 1973).

All the mathematical models are quantitatively agreeing and are showing the expected absorption peaks in the visible and NIR part of the spectrum (Fig. 6.1, B dashed-lines). Also the absorption coefficient of Simpson et al. (Simpson et al., 1998) derived from indirect optical measurements in the range 600-1000 nm is showing the expected water peak at 970 nm and quantitatively agreeing with the mathematical models (Fig. 6.1, B).

On the contrary, experimentally obtained datasets of Salomatina (Salomatina et al., 2006) and Anderson (Anderson and Parrish, 1981) do not reveal any of these expected spectral properties (Fig. 6.1, B) and show higher global absorption level than most datasets. A possible explanation could be that the rinsing with PBS and the rehydration with saline may have altered the content of the dermis and therefore the measurement of Salomatina (Salomatina et al., 2006) (Tables 6.1, 6.3 and 6.4).

6.2.3 Absorption coefficient of the subcutaneous fat layer

The main components of the subcutaneous fat layer are lipids and water (Woodard and White, 1986). The absorption spectrum of purified pig fat (Veen et al., 2004) was reported and shows a characteristic absorption peak at 930 nm.

No distinct clusters of the reported optical properties of subcutaneous (Fig. 6.1,

C) was observed, except for a quantitative agreement of the model of Meglinski (Meglinski and Matcher, 2002) and the experimental measurement of Simpson (Simpson et al., 1998) in the spectral range 600-1000 nm (Fig. 6.1, C).

Only the dataset of Simpson (Simpson et al., 1998) is showing the fat-related absorption peak at 930 nm (Fig. 6.1, C). The model of Meglinski (Meglinski and Matcher, 2002) does not show a specific fat-related absorption features but is quantitatively agreeing with the measurements of Simpson (Simpson et al., 1998). Strangely Meglinski (Meglinski and Matcher, 2002) did not consider the fat as an absorbing component of the subcutaneous layer, and only considered blood and water (composition includes 5 % blood and 70 % water and no lipids). This perhaps explains why in his dataset the fat-related absorption peak was not be present. Naturally, given the molecular composition of the subcutis, one should genuinely expect that a significant contribution of fat absorption (Veen et al., 2004). Following the general equation for the absorption of a layer in the review by Jacques (Jacques, 2013), a possible update when considering the absorption of the subcutaneous fat layer in the model of Meglinski (Meglinski and Matcher, 2002) would be to use the purified fat absorption spectrum from van Veen (Veen et al., 2004).

6.2.4 Scattering coefficient of all layers

The values of the scattering coefficient reported in analyzed literature references are not forming any cluster for any layer (Fig. 6.1, D, E, F). All references tend to show a relative agreement regarding the variation of their coefficient with wavelength.

6.3 Selection of the datasets of optical properties

As stated earlier the purpose of this study was to select subsets of the optical properties of the skin layers, presumably most closely representing realistic values

Author	Layer	Absorbers / scatterers included	Supporting bibliographic reference
Jacques	Epidermis	Skin baseline and melanin	Skin baseline absorption extracted from absorption measurement on *in vitro* neonatal skin samples using an integrating sphere (Jacques and McAuliffe, 1991). The absorption of melanin was measured (Jacques, Alter, and Prahl, 1987). Volume fraction of the epidermis filled by melanin is set to 4% (Jacques and McAuliffe, 1991)
	Dermis	Skin baseline and blood	Skin baseline absorption extracted from absorption measurement on *in vitro* neonatal skin samples using an integrating sphere (Jacques and McAuliffe, 1991). The absorption of blood is taken from literature based on the absorption of oxy- and deoxy-haemoglobin (Jacques, 2013). Volume fraction of the dermis filled by blood is set to 2%
Svaasand	Epidermis	Skin baseline and melanin	Skin baseline absorption is set as a single values corresponding to the absorption,of low-absorbing tissue such as human eye and uterine at 694 nm (Svaasand et al., 1995),The absorption of melanin is set to an empirical value at 694 nm (derived from skin reflectance measurement) and the variation with wavelength is assumed to be a law in ($1/\lambda^4$)
	Dermis	Skin baseline and blood	Skin baseline absorption is set as a single values corresponding to the absorption of low-absorbing tissue such as human eye and uterine at 694 nm. Blood absorption is set via a proper empirical analytical approximation. Volume fraction of the dermis occupied by blood is set to 1%
Meglinski	Any layer	Skin baseline, blood, water, melanin	Skin baseline absorption extracted from absorption measurement on in vitro neonatal skin samples using an integrating sphere35. Melanin absorption is extracted from Jacques12 measurement. Oxy-,and deoxy- haemoglobin absorption14. The absorption of water is extracted from Jacques (Jacques and McAuliffe, 1991). Blood, water contents estimated from multiple reports, see article for details.
Altshuler	Any layer	Skin baseline, blood, water, melanin	Skin baseline absorption is assumed independent of wavelength and was derived from an empirical measurement of the skin reflectance at 800nm. The absorption of blood is based on Jacques (Jacques and McAuliffe, 1991). Water absorption (Jacques, 2013). Melanin absorption is obtained from measurement of the optical density of the epidermis and other (Jacques, 2013)

Table 6.1: Factors included in the mathematical models for estimating the optical properties of the skin layers in the bibliographic references included in the study (absorption coefficient).

Author	Layer	Absorbers / scatterers included	Supporting bilbiographic reference
Jacques	Any layer	Collagen fibers and components and others	The scattering of epidermis is assumed to be similar to the one dermis. Mie scattering component is extrapolated from the scattering of large cylindrical dermal collagen fibers (Saidi, Jacques, and Tittel, 1995). Rayleigh scattering component is extrapolated from the scattering of small-scale structure associated with the collagen fibers and other cellular structures (Jacques and McAuliffe, 1991)
Svaasand	Any layer	Empirical relation	The scattering of epidermis is assumed to be similar to the one of the dermis. The scattering of epidermis/dermis is set to an empirical value at 577 nm and the variation with wavelength is assumed to be a law in $(1/\lambda)$ (Svaasand et al., 1995)
Meglinski	N.A.	N.A.	N.A.
Altshuler	Any layer	Skin baseline and blood	The skin baseline scattering is based on the formula proposed by Jacques (Jacques and McAuliffe, 1991). The scattering,formula is extended to the NIR range from Troy et al. (Troy and Thennadil, 2001) The scattering of blood is adapted from Svaasand formula (Svaasand et al., 1995)

Table 6.2: Factors included in the mathematical models for estimating the optical properties of the skin layers in the bibliographic references included in the study (scattering coefficient).

Author	Sample origin	Body location	Skin Handling before measurement	Optical method	Statistics
Marchesini	Caucasian skin, whole measurement performed within 1 hour post surgery	upper leg, lower back, breast, thigh, abdomen, groin	Removal of fat by scraping, thermal heating of dermis in contact with heating plate, epidermis was carefully extracted and placed in a saline solution then directly put on a metal frame	Transmittance and reflectance measurement. 1-D diffusion approximation for back-calculation of the absorption and scattering coefficients. Comparison with'*in vivo* measurements	10
Salomatina	Freshly discarded specimens obtained from surgeries within 7 hours	face, scalp, neck and back	Sample rinsed in PBS and sectioned with microcryotome, followed by thickness measurement, then rehydration with saline, sealed between a coverslip and slide with rapid mounting media to prevent desiccation	Integrating-sphere measurement of diffuse reflectance and total transmittance. Inverse Monte Carlo technique to retrieve the optical properties of the skin layers	10
Anderson	N.A.	N.A.	200 microns thick slice	Reflectance and transmittance. Back calculation using the Kubelka Munk Model.	1
Simpson	Caucasian (N=4) and negroid (N=1) skin samples from plastic surgery or post-mortem. All samples were used within 5 days from excision.	Abdominal and breast	Refrigerated for storage, and brought naturally to ambient temperature for measurement. Layers were separated using a razor (dermis and fat). Punches of the samples were then put between two coverslips to avoid desiccation.	Integrating-sphere measurement of diffuse reflectance and total transmittance. Inverse Monte Carlo technique to recover the optical properties of the skin layers	4

Table 6.3: Sample origin and methods used in the experimental measurements of the optical properties of the skin layers in the bibliographic references included in the study (Part I).

Author	Sample origin	Body location	Skin Handling before measurement	Optical method	Statistics
Wan	Samples from autopsy and surgical specimens. Seven fair Caucasian and one tanned and one dark skin.	Abdominal and breast	Removal of fat by scraping. Separation of dermis and epidermis by water bath 60 degrees for 30 s. Sample was mounted between two quartz diffuser (1 mm thickness), quartz-sample-quartz measurement	Reflectance and transmittance. Back calculation using the Kubelka Munk Model.	8
Bashkatov	Post-mortem and fresh subcutaneous human tissue. Storage of sample in saline. Measurement within 2-3h after biopsies.	Peritoneum area	Sample sandwiched between 2 glass slides without compression.	Total transmittance and diffuse reflectance measurement with integrating sphere. Inverse-adding doubling method for iterative back-calculation.	6
Ding	Samples from Caucasian (N = 10) and African American female skins after abdominoplasty surgery, age between 27 and 63 yo. Stored in ice in the fridge. Sample of 1x1 cm were prepared and the hairs were removed. Every measurement were done within 30h after excision.	Abdomen (N=11), Arm (N=1)	Fat was removed using a razor. Sample was brought to ambient temperature. Rehydrated with saline. Epidermis and dermis were not separated, either side was pressed against the prims for measurement.	Coherent reflectance measurement versus incidence angle. Theoretical back-calculation of the index of refraction.	12

Table 6.4: Sample origin and methods used in the experimental measurements of the optical properties of the skin layers in the bibliographic references included in the study (Part 2, continued).

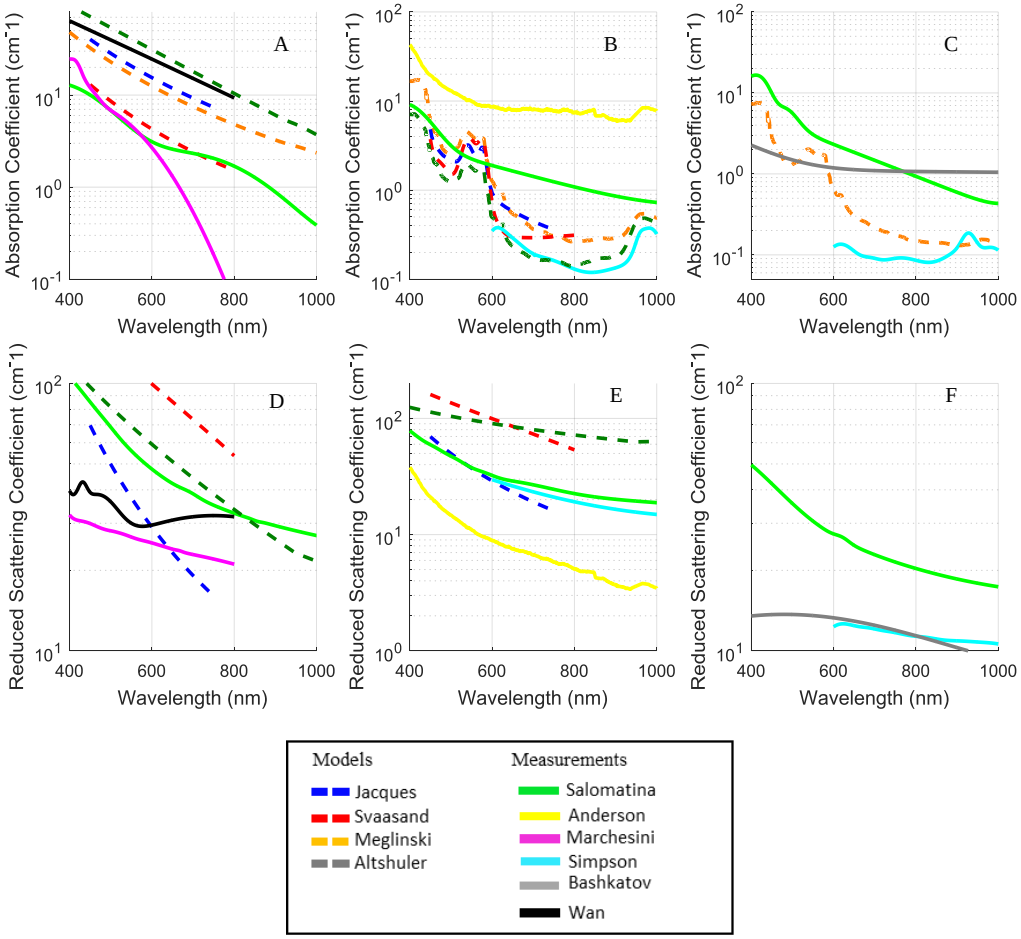

Figure 6.1: Absorption and scattering coefficients versus wavelength from bibliographic sources for epidermis (A, D), dermis (B, E) and subcutaneous fat layer (C, F). Full lines are extracted from experimental measurements, dashed-lines are extracted from mathematical models.

using a rational-based approach.

Only the most coherent datasets reflecting contribution of the major chromophores of the skin compartments were retained (Table 3).

They were combined in 4 skin datasets containing the optical properties of each of the 3 main skin layers (Table 4). The remaining datasets for the subcutaneous fat layer were not numerous enough and only one subcutaneous dataset was created combining the ones from (Simpson et al., 1998), Meglinski (Meglinski and Matcher, 2002) and Bashkatov (Bashkatov et al., 2005).

Reference	Remarks	Included/Not Included
Jacques	None	Included
Svaasand	Significantly lower contribution of melanin in the absorption coefficient of epidermis than expected target with overall much lower absorption	Not included
Meglinski	Absence of characteristic absorption band of fat at 930 nm, while the order of magnitude is in agreement with the values of Simpson (Simpson et al., 1998)	Included
Altshuler	None	Included
Salomatina	Significantly lower contribution of melanin in the absorption coefficient of epidermis than expected target; Absence of characteristic absorption peaks of hemaglobin and water in the dermal absorption coefficient; High absorption of the subcutaneous fat layer	Not Included
Anderson	Absence of characteristic absorption peaks of blood and water in the dermal absorption coefficient; High absorption of the dermal layer; Low scattering of the dermal layer	Not Included
Marchesini	Significantly lower contribution of melanin in the absorption coefficient of epidermis than expected target; Steep variation of the absorption of the epidermis in the NIR	Not Included
Simpson	None	Included
Bashkatov	High absorption of the subcutaneous fat layer	Included (only for scattering)
Wan	None	Included

Table 6.5: Summary of the rational for the inclusion or exclusion of bibliographic references from analysis

Dataset #	Reference epidermis	Reference dermis	Reference subcutaneous fat layer
1	Jacques	Jacques	Simpson Meglinski / Simpson Bashkatov
2	Wan	Simpson Jacques / Simpson Jacques	Simpson Meglinski / Simpson Bashkatov
3	Meglinski / Altshuler	Meglinski / Altshuler	Simpson Meglinski / Simpson Bashkatov
4	Altshuler	Altshuler	Simpson Meglinski / Simpson Bashkatov

Table 6.6: Selected datasets used in simulations together with the bibliographic references for the absorption and scattering coefficients (absorption / scattering) of epidermis, dermis and subcutaneous fat layer

6.4 Predicted photon density distribution in depth, beam profiles and skin reflectance versus the skin layer optical properties datasets

The resulting quantitative predictions of light distribution over the depth in the skin obtained using a Monte Carlo model and the four selected datasets are falling within a range where the minimum and maximum values of photon densities are different by a factor 6, in absolute terms. The maximum difference is observed when looking at a ratio between the maximum of photon density at 655nm between the datasets 1 (Jacques (Jacques, 2013)) and 4 (Altshuler (Altshuler, Smirnov, and Yaroslavsky, 2005)) (Table 6.7).

Overall the ratios between the estimated photon densities obtained using the four selected datasets is stable over the 4 tested wavelengths. In particular, the dataset 1 is systematically predicting the lowest maximal photon density, reaching around $1/4$ of the magnitude obtained using dataset 4. Distribution of light obtained using the remaining datasets, those of Wan (Wan et al., 1981)/Simpson (Simpson et al., 1998) and Meglinski (Meglinski and Matcher, 2002) demonstrate more resemblance to that obtained using the dataset 4. Specifically, the values estimated using the dataset 2 (Wan (Wan et al., 1981)/Simpson (Simpson et al., 1998)) and the dataset 3 ((Meglinski and Matcher, 2002)) are reaching $1/2$ and $3/4$ of the maximum when using the dataset 4, respectively (Table 6.7).

At 655 nm, a decrease of the ratios between the maximum of photon density obtained with the datasets 1 and 3 compared to the same ratios at the three other wavelengths was observed, while the dataset 2 increased its maximum (Table 6.7). These effects were associated to the low epidermal absorption reported by Jacques (Jacques, 2013) and Meglinski (Meglinski and Matcher, 2002) as compared to the higher epidermal absorption estimated by Wan (Wan et al., 1981) and Altshuler (Altshuler, Smirnov, and Yaroslavsky, 2005) (Fig. 6.4).

When looking at the predictions of photon density level in depth using the four

datasets, a good agreement in relative terms is observed. In particular, the maximum difference of factor of < 2 is reached at 2 mm depth between the photon density estimated using datasets 1 and 4 at 450 nm (Fig. 6.2).

Furthermore, estimated axial beam profiles expressed in terms of photon density in the upper dermis (700 micrometers below the skin surface) vary within a factor 5, which is reached again between the datasets 1 and 4 at 450 nm (Fig. 6.3). Within 2 mm distance from the irradiation point at a position of upper dermis, the relative quantitative difference between the predictions using each of the datasets is falling under a factor 2.

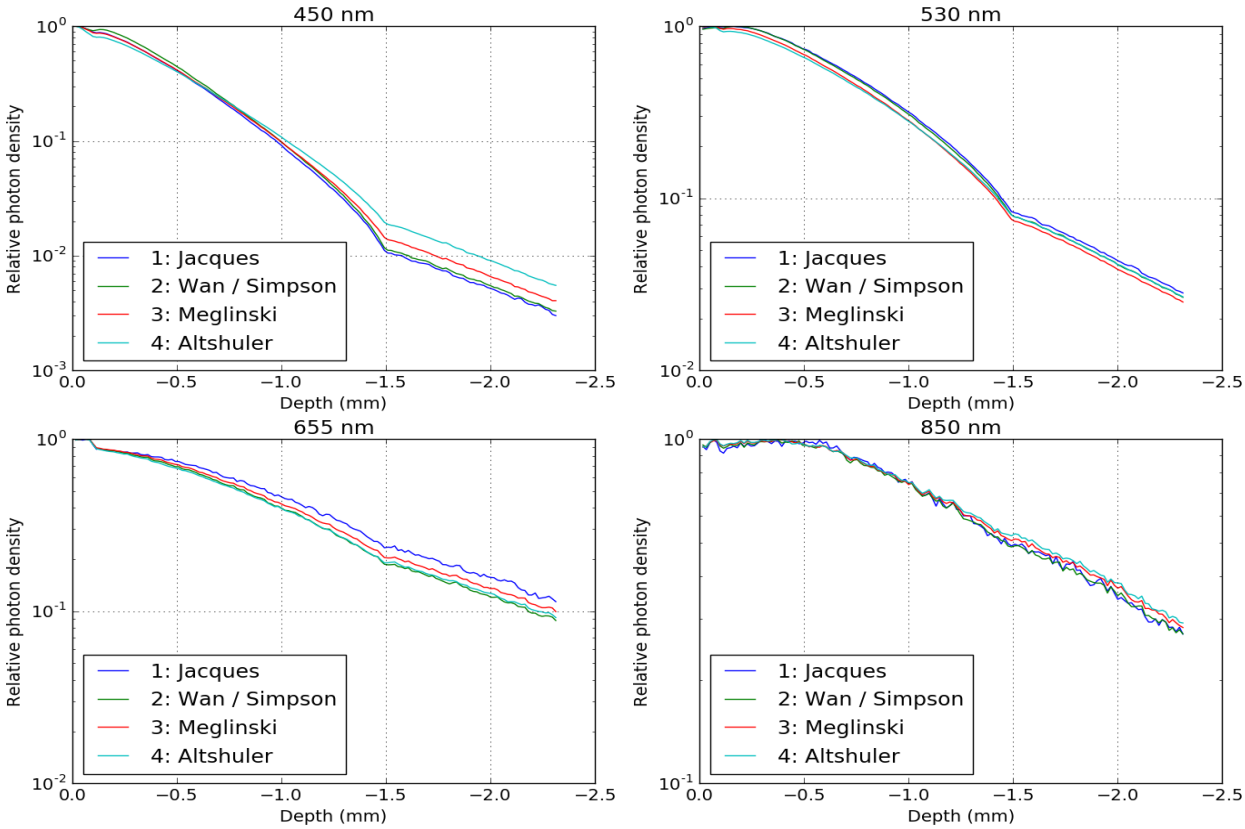

Figure 6.2: Relative photon density versus depth obtained from the Monte Carlo predictions of optical transport in a three-layer human skin model using the selected optical properties datasets, shown in semi-logarithmic scale. The photon density presented was extracted from a rectangular cylinder of sizes 400 μm by 400 μm centered on the propagation axis.

At 530 nm, and 850 nm, a similar decrease of the photon density level is ob-

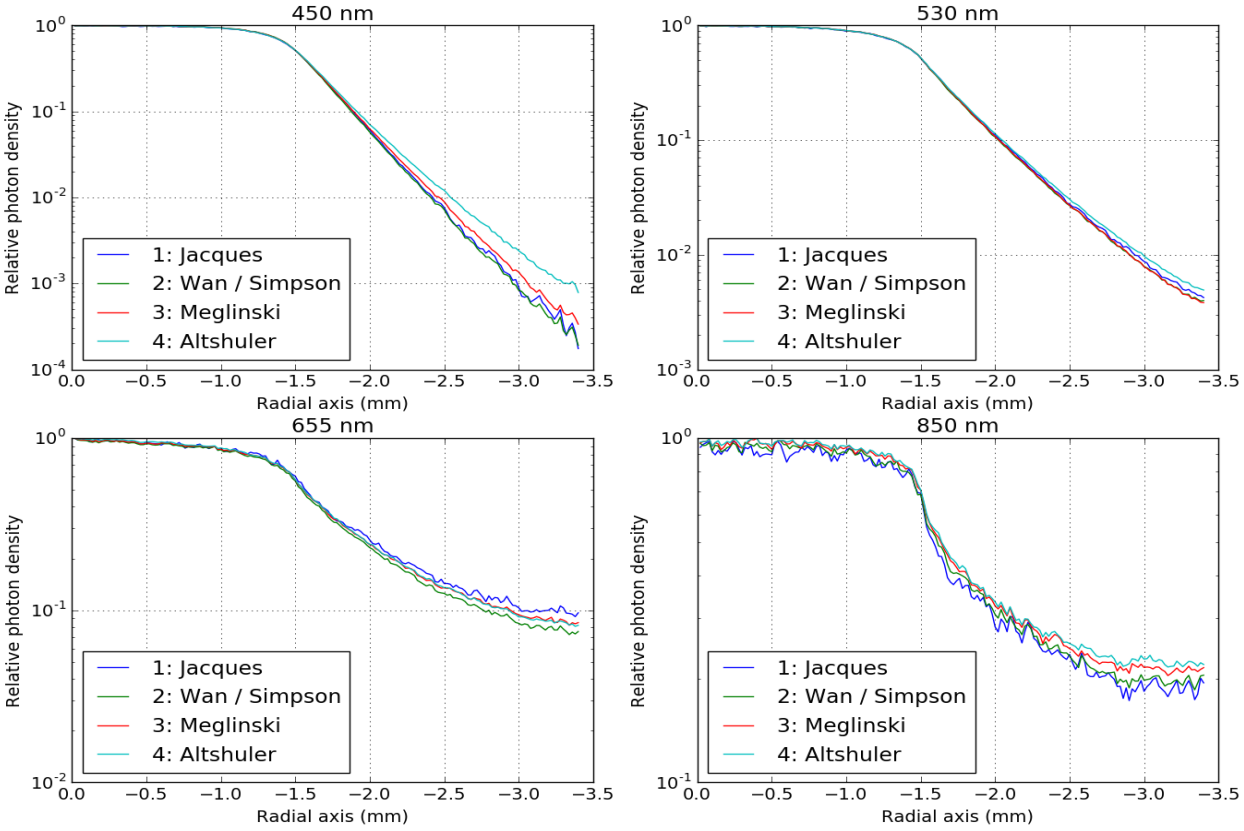

Figure 6.3: Beam profile in the dermal layer (photon density) versus radial axis obtained from the Monte Carlo predictions of optical transport in a three-layer human skin model using the selected optical properties datasets, shown in semi-logarithmic scale. The photon density presented is the beam profile measured at 700 μm under the skin surface and averaged over 164 μm in the direction perpendicular to the propagation axis

served in depth and in profile using all datasets (Fig. 6.2 and 6.3), where there is a quantitative agreement between them within a factor 2 at all spatial locations. At 450 nm, however, the dataset 4 is standing out, where the photon density associated with it has a steeper decrease with depth in the epidermal layer and a slower decrease with depth in the dermal layer compared to the other datasets (Fig. 6.2). As such, this resulted in a lower relative photon density in the epidermis and a higher photon density in the dermis as compared to other datasets (Fig. 6.2, 450 nm). This trend originates due to relatively higher epidermal absorption and scattering as well as due to lower dermal absorption and scattering associated with the dataset of Altshuler (Altshuler, Smirnov, and Yaroslavsky, 2005)

Wavelength (nm)	450	530	655	850
Jacques	0.249	0.242	0.174	0.248
Wan/Simpson	0.473	0.486	0.526	0.487
Meglinski	0.753	0.760	0.621	0.747

Table 6.7: Ratios between the maximum of photon density reached in the skin with the datasets 1 (Jacques (Jacques, 2013)), 2 (Wan (Wan et al., 1981) /Simpson (Simpson et al., 1998)) and 3 (Meglinski (Meglinski and Matcher, 2002)) over the maximum obtained with the dataset 4 (Altshuler, Smirnov, and Yaroslavsky, 2005).

(Fig. 6.4).

Similar difference is also observable at 530 nm (Fig. 6.2), however, to a lower extent as the absorption and scattering coefficients associated with dataset 4 are quantitatively closer to the ones originating from the other three datasets (Fig. 6.4).

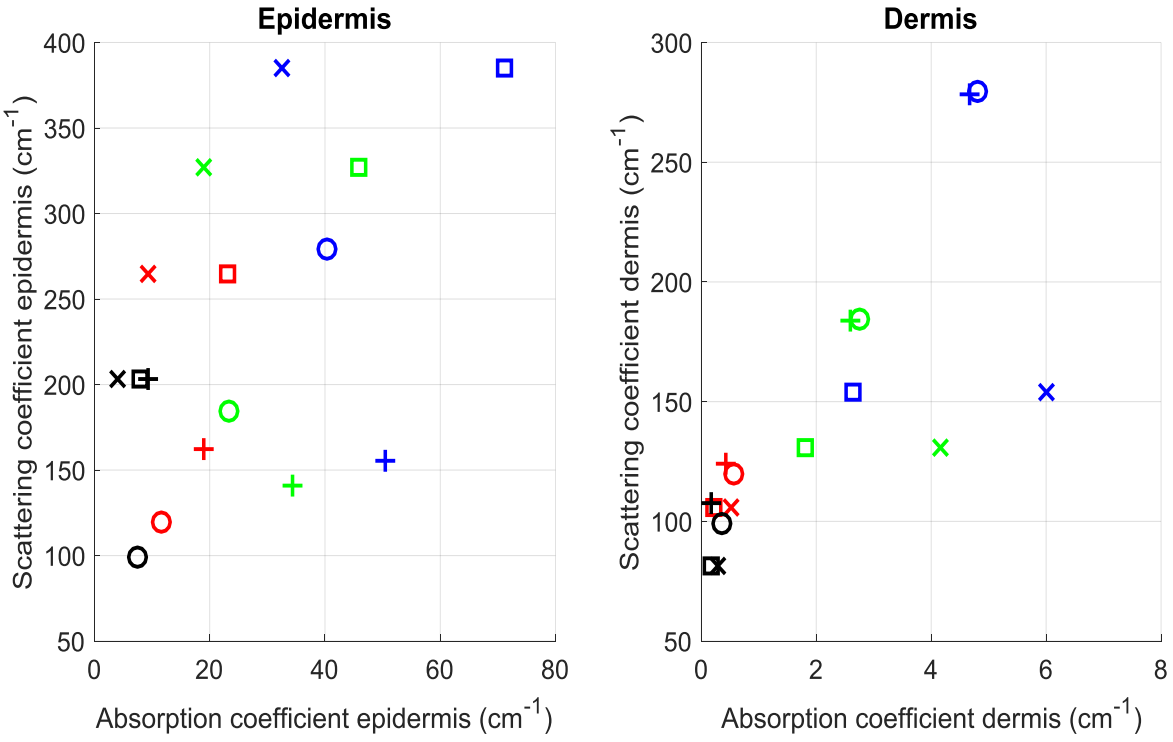

Figure 6.4: Absorption versus scattering coefficients corresponding to datasets 1, 2, 3 and 4 for the epidermis (left) and dermis (right). The symbol indicates the dataset: 1 (○), 2 (+), 3 (x) and 4 (□). The colour of the dots indicates the wavelength, blue 450 nm, green 530 nm, red 655 nm and black 850 nm.

6.5 Comparison of the skin diffuse reflectance estimated using Monte Carlo model and selected optical properties to an independent source of in vivo measurements

As the next step, the comparison of the skin reflectance estimated using Monte Carlo model and selected optical properties with an independently obtained *in vivo* measurements of reflectance of human skin was performed. The independent human skin reflectance was measured on 28 individuals with Caucasian skin type, information which is available at the National Institute of Standards and Technology (NIST) (Cooksey, Tsai, and Allen, 2014).

In the first instance one can see that the variability of the diffuse reflectance originating from individual human subjects as reported by the NIST reaches about 30% (Fig. 6.5, dotted-black lines).

Furthermore, what is very encouraging is that when comparing the quantitative values of the diffuse reflectance of human skin, extracted from the NIST source to those estimated using Monte Carlo model, the diffuse reflectance associated with all of the four selected datasets are falling within the range reported by the NIST, specifically for the visible wavelengths (Fig. 6.5, 450, 530, 655 nm).

What is seen however, that at all wavelengths, and particularly at 655 nm, the diffuse reflectance associated with the datasets of Altshuler (Altshuler, Smirnov, and Yaroslavsky, 2005) and Wan (Wan et al., 1981)/ Simpson (Simpson et al., 1998) is higher than that associated with the two other datasets of Meglinski (Meglinski and Matcher, 2002) and Jacques (Jacques, 2013) (Fig. 6.5). One can easily recognize here two clusters when looking at diffuse reflectance corresponding to 655 nm: the one originating when using the data of Altshuler (Altshuler, Smirnov, and Yaroslavsky, 2005) and Simpson (Simpson et al., 1998) and the other - Jacques (Jacques, 2013) and Meglinski (Meglinski and Matcher, 2002) (Fig. 6.5, 655 nm). The origin of these two clusters is rooted back in the differences of absorption

coefficients of the epidermis and dermis between these two pairs of datasets, in particular for wavelength longer than 600 nm (Fig. 6.1, A B).

At 450 nm and 530 nm, the diffuse reflectance associated with the dataset of Meglinski (Meglinski and Matcher, 2002) is particularly lower than that associated with the rest of the datasets (Fig. 6.5). A possible explanation for this differences is the combined effect of a higher dermal absorption, as well as a lower epidermal absorption as discussed earlier (Fig. 6.4).

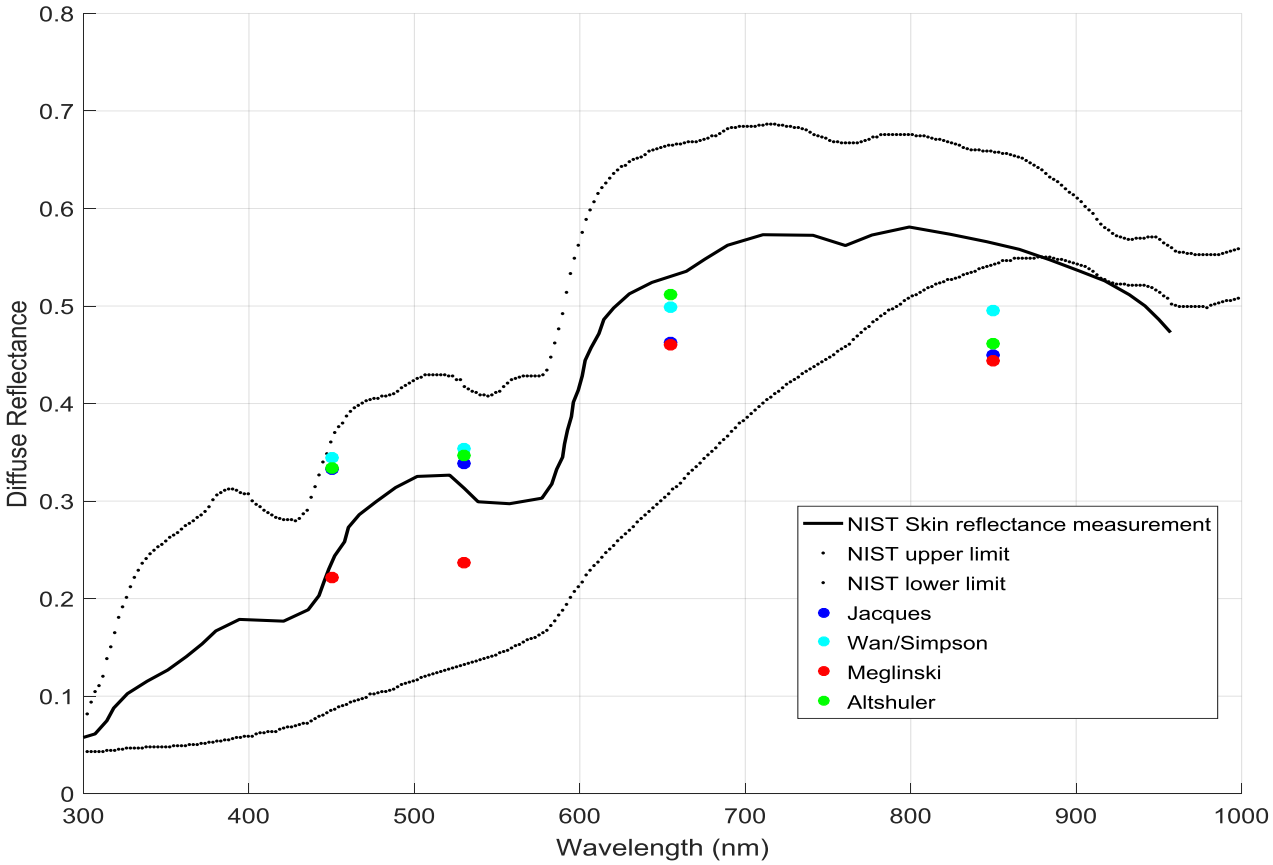

Figure 6.5: Diffuse reflectance of human skin computed from the Monte Carlo predictions of the propagation of light in a three-layer skin model using the selected optical properties datasets. Also shown is an empirical measurement of the diffuse reflectance of human Caucasian skin as measured by the NIST (Cooksey, Tsai, and Allen, 2014)

6.6 Discussion

Our review of the literature found 4 mathematical models and 6 experimental measurements reporting the optical properties of one or several of the skin layers, where a large spread of the reported values of optical properties of the skin layers. More specifically, published values of the absorption and scattering coefficients of the epidermis, dermis and subcutaneous fat layer were found to extend over a large range, where up to 100-fold difference are present for one coefficient of one skin layer (Fig. 6.1). This existing dramatic variation poses a major problem for application of Monte Carlo optical model for the prediction of the light propagation in human skin and further selection of treatment parameters and interpretation of values in skin diagnostics, as the calculated photon density will be directly and very strongly impacted by the choice of absorption and scattering coefficients for the skin components. Furthermore such a large spread in the reported values raises a question about the validity of the references reporting the optical properties of the skin layers.

Therefore, the purpose of this work was to select subsets of the optical properties of the skin layers, presumably most closely representing realistic values using a rational-based approach.

In attempt to achieve this, a rational-based approach was adopted, guided by a simple yet a very powerful idea (Jacques, 2013), stating that the absorption and scattering of any tissue, and particularly of any homogeneous skin layer, should simply find their origins in the biological composition of the layer.

This idea was implemented on practice by, in the first instance, evaluating each of the reported dataset in terms of presence of the absorption bands of the strongest chromophores over visible to NIR range, specific for each of the skin layers: melanin - in epidermis, haemoglobin - in dermis, and lipids – in subcutaneous fat.

Secondly, the sample preparation and handling during optical measurements was also extracted trying to link differences in the reported value with variations in ex-

perimental lab protocol.

And finally, the coherence or clustering between the datasets originating from different research investigations was analyzed.

As a result of these steps, it was possible to exclude from further considerations three sets of the optical properties estimated based on experimental measurements (Salomatina (Salomatina et al., 2006), Anderson (Anderson and Parrish, 1981) and Marchesini (Marchesini et al., 1992)) and one – based on mathematical model (Svaasand (Svaasand et al., 1995)). All these datasets were discarded as they did not contain the spectroscopic features that one should expect to be present based on the biochemical content of the skin layers. In particular, the mathematical model of Svaasand (Svaasand et al., 1995) and the experimental measurements of Salomatina (Salomatina et al., 2006), Anderson (Anderson and Parrish, 1981) and Marchesini (Marchesini et al., 1992) were all not showing the expected spectroscopic features in the quantitative values of their respective absorption coefficient (Tab. 6.5). Finally as a result of such a screening, 5 publications were retained (Wan (Wan et al., 1981), Simpson (Simpson et al., 1998), Jacques (Jacques, 1996), Meglinski (Meglinski and Matcher, 2002) and Altshuler (Altshuler, Smirnov, and Yaroslavsky, 2005)) reporting the most coherent with each other and realistic optical properties, reflecting contribution of the major chromophores of the skin compartments. Across these datasets the variability of the absorption and scattering coefficients decreased from a factor 100 to under a factor 3 at fixed wavelength (Fig. 6.4).

Looking at the sample preparation and handling, it seems important that any experimental measurement of the optical properties of the skin layers should as less as possible alter the biochemical content of the skin layers. The importance of the sample handling routine should not be underestimated. For example, the quantitative values of the optical properties measured by Salomatina (Salomatina et al., 2006) are showing signs that the chemical composition of the layers was severely affected during measurement, potentially during the washing/rinsing phase. The absorption peaks of blood, water and fat were not visible in the corresponding

layers (dermis and fat). Besides, the absorption coefficient of all layers (epidermis, dermis and subcutaneous fat layer) were quantitatively too similar: a slow decrease from around $10\ cm^{-1}$ at 400 nm to $0.5\ cm^{-1}$ at 1000 nm, while their composition is clearly distinct (Raicu and Feldman, 2015). The measurements of the optical properties should ensure that the pigments and optically active compounds are preserved in their original state.

Likewise, for the mathematical models applied to calculate the optical properties of a specific layer based on its baseline properties and additional chromophores, the addition of all the contributions of the relevant pigments to the absorption of the layer is recommended. For example, the addition of the absorption of fat to the absorption coefficient of the subcutaneous fat layer in the model of Meglinski (Meglinski and Matcher, 2002) may be necessary.

Taken together a recommendation can be formulated: one would benefit from preferentially using the datasets reported by Wan (Wan et al., 1981), Simpson (Simpson et al., 1998), Jacques (Jacques, 1996), Meglinski (Meglinski and Matcher, 2002) and Altshuler (Altshuler, Smirnov, and Yaroslavsky, 2005).

Prior performing Monte Carlo calculations of light propagation in the skin using the selected sources of literature, to evaluate the impact of yet remaining spread in reported values, 4 complete datasets were constructed by merging individual datasets from 6 sources in total (Wan (Wan et al., 1981), Simpson (Simpson et al., 1998), Jacques (Jacques, 1996), Meglinski (Meglinski and Matcher, 2002) and Altshuler (Altshuler, Smirnov, and Yaroslavsky, 2005), Bashkatov (Bashkatov et al., 2005)). This was necessary as in some cases each of the publications did not report the complete set of the optical parameters over the total visible to NIR range for all three optical properties (absorption and scattering coefficients and anisotropy of scattering) for each of the three skin layers (epidermis, dermis, subcutaneous fat).

The next steps were to calculate light propagation in the skin model using Monte Carlo model and selected optical properties and to evaluate the resulting differences in photon densities originating based on several data sources in terms of

dependency on the wavelength-, depth- and radial dimension. More specifically, this project has reported the resulting impact of variability of the optical properties on the output photon densities and thus on the uncertainty in Monte Carlo prediction.

Despite the reduction of the variabilities of the optical properties of the skin layers, the simulations of light propagation in the skin still revealed a quantitative disagreement of the calculated photon density, up to a factor 6, between the 4 selected datasets (Tab. 6.7).

This variability could be reduced by tuning the mathematical models even further and reducing the variability of the optical properties of the datasets further. Indeed, most mathematical models have many factors which are estimated and might not be set to the most realistic values (melanin content of the epidermis, blood content of the dermis, absorbers of the layer, etc.). However, it will never be possible to find exactly defined single value for those due to the variability of the skin properties existing between individuals, body location, skin type, etc. For example, the melanosome content of the epidermis was shown to vary between 1 to 6 % in volume fraction of epidermis in light-skinned adults (Jacques and McAuliffe, 1991). Variability in the optical properties of the skin layers will always exist. Thus, this remaining variability between the selected datasets might be partly due to a natural variability existing in large group of individuals. Therefore, the quantitative disagreement of the calculated photon density, due to the variability of the optical properties of the skin layers, might only be partly solved with a ‘better’ measurement or model of the optical properties of the skin layers.

The last step towards narrowing down a parameter window was verification of the estimated the values of diffuse reflectance from human skin using Monte Carlo model with respect to an independent source of data: *in vivo* diffuse reflectance measurements on human subjects originating from an independent source of data (Cooksey, Tsai, and Allen, 2014). Here a good agreement was observed, where while variability of the diffuse reflectance originating from individual human subjects as reported by the NIST was about 30% (Fig. 6.5, dotted-black lines), the

diffuse reflectance calculated using Monte Carlo model and associated with all of the four selected datasets were falling within the range reported by the NIST, specifically for the visible wavelengths (Fig. 6.5, 450, 530, 655 nm). This verification step supports proposed selection of the datasets of the optical properties.

6.7 Summary

In this chapter, the accuracy of the Monte Carlo optical model was investigated. In particular, the impact of the variability of the optical properties of the skin layers on the output of the model was evaluated. The main results are:

- 4 mathematical models and 6 experimental measurements of the optical properties (absorption and scattering coefficients) of the skin layers published between 1981 and 2013 were found in the literature. The quantitative values of the absorption and scattering coefficients originating from the publications were extending over two orders of magnitude for the same property of any layer at a given wavelength.

- The careful selection of the most trust-worthy dataset, based on the spectral properties of the biochemical content of the skin layers, allowed the reduction of the spread of the skin layers optical properties to be under a factor 3 at a given wavelength

- 5 publications were retained (Wan (Wan et al., 1981), Simpson (Simpson et al., 1998), Jacques (Jacques, 1996), Meglinski (Meglinski and Matcher, 2002) and Altshuler (Altshuler, Smirnov, and Yaroslavsky, 2005)) reporting the most coherent with each other and realistic skin layers optical properties, reflecting contribution of the major chromophores of the skin compartments.

Chapter 7: Conclusion

In the introduction of this thesis I explored four key gaps emerging from the literature in photobiomodulation in dermatology. These included: the unidentified chromophore(s) responsible for the reception of light in human skin and human skin cells, the misunderstood mechanisms of actions of light in human skin cells, the lack of rationality in the selection of optical treatment settings in photobiomodulation studies and the lack of translational tools for the extrapolation from *in vitro* study to *in vivo* applications. Results demonstrated in this project were able to partly address some of these gaps.

The literature review of chapter 3 provides a more detailed overview of the inconsistencies surrounding the current knowledge in the fundamentals of photobiomodulation in dermatology. The practical aim of this review was to seek greater clarity and rationality, specifically for the selection of optical parameters for hair regrowth and wound healing. Its investigation of 90 reports published between 1985 and 2015 revealed major inconsistencies in the selection of optical parameters for clinical applications. Moreover, it is now understood that many photoreceptors expressed in human skin such as cytochrome c oxidase, cryptochromes, opsins, ion-gated channel etc. may trigger different molecular mechanisms simultaneously in skin cells. All this could explain the plethora of reported physiological effects of light. Furthermore, there is a need for a more systematic approach to derive parameters for optimal clinical efficacy of photobiomodulation, supported by a more rational approach to underpin clinical studies, with research on molecular targets and pathways using well-defined biological model systems. This will pave the way to enable translation of optical parameters from *in vitro* to *in vivo*.

Puzzled by the strong inconsistencies in the parameter-effect space in photo-

biomodulation, chapter 4 presented a rational approach for the selection of the optical treatment parameters in photobiomodulation. It investigated the appropriateness of a range of previously-reported treatment parameters, including light wavelength, irradiance and radiant exposure, as well as cell culture conditions (e.g., serum concentration, cell confluency, medium refreshment, direct/indirect treatment, oxygen concentration, etc.), in primary cultures of normal human dermal fibroblasts exposed to visible and near infra-red (NIR) light. Apart from irradiance, all study parameters impacted significantly on fibroblast metabolic activity. Moreover, when cells were grown at atmospheric O2 levels (i.e. 20%) short wavelength light inhibited cell metabolism, while negligible effects were seen with long visible and NIR wavelength. By contrast, NIR stimulated cells when exposed to dermal tissue oxygen levels (approx. 2%). The impact of culture conditions was further seen when inhibitory effects of short wavelength light were reduced with increasing serum concentration and cell confluency. This chapter concludes that a significant source of problematic interpretations in photobiomodulation reports derives from poor optimization of study design. Further development of this field using *in vitro*/*ex vivo* models should embrace significant standardization of study design, ideally within a design-of-experiment setting.

Strengthened by this project's rational investigation of the critical factors involved in the photobiomodulation interaction in human dermal fibroblasts, an optimized *in vitro* model of human dermal fibroblasts was developed and was treated by a restricted parameter window of optical treatment parameters. In chapter 5, complete dose-response curves at 6 visible and NIR wavelengths measured on the metabolic activity of human dermal fibroblasts revealed a stronger impact of short visible wavelengths compared to long visible and NIR wavelengths even over large dose range (0-250 $J.cm^{-2}$). Furthermore, a the dose response of human dermal fibroblasts to short visible wavelengths was found to fit a biphasic dose response curve, with successively inhibition and cytotoxicity. Next, I explored the live-induction of ROS in human dermal fibroblasts in response to short visible wavelengths. The creation of ROS species was linearly dependant on the dose

of visible light. Besides, the localization of the light-induced ROS showed a good correlation with a mitochondria tracker, indicating that ROS species might directly originate from the expression pattern of a mitochondria in the cells. On the contrary, NIR wavelengths did not induce any significant amount of ROS species upon irradiation. Lastly, the impact of short and long visible wavelengths on explanatory and functional readouts was investigated. The impact of three light parameters at the gene expression levels was assessed in human dermal fibroblasts subpopulations. The results showed that blue light (450 nm) down-regulated multiple pathways involved in proliferation, metabolic activity and protein synthesis in a dose-dependant manner. Additionally, blue light down-regulated the TGF-B signalling pathways, and specifically TGFB2 gene, for all populations and all light radiant exposures tested. Likewise, blue light also down-regulated the procollagen production by both subpopulations of human dermal fibroblasts in a dose-dependent manner (increased down-regulation with increasing dose). This was associated with the down-regulation of collagen fibers genes and integrins and up-regulation of MMP1 at the gene level. Importantly, consistent results between the gene expression study and the cellular assays were found.

In parallel, the chapter 6 presents an investigation of the potential use of Monte Carlo optical model for the translation of the results of photobiomodulation *in vitro* to *in vivo* applications. As the quantitative spread of the optical properties of the skin layers is known to be large, the accuracy of such model is known to be low, and therefore it reduces the adequacy of using such a model when accurate treatment needs to be provided. The literature review of chapter 6 actually revealed that the absorption and scattering coefficients of each skin layer varied by as much as two orders of magnitude. This variation was reduced to a factor 3 by the careful selection of the most 'trust-worthy' bibliographic datasets, whose selection was based on the spectroscopic features expected from the biological content of the skin layers. The remaining variability was translated to a factor of 6 in the calculated photon densities in absolute terms, and a factor of 2 in relative terms within 2 mm distance from the irradiation centre in the skin. The diffuse reflectance ex-

tracted from the Monte Carlo simulations were consistent with an independent measurement of human skin reflectance *in vivo*. It may therefore be concluded with a recommendation to use of trust-worthy optical property datasets which show the expected absorption features associated to the biochemical content of the skin layers. This could increase the accuracy of the prediction of the quantitative photon density level in the skin, and therefore help to standardize the photon density originating from the same optical input at most location in the skin.

The field of photobiomodulation is receiving an increasing attention. Future research will probably include simultaneous investigations *in vitro*, *ex vivo* and *in vivo*.

The mystery around the 'how' and 'what' of the action of light in photobiomodulation still exists. The use of *in vitro* research is fundamental, due to the practicability of the design and analysis of the response of *in vitro* models. Indeed, the interpretation of results is much more straightforward than with *in vivo* models. A particular area of future research could be the development of more realistic *in vitro* models, with higher and closer approximations to *in vivo* conditions. This could include a similar composition of the extracellular matrix or the introduction of mechanical flow to mimic the body's live mechanisms of fluid movement. The introduction of mechanical stress in *in vitro* models might become relevant as it has been shown to be fundamental in driving the behavior of cells *in vivo* (Evans et al., 2013). More research is needed to understand the action of light on individual cell layers, from parameter studies, action spectrum and on to pathway analysis. Some specific suggestions include the understanding of the mediation of the action of light: directly by the cell's components and/or indirectly via the culture medium. Indeed a large amount of interaction might be mediated by or via the culture medium including the activation of extracellular growth factors, cytokines via 'bystander' effects. In order to understand the molecular pathways triggered by light in the cells, relative changes in gene expression after irradiation represent a key opportunity.

The development of 3D *in vitro* models and *ex vivo/in vivo* models will most probably become more and more important in photobiomodulation research. Indeed,

contrary to single-cell *in vitro* models, they have the realness required from a biological model and which is critical to draw strong conclusions. However, the understanding becomes immediately more complex as many more interacting targets are involved. Future research in that area will need to address the propagation of light in the skin. Indeed, researchers are required to understand how a specific light treatment will reach the different skin layers and cell populations. This will help for the reporting of more robust results and a better understanding of empirical observations.

Last but not least, combining both real *in vivo* complexity and *in vitro* practicability, numerical modelling of biology systems might become relevant. They are better able to predict the dynamic behavior of multicellular organs such as the skin. Therefore, knowing the individual responses of individual skin cells to visible light, numerical agent-based models of the skin could be used to get a better understanding of the action of light on an interactive multi-cellular model. For example, the dynamic time-evolution of the epidermis in normal and diseased conditions was numerically predicted (González et al., 2003; Li, Chen, and Huang, 2013; Zhang et al., 2015). The model include many features such as inter-cellular signalling, proliferation, differentiation or even stem cell-ness (González et al., 2003; Li, Chen, and Huang, 2013; Zhang et al., 2015). Potential next steps would most probably include wound healing, inflammation or even psoriasis (Mi et al., 2007; Zhang et al., 2015). These models could be used and adapted to predict the response to light treatment knowing the responses of each individual cell populations. As photobiomodulation is a dose-dependant interaction, this would need to be combined with the prediction of photon density in the skin as calculated with Monte Carlo methods for example.

Bibliography

Abdelhalim, N M (2014). “Efficacy of low level laser therapy in the treatment of alopecia areata”. In: *International Journal of Physiotherapy and Research* 2.2, pp. 460–465.

Abergel, R P et al. (1987). “Biostimulation of Wound Healing by Lasers: Experimental Approaches in Animal Models and in Fibroblast Cultures”. In: *J. Dermatology Surgery Oncology*.

Administration, U S Food and Drugs (2016). “Light-based hair regrowth devices with 510(k) premarket notification”. In: *http://www.accessdata.fda.gov/scripts/cdrh/cfdocs/* 15/02/2016. URL: http://www.accessdata.fda.gov/scripts/cdrh/cfdocs/cfPMN/pmn.cfm?start_search=1&Center=&Panel=&ProductCode=OAP&KNumber=&Model=&Applicant=&DeviceName=&Type=&ThirdPartyReviewed=&ClinicalTrials=&ExpeditedReview=&Decision=&DecisionDateFrom=&DecisionDateTo 02/1.

Afifi, L et al. (2016). “Low-level laser therapy as a treatment for androgenetic alopecia”. In: *Lasers Surg Med*. ISSN: 1096-9101. DOI: 10.1002/lsm.22512. URL: https://www.ncbi.nlm.nih.gov/pubmed/27114071.

Altshuler, Gregory, Mikhail Smirnov, and Ilya Yaroslavsky (2005). “Lattice of optical islets: a novel treatment modality in photomedicine”. In: *Journal of Physics D: Applied Physics* 38.15, pp. 2732–2747. ISSN: 0022-3727. DOI: 10.1088/0022-3727/38/15/027. URL: http://stacks.iop.org/0022-3727/38/i=15/a=027http://stacks.iop.org/0022-3727/38/i=15/a=027?key=crossref.c662fd4db0bd1864fe31db56ecdf62fc.

Anders, J J, S Geuna, and S Rochkind (2004). “Phototherapy promotes regeneration and functional recovery of injured peripheral nerve”. In: *Neurol Res* 26.2,

pp. 233–239. ISSN: 0161-6412. DOI: 10.1179/016164104225013914. URL: https://www.ncbi.nlm.nih.gov/pubmed/15072645.

Anders, Juanita et al. (2008). “Light Supports Neurite Outgrowth of Human Neural Progenitor Cells In Vitro : The Role of P2Y Receptors”. In: 14.1, pp. 118–125.

Anders, Juanita et al. (2010). “The Combination of Light and Stem Cell Therapies: A Novel Approach in Regenerative Medicine”. In: *American Institute of Physics* 3, pp. 3–10. ISSN: 9780735407701. DOI: 10.1063/1.3453785. URL: http://scitation.aip.org/content/aip/proceeding/aipcp/10.1063/1.3453785.

Anders, Juanita J., Raymond J. Lanzafame, and Praveen R. Arany (2015). “Low-level light/laser therapy versus photobiomodulation therapy”. In: *Photomed Laser Surg* 33.4, pp. 183–184. ISSN: 1557-8550 (Electronic) 1549-5418 (Linking). DOI: 10.1089/pho.2015.9848. URL: http://online.liebertpub.com/doi/10.1089/pho.2015.9848http://www.ncbi.nlm.nih.gov/pubmed/25844681.

Anderson, R Rox and John A Parrish (1981). “The Optics of Human Skin”. In: *Journal of Investigative Dermatology* 77.1, pp. 13–19. ISSN: 0022-202X. DOI: 10.1111/1523-1747.ep12479191. URL: http://dx.doi.org/10.1111/1523-1747.ep12479191.

Arany, P. R. et al. (2014). “Multi-lineage MSC Differentiation via Engineered Morphogen Fields”. In: *Journal of Dental Research* 93, pp. 1250–1257. ISSN: 0022-0345. DOI: 10.1177/0022034514542272. URL: http://jdr.sagepub.com/cgi/doi/10.1177/0022034514542272.

Arthaut, Louis-David et al. (2017). “Blue-light induced accumulation of reactive oxygen species is a consequence of the Drosophila cryptochrome photocycle”. In: *PLOS ONE* 12.3. Ed. by Ilia Solov’yov, e0171836. ISSN: 1932-6203. DOI: 10.1371/journal.pone.0171836. URL: http://dx.plos.org/10.1371/journal.pone.0171836.

Avci, Pinar et al. (2014). “Low-level laser (light) therapy (LLLT) for treatment of hair loss.” In: *Lasers in surgery and medicine* 46.2, pp. 144–51. ISSN: 1096-9101.

DOI: 10.1002/lsm.22170. URL: http://www.ncbi.nlm.nih.gov/pubmed/23970445https://www.ncbi.nlm.nih.gov/pubmed/23970445.

Azevedo, Luciane Hiramatsu et al. (2006). “Influence of different power densities of LILT on cultured human fibroblast growth : a pilot study.” In: *Lasers in medical science* 21.2, pp. 86–9. ISSN: 0268-8921. DOI: 10.1007/s10103-006-0379-9. URL: http://www.ncbi.nlm.nih.gov/pubmed/16699912.

Azzam, Edouard I, Jean-Paul Jay-Gerin, and Debkumar Pain (2012). “Ionizing radiation-induced metabolic oxidative stress and prolonged cell injury.” In: *Cancer letters* 327.1-2, pp. 48–60. ISSN: 1872-7980. DOI: 10.1016/j.canlet.2011.12.012. URL: http://www.ncbi.nlm.nih.gov/pubmed/22182453http://www.pubmedcentral.nih.gov/articlerender.fcgi?artid=PMC3980444.

Babilas, P et al. (2010). “Intense pulsed light (IPL): a review”. In: *Lasers Surg Med* 42.2, pp. 93–104. ISSN: 1096-9101 (Electronic) 0196-8092 (Linking). DOI: 10.1002/lsm.20877. URL: http://www.ncbi.nlm.nih.gov/pubmed/20166155.

Baker, Monya (2016). “Reproducibility: Respect your cells!” In: *Nature* 537.7620, pp. 433–435. ISSN: 0028-0836. DOI: 10.1038/537433a. URL: http://www.nature.com/doifinder/10.1038/537433a.

Barolet, Daniel et al. (2009). “Regulation of skin collagen metabolism in vitro using a pulsed 660 nm LED light source: clinical correlation with a single-blinded study.” In: *The Journal of investigative dermatology* 129.12, pp. 2751–2759. ISSN: 1523-1747. DOI: 10.1038/jid.2009.186. URL: http://www.ncbi.nlm.nih.gov/pubmed/19587693.

Barolet, Daniel et al. (2010). “Importance of pulsing illumination parameters in low-level-light therapy”. In: *Journal of biomedical optics* 15.4, p. 048005. ISSN: 1560-2281. DOI: 10.1117/1.3477186. URL: http://www.ncbi.nlm.nih.gov/pubmed/20799848http://biomedicaloptics.spiedigitallibrary.org/article.aspx?doi=10.1117/1.3477186.

Bashkatov, A N et al. (2005). “Optical properties of human skin , subcutaneous and mucous tissues in the wavelength range from 400 to 2000 nm”. In: *Journal of Physics D: Applied Physics* 38.15, pp. 2543–2555. ISSN: 0022-3727. DOI:

10.1088/0022-3727/38/15/004. URL: http://stacks.iop.org/0022-3727/38/i=15/a=004.

Basso, Fernanda G et al. (2013). “Biostimulatory effect of low-level laser therapy on keratinocytes in vitro.” In: *Lasers in medical science* 28.2, pp. 367–374. ISSN: 1435-604X. DOI: 10.1007/s10103-012-1057-8. URL: http://www.ncbi.nlm.nih.gov/pubmed/22314560.

Becker, Anja et al. (2015). “Impact of blue LED irradiation on proliferation and gene expression of cultured human keratinocytes”. In: *Proc. of SPIE* 9309, p. 930909. DOI: 10.1117/12.2083010. URL: http://proceedings.spiedigitallibrary.org/proceeding.aspx?doi=10.1117/12.2083010.

Becker, Anja et al. (2016). “Gene expression profiling reveals aryl hydrocarbon receptor as a possible target for photobiomodulation when using blue light”. In: *Scientific Reports* 6, p. 33847. ISSN: 2045-2322. DOI: 10.1038/srep33847. URL: http://www.nature.com/articles/srep33847.

Bellono, Nicholas W et al. (2013). “UV light phototransduction activates transient receptor potential A1 ion channels in human melanocytes.” In: *Proceedings of the National Academy of Sciences of the United States of America* 110.6, pp. 2383–8. ISSN: 1091-6490. DOI: 10.1073/pnas.1215555110. URL: http://www.pubmedcentral.nih.gov/articlerender.fcgi?artid=3568351&tool=pmcentrez&rendertype=abstract.

Blum, Kenneth et al. (2014). “”Cold” X5 Hairlaser used to treat male androgenic alopecia and hair growth: an uncontrolled pilot study”. In: *BMC Research Notes* 7.1, pp. 1–13. ISSN: 1756-0500 (Electronic) 1756-0500 (Linking). DOI: 10.1186/1756-0500-7-103. URL: http://dx.doi.org/10.1186/1756-0500-7-103http://www.ncbi.nlm.nih.gov/pubmed/24559020.

Booth, R. a. D, B. a. Goddard, and A. Paton (1966). “Measurement of fat thickness in man: a comparison of ultrasound, Harpenden calipers and electrical conductivity”. In: *Br J Nutr* 20.4, pp. 719–725. ISSN: 0007-1145. DOI: 10.1079/BJN19660073. URL: http://www.journals.cambridge.org/abstract_S0007114566000746http://www.ncbi.nlm.nih.gov/pubmed/5956158.

Bouly, Jean-Pierre et al. (2007). “Cryptochrome blue light photoreceptors are activated through interconversion of flavin redox states.” In: *The Journal of biological chemistry* 282.13, pp. 9383–9391. ISSN: 0021-9258. DOI: 10.1074/jbc.M609842200. URL: http://www.ncbi.nlm.nih.gov/pubmed/17237227.

Brondon, Philip, Istvan Stadler, and Raymond J Lanzafame (2009). “Pulsing influences photoradiation outcomes in cell culture.” In: *Lasers in surgery and medicine* 41.3, pp. 222–226. ISSN: 1096-9101. DOI: 10.1002/lsm.20740. URL: http://www.ncbi.nlm.nih.gov/pubmed/19291749.

Brooks, J L, a Sucheta, and O Einarsdóttir (1997). “Light-induced spectral changes in fully oxidized cytochrome c oxidase in the presence of oxygen.” In: *Biochemistry* 36.21, pp. 6336–42. ISSN: 0006-2960. DOI: 10.1021/bi9630321. URL: http://www.ncbi.nlm.nih.gov/pubmed/9174348.

Brown, P K and G Wald (1964). “Visual pigments in single rods and cones of the human retina. Direct measurements reveal mechanisms of human night and color vision”. In: *Science* 144.3614, pp. 45–52. ISSN: 0036-8075 (Print) 0036-8075 (Linking). URL: http://www.ncbi.nlm.nih.gov/pubmed/14107460.

Buscone, Serena et al. (2017). “A new path in defining light parameters for hair growth: Discovery and modulation of photoreceptors in human hair follicle”. In: *Lasers in Surgery and Medicine*. ISSN: 01968092. DOI: 10.1002/lsm.22673. URL: http://www.ncbi.nlm.nih.gov/pubmed/28418107http://doi.wiley.com/10.1002/lsm.22673.

Carreau, Aude et al. (2011). “Why is the partial oxygen pressure of human tissues a crucial parameter? Small molecules and hypoxia.” In: *Journal of cellular and molecular medicine* 15.6, pp. 1239–53. ISSN: 1582-4934. DOI: 10.1111/j.1582-4934.2011.01258.x. URL: http://www.ncbi.nlm.nih.gov/pubmed/21251211http://www.pubmedcentral.nih.gov/articlerender.fcgi?artid=PMC4373326.

Carroll, J (2015). *Pubmed to adopt “Photobiomodulation Therapy” as a MeSH term*.

Cashmore, A R. et al. (1999). “Cryptochromes: blue light receptors for plants and animals”. In: *Science* 284.5415, pp. 760–765. ISSN: 0036-8075 (Print) 0036-8075 (Linking). DOI: 10.1126/science.284.5415.760. URL: http://www.sciencemag.org/cgi/doi/10.1126/science.284.5415.760http://www.ncbi.nlm.nih.gov/pubmed/10221900.

Caughey, W et al. (1975). “Heme A of Cytochrome c Oxidase”. In: *Journal of Biological Chemistry*.

Chan, K-S, C-G Koh, and H-Y Li (2012). “Mitosis-targeted anti-cancer therapies: where they stand.” In: *Cell death & disease* 3.10, e411. ISSN: 2041-4889. DOI: 10.1038/cddis.2012.148. URL: http://www.ncbi.nlm.nih.gov/pubmed/23076219http://www.pubmedcentral.nih.gov/articlerender.fcgi?artid=PMC3481136.

Chu, T W, L Santos, and K J McElwee (2015). “Biology of the hair follicle and mechanisms of nonscarring and scarring alopecia”. In: *Semin Cutan Med Surg* 34.2, pp. 50–56. ISSN: 1085-5629 (Print) 1085-5629 (Linking). DOI: 10.12788/j.sder.2015.0133. URL: http://www.ncbi.nlm.nih.gov/pubmed/26176280.

Chung, Hoon et al. (2012). “The nuts and bolts of low-level laser (light) therapy.” In: *Annals of biomedical engineering* 40.2, pp. 516–533. ISSN: 1573-9686. DOI: 10.1007/s10439-011-0454-7. URL: http://www.ncbi.nlm.nih.gov/pubmed/22045511http://www.pubmedcentral.nih.gov/articlerender.fcgi?artid=3288797&tool=pmcentrez&rendertype=abstract.

Consentino, L et al. (2015). “Blue-light dependent reactive oxygen species formation by Arabidopsis cryptochrome may define a novel evolutionarily conserved signaling mechanism”. In: *New Phytol* 206.4, pp. 1450–1462. ISSN: 1469-8137 (Electronic) 0028-646X (Linking). DOI: 10.1111/nph.13341. URL: http://www.ncbi.nlm.nih.gov/pubmed/25728686.

Cooksey, Catherine C., Benjamin K. Tsai, and David W. Allen (2014). “A collection and statistical analysis of skin reflectance signatures for inherent variability over the 250 nm to 2500 nm spectral range.” In: *Proc. SPIE* 9082,

pp. 908206–908211. DOI: 10.1117/12.2053604. URL: http://proceedings.spiedigitallibrary.org/proceeding.aspx?doi=10.1117/12.2053604.

Dai, Manhong et al. (2005). “Evolving gene/transcript definitions significantly alter the interpretation of GeneChip data.” In: *Nucleic acids research* 33.20, e175. ISSN: 1362-4962. DOI: 10.1093/nar/gni179. URL: http://www.ncbi.nlm.nih.gov/pubmed/16284200http://www.pubmedcentral.nih.gov/articlerender.fcgi?artid=PMC1283542.

Damante, Carla Andreotti et al. (2009). “Effect of laser phototherapy on the release of fibroblast growth factors by human gingival fibroblasts.” In: *Lasers in medical science* 24.6, pp. 885–891. ISSN: 1435-604X. DOI: 10.1007/s10103-008-0582-y. URL: http://www.ncbi.nlm.nih.gov/pubmed/18600291.

Danno, Kiichiro et al. (2001). “Near-infrared irradiation stimulates cutaneous wound repair: laboratory experiments on possible mechanisms”. In: *Photodermatology Photoimmunology and Photomedecine*, pp. 261–265.

Dartnall, H. J. A, J. K Bowmaker, and J. D Mollon (1983). “Human Visual Pigments: Microspectrophotometric results from the eyes of seven persons”. In: *Proc. R. Sic. Lond.*

Denda, Mitsuhiro and Shigeyoshi Fuziwara (2008). “Visible radiation affects epidermal permeability barrier recovery: selective effects of red and blue light.” In: *The Journal of investigative dermatology* 128.November 2007, pp. 1335–1336. ISSN: 0022-202X. DOI: 10.1038/sj.jid.5701168. URL: http://www.ncbi.nlm.nih.gov/pubmed/18007581.

Di Veroli, G Y et al. (2015). “An automated fitting procedure and software for dose-response curves with multiphasic features”. In: *Sci Rep* 5, p. 14701. ISSN: 2045-2322. DOI: 10.1038/srep14701. URL: http://www.nature.com/articles/srep14701https://www.ncbi.nlm.nih.gov/pubmed/26424192.

Ding, Huafeng et al. (2006). “Refractive indices of human skin tissues at eight wavelengths and estimated dispersion relations between 300 and 1600 nm”. In: *Physics in Medicine and Biology* 51.6, p. 1479. ISSN: 0031-9155. DOI:

10.1088/0031-9155/51/6/008. URL: http://www.ncbi.nlm.nih.gov/pubmed/16510957http://stacks.iop.org/0031-9155/51/i=6/a=008.

Douven, Lucien F A and Gerald W Lucassen (2000). “Retrieval of optical properties of skin from measurement and modeling the diffuse reflectance”. In: *Proc. SPIE* 3914, pp. 312–323. DOI: 10.1117/12.388058.

Driskell, Ryan R et al. (2011). “Hair follicle dermal papilla cells at a glance.” In: *Journal of cell science* 124.Pt 8, pp. 1179–82. ISSN: 1477-9137. DOI: 10.1242/jcs.082446. URL: http://www.pubmedcentral.nih.gov/articlerender.fcgi?artid=3115771&tool=pmcentrez&rendertype=abstract.

Driskell, Ryan R. et al. (2013). “Distinct fibroblast lineages determine dermal architecture in skin development and repair.” In: *Nature* 504.7479, pp. 277–81. ISSN: 1476-4687. DOI: 10.1038/nature12783. URL: http://www.pubmedcentral.nih.gov/articlerender.fcgi?artid=3868929&tool=pmcentrez&rendertype=abstracthttp://www.nature.com/doifinder/10.1038/nature12783.

Driskell, Ryan R et al. (2015). “Understanding fibroblast heterogeneity in the skin.” In: *Trends in cell biology* 25.2, pp. 92–9. ISSN: 1879-3088. DOI: 10.1016/j.tcb.2014.10.001. URL: http://www.ncbi.nlm.nih.gov/pubmed/25455110.

Dykes, P.J J, M.B Marks, and R Marks (1977). “Measurement of skin thickness: a comparison of two in vivo techniques with a conventional histometric method”. In: *Journal of Investigative Dermatology* 69.3, pp. 275–278. ISSN: 0022-202X. DOI: http://dx.doi.org/10.1111/1523-1747.ep12507488. URL: http://www.sciencedirect.com/science/article/pii/S0022202X15451048.

Edelhoch, H (1967). “Spectroscopic determination of tryptophan and tyrosine in proteins.” In: *Biochemistry* 6, pp. 1948–1954. ISSN: 0006-2960. DOI: 10.1021/bi00859a010.

[Editorial] (2016). “Reality check on reproducibility”. In: *Nature* 533.7604, pp. 437–437. ISSN: 0028-0836. DOI: 10.1038/533437a. URL: http://www.nature.com/doifinder/10.1038/533437a.

Ejiri, Kenichiro et al. (2014). “High-frequency low-level diode laser irradiation promotes proliferation and migration of primary cultured human gingival epithelial

cells.” In: *Lasers in medical science* 29.4, pp. 1339–47. ISSN: 1435-604X. DOI: 10.1007/s10103-013-1292-7. URL: http://www.ncbi.nlm.nih.gov/pubmed/23515630.

Esmaeelinejad, Mohammad et al. (2014). “The effects of low-level laser irradiation on cellular viability and proliferation of human skin fibroblasts cultured in high glucose mediums.” In: *Lasers in medical science* 29.1, pp. 121–9. ISSN: 1435-604X. DOI: 10.1007/s10103-013-1289-2. URL: http://www.ncbi.nlm.nih.gov/pubmed/23455657.

Evans, Denise Hawkins and Heidi Abrahamse (2008). “Efficacy of three different laser wavelengths for in vitro wound healing.” In: *Photodermatology, photoimmunology & photomedicine* 24.4, pp. 199–210. ISSN: 1600-0781. DOI: 10.1111/j.1600-0781.2008.00362.x. URL: http://www.ncbi.nlm.nih.gov/pubmed/18717961.

Evans, Nicholas D. et al. (2013). “Epithelial mechanobiology, skin wound healing, and the stem cell niche”. In: *Journal of the Mechanical Behavior of Biomedical Materials* 28, pp. 397–409. ISSN: 17516161. DOI: 10.1016/j.jmbbm.2013.04.023. URL: http://www.ncbi.nlm.nih.gov/pubmed/23746929http://linkinghub.elsevier.com/retrieve/pii/S1751616113001550.

Fushimi, Tomohiro et al. (2012). “Green light emitting diodes accelerate wound healing: characterization of the effect and its molecular basis in vitro and in vivo.” In: *Wound repair and regeneration : official publication of the Wound Healing Society [and] the European Tissue Repair Society* 20.2, pp. 226–35. ISSN: 1524-475X. DOI: 10.1111/j.1524-475X.2012.00771.x. URL: http://www.ncbi.nlm.nih.gov/pubmed/22380691.

Gambichler, Thilo et al. (2006). “In vivo data of epidermal thickness evaluated by optical coherence tomography: Effects of age, gender, skin type, and anatomic site”. In: *Journal of Dermatological Science* 44.3, pp. 145–152. ISSN: 0923-1811. DOI: http://dx.doi.org/10.1016/j.jdermsci.2006.09.008. URL: http://www.ncbi.nlm.nih.gov/pubmed/17071059http://www.sciencedirect.com/science/article/pii/S0923181106002623.

Gandjbakhche, A H, R F Bonner, and R Nossal (1992). “Scaling relationships for anisotropic random walks”. In: *Journal of Statistical Physics* 69.1, pp. 35–53. ISSN: 1572-9613. DOI: 10.1007/BF01053781. URL: http://dx.doi.org/10.1007/BF01053781.

Gavish, Lilach et al. (2004). “Low level laser irradiation stimulates mitochondrial membrane potential and disperses subnuclear promyelocytic leukemia protein.” In: *Lasers in surgery and medicine* 35.5, pp. 369–376. ISSN: 0196-8092. DOI: 10.1002/lsm.20108. URL: http://www.ncbi.nlm.nih.gov/pubmed/15611960.

Ghisla, S (1980). “Fluorescence and optical characteristics of reduced flavins and flavoproteins.” In: *Methods in enzymology* 66.1969, pp. 360–73. ISSN: 0076-6879. URL: http://www.ncbi.nlm.nih.gov/pubmed/7374479.

González, Pedro Pablo et al. (2003). “Cellulat: an agent-based intracellular signalling model.” In: *Bio Systems* 68.2-3, pp. 171–85. ISSN: 0303-2647. URL: http://www.ncbi.nlm.nih.gov/pubmed/12595116.

Goto, M et al. (2011). “Phosphodiesterase inhibitors block the acceleration of skin permeability barrier repair by red light”. In: *Exp Dermatol* 20.7, pp. 568–571. ISSN: 1600-0625 (Electronic) 0906-6705 (Linking). DOI: 10.1111/j.1600-0625.2011.01255.x. URL: http://www.ncbi.nlm.nih.gov/pubmed/21410772.

Grossman, N et al. (1998). “780 Nm Low Power Diode Laser Irradiation Stimulates Proliferation of Keratinocyte Cultures: Involvement of Reactive Oxygen Species.” In: *Lasers in surgery and medicine* 22.4, pp. 212–218. ISSN: 0196-8092. URL: http://www.ncbi.nlm.nih.gov/pubmed/9603282.

Gueymard, C. a., D. Myers, and K. Emery (2002). “Proposed reference irradiance spectra for solar energy systems testing”. In: *Solar Energy* 73.6, pp. 443–467. ISSN: 0038092X. DOI: 10.1016/S0038-092X(03)00005-7.

Guffey, J et al. (2014). “Inhibition of Mycobacterium smegmatis using near-IR and blue light”. In: *International Journal of Research in Medical Sciences* 2.1, p. 42.

ISSN: 2320-6071. DOI: 10.5455/2320-6012.ijrms20140209. URL: http://www.scopemed.org/?mno=47386.

Gupta et al. (1998). “The Use of low energy photon therapy (LEPT) in Venous Leg Ulcers: A double-blind, Placebo-controlled Study”. In: *The American Society for Dermalogic Surgery*.

Haas, Ann F. et al. (1990). “Low-Energy Helium-Neon Laser Irradiation Increases the Motility of Cultured Human Keatinocytes”. In: *The Society for Investigative Dermatology, Inc*.

Habbema, L et al. (2012). “Minimally invasive non-thermal laser technology using laser-induced optical breakdown for skin rejuvenation”. In: *J Biophotonics* 5.2, pp. 194–199. ISSN: 1864-0648 (Electronic) 1864-063X (Linking). DOI: 10.1002/jbio.201100083. URL: http://www.ncbi.nlm.nih.gov/pubmed/22045580.

— (2013). “Efficacy of minimally invasive nonthermal laser-induced optical breakdown technology for skin rejuvenation”. In: *Lasers Med Sci* 28.3, pp. 935–940. ISSN: 1435-604X (Electronic) 0268-8921 (Linking). DOI: 10.1007/s10103-012-1179-z. URL: http://www.ncbi.nlm.nih.gov/pubmed/22890872.

Hadis, M A et al. (2016). “The dark art of light measurement: accurate radiometry for low-level light therapy”. In: *Lasers Med Sci* 31.4, pp. 789–809. ISSN: 1435-604X. DOI: 10.1007/s10103-016-1914-y. URL: https://www.ncbi.nlm.nih.gov/pubmed/26964800.

Hale, G M and M R Querry (1973). “Optical Constants of Water in the 200-nm to 200-μm Wavelength Region”. In: *Appl. Opt.* 12.3, pp. 555–563. DOI: 10.1364/AO.12.000555. URL: http://ao.osa.org/abstract.cfm?URI=ao-12-3-555.

Haltaufderhyde, Kirk et al. (2015). “Opsin Expression in Human Epidermal Skin”. In: *Photochemistry and photobiology* 91.July, pp. 1–7. ISSN: 00318655. DOI: 10.1111/php.12354. URL: http://www.ncbi.nlm.nih.gov/pubmed/25267311http://www.pubmedcentral.nih.gov/articlerender.fcgi?artid=

PMC4303996http://doi.wiley.com/10.1111/php.12354http://onlinelibrary.wiley.com/doi/10.1111/php.12354/full.

Hamblin, Michael, Ronald W Waynant, and Juanita Anders (2010). *Mechanisms of low-level light therapy V*. Vol. 7552. Progress in Biomedical Optics and Imaging. Proceedings of SPIE: SPIE.

Han, Kwang-Ho et al. (2005). "Alteration of the TGF-β/SMAD pathway in intrinsically and UV-induced skin aging". In: *Mechanisms of Ageing and Development* 126.5, pp. 560–567. ISSN: 00476374. DOI: 10.1016/j.mad.2004.11.006. URL: http://www.ncbi.nlm.nih.gov/pubmed/15811425http://linkinghub.elsevier.com/retrieve/pii/S0047637404002994.

Hanson, Kerry M and Robert M Clegg (2002). "Observation and quantification of ultraviolet-induced reactive oxygen species in ex vivo human skin." In: *Photochemistry and photobiology* 76.1, pp. 57–63. ISSN: 0031-8655. URL: http://www.ncbi.nlm.nih.gov/pubmed/12126308.

Hashiramoto, A et al. (2010). "Mammalian clock gene Cryptochrome regulates arthritis via proinflammatory cytokine TNF-alpha". In: *J Immunol* 184.3, pp. 1560–1565. ISSN: 1550-6606 (Electronic) 0022-1767 (Linking). DOI: 10.4049/jimmunol.0903284. URL: http://www.ncbi.nlm.nih.gov/pubmed/20042581.

Hashmi, J T et al. (2011). "Role of Low-Level Laser Therapy in Neurorehabilitation". In: *The American Academy of Physical Medicine and Rehabilitation* 2.12 Suppl 2, pp. 1–25. ISSN: 1934-1482. DOI: 10.1016/j.pmrj.2010.10.013.Role. URL: https://www.ncbi.nlm.nih.gov/pubmed/21172691.

Hawkins, D. and Heidi Abrahamse (2006). "The Role of Laser Fluence in Cell Viability, Proliferation, and Membrane Integrity of Wounded Human Skin Fibroblasts Following Helium-Neon Irradiation". In: *Lasers in surgery and medicine*.

Hay, R J et al. (2014). "The global burden of skin disease in 2010: an analysis of the prevalence and impact of skin conditions". In: *J Invest Dermatol* 134.6, pp. 1527–1534. ISSN: 1523-1747 (Electronic) 0022-202X (Linking). DOI: 10.1038/jid.2013.446. URL: http://www.ncbi.nlm.nih.gov/pubmed/24166134.

Hoang, Nathalie et al. (2008). “Human and Drosophila Cryptochromes Are Light Activated by Flavin Photoreduction in Living Cells”. In: *PLoS Biology* 6.7. DOI: 10.1371/journal.pbio.0060160.

Holanda, Vanessa Milanesi et al. (2017). “The mechanistic basis for photobiomodulation therapy of neuropathic pain by near infrared laser light”. In: *Lasers in Surgery and Medicine*. ISSN: 01968092. DOI: 10.1002/lsm.22628. URL: http://doi.wiley.com/10.1002/lsm.22628.

Hopkins, J Ty et al. (2004). “Low-Level Laser Therapy Facilitates Superficial Wound Healing in Humans: A triple-blind, sham-controlled Study”. In: *Journal of Athletic Training* 39.3, pp. 223–229.

Houreld, N. et al. (2008). “Laser light influences cellular viability and proliferation in diabetic-wounded fibroblast cells in a dose- and wavelength-dependent manner.” In: *Lasers in medical science* 23.1, pp. 11–18. ISSN: 0268-8921. DOI: 10.1007/s10103-007-0445-y. URL: http://www.ncbi.nlm.nih.gov/pubmed/17361392.

Houreld; N. et al. (2014). “Expression of genes in normal fibroblast cells (WS1) in response to irradiation at 660nm.” In: *Journal of photochemistry and photobiology. B, Biology* 130, pp. 146–152. ISSN: 1873-2682. DOI: 10.1016/j.jphotobiol.2013.11.018. URL: http://www.ncbi.nlm.nih.gov/pubmed/24333762.

Hsu, D S et al. (1996). “Putative human blue-light photoreceptors hCRY1 and hCRY2 are flavoproteins.” In: *Biochemistry* 35.44, pp. 13871–13877. ISSN: 0006-2960. DOI: 10.1021/bi962209o. URL: http://www.ncbi.nlm.nih.gov/pubmed/8909283.

Huang, D. W., B. T. Sherman, and R. A. Lempicki (2009). “Bioinformatics enrichment tools: paths toward the comprehensive functional analysis of large gene lists”. In: *Nucleic Acids Research* 37.1, pp. 1–13. ISSN: 0305-1048. DOI: 10.1093/nar/gkn923. URL: http://www.ncbi.nlm.nih.gov/pubmed/19033363http://www.pubmedcentral.nih.gov/articlerender.fcgi?artid=

PMC2615629https://academic.oup.com/nar/article-lookup/doi/10.1093/nar/gkn923.

Hugh Rushton, D, Michael J Norris, and Dominique Van Neste (2016). “Hair regrowth in male and female pattern hair loss does not involve the conversion of vellus hair to terminal hair”. In: *Experimental Dermatology*, n/a–n/a. ISSN: 1600-0625. DOI: 10.1111/exd.12945. URL: http://dx.doi.org/10.1111/exd.12945.

Izumi, T, S Tajima, and T Nishikawa (1995). “Differential expression of alpha 1 and alpha 2 chains of type VI collagen in the upper, middle, and lower dermal fibroblasts in vitro.” In: *Journal of biochemistry* 117, pp. 1004–1007. ISSN: 0021-924X.

Jacques, S L (1996). “Origins of Optical Properties in the UVA, Visible and NIR Regions”. In: *Advances in Optical Imaging and Photon Migration*. Ed. by R R Alfano Fujimoto and J G. Vol. 2. OSA, p. 70.

Jacques, Steven L (1992). “Laser-tissue interactions. Photochemical, photothermal, and photomechanical.” In: *Surg. Clin. North Am.* 72.3, pp. 531–558.

— (2013). “Optical properties of biological tissues: a review.” In: *Physics in medicine and biology* 58.11, pp. 37–61. ISSN: 1361-6560. DOI: 10.1088/0031-9155/58/11/R37. URL: http://www.ncbi.nlm.nih.gov/pubmed/23666068http://stacks.iop.org/0031-9155/58/i=11/a=R37.

Jacques, Steven L, C.A Alter, and S. A. Prahl (1987). “Angular Dependence of HeNe Laser Light Scattering by Human Dermis”. In: *Lasers in the Life Sciences*.

Jacques, Steven L and Daniel J McAuliffe (1991). “The melanosome: threshold temperature for explosive vaporisation and internal absorption coefficient during pulsed laser irradiation”. In: *Photochemistry and Photobiology* 53.6, pp. 769–775. ISSN: 1751-1097. DOI: 10.1111/j.1751-1097.1991.tb09891.x. URL: http://dx.doi.org/10.1111/j.1751-1097.1991.tb09891.x.

Janson, D G et al. (2012). “Different gene expression patterns in human papillary and reticular fibroblasts”. In: *J Invest Dermatol* 132.11, pp. 2565–2572. ISSN:

1523-1747. DOI: 10.1038/jid.2012.192. URL: https://www.ncbi.nlm.nih.gov/pubmed/22696053.

Janson, David et al. (2013). “Papillary fibroblasts differentiate into reticular fibroblasts after prolonged in vitro culture”. In: *Experimental Dermatology* 22.1, pp. 48–53. ISSN: 09066705. DOI: 10.1111/exd.12069. URL: https://www.ncbi.nlm.nih.gov/pubmed/23278894.

Jenkins, P A and J D Carroll (2011). “How to report low-level laser therapy (LLLT)/photomedici
dose and beam parameters in clinical and laboratory studies”. In: *Photomed Laser Surg* 29.12, pp. 785–787. ISSN: 1557-8550. DOI: 10.1089/pho.2011.9895. URL: https://www.ncbi.nlm.nih.gov/pubmed/22107486.

Jimenez, Joaquin J et al. (2014). “Efficacy and Safety of a Low-level Laser Device in the Treatment of Male and Female Pattern Hair Loss : A Multicenter ,” in: *American Journal Clinical Dermatology*. ISSN: 4025701300606. DOI: 10.1007/s40257-013-0060-6.

Johnson, J L et al. (1988). “Identification of the second chromophore of Escherichia coli and yeast DNA photolyases as 5,10-methenyltetrahydrofolate.” In: *Proceedings of the National Academy of Sciences of the United States of America* 85.7, pp. 2046–2050. ISSN: 0027-8424. URL: http://www.pubmedcentral.nih.gov/articlerender.fcgi?artid=279925&tool=pmcentrez&rendertype=abstract.

Kajagar, Basavaraj M et al. (2012). “Efficacy of low level laser therapy on wound healing in patients with chronic diabetic foot ulcers-a randomised control trial.” In: *The Indian journal of surgery* 74.5, pp. 359–363. ISSN: 0972-2068. DOI: 10.1007/s12262-011-0393-4. URL: http://www.pubmedcentral.nih.gov/articlerender.fcgi?artid=3477409&tool=pmcentrez&rendertype=abstract.

Karu, Tiina I (2003). “Low-Power Laser Therapy”. In: *Biomedical Photonics Handbook*, pp. 1–26. ISBN: 0849311160.

— (2014). “Cellular and Molecular Mechanisms of Photobiomodulation (Low-Power Laser Therapy)”. In: *IEEE Journal of Selected Topics in Quantum Electronics*

20.2, pp. 143–148. ISSN: 1077-260X. DOI: 10.1109/JSTQE.2013.2273411. URL: http://ieeexplore.ieee.org/lpdocs/epic03/wrapper.htm?arnumber=6603355.

Karu, Tiina I and SF F Kolyakov (2005). “Exact action spectra for cellular responses relevant to phototherapy”. In: *Photomedicine and Laser Therapy* 23.4, pp. 355–361. URL: http://online.liebertpub.com/doi/abs/10.1089/pho.2005.23.355.

Kawagishi, Hiroyuki and Toren Finkel (2014). “Unraveling the Truth About Antioxidants: ROS and disease: finding the right balance.” In: *Nature medicine* 20.7, pp. 711–3. ISSN: 1546-170X. DOI: 10.1038/nm.3625. URL: http://www.ncbi.nlm.nih.gov/pubmed/24999942.

Keszler, A et al. (2014). “Far red/near infrared light-induced protection against cardiac ischemia and reperfusion injury remains intact under diabetic conditions and is independent of nitric oxide synthase”. In: *Front Physiol* 5, p. 305. ISSN: 1664-042X (Electronic) 1664-042X (Linking). DOI: 10.3389/fphys.2014.00305. URL: http://www.ncbi.nlm.nih.gov/pubmed/25202275.

Khan, Imran, Elieza Tang, and Praveen Arany (2015). “Molecular pathway of near-infrared laser phototoxicity involves ATF-4 orchestrated ER stress”. In: *Scientific Reports* 5, p. 10581. ISSN: 2045-2322. DOI: 10.1038/srep10581. URL: http://www.nature.com/doifinder/10.1038/srep10581.

Kim, Hyojin et al. (2013a). “Low-level light therapy for androgenetic alopecia: a 24-week, randomized, double-blind, sham device-controlled multicenter trial”. In: *Dermatol Surg* 39.8, pp. 1177–1183. ISSN: 1524-4725 (Electronic) 1076-0512 (Linking). DOI: 10.1111/dsu.12200. URL: http://www.ncbi.nlm.nih.gov/pubmed/23551662.

Kim, Hyoung-June June et al. (2013b). “Violet Light Down-Regulates the Expression of Specific Differentiation Markers through Rhodopsin in Normal Human Epidermal Keratinocytes”. In: *PLoS ONE* 8.9, pp. 1–10. ISSN: 1932-6203. DOI: 10.1371/journal.pone.0073678. URL: http://www.pubmedcentral.nih.

gov/articlerender.fcgi?artid=3775733&tool=pmcentrez&rendertype=abstract.

Klammer, Holger et al. (2015). “Bystander effects as manifestation of intercellular communication of DNA damage and of the cellular oxidative status”. In: *Cancer Letters* 356.1, pp. 58–71. ISSN: 03043835. DOI: 10.1016/j.canlet.2013.12.017. URL: http://linkinghub.elsevier.com/retrieve/pii/S0304383513008550.

Kojima, Daisuke et al. (2011). “UV-sensitive photoreceptor protein OPN5 in humans and mice”. In: *PLoS ONE* 6.10. ISSN: 1932-6203 (Electronic)\n1932-6203 (Linking). DOI: 10.1371/journal.pone.0026388.

Kopera, D et al. (2005). “Does the use of low-level laser influence wound healing in chronic venous leg ulcers?” In: *J Wound Care* 14.8, pp. 391–394. ISSN: 0969-0700 (Print) 0969-0700 (Linking). DOI: 10.12968/jowc.2005.14.8.26825. URL: http://www.ncbi.nlm.nih.gov/pubmed/16178295.

Koyanagi, Mitsumasa et al. (2013). “Homologs of vertebrate Opn3 potentially serve as a light sensor in nonphotoreceptive tissue.” In: *Proceedings of the National Academy of Sciences of the United States of America* 110.13, pp. 4998–5003. ISSN: 1091-6490. DOI: 10.1073/pnas.1219416110. URL: http://www.pubmedcentral.nih.gov/articlerender.fcgi?artid=3612648&tool=pmcentrez&rendertype=abstract.

Kupermanbeade, Marina, Vicki J. Levine, and Robin Ashinoff (2001). “Laser Removal of Tattoos”. In: *American Journal of Clinical Dermatology* 2.1, pp. 21–25. ISSN: 1175-0561. DOI: 10.2165/00128071-200102010-00004. URL: http://link.springer.com/10.2165/00128071-200102010-00004.

Kuse, Yoshiki et al. (2014). “Damage of photoreceptor-derived cells in culture induced by light emitting diode-derived blue light”. In: *Scientific Reports* 4, pp. 497–505. ISSN: 2045-2322. DOI: 10.1038/srep05223. URL: http://www.nature.com/articles/srep05223.

Lamola, Angelo a et al. (2013). “The effect of hematocrit on the efficacy of phototherapy for neonatal jaundice.” In: *Pediatric research* 74.1, pp. 54–60. ISSN:

1530-0447. DOI: 10.1038/pr.2013.67. URL: http://www.ncbi.nlm.nih.gov/pubmed/23604171.

Lanzafame, R J et al. (2014). “The growth of human scalp hair in females using visible red light laser and LED sources”. In: *Lasers Surg Med* 46.8, pp. 601–607. ISSN: 1096-9101 (Electronic) 0196-8092 (Linking). DOI: 10.1002/lsm.22277. URL: http://www.ncbi.nlm.nih.gov/pubmed/25124964.

Lanzafame, Raymond J et al. (2013). “The growth of human scalp hair mediated by visible red light laser and LED sources in males.” In: *Lasers in surgery and medicine* 45.8, pp. 487–95. ISSN: 1096-9101. DOI: 10.1002/lsm.22173. URL: http://www.ncbi.nlm.nih.gov/pubmed/24078483.

Leavitt, Matt et al. (2009). “HairMax LaserComb Laser Phototherapy Device in the Treatment of Male Androgenetic Alopecia”. In: *Clinical Drug Investigation* 29.5, pp. 283–292.

Lee, T H, A B Lerner, and R J Halberg (1953). “Water soluble vitamins in normal human skin”. In: *J Invest Dermatol* 20.1, pp. 19–26. ISSN: 0022-202X. URL: https://www.ncbi.nlm.nih.gov/pubmed/13023026.

Lemons, Johanna M S et al. (2010). “Quiescent fibroblasts exhibit high metabolic activity.” In: *PLoS biology* 8.10, e1000514. ISSN: 1545-7885. DOI: 10.1371/journal.pbio.1000514. URL: http://www.ncbi.nlm.nih.gov/pubmed/21049082http://www.pubmedcentral.nih.gov/articlerender.fcgi?artid=PMC2958657.

Lewis, Jeffrey a and Jorge C Escalante-Semerena (2006). “The FAD-dependent tricarballylate dehydrogenase (TcuA) enzyme of Salmonella enterica converts tricarballylate into cis-aconitate.” In: *Journal of bacteriology* 188.15, pp. 5479–86. ISSN: 0021-9193. DOI: 10.1128/JB.00514-06. URL: http://www.pubmedcentral.nih.gov/articlerender.fcgi?artid=1540016&tool=pmcentrez&rendertype=abstract.

Li, Wen-Tyng, Chih-Wei Chen, and Po-Ya Huang (2013). “Effects of low level light irradiation on the migration of mesenchymal stem cells derived from rat bone marrow.” In: *Conference proceedings : ... Annual International Conference of*

the IEEE Engineering in Medicine and Biology Society. IEEE Engineering in Medicine and Biology Society. Conference 2013.passage 0, pp. 4121–4. ISSN: 1557-170X. DOI: 10.1109/EMBC.2013.6610452. URL: http://www.ncbi.nlm.nih.gov/pubmed/24110639.

Liebel, Frank et al. (2012). "Irradiation of Skin with Visible Light Induces Reactive Oxygen Species and Matrix-Degrading Enzymes". In: *Journal of Investigative Dermatology* 132.7, pp. 1901–1907. ISSN: 0022-202X. DOI: 10.1038/jid.2011.476. URL: http://dx.doi.org/10.1038/jid.2011.476.

Liebmann, Joerg, Matthias Born, and Victoria Kolb-Bachofen (2010). "Blue-light irradiation regulates proliferation and differentiation in human skin cells." In: *The Journal of investigative dermatology* 130.1, pp. 259–269. ISSN: 1523-1747. DOI: 10.1038/jid.2009.194. URL: http://www.ncbi.nlm.nih.gov/pubmed/19675580http://dx.doi.org/10.1038/jid.2009.194.

Lim, H W et al. (2015). "Phototherapy in dermatology: A call for action". In: *J Am Acad Dermatol* 72.6, pp. 1078–1080. ISSN: 1097-6787 (Electronic) 0190-9622 (Linking). DOI: 10.1016/j.jaad.2015.03.017. URL: http://www.ncbi.nlm.nih.gov/pubmed/25981004.

Ling, Z, J C Hannaert, and D Pipeleers (1994). "Effect of nutrients, hormones and serum on survival of rat islet beta cells in culture." In: *Diabetologia* 37.1, pp. 15–21. ISSN: 0012-186X. URL: http://www.ncbi.nlm.nih.gov/pubmed/7512059.

Lipovsky, Anat et al. (2013). "Low-level visible light (LLVL) irradiation promotes proliferation of mesenchymal stem cells." In: *Lasers in medical science* 28.4, pp. 1113–1117. ISSN: 1435-604X. DOI: 10.1007/s10103-012-1207-z. URL: http://www.ncbi.nlm.nih.gov/pubmed/23007630.

Lockwood, Daniel B. et al. (2005). "Blue light generates reactive oxygen species (ROS) differentially in tumor vs. normal epithelial cells". In: *Dental Materials* 21.7, pp. 683–688. ISSN: 01095641. DOI: 10.1016/j.dental.2004.07.022. URL: http://www.ncbi.nlm.nih.gov/pubmed/15978279http://linkinghub.elsevier.com/retrieve/pii/S0109564105000345.

Malm, M (1991). “EFFECT OF LOW POWER GALLIUM ARSENIDE LASER ON HEALING”. In: *Scandinavian Journal of Plastic Recontructive and Hand Surgery*, pp. 249–251.

Mamalis, Andrew, Manveer Garcha, and Jared Jagdeo (2015). “Light emitting diode-generated blue light modulates fibrosis characteristics: Fibroblast proliferation, migration speed, and reactive oxygen species generation”. In: *Lasers in Surgery and Medicine* 47.August 2014, pp. 210–215. ISSN: 01968092. DOI: 10.1002/lsm.22293. URL: http://doi.wiley.com/10.1002/lsm.22293.

Marchesini, Renato et al. (1992). “Optical properties of in vitro epidermis and their possible relationship with optical properties of in vivo skin”. In: *Journal of Photochemistry and Photobiology B: Biology* 16.2, pp. 127–140. ISSN: 1011-1344. DOI: http://dx.doi.org/10.1016/1011-1344(92)80004-F. URL: http://www.sciencedirect.com/science/article/pii/101113449280004F.

Mason, M G, P Nicholls, and C E Cooper (2014). “Re-evaluation of the near infrared spectra of mitochondrial cytochrome c oxidase: Implications for non invasive in vivo monitoring of tissues”. In: *Biochim Biophys Acta* 1837.11, pp. 1882–1891. ISSN: 0006-3002 (Print) 0006-3002 (Linking). DOI: 10.1016/j.bbabio.2014.08.005. URL: http://www.ncbi.nlm.nih.gov/pubmed/25175349.

Massey, V and H Ganther (1965). “On the interpretation of the absorption spectra of flavoproteins with special reference to D-amino acid oxidase.” In: *Biochemistry* 4.June, pp. 1161–1173. ISSN: 0006-2960.

Matsuyama, Take et al. (2012). “Photochemical properties of mammalian melanopsin.” In: *Biochemistry* 51.27, pp. 5454–5462. ISSN: 1520-4995. DOI: 10.1021/bi3004999. URL: http://www.ncbi.nlm.nih.gov/pubmed/22670683.

McDaniel, D H et al. (2010). “Varying ratios of wavelengths in dual wavelength LED photomodulation alters gene expression profiles in human skin fibroblasts.” In: *Lasers in surgery and medicine* 42.6, pp. 540–545. ISSN: 1096-9101. DOI: 10.1002/lsm.20947. URL: http://www.ncbi.nlm.nih.gov/pubmed/20662030.

McFarland, Kevin L et al. (2011). “Culture medium and cell density impact gene expression in normal skin and abnormal scar-derived fibroblasts.” In: *Journal of burn care & research : official publication of the American Burn Association* 32.4, pp. 498–508. ISSN: 1559-0488. DOI: 10.1097/BCR.0b013e3182223cb1. URL: http://www.ncbi.nlm.nih.gov/pubmed/21747336.

Meglinski, Igor V and Stephen J Matcher (2002). “Quantitative assessment of skin layers absorption and skin reflectance spectra simulation in the visible and near-infrared spectral regions”. In: *Physiological Measurement* 23.4, p. 741. ISSN: 0967-3334. URL: http://stacks.iop.org/0967-3334/23/i=4/a=312.

Melyan, Z. et al. (2005). “Addition of human melanopsin renders mammalian cells photoresponsive”. In: *Nature* 433.7027, pp. 741–745. ISSN: 0028-0836. DOI: 10.1038/nature03344. URL: http://www.ncbi.nlm.nih.gov/pubmed/15674244http://www.nature.com/doifinder/10.1038/nature03344.

Merbs, S and J Nathans (1992). “Absorption Spectra of human cone pigments”. In: *Nature*.

Mester, E, B Szende, and P Gartner (1968). “[The effect of laser beams on the growth of hair in mice]”. In: *Radiobiol Radiother (Berl)* 9.5, pp. 621–626. ISSN: 0033-8184 (Print) 0033-8184 (Linking). URL: http://www.ncbi.nlm.nih.gov/pubmed/5732466.

Metelitsa, Andrei I and Jeremy B Green (2011). “Home-use laser and light devices for the skin: an update.” In: *Seminars in cutaneous medicine and surgery* 30.3, pp. 144–7. ISSN: 1558-0768. DOI: 10.1016/j.sder.2011.05.005. URL: http://www.ncbi.nlm.nih.gov/pubmed/21925367.

Mi, Qi et al. (2007). “Agent-based model of inflammation and wound healing: insights into diabetic foot ulcer pathology and the role of transforming growth factor-β1”. In: *Wound Repair and Regeneration* 15.5, pp. 671–682. ISSN: 10671927. DOI: 10.1111/j.1524-475X.2007.00271.x. URL: http://www.ncbi.nlm.nih.gov/pubmed/17971013http://doi.wiley.com/10.1111/j.1524-475X.2007.00271.x.

Mignon, C. et al. “Investigation of the origin of the variability of the values of the skin layers optical properties for a more accurate prediction of the light propagation in the skin”. In: *(in preparation)*.

Mignon, C. et al. “Reticular and papillary fibroblasts exhibit a differential response to visible and NIR light”. In: *(in preparation)*.

Mignon, C. et al. (2015a). “A systematic approach to unravel how light impacts primary human dermal fibroblasts”. In: *Lasers in surgery and medicine*, ASLMS Kissimmee 2015.

— (2015b). “Light Parameters in Low-Level Light Therapy. A systematic literature review.” In: *Lasers in surgery and medicine*, ASLMS Kissimmee 2015.

Mignon, C. et al. (2016a). “Impact of variability of the optical properties of skin layers on prediction of photon density using a Monte Carlo model.” In: *Lasers in surgery and medicine*. 111 RIVER ST, HOBOKEN 07030-5774, NJ USA: Wiley-Blackwell, p. 48.

Mignon, C et al. (2016b). “Photobiomodulation devices for hair regrowth and wound healing: a therapy full of promise but a literature full of confusion”. In: *Exp Dermatol*. ISSN: 1600-0625. DOI: 10.1111/exd.13035. URL: https://www.ncbi.nlm.nih.gov/pubmed/27095546.

Mignon, C et al. (2016c). “Photobiomodulation of distinct lineages of human dermal fibroblasts: a rational approach towards the selection of effective light parameters for skin rejuvenation and wound healing”. In: *Proc. SPIE* 9695, pp. 969508–969516. DOI: 10.1117/12.2208574.

Mignon, C. et al. (2016d). “Visible light differentially influences distinct human dermal fibroblast lineages and may be exploitable for wound-healing therapy”. In: *British Journal of Dermatology* 174.5, e72. ISSN: 0007-0963.

Mignon, C. et al. (2017a). “Optical settings, cell culture conditions and treatment protocols all significantly impact on interpretation of photobiomodulation responses in primary human dermal fibroblasts”. In: *BSID Manchester 2017*.

Mignon, C. et al. (2017b). “Photobiomodulation of human dermal fibroblasts in vitro: decisive role of cell culture conditions and treatment protocols on exper-

imental outcome". In: *Scientific Reports* 7.1, p. 2797. ISSN: 2045-2322. DOI: 10.1038/s41598-017-02802-0. URL: http://www.ncbi.nlm.nih.gov/pubmed/28584230http://www.pubmedcentral.nih.gov/articlerender.fcgi?artid=PMC5459822http://www.nature.com/articles/s41598-017-02802-0.

Mignon, C. et al. (2017c). "The importance of the selection of optical parameters, cell culture conditions and treatment protocols in photobiomodulation in vitro: a multi-factorial analysis of the response of primary human dermal fibroblasts to visible and NIR light". In: *ASLMS San Diego 2017 (Travel grant)*.

Mignon, Charles et al. (2016e). "Fractional laser photothermolysis using Bessel beams". In: *Biomedical Optics Express* 7.12, p. 4974. ISSN: 2156-7085. DOI: 10.1364/BOE.7.004974. URL: https://www.osapublishing.org/abstract.cfm?URI=boe-7-12-4974.

Milton Prabu, S, K Shagirtha, and J Renugadevi (2010). "Quercetin in combination with vitamins (C and E) improves oxidative stress and renal injury in cadmium intoxicated rats." In: *European review for medical and pharmacological sciences* 14.11, pp. 903–14. ISSN: 1128-3602. URL: http://www.ncbi.nlm.nih.gov/pubmed/21284339.

Minatel, Debora G et al. (2009). "Phototherapy promotes healing of chronic diabetic leg ulcers that failed to respond to other therapies." In: *Lasers in surgery and medicine* 41.6, pp. 433–41. ISSN: 1096-9101. DOI: 10.1002/lsm.20789. URL: http://www.ncbi.nlm.nih.gov/pubmed/19588536.

Mine, Solène et al. (2008). "Aging alters functionally human dermal papillary fibroblasts but not reticular fibroblasts: A new view of skin morphogenesis and aging". In: *PLoS ONE* 3.12. ISSN: 19326203. DOI: 10.1371/journal.pone.0004066.

Moody, John (2005). *Tissue Spectra*. URL: http://www.ucl.ac.uk/medphys/research/borl/intro/spectra.

Mosmann, T (1983). "Rapid colorimetric assay for cellular growth and survival: application to proliferation and cytotoxicity assays." In: *Journal of immunological*

methods 65.1-2, pp. 55–63. ISSN: 0022-1759. URL: http://www.ncbi.nlm.nih.gov/pubmed/6606682.

Mysore, V (2012). “Finasteride and sexual side effects”. In: *Indian Dermatol Online J* 3.1, pp. 62–65. ISSN: 2249-5673 (Electronic) 2229-5178 (Linking). DOI: 10.4103/2229-5178.93496. URL: http://www.ncbi.nlm.nih.gov/pubmed/23130269.

Nakao, A (2014). “Temporal regulation of cytokines by the circadian clock”. In: *J Immunol Res* 2014, p. 614529. ISSN: 2314-7156 (Electronic) 2314-7156 (Linking). DOI: 10.1155/2014/614529. URL: http://www.ncbi.nlm.nih.gov/pubmed/24809063.

Narasimamurthy, R et al. (2012). “Circadian clock protein cryptochrome regulates the expression of proinflammatory cytokines”. In: *Proc Natl Acad Sci U S A* 109.31, pp. 12662–12667. ISSN: 1091-6490 (Electronic) 0027-8424 (Linking). DOI: 10.1073/pnas.1209965109. URL: http://www.ncbi.nlm.nih.gov/pubmed/22778400.

Narayanan, P K et al. (1999). “Alpha particles induce the production of interleukin-8 by human cells.” In: *Radiation research* 152.1, pp. 57–63. ISSN: 0033-7587. URL: http://www.ncbi.nlm.nih.gov/pubmed/10381841.

North, J, D Rein, and L Tappel (1996). “Multicomponent analysis of heme protein spectra in biological materials.” In: *Analytical biochemistry* 233.1, pp. 115–123. ISSN: 0003-2697. DOI: 10.1006/abio.1996.0015. URL: http://www.ncbi.nlm.nih.gov/pubmed/8789155.

Ohara, Masayuki, Tatsuo Fujikura, and Hiroshi Fujiwara (2003). “Augmentation of the inhibitory effect of blue light on the growth of B16 melanoma cells by riboflavin”. In: *Int J Oncol* 22.6, pp. 1291–1295. ISSN: 1019-6439 (Print) 1019-6439 (Linking). URL: http://www.ncbi.nlm.nih.gov/pubmed/12738996.

Olesen, B W (1982). “Thermal comfort”. In: *Technical Review*.

Olsen, Rikke K J et al. (2016). “Riboflavin-Responsive and -Non-responsive Mutations in FAD Synthase Cause Multiple Acyl-CoA Dehydrogenase and Combined Respiratory-Chain Deficiency.” In: *American journal of human genetics*

98.6, pp. 1130–45. ISSN: 1537-6605. DOI: 10.1016/j.ajhg.2016.04.006. URL: http://www.ncbi.nlm.nih.gov/pubmed/27259049http://www.pubmedcentral.nih.gov/articlerender.fcgi?artid=PMC4908180.

Oplander, C et al. (2011). “Effects of blue light irradiation on human dermal fibroblasts.” In: *Journal of photochemistry and photobiology. B, Biology* 103.2, pp. 118–125. ISSN: 1873-2682. DOI: 10.1016/j.jphotobiol.2011.02.018. URL: http://www.ncbi.nlm.nih.gov/pubmed/21421326.

Opländer, Christian et al. (2013). “Mechanism and biological relevance of blue-light (420-453 nm)-induced nonenzymatic nitric oxide generation from photolabile nitric oxide derivates in human skin in vitro and in vivo”. In: *Free Radical Biology and Medicine* 65, pp. 1363–1377. ISSN: 08915849. DOI: 10.1016/j.freeradbiomed.2013.09.022. URL: http://www.ncbi.nlm.nih.gov/pubmed/24121056http://dx.doi.org/10.1016/j.freeradbiomed.2013.09.022.

Panda, Satchidananda et al. (2005). “Illumination of the melanopsin signaling pathway”. In: *Science* 307.5709, pp. 600–604. ISSN: 1095-9203 (Electronic) 0036-8075 (Linking). DOI: 10.1126/science.1105121. URL: http://www.ncbi.nlm.nih.gov/pubmed/15681390.

Pellicioli, Ana et al. (2014). “Laser phototherapy accelerates oral keratinocyte migration through the modulation of the mammalian target of rapamycin signaling pathway”. In: *Journal of Biomedical Optics* 19(2). DOI: 10.1117/1.JBO.19.2.028002.

Pfaff, S et al. (2015). “Prospective Randomized Long-Term Study on the Efficacy and Safety of UV-Free Blue Light for Treating Mild Psoriasis Vulgaris”. In: *Dermatology* 231.1, pp. 24–34. ISSN: 1421-9832 (Electronic) 1018-8665 (Linking). DOI: 10.1159/000430495. URL: http://www.ncbi.nlm.nih.gov/pubmed/26044167.

Pillai, S., C. Oresajo, and J. Hayward (2005). “Ultraviolet radiation and skin aging: roles of reactive oxygen species, inflammation and protease activation, and strategies for prevention of inflammation-induced matrix degradation - a review”. In: *International Journal of Cosmetic Science* 27.1, pp. 17–34. ISSN:

0142-5463. DOI: 10.1111/j.1467-2494.2004.00241.x. URL: http://www.ncbi.nlm.nih.gov/pubmed/18492178http://doi.wiley.com/10.1111/j.1467-2494.2004.00241.x.

Poon, Vincent K M, Lin Huang, and Andrew Burd (2005). "Biostimulation of dermal fibroblast by sublethal Q-switched Nd:YAG 532 nm laser: collagen remodeling and pigmentation." In: *Journal of photochemistry and photobiology. B, Biology* 81.1, pp. 1–8. ISSN: 1011-1344. DOI: 10.1016/j.jphotobiol.2005.05.006. URL: http://www.ncbi.nlm.nih.gov/pubmed/16019220.

Preissig, Jason, Kristy Hamilton, and Ramsey Markus (2012). "Current Laser Resurfacing Technologies: A Review that Delves Beneath the Surface." In: *Seminars in plastic surgery* 26.3, pp. 109–16. ISSN: 1535-2188. DOI: 10.1055/s-0032-1329413. URL: http://www.ncbi.nlm.nih.gov/pubmed/23904818http://www.pubmedcentral.nih.gov/articlerender.fcgi?artid=PMC3580982.

Prise, Kevin M and Joe M O'Sullivan (2009). "Radiation-induced bystander signalling in cancer therapy." In: *Nature reviews. Cancer* 9.5, pp. 351–60. ISSN: 1474-1768. DOI: 10.1038/nrc2603. URL: http://www.ncbi.nlm.nih.gov/pubmed/19377507http://www.pubmedcentral.nih.gov/articlerender.fcgi?artid=PMC2855954.

Quan, TaiHao et al. (2002). "Ultraviolet Irradiation Alters Transforming Growth Factor β/Smad Pathway in Human Skin In Vivo". In: *Journal of Investigative Dermatology* 119.2, pp. 499–506. ISSN: 0022202X. DOI: 10.1046/j.1523-1747.2002.01834.x. URL: http://www.ncbi.nlm.nih.gov/pubmed/12190876http://linkinghub.elsevier.com/retrieve/pii/S0022202X15417506.

Raicu, V and Y Feldman (2015). *Dielectric Relaxation in Biological Systems*. Oxford.

Rajagopalan, K V and P Handler (1964). "The Absorption Spectra of Iron-Flavoproteins". In: *The Journal of biological chemistry* 239.5.

Raulin, Christian, Barbel Greve, and Hortensia Grema (2003). "IPL technology: A review". In: *Lasers in Surgery and Medicine* 32.2, pp. 78–87. ISSN: 0196-8092. DOI: 10.1002/lsm.10145. URL: http://doi.wiley.com/10.1002/lsm.10145.

Ribeiro, Martha Simões et al. (2004). “Effects of low-intensity polarized visible laser radiation on skin burns: a light microscopy study.” In: *Journal of clinical laser medicine & surgery* 22.1, pp. 59–66. ISSN: 1044-5471. DOI: 10.1089/104454704773660994. URL: http://www.ncbi.nlm.nih.gov/pubmed/15117489.

Rieder, Conly L. and Helder Maiato (2004). “Stuck in Division or Passing through: What Happens When Cells Cannot Satisfy the Spindle Assembly Checkpoint”. In: *Developmental Cell* 7.5, pp. 637–651. ISSN: 15345807. DOI: 10.1016/j.devcel.2004.09.002.

Rigau, J et al. (1994). “Effects of the 633nm laser on the behavior and morphology of primary fibroblast culture”. In: *Proceedings of SPIE* 2630.2, pp. 38–42.

Rinaldi, F (2008). “Laser: a review”. In: *Clin Dermatol* 26.6, pp. 590–601. ISSN: 0738-081X (Print) 0738-081X (Linking). DOI: 10.1016/j.clindermatol.2007.09.014. URL: http://www.ncbi.nlm.nih.gov/pubmed/18940539.

Rinnerthaler, Mark et al. (2015). “Oxidative stress in aging human skin.” In: *Biomolecules* 5.2, pp. 545–89. ISSN: 2218-273X. DOI: 10.3390/biom5020545. URL: http://www.ncbi.nlm.nih.gov/pubmed/25906193http://www.pubmedcentral.nih.gov/articlerender.fcgi?artid=PMC4496685.

Roggan, A et al. (1999). “Optical Properties of Circulating Human Blood in the Wavelength Range 400–2500 nm”. In: *Journal of Biomedical Optics* 4.1, pp. 36–46. ISSN: 1083-3668. DOI: 10.1117/1.429919.

Ross, E V et al. (1999). “Theoretical considerations in laser hair removal”. In: *Dermatol Clin* 17.2, pp. 333–55. ISSN: 0733-8635. URL: http://www.ncbi.nlm.nih.gov/pubmed/10327301.

Rushton, D H, J J H Gilkes, and D J J Van Neste (2012). “No improvement in male-pattern hair loss using laser hair-comb therapy: a 6-month, half-head, assessor-blinded investigation in two men”. In: *Clinical and Experimental Dermatology* 37.3, pp. 313–315. ISSN: 1365-2230. DOI: 10.1111/j.1365-2230.2011.04208.x. URL: http://dx.doi.org/10.1111/j.1365-2230.2011.04208.x.

Saidi, I S, S L Jacques, and F K Tittel (1995). “Mie and Rayleigh modeling of visible-light scattering in neonatal skin”. In: *Appl. Opt.* 34.31, pp. 7410–7418. DOI: 10.1364/AO.34.007410. URL: http://ao.osa.org/abstract.cfm?URI=ao-34-31-7410.

Salomatina, Elena et al. (2006). “Optical properties of normal and cancerous human skin in the visible and near-infrared spectral range”. In: *Journal of Biomedical Optics* 11.6, pp. 64026–64029. ISSN: 1083-3668. DOI: 10.1117/1.2398928. URL: http://www.ncbi.nlm.nih.gov/pubmed/17212549.

Sancar, A (2000). “Cryptochrome: the second photoactive pigment in the eye and its role in circadian photoreception.” In: *Annual review of biochemistry* 69, pp. 31–67. ISSN: 0066-4154. DOI: 10.1146/annurev.biochem.69.1.31. URL: http://www.ncbi.nlm.nih.gov/pubmed/10966452.

Satino, John L and Michael Markou (2003). “Hair Regrowth and Increased Hair Tensile Strength Low-Level Laser Therapy”. In: *International journal of cosmetic surgery and aesthetic dermatology* 5.2, pp. 113–118.

Sato, K et al. (1995). *The primary cytotoxicity in ultraviolet-a-irradiated riboflavin solution is derived from hydrogen peroxide.* DOI: 10.1111/1523-1747.ep12323724.

Schindl, A et al. (1998). “Low-intensity laser irradiation improves skin circulation in patients with diabetic microangiopathy”. In: *Diabetes Care* 21.4, pp. 580–584. ISSN: 0149-5992 (Print) 0149-5992 (Linking). URL: http://www.ncbi.nlm.nih.gov/pubmed/9571346.

Schindl, Andreas, M Schindl, and L Schindl (1997). “Successful treatment of a persistent radiation ulcer by low power laser therapy.” In: *Journal of the American Academy of Dermatology* 37.4, pp. 646–8. ISSN: 0190-9622. URL: http://www.ncbi.nlm.nih.gov/pubmed/9344208.

Schindl, Andreas et al. (2002). “Systemic Effects of Low-Intensity Laser Irradiation on Skin Microcirculation in Patients with Diabetic Microangiopathy”. In: *Microvascular Research* 64.2, pp. 240–246. ISSN: 00262862. DOI: 10.1006/mvre.2002.2429. URL: http://linkinghub.elsevier.com/retrieve/pii/S0026286202924295http://www.ncbi.nlm.nih.gov/pubmed/12204648.

Seltman, H.J. (2015). *Experimental Design and Analysis*. URL: http://www.stat.cmu.edu/~hseltman/309/Book/Book.pdf.

Seo, Min-Duk et al. (2012). “HaCaT Keratinocytes and Primary Epidermal Keratinocytes Have Different Transcriptional Profiles of Cornified Envelope-Associated Genes to T Helper Cell Cytokines”. In: *Biomolecules and Therapeutics* 20.2, pp. 171–176. ISSN: 1976-9148. DOI: 10.4062/biomolther.2012.20.2.171. URL: http://koreascience.or.kr/journal/view.jsp?kj=OOOMB4&py=2012&vnc=v20n2&sp=171.

Sheen, Yi-Shuan et al. (2015). “Visible red light enhances physiological anagen entry in vivo and has direct and indirect stimulative effects in vitro”. In: *Lasers in Surgery and Medicine* 47.October 2014, pp. 50–59. ISSN: 01968092. DOI: 10.1002/lsm.22316. URL: http://doi.wiley.com/10.1002/lsm.22316.

Sikka, Gautam et al. (2014). “Melanopsin mediates light-dependent relaxation in blood vessels”. In: *Proceedings of the National Academy of Sciences* 111.50, pp. 17977–17982. ISSN: 0027-8424. DOI: 10.1073/pnas.1420258111. URL: http://www.pnas.org/lookup/doi/10.1073/pnas.1420258111.

Simpson, C R et al. (1998). “Near-infrared optical properties of ex vivo human skin and subcutaneous tissues measured using the Monte Carlo inversion technique”. In: *Physics in Medicine and Biology* 43.9, p. 2465. ISSN: 0031-9155. URL: http://stacks.iop.org/0031-9155/43/i=9/a=003http://www.ncbi.nlm.nih.gov/pubmed/9755939.

Sliney, David H (2007). “Radiometric quantities and units used in photobiology and photochemistry: recommendations of the Commission Internationale de L’Eclairage (International Commission on Illumination).” In: *Photochemistry and photobiology* 83.2, pp. 425–32. ISSN: 0031-8655. DOI: 10.1562/2006-11-14-RA-1081. URL: http://www.ncbi.nlm.nih.gov/pubmed/17115802.

Smith, Kendric C (2007). “Ten Lectures on Basic Science of Laser Phototherapy”. In: *Photochemistry and Photobiology* 83.6, pp. 1539–1540. ISSN: 1751-1097. DOI: 10.1111/j.1751-1097.2007.00229.x. URL: http://dx.doi.org/10.1111/j.1751-1097.2007.00229.x.

Sorrell, J M and A I Caplan (2004). “Fibroblast heterogeneity: more than skin deep”. In: *J Cell Sci* 117.Pt 5, pp. 667–675. ISSN: 0021-9533. DOI: 10.1242/jcs.01005. URL: https://www.ncbi.nlm.nih.gov/pubmed/14754903.

Stenkamp, R E, D C Teller, and K Palczewski (2002). “Crystal structure of rhodopsin: a G-protein-coupled receptor.” In: *Chembiochem : a European journal of chemical biology* 3.10, pp. 963–967. ISSN: 1439-4227. DOI: 10.1002/1439-7633(20021004)3:10<963::AID-CBIC963>3.0.CO;2-9. URL: http://www.ncbi.nlm.nih.gov/pubmed/12362360.

Stern, R S (2007). “Psoralen and ultraviolet a light therapy for psoriasis”. In: *N Engl J Med* 357.7, pp. 682–690. ISSN: 1533-4406 (Electronic) 0028-4793 (Linking). DOI: 10.1056/NEJMct072317. URL: http://www.ncbi.nlm.nih.gov/pubmed/17699818.

Stoppiglia, Luiz F et al. (2002). “Protective effect of d-glucose, l-leucine and fetal calf serum against oxidative stress in neonatal pancreatic islets”. In: *Biochimica et Biophysica Acta (BBA) - Molecular Basis of Disease* 1588.2, pp. 113–118. ISSN: 09254439. DOI: 10.1016/S0925-4439(02)00154-0.

Subramanian, Aravind et al. (2005). “Gene set enrichment analysis: a knowledge-based approach for interpreting genome-wide expression profiles.” In: *Proceedings of the National Academy of Sciences of the United States of America* 102.43, pp. 15545–50. ISSN: 0027-8424. DOI: 10.1073/pnas.0506580102. URL: http://www.ncbi.nlm.nih.gov/pubmed/16199517http://www.pubmedcentral.nih.gov/articlerender.fcgi?artid=PMC1239896.

Svaasand, Lars O et al. (1995). “Tissue parameters determining the visual appearance of normal skin and port-wine stains”. In: *Lasers in Medical Science* 10.1, pp. 55–65. ISSN: 1435-604X. DOI: 10.1007/BF02133165. URL: http://dx.doi.org/10.1007/BF02133165.

Taflinski, L et al. (2014). “Blue light inhibits transforming growth factor-beta1-induced myofibroblast differentiation of human dermal fibroblasts”. In: *Exp Dermatol* 23.4, pp. 240–246. ISSN: 1600-0625 (Electronic) 0906-6705 (Linking).

DOI: 10.1111/exd.12353. URL: http://www.ncbi.nlm.nih.gov/pubmed/24533842.

Tonder, Alet van et al. (2015). “Limitations of the 3-(4,5-dimethylthiazol-2-yl)-2,5-diphenyl-2H-tetrazolium bromide (MTT) assay when compared to three commonly used cell enumeration assays”. In: *BMC Research Notes* 8.1, p. 47. ISSN: 1756-0500. DOI: 10.1186/s13104-015-1000-8. URL: http://www.biomedcentral.com/1756-0500/8/47.

Troy, T L and S N Thennadil (2001). “Optical properties of human skin in the near infrared wavelength range of 1000 to 2200 nm”. In: *Journal of Biomedical Optics* 6.2, pp. 167–176. ISSN: 1083-3668. DOI: 10.1117/1.1344191.

Tsutsumi, Moe et al. (2009). “Expressions of rod and cone photoreceptor-like proteins in human epidermis.” In: *Experimental dermatology* 18.6, pp. 567–570. ISSN: 1600-0625. DOI: 10.1111/j.1600-0625.2009.00851.x. URL: http://www.ncbi.nlm.nih.gov/pubmed/19493002.

Upton, James H et al. (2015). “Oxidative stress-associated senescence in dermal papilla cells of men with androgenetic alopecia.” In: *The Journal of investigative dermatology* 135.5, pp. 1244–52. ISSN: 1523-1747. DOI: 10.1038/jid.2015.28. URL: http://www.ncbi.nlm.nih.gov/pubmed/25647436.

Vahlquist, A et al. (1982). “Vitamin A in Human Skin: II Concentrations of Carotene, Retinol and Dehydroretinol in Various Components of Normal Skin”. In: *The Journal of investigative dermatology* 79.2.

Varghese, Babu et al. (2016). “Effects of polarization and absorption on laser induced optical breakdown threshold for skin rejuvenation”. In: pp. 97400I–97400I–6. DOI: 10.1117/12.2232894. URL: http://proceedings.spiedigitallibrary.org/proceeding.aspx?articleid=2502683.

Veen, R L P van et al. (2004). “Determination of VIS- NIR absorption coefficients of mammalian fat, with time- and spatially resolved diffuse reflectance and transmission spectroscopy”. In: *Biomedical Topical Meeting*, SF4. DOI: 10.1364/BIO.2004.SF4. URL: http://www.osapublishing.org/abstract.cfm?URI=BIO-2004-SF4.

Vieira, Jacqueline et al. (2012). “Human cryptochrome-1 confers light independent biological activity in transgenic drosophila correlated with flavin radical stability”. In: *PLoS ONE* 7.3. ISSN: 1932-6203 (Electronic)\n1932-6203 (Linking). DOI: 10.1371/journal.pone.0031867.

Waiz, Makram et al. (2006). “Use of the pulsed infrared diode laser (904 nm) in the treatment of alopecia areata.” In: *Journal of cosmetic and laser therapy : official publication of the European Society for Laser Dermatology* 8.1, pp. 27–30. ISSN: 1476-4172. DOI: 10.1080/14764170600607368. URL: http://www.ncbi.nlm.nih.gov/pubmed/16581682.

Wan, San et al. (1981). “Analytical modeling for the optical properties of the skin with in vitro and in vivo applications.” In: *Photochemistry and photobiology* 34.4, pp. 493–9. ISSN: 0031-8655. DOI: 10.1111/j.1751-1097.1981.tb09030.x. URL: http://dx.doi.org/10.1111/j.1751-1097.1981.tb09030.xhttp://www.ncbi.nlm.nih.gov/pubmed/7312955.

Wang, L, SL L Jacques, and L Zheng (1995). “MCML - Monte Carlo modeling of light transport in multi-layered tissues”. In: *Computer methods and Programs in Biomedicine*.

Wang, Wen (2005). “Oxygen partial pressure in outer layers of skin: simulation using three-dimensional multilayered models.” In: *Microcirculation (New York, N.Y. : 1994)* 12.2, pp. 195–207. ISSN: 1073-9688. DOI: 10.1080/10739680590905062. URL: http://www.ncbi.nlm.nih.gov/pubmed/15824040.

Wang, Yuguang et al. (2016). “Photobiomodulation (blue and green light) encourages osteoblastic-differentiation of human adipose-derived stem cells: role of intracellular calcium and light-gated ion channels.” In: *Scientific reports* 6, p. 33719. ISSN: 2045-2322. DOI: 10.1038/srep33719. URL: http://www.ncbi.nlm.nih.gov/pubmed/27650508http://www.pubmedcentral.nih.gov/articlerender.fcgi?artid=PMC5030629.

Waynant, Ronald and Darrell B Tata (2008). *Proceedings of light-activated tissue regenaration and therapy conference*. 1st ed. Vol. 12. Lectures notes in electrical engineering. Springer, p. 443.

Webb, Cecilia, M Dyson, and W H Lewis (1998). “Stimulatory effect of 660 nm low level laser energy on hypertrophic scar-derived fibroblasts: possible mechanisms for increase in cell counts.” In: *Lasers in surgery and medicine* 22.5, pp. 294–301. ISSN: 0196-8092. URL: http://www.ncbi.nlm.nih.gov/pubmed/9671996.

Webb, Cecilia and Mary Dyson (2003). “The effect of 880 nm low level laser energy on human fibroblast cell numbers: a possible role in hypertrophic wound healing.” In: *Journal of photochemistry and photobiology. B, Biology* 70.1, pp. 39–44. ISSN: 1011-1344. URL: http://www.ncbi.nlm.nih.gov/pubmed/12745245.

Weinstabl, A et al. (2011). “Prospective Randomized Study on the Efficacy of Blue Light in the Treatment of Psoriasis Vulgaris”. In: *Karger Dermatology* 223.3.

Wharton, D C and A Tzagoloff (1964). “Studies on the Electron Transfer System. Lvii. The near Infrared Absorption Band of Cytochrome Oxidase”. In: *J Biol Chem* 239, pp. 2036–2041. ISSN: 0021-9258 (Print) 0021-9258 (Linking). URL: http://www.ncbi.nlm.nih.gov/pubmed/14213394.

Whelan, Harry T and Scott G Turner (2001). “Effect of Light-emitting Diode Irradiation on Wound Healing”. In: 19.6. DOI: 10.1089/104454701753342758.This.

Wicks, N L et al. (2011). “UVA phototransduction drives early melanin synthesis in human melanocytes”. In: *Curr Biol* 21.22, pp. 1906–1911. ISSN: 1879-0445. DOI: 10.1016/j.cub.2011.09.047. URL: http://www.ncbi.nlm.nih.gov/pubmed/22055294.

Wong-Riley, Margaret T T. et al. (2005). “Photobiomodulation directly benefits primary neurons functionally inactivated by toxins: role of cytochrome c oxidase.” In: *The Journal of biological chemistry* 280.6, pp. 4761–4771. ISSN: 0021-9258. DOI: 10.1074/jbc.M409650200. URL: http://www.ncbi.nlm.nih.gov/pubmed/15557336.

Woodard, H Q and D R White (1986). “The composition of body tissues”. In: *The British Journal of Radiology* 59.708, pp. 1209–1218. ISSN: 0007-1285. DOI:

10.1259/0007-1285-59-708-1209. URL: http://dx.doi.org/10.1259/0007-1285-59-708-1209.

Woodley, David T. (2017). “Distinct Fibroblasts in the Papillary and Reticular Dermis: Implications for Wound Healing”. In: *Dermatologic Clinics* 35.1, pp. 95–100. ISSN: 07338635. DOI: 10.1016/j.det.2016.07.004.

Woodruff, Lynda D et al. (2004). “The efficacy of laser therapy in wound repair: a meta-analysis of the literature”. In: *Photomed Laser Surg* 22.3, pp. 241–247. ISSN: 1549-5418 (Print) 1549-5418 (Linking). DOI: 10.1089/1549541041438623. URL: http://www.ncbi.nlm.nih.gov/pubmed/15315732.

Young, Antony R. (2006). “Acute effects of UVR on human eyes and skin”. In: *Progress in Biophysics and Molecular Biology* 92.1, pp. 80–85. ISSN: 00796107. DOI: 10.1016/j.pbiomolbio.2006.02.005. URL: http://www.ncbi.nlm.nih.gov/pubmed/16600340http://linkinghub.elsevier.com/retrieve/pii/S0079610706000198.

Yu, Hsin-Su et al. (1996). “Low-Energy Helium Neon Laser Irradiation stimulates interleukin-1alpha and interleukin-8 release from cultured Human Keratinocytes”. In: *The Society for Investigative Dermatology, Inc*.

Zhang, Hong et al. (2015). “Modelling epidermis homoeostasis and psoriasis pathogenesis”. In: *Journal of The Royal Society Interface* 12.103.

Zhang, S Z et al. (1990). “Neutral red (NR) assay for cell viability and xenobiotic-induced cytotoxicity in primary cultures of human and rat hepatocytes.” In: *Cell biology and toxicology* 6.2, pp. 219–34. ISSN: 0742-2091. URL: http://www.ncbi.nlm.nih.gov/pubmed/2113829.

Zhang, Yaou et al. (2003). “cDNA microarray analysis of gene expression profiles in human fibroblast cells irradiated with red light.” In: *The Journal of investigative dermatology* 120.5, pp. 849–857. ISSN: 0022-202X. DOI: 10.1046/j.1523-1747.2003.12133.x. URL: http://www.ncbi.nlm.nih.gov/pubmed/12713592.

Zhou, Jian-da, Cheng-qun Luo, and Xie (2008). “Increased expression of heat shoch protein 70 and heat shoch factor 1 in chronic dermal ulcer tissues treated

with alser-aided therapy". In: *Chinese Medical Journal* 121.30672035, pp. 1269–1273.

Appendices

Chapter A: Essential definitions and concepts in Photobiology

In this section we review the principles and nomenclature relating to the quantification of light, that are essential for photobiology, basics of biomedical optics for light propagation in tissue. First, definitions of photobiological units will be given to assure consistency throughout the entire report. These units are defined by the CIE (Commission Internationale de l'Eclairage) and have been summarized by Sliney et al (Sliney, 2007).

A.1 Photobiological units

When it comes to light interaction with biological tissues and specifically to photobiology, it is essential to use relevant and consistent nomenclature for the quantification of light. Unfortunately, the vast majority of scientific articles reporting on both *in vivo* and clinical studies and on *in vitro* studies lack such a rigorous and consistent approach. This make it very difficult, and often impossible, to relate treatment parameters with clinical outcomes, to compare interaction outcome between different parameters (e.g. power, dose, irradiance, radiant exposure). It also excludes any possibility to make further predictions towards settings that could lead to improved efficacy of treatment.

Below the most essential parameters and possible variability of each of them are listed:

- Light Energy: Wavelength, Power, Dose, Irradiance, Radiant Exposure, Cumulative Radiant Exposure

- Light Regime: Continuous Wave, Pulsed Wave
- Light Coherence: Time and Spatial Coherence

A summary table containing every unit described here is showed on table A.1.

A.1.1 Light energy

Every light source is characterized by its light emission or by how much output power exits the source and in which direction. The latter two parameters, Output Power and Spatial Distribution, are of primary importance when characterizing a photobiological interaction. Output power is linked to the light source, and to the choice of wavelength. The energy of photons depends on the wavelength of light. While power is defined as the number of photons exiting the light source per unit of time, and is expressed in Watts (W), equivalent to Joule per second ($J.s^{-1}$). Spatial distribution of light will give the spatial allocation of these photons, and can be expressed as a photon density map. Power and Spatial Distribution directly input the Irradiance and Radiant Exposure (and cumulative Radiant Exposure); key parameters in photobiology, which will also be used throughout this Report. Irradiance I is defined as the number of photons impinging on a surface per unit of area and per unit of time. In photobiology it is generally expressed in $mW.cm^{-2}$; while radiant exposure RE is the number of photon impinging on a surface per unit of surface over a defined time, generally expressed in $J.cm^{-2}$. Both units are linked by the exposure time δT.

To summarize, Irradiance and Radiant Exposure are the most essential parameters that define the effect of light on biological tissues. Moreover, each of them can have an impact on the biological response. A good illustration of the importance of both Irradiance and Radiant Exposure can be found in the article by Anders et al. (Anders et al., 2010). Anders et al. treated neural cells using a range of irradiances and radiant exposures and demonstrated different effects as a function of irradiance, even when the radiant exposure was kept the same. Similar behaviour was observed as a function of radiant exposure, while irradiance

remained constant. Therefore, both these parameters should always be provided.

A.1.2 Light regime

The second important parameter in photobiology is the regime of light, whereby samples can be treated either using continuous wave light (which is most often reported in the articles describing clinical studies using light for skin and hair treatment) or pulsed light. In case of a continuous wave regime, it is entirely characterized by Irradiance and Radiant Exposure parameters. Treatment using pulsed light is less common reported in literature. It is somewhat more complex and at least 2 other parameters are necessary to describe a pulsing regime, and 4 other could be necessary to describe complex pulsing regime.

The most important are Pulse Duration and Duty Cycle. Pulse Duration τ represents the time during which the light source is turned on, while the duty cycle DC represents the total period or the sum of the on- and off- time of the light source. More complex pulsing regimes could include pulse trains of a defined frequency and duration τ_1, separated by a time interval of τ_2. Pulse trains are characterized by the number of pulses per train PPT and the train interval TI. Barolet et.al demonstrated importance of pulsing and pulse parameters on stimulative or inhibitory effect of light on collagen production in fibroblasts cells (Barolet et al., 2010).

A.1.3 Light coherence

The third parameter important in phototherapy is light coherence. Incandescent lamps and light emitting diodes (LEDs) have low spatial- and time coherence (which could be only a few hundreds of microns for an LED source), whereas laser sources emit light waves of high time- and spatial coherence (coherence length can be as long as several tens of meters). Until now no solid evidence has been reported demonstrating the importance of light coherence on photobiological effects. Alas, many researchers use lasers, LEDs and sometimes broad-band

Name	Symbol	Units
Power	P	W
Dose	D	J
Irradiance	I	$mW.cm^{-2}$
Radiant Exposure	RE	$J.cm^{-2}$
Exposition Time	δT	s
Pulse Duration	τ	s
Duty Cycle	DC	%
Pulse Per Train	PPT	$No\,Units$
Train Interval	TI	s

Table A.1: Quantities in photobiology

lamps, assuming there is no difference between them in this regard. Karu in (Karu, 2003) proposed a hypothesis that light coherence may play a role in photobiological effects, in cases where light traverses through a thick enough turbid medium, as coherence of a light source will impact on a phase of the light. A similar remark could be made on polarization, another light property that is very poorly represented in investigations.

A.1.4 Elecromagnetic spectrum and solar reference

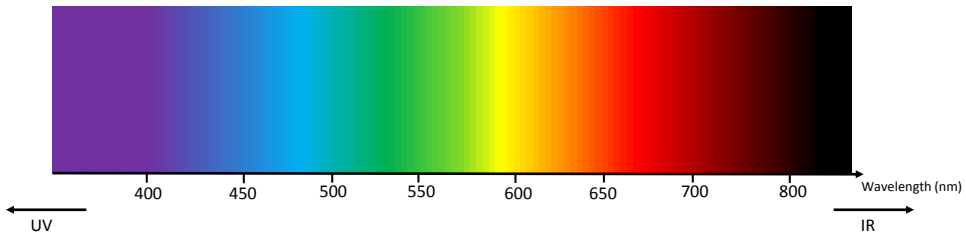

Figure A.1: Electro-magnetic spectrum of the visible and NIR range

It is interesting to put the quantitative values of the optical settings used in literature in comparison with a the output of the sun. Accurate and detailed spectra are openly available from the DOE/NREL/ALLIANCE website (http://rredc.nrel.gov/), providing several types of Solar Irradiances (direct or $30\ ^\circ$ tilted), also described by Gueymard et al. (Gueymard, Myers, and Emery, 2002). Out of these data, an order of magnitude of irradiance within the visible spectrum can be obtained: $0.1\ mW.cm^{-}2.nm^{-}1$. After 1 hour under the sun a total broadband dose of $200\ J.cm^{-}2$ could be received. In order to create a relevant comparison, we should compare with a typical bandwidth of light sources used in photobiomodulation. The bandwidths would be of $0.01\ nm$ and $10\ nm$ for a HeNe laser and typical LED. The result is that a laser with an irradiance less than $10\ mW.cm^{-}2$ will not provide more than what the sun is already sending, while the same value would be $0.005\ mW.cm^{-}2$ for a LED. In one hour, a laser with the sun irradiance will then give a dose of $3.6\ mJ.cm^{-}2$, while a LED, with the same irradiance, will give $3.6\ J.cm^{-}2$. The large difference between both light sources come from the bandwidth. A laser has a significantly tiny bandwidth compared to the LED, figuratively a LED is sending

thousands of laser-wavelengths all different and close to each other.

Chapter B: Technical characterization and safety considerations of light-based prototypes

B.1 Environmental influence of the optical output

The devices have been characterized at ambient temperature. The emission power of the LED are dependant on the temperature of the heat sink (information which is displayed in the software). As shown in the section B.1, the temperature of the environment can have an influence on the optical output; especially if the environment is a close box such as an incubator. The user should be aware that the optical output should stay within 10 % of the characterized value only if the temperature is inferior to $75°$. If a very high temperature is reached the LED will be damaged, or even broken. The illumination will then stop without further risks.

Sirius-24 characterization

Temperature/Power variation

LED are component whose emission variate with temperature. In the case of Sirius-24, the LED are manufactured by Lumileds mainly and OSLON for the infrared LED. In the datasheet, variation of the emission due to temperature is available. As a rapid summary the following should be kept:

- Blue, Red and Infrared have very low variation of emission with temperature
- Green and Cyan have slight emission variation with temperature
- Yellow have significant emission variation with temperature

It has been checked experimentally, roughly. In air environment, the irradiance was measured two times:

- Initial temperature
- Stabilized temperature

The following results were obtained shown in table B.1.

Box	Wavelength	Initial Temp. 28 ∘	Stabilized Temp. 34 ∘	Variation
”Blue” Box	447	50	50	Not measurable*
	505	39	38.4	Measurable
	530	30	29.3	Measurable
”Red” Box	591	6.8	6	Measurable
	655	68	68	Not measurable*
	850	75	75	Not measurable*

Table B.1: Sirius-24: Irradiances at $13\ mm$ distance from the LED chip, measured under the maximum (software) current of $700\ mA$ using Ophir Powermeter Nova II and sensor PD300-3W-V1 calibrated Oct-2014, at two different temperatures, initial and after stabilization (long exposure). *Within the accuracy of measurement

Sirius-8 characterization

Later on, the different light sources within Sirius-8 will be designated by letter and number as showed on figure B.1. The letter stands for the color of the light source and the number for the row index.

Irradiance of the light-based device Sirius-8 at the working distance ($50\ mm$)

The irradiances (Fig. B.2) reached with the light-based prototype Siriu-8 were measured at the bottom of a 35 mm culture dish placed on the device using an Ophir Nova II powermeter with PD-300 3W sensor. The 8 light sources have different irradiances reached at the bottom of the dish due to difference in the LEDs themselves but also in the current which flows in both paths.

Temperature/Power Variation

LED are component whose emission variate with temperature. In the case of Sirius-8, the LED are manufactured by Lumileds for the visible and OSLON for

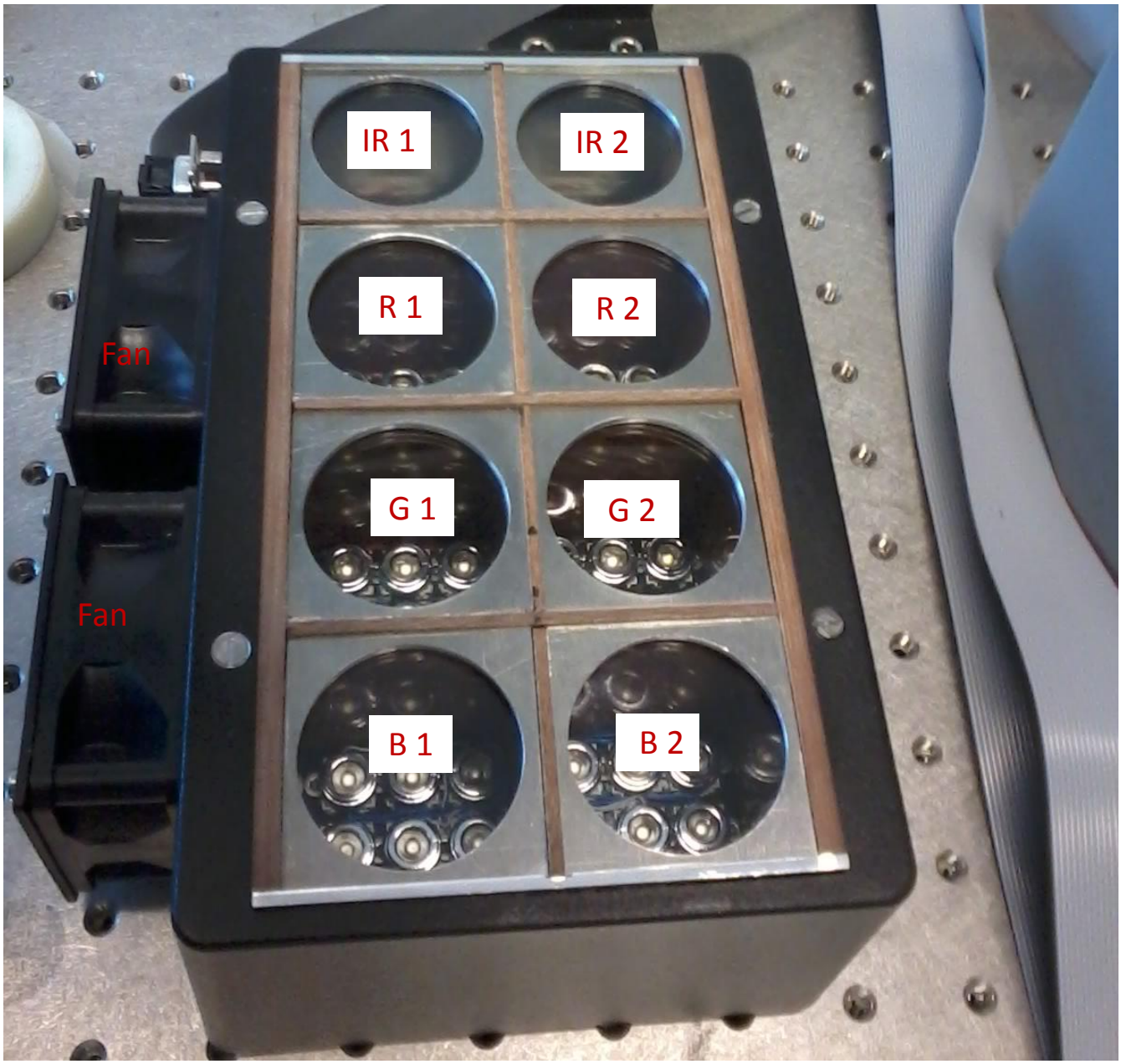

Figure B.1: Photograph of the light-based prototype Sirius-8

Current (A)	IR 1	IR 2	R 1	R 2	G 1	G 2	B 1	B 2
0.005	0.1	0.1	0.9	1	0.7	0.7	1.5	1.5
0.01	0.7	0.7	2	2.1	1.8	1.8	3.4	3.5
0.05	8.1	7.5	10.9	11.3	9.4	9.3	19.2	19.7
0.1	16.5	15.5	22.2	23.1	17.4	17.2	37.9	38.8
0.3	56.4	54.2	67.5	69.6	41.5	41.2	105.3	107.5
0.5	92.6	89.4	113	117.1	59.1	58.6	165	168.6
0.7	124.5	122.1	157.7	162.3	72.8	72.1	220.2	225.6

Table B.2: Irradiances of the LED sources of the light-based device Sirius-8 (all values in $mW.cm^{-}2$).

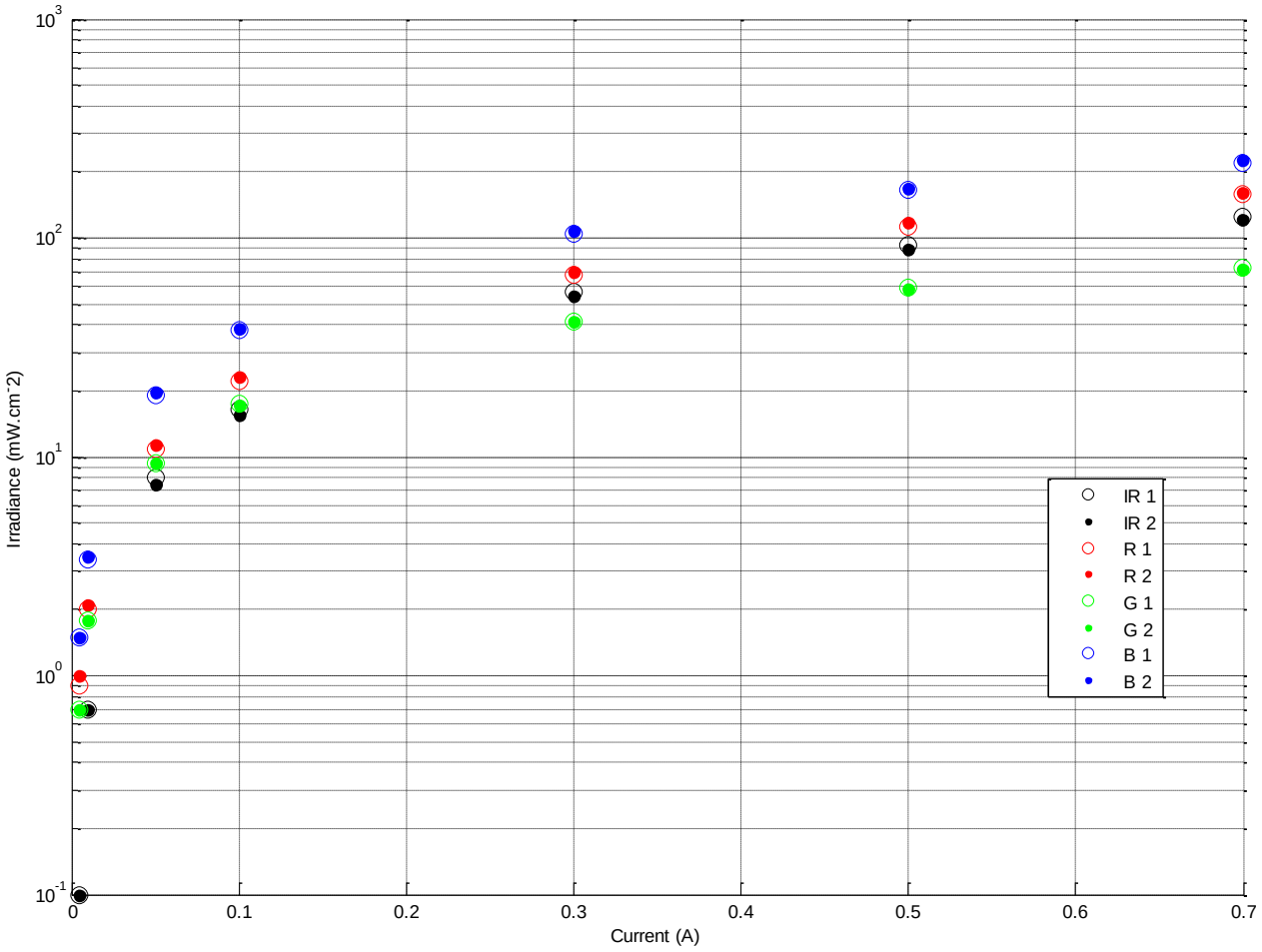

Figure B.2: Irradiance levels reached by each of the 8 light sources of the light-based device Sirius-8 versus input current.

the infrared. In the datasheet, variation of the emission due to temperature is available. However, rapid measurement were performed. The following results were obtained shown in table B.3.

Box	Wavelength	Initial Temp. 45 ∘	Stabilized Temp. 60 ∘	Variation
”Blue” Box	447	210	210	Not measurable*
	530	75	74	Measurable
	655	170	170	Not measurable*
	850	100	100	Not measurable*

Table B.3: Sirius-8: Irradiances at $50\ mm$ distance from the LED chip, measured under the maximum (software) current of $700\ mA$ using Ophir Powermeter Nova II and sensor PD300-3W-V1 calibrated Oct-2014, at two different temperatures, initial and after stabilization (long exposure). *Within the accuracy of measurement

The same experiment has been made inside a stove set at $37\ ^{\circ}C$. The experiment was stopped after the temperature reached 80 degrees on the heat sink. The conclusion was that the temperature of the stove was too disturbed ($50\ ^{\circ}C$ reached within 300 seconds) by the light-based devices.

Box	Wavelength	Initial Temp. 45 ∘	Stabilized Temp. 75 ∘	Variation
”Blue” Box	447	210	210	Nonsignificant*
	530	75	70	Measurable
	655	172	170	Nonsignificant*
	850	100	105	Nonsignificant*

Table B.4: Sirius-8: Irradiances at $50\ mm$ distance from the LED chip, measured under the maximum (software) current of $700\ mA$ using Ophir Powermeter Nova II and sensor PD300-3W-V1 calibrated Oct-2014, at two different temperatures, initial and after stabilization (long exposure) inside the stove set at $37\ ^{\circ}C$. *Within the accuracy of measurement

B.2 Safety & risks

B.2.1 Electrical safety

The contact person who performed the test is Frank Jaartsveld (frank.jaartsveld@philips.com)

The electrical safety assessment of both devices was performed by Frank Jaartsveld in accordance with standard IEC 61010 Safety requirements for electrical equipment for measurement, control, and laboratory use. Both devices passed the tests ensuring that there are no risk of fire, no mechanical risks or risks due to electrical

shocks that could be foreseen. Test reports will be available within the Technical Construction File.

B.2.2 Electromagnetic Compatibility (EMC)

The contact person who performed the test is Rene Kragt (rene.kragt@philips.com)
The EMC safety assessment of both devices was performed by Rene Kragt in accordance with standard IEC 61326 Electrical equipment for measurement, control and laboratory use – EMC requirements –. Both devices passed the tests ensuring that there are no EMC requirements that are not matched within the devices. Tests reports are available within the Technical Construction File.

B.2.3 Optical safety

The contact persons who performed the tests are Peter Jutte, Arno Ras and Charles Mignon (peter.jutte@philips.com / a.j.m.ras@philips.com / charles-antoine.mignon@
The Optical safety assessment of both devices was performed by Charles Mignon and reviewed by Peter Jutte, Arno Ras in accordance with standards IEC 62471 Photobiological Safety of lamps and lamp systems and IEC 60825 Safety of laser Products. Tests reports and evaluation are available within the Technical Construction File.
Based on safety risk assessment using 2 methods:

- Comparison between measurements/calculations of Radiances impinging on the eye and Standard Limits from EN 62471:2008 ”Photobiological Safety of lamps and lamp systems”
- Eye Safety Program (Laser Safe PC), calculating the eye exposure at a defined distance and relating it to the MPE (Maximum Permissible Exposure), using the specifications of the light source in accordance with standard IEC 60825 Safety of laser Products

and based on discussion with experts Arno Ras and Peter Jutte, it was concluded that the highest risk group is 2: Moderate Risk (only for 447 nm wavelength).

A specific case worths to be reminded: the Infrared LED in Sirius-24. The safe distance of that LED has to be at least $30\ mm$. Under mechanical conditions distances smaller than the safe distance are reachable. Although under intended use, there is a culture plate on top of the device, ensuring that the distance eye to LED is always superior to the safe distance of the Infrared LED. The recommendations taken out of this study are the labelling of the devices (necessary), writing of user-notice provided with good practical use advice (necessary) and the use of protective goggles (not necessary).

B.3 Assessment of the retina related risks & risk group classification

Both devices contain light sources with wavelength ranging from $440\ nm$ to $850\ nm$. Three types of hazards can occur according the standard 62471 introduced earlier, depending on a wavelength of a source:

- Blue light hazard: retina hazard when using blue light, which is photochemical by nature.
- The retinal thermal hazard occurring when the retina is heated extensively.
- The retinal thermal hazard when using light producing weak visual signal; causing potentially extensive heating

Both hazards will be assessed comparing radiance levels available in the devices with limits of exposure defined in the standard 62471.
Before presenting the results, several key parameters can be introduced:

- Array of LED versus single LED
- Blue hazard factor and burn hazard factor: $B(\lambda)$ and $R(\lambda)$
- Solid angles Ω and acceptance angles α

- The distance where the hazard should be evaluated D, this distance is $200\ mm$ in the IEC62471 standard because it is the shortest distance at which eye can accommodate.
- The basetimes which should be considered τ

Array of LEDs versus single LED

Both devices are build as arrays of LED. In the version 24, the LED array is composed of 24 LEDs which are separated by $15\ mm$ laterally in 4 lines of 6 LEDs. In the version 8, the array of 72 LEDs is divided in 8 separated smaller arrays of 9 LEDs each. These LEDs are $10\ mm$ from each other. Referring to figure 5.2 of the standard EN 62471:2008 "Photobiological Safety of lamps and lamp systems", we can calculate the size of the area that an human eye can focus at a distance D of $200\ mm$ from the source. The size Φ is directly linked to the maximum acceptance angle of the eye, ie. $0.011\ rad$ for middle exposure time ($0.25 < Exposure < 10000\ sec$). The numerical application is the following:

$$\Phi = 2 * D * \tan\frac{0.011}{2} = 2.2\ mm \tag{B.1}$$

LED array in Sirius-8 have always larger spatial separation between their single LEDs. Therefore, human eye can only focus on one LED at a time. Every LED of the arrays can only be imaged at different positions of the retina. As a consequence, checking for the safety of the device is reduced to assessing the safety of every LED separately.

Blue & Burn hazards Factors

Blue hazard and burn hazard factors need to be used as weighting to compensate for the differences between wavelengths and their influence on both hazards. All coefficients are available within the standard. Weighting factors corresponding to wavelengths used in the devices are shown in table B.5.

Wavelength	Blue Hazard Factor	Burn Hazard Factor
447	0.955	9.55
505	0.0794	1
530	0.0251	1
591	0.0015	1
655	0.001	1
850	0	0.5012

Table B.5: Optical safety assessment: blue & burn hazards factors

B.3.1 Solid angles Ω, acceptance angles α, and evaluation distance

The standard requires, for non-medical device, that the eye hazard is evaluated at 200 mm from the source. The main quantity regulating the calculation is the acceptance angle to consider, it is the one of a LED chip (size a 1 mm or 2 mm depending on the LED) over a 200 mm distance:

$$\alpha = \frac{a}{D}$$

The actual used acceptance angle will be defined in the next section. It is dependant on the risk itself and on the exposure time.

The solid angle is then directly calculated from the following formula:

$$\Omega = \frac{\pi * \alpha^2}{4}$$

The radiance L is directly linked to the irradiance I by the following relation:

$$L = \frac{I}{\Omega}$$

Basetimes consideration

There are basetimes to consider: one for the pulsing regime and the other for continuous regime. Both, require the use of different acceptance angle for the calculations.

The standard considers a light source as pulsed if it can produce pulse of light of 0.25 second or less, linked to the retinal reflex. The devices Sirius-8 and Sirius-24 allow pulsing but do not change the peak power. In our case, the pulsing On &

Off times can vary over a wide range, Hz to kHz frequencies. Although the energy contained in the peak pulse is only dependant on the length of the peak. To evaluate the hazard provoked by the pulsing we can then use the maximum pulse length, ie. 0.25 second (as defined by the retinal reflex). In that case the standard advise to use $1.7\ mrad$ as an acceptance angle. It represents the smallest image that can be formed on a still eye.

The second basetime to consider is for continuous regime, or exposition time of more than 0.25 second. In that case the acceptance angle should be $11\ mrad$. Another nuance is for exposure times superior to 10000 seconds, where movements of the eye will average the exposure over a larger area, the acceptance angle should be $0.1\ rad$, always according to the standard.

Blue light and retinal burn hazards

Exposure limits In the standard Photobiological safety of lamps 62471, table 6.1, exposition limits are listed. We extract and quote here the most essential values for our case. They are shown in tables B.6 and B.7 for continuous and pulsed conditions respectively.

Risk	Action Spectrum	Symbol	Exempt Limit	Low Risk Limit	Mod. Risk Limit
Blue light	$B(\lambda)$	L_B	100	10000	4000000
Retinal Thermal	$R(\lambda)$	L_R	$\frac{28000}{\alpha}$	N.A	$\frac{71000}{\alpha}$
Retinal Thermal, NIR	$R(\lambda)$	L_{IR}	$\frac{6000}{\alpha}$	N.A	N.A

Table B.6: Blue & burn hazards: exposition limits in continuous regime, directly from EN 62471:2008 ”Photobiological Safety of lamps and lamp systems”. The unit of the quantities is $W.m^{-2}.sr^{-1}$.

Risk	Action Spectrum	Symbol	Limit
Blue light	$B(\lambda)$	L_B	$\frac{1000000}{\tau}$
Retinal Thermal	$R(\lambda)$	L_R	$\frac{50000}{\alpha * \tau^{0.25}}$
Retinal Thermal, NIR	$R(\lambda)$	L_{IR}	$\frac{6000}{\alpha}$

Table B.7: Blue & burn hazards: exposition limits in pulsed regime, directly from EN 62471:2008 ”Photobiological Safety of lamps and lamp systems”. The unit of the quantities is $W.m^{-2}.sr^{-1}$.

Risk group assessment for continuous wave regime

Risk group is assigned by comparing he Risk Groups limits (as defined in the previous sections) with the corresponding weighted radiances L_B, L_R and L_{IR}. The first step is to evaluate the radiance with the three involved acceptance angles defined in the previous section. Then we can compare to the different limits and assess in which risk group every LED belongs. The results for Sirius-24 are presented in tables B.8 and B.9, showing the weighted radiances, groups limits and group classification for every LED; the same was done for Sirius-8 in tables B.10 and B.11.

Overall only two cases fall under the Risk Group 2: blue light 447 nm in Sirius-24 and Sirius-8 with acceptance angle $0.011\ rad$. The standard IEC 60601:2006 Medical electrical equipment requires distance information for theses cases to fall back in the risk group 1. The following distances have been back calculated:

- Sirius-24: Over $300\ mm$, the blue hazard weighted radiance falls back into Risk Group 1 under middle exposure time ($0.25 < \ Exposure \ < \ 10000\ sec$) of the light source at $447\ nm$.
- Sirius-8: Over $800\ mm$, the blue hazard weighted radiance falls back into Risk Group 1 under middle exposure time ($0.25 < \ Exposure \ < \ 10000\ sec$) of the light source at $447\ nm$.

Risk group assessment for pulsed wave regime

Similarly risk group were assessed for a pulsed regime, with a pulse of 0.25 second and equal peak irradiance to that of Continuous Wave Mode. Another small difference relies in the use of a very small acceptance angle $1.7\ mrad$, which is smaller than the actual subtended angle of a LED chip ($1\ mm$ or $2\ mm$ size) at the evaluation distance $200\ mm$, ie. $5\ mrad$. The actual entire chip of the LED cannot be focused by the human eye with such small acceptance angle. Using equation B.1, the area corresponding to the subtended angle $1.7\ mrad$ is approximately $0.37\ mm^2$. I would give a further factor on the measured irradiance to only take the part which is coming from the focused area. This factor will be further used

when making calculations for pulsing regime, and is defined in equation B.2. It links the measured irradiance I_{5mrad} (corresponding to the full subtended angle $5\ mrad$) with the actual irradiance received by the eye in the small acceptance angle required when assessing pulsing regime safety $I_{1.7mrad}$, and the ratio of surfaces of the LED S_{LED} for one part and of the area focused by the eye $0.37\ mm^2$ for the other part. The surface of the LED is always $1\ mm^2$ except for the blue LED used in Sirius-8 where it becomes $4\ mm^2$.

$$I_{1.7\ mrad} \ = \ I_{5\ mrad} * \frac{0.37}{S_{LED}} \tag{B.2}$$

A table summarizing the factors applied to the measured irradiances and the actual used irradiances for the pulsing regime risk assessment was made and is shown on figure B.12.

The results for Sirius-24 are presented in tables B.13 and B.14, showing the weighted radiances, groups limits and group classification for every LED of the device. The same calculation have been performed for Sirius-8, shown on table B.15 and B.16.

Overall, both device fall onto the exempt group at all wavelength. A special care should be taken when using the blue light source ($447\ nm$) of Sirius-8 which have a weighted radiance very close to the limit of the risk Group 2.

Acceptance Angle (rad)	Wavelength	Radiance ($W.m^{-2}.sr^{-1}$)	L_B	ER Limit	G1 Limit	G2 Limit	Group Class
0.11	447	225	215	100	1×10^4	4×10^6	G1
	501	178	15	100	1×10^4	4×10^6	Exempt
	530	134	3.5	100	1×10^4	4×10^6	Exempt
	591	45	0.07	100	1×10^4	4×10^6	Exempt
	655	290	0.3	100	1×10^4	4×10^6	Exempt
	850	355	0	100	1×10^4	4×10^6	Exempt
0.011	447	2.22×10^4	2.12×10^4	100	1×10^4	4×10^6	G2
	501	1.78×10^4	1.4×10^3	100	1×10^4	4×10^6	G1
	530	1.33×10^4	335	100	1×10^4	4×10^6	G1
	591	4.45×10^3	7	100	1×10^4	4×10^6	Exempt
	655	2.89×10^4	30	100	1×10^4	4×10^6	Exempt
	850	3.56×10^4	0	100	1×10^4	4×10^6	Exempt

Table B.8: Sirius-24: blue risk weighted radiance L_B & group classification, continuous regime

Acceptance Angle (rad)	Wavelength	Radiance ($W.m^{-2}.sr^{-1}$)	L_R	ER Limit	G1 Limit	G2 Limit	Group
0.11	447	223	2160	2.55×10^5	X	6.45×10^5	Exempt
	501	180	180	2.55×10^5	X	6.45×10^5	Exempt
	530	135	135	2.55×10^5	X	6.45×10^5	Exempt
	591	45	45	2.55×10^5	X	6.45×10^5	Exempt
	655	300	300	2.55×10^5	X	6.45×10^5	Exempt
	850	355	$L_{IR} = 180$	5.45×10^4	X	X	Exempt
0.011	447	2.22×10^4	2.12×10^5	2.55×10^6	X	6.45×10^6	Exempt
	501	1.78×10^4	1.78×10^4	2.55×10^6	X	6.45×10^6	Exempt
	530	1.33×10^4	1.33×10^4	2.55×10^6	X	6.45×10^6	Exempt
	591	4.5×10^3	4.5×10^3	2.55×10^6	X	6.45×10^6	Exempt
	655	2.89×10^4	2.89×10^4	2.55×10^6	X	6.45×10^6	Exempt
	850	3.56×10^4	$L_{IR} = 1.78 \times 10^4$	5.45×10^5	X	X	Exempt

Table B.9: Sirius-24: burn risk weighted radiances L_R and L_{IR} & group classification, continuous regime

Acceptance Angle (rad)	Wavelength	Radiance ($W.m^{-2}.sr^{-1}$)	L_B	ER Limit	G1 Limit	G2 Limit	Group Class
0.11	447	1.64×10^3	1.57×10^3	100	1×10^4	4×10^6	G1
	530	533	13.4	100	1×10^4	4×10^6	Exempt
	655	1.19×10^3	1.19	100	1×10^4	4×10^6	Exempt
	850	913	0	100	1×10^4	4×10^6	Exempt
0.011	447	1.64×10^5	1.57×10^5	100	1×10^4	4×10^6	G2
	530	5.33×10^4	1.34×10^3	100	1×10^4	4×10^6	G1
	655	1.19×10^5	119	100	1×10^4	4×10^6	G1
	850	9.13×10^4	0	100	1×10^4	4×10^6	Exempt

Table B.10: Sirius-8: blue risk weighted radiance L_B & group classification, continuous regime

Acceptance Angle (rad)	Wavelength	Radiance ($W.m^{-2}.sr^{-1}$)	L_R	ER Limit	G1 Limit	G2 Limit	Group
0.11	447	1.64×10^3	1.57×10^4	2.55×10^5	X	6.45×10^5	Exempt
	530	533	533	2.55×10^5	X	6.45×10^5	Exempt
	655	1120	1120	2.55×10^5	X	6.45×10^5	Exempt
	850	913	$L_{IR} = 458$	5.45×10^4	X	X	Exempt
0.011	447	1.64×10^5	1.57×10^6	2.55×10^6	X	6.45×10^6	Exempt
	530	5.33×10^4	5.33×10^4	2.55×10^6	X	6.45×10^6	Exempt
	655	1.19×10^5	1.19×10^5	2.55×10^6	X	6.45×10^6	Exempt
	850	9.13×10^4	$L_{IR} = 4.58 \times 10^4$	5.45×10^5	X	X	Exempt

Table B.11: Sirius-8: burn risk weighted radiances L_R and L_{IR} & group classification, continuous regime

Device	Wavelength	Factors	"Corrected" Irradiance ($mW.cm^{-2}$)
Sirius-24	447	0.37	18.5
	501	0.37	15
	530	0.37	11.1
	591	0.37	3.7
	655	0.37	24
	850	0.37	30
Sirius-8	447	$\frac{1}{9} * \frac{0.37}{4}$	2.3
	530	$\frac{1}{9} * \frac{0.37}{1}$	3
	655	$\frac{1}{9} * \frac{0.37}{1}$	6.7
	850	$\frac{1}{9} * \frac{0.37}{1}$	5.2

Table B.12: Sirius-24 & Sirius-8: "Corrected" irradiances at working distances in the small acceptance angle case, pulsed regime

Acceptance Angle (rad)	Wavelength	Radiance ($W.m^{-2}.sr^{-1}$)	L_B	Limit	Group Class
0.0017	447	3.44×10^5	3.29×10^5	4×10^6	Exempt
	501	2.75×10^5	2.19×10^4	4×10^6	Exempt
	530	2.07×10^5	5.19×10^3	4×10^6	Exempt
	591	6.89×10^4	103	4×10^6	Exempt
	655	4.48×10^5	448	4×10^6	Exempt
	850	5.51×10^5	0	4×10^6	Exempt

Table B.13: Sirius-24: blue risk weighted radiance L_B & group classification, pulsed regime

Acceptance Angle (rad)	Wavelength	Radiance ($W.m^{-2}.sr^{-1}$)	L_R	Limit	Group Class
0.0017	447	3.44×10^5	3.29×10^6	4.16×10^7	Exempt
	501	2.75×10^5	2.75×10^5	4.16×10^7	Exempt
	530	2.07×10^5	2.07×10^5	4.16×10^7	Exempt
	591	6.89×10^4	6.89×10^4	4.16×10^7	Exempt
	655	4.48×10^5	4.48×10^5	4.16×10^7	Exempt
	850	5.51×10^5	$L_{IR} = 2.76 \times 10^5$	3.53×10^6	Exempt

Table B.14: Sirius-24: burn risk weighted radiances L_R and L_{IR} & group classification, pulsed regime

Acceptance Angle (rad)	Wavelength	Radiance ($W.m^{-2}.sr^{-1}$)	L_B	Limit	Group Class
0.0017	447	6.37×10^5	6.08×10^5	4×10^6	Exempt
	530	8.26×10^5	2.07×10^4	4×10^6	Exempt
	655	1.85×10^6	1.85×10^3	4×10^6	Exempt
	850	1.42×10^6	0	1.92×10^6	Exempt

Table B.15: Sirius-8: blue risk weighted radiance L_B & group classification, pulsed regime

Acceptance Angle (rad)	Wavelength	Radiance ($W.m^{-2}.sr^{-1}$)	L_R	Limit	Group Class
0.0017	447	6.37×10^5	6.08×10^6	4.2×10^7	Exempt
	530	8.26×10^5	8.26×10^5	4.2×10^7	Exempt
	655	1.85×10^6	1.85×10^6	4.2×10^7	Exempt
	850	1.46×10^6	$L_{IR} = 7.09 \times 10^5$	3.53×10^6	Exempt

Table B.16: Sirius-8: burn risk weighted radiances L_R and L_{IR} & group classification, pulsed regime

Chapter C: Gene expression analysis: Lists of significant pathways and associated genes per light treated group

Table C.1: KEGG Pathways significantly up- or down-regulated by light treatment in papillary fibroblasts (450 nm, $30\ J.cm^{-2}$) together with the NES (normalized enrichment score) and the names of the genes significantly expressed in the treated group compared to the control group. Pathway significance was evaluated on p-value ($p < 0.05$) and and false discovery rate ($FDR < 0.1$). Gene expression significance is evaluated on p-value ($p < 0.05$) (N=1, reticular and papillary, 3 replicates).

Pathway name	NES	Genes downregulated	Genes up-regulated	Number of gene
Cell cycle	-1.605136	CCND2, PLK1, CDC20	MDM2	124
Steroid hormone biosynthesis	1.8632389	none	AKR1C1, AKR1C2, AKR1C3, COMT	58
TGF-beta signaling pathway	-1.7416905	NOG, TGFB2, INHBB, FST, MYC, SMURF2, ZFYVE9, ID2, ID4	LTBP1, DCN	84
Peroxisome	1.5853581	none	none	83
Lysosome	1.6117865	CTSC, CLTCL1	CD68, CTSK, CTSB,CTSK, CTSS,GBA, HEXB, CD68, SCARB2, SLC17A5, LAPTM4B, CD164, FUCA1	123
Ribosome	-1.933875	N.A.	N.A.	N.A.
Aminoacyl-tRNA biosynthesis	-2.0876231	IARS, WARS, LARS, EPRS, MARS, YARS, AARS, CARS, TARS, GARS, SARS, NARS	none	66
Biosynthesis of amino acids	-1.704959	N.A.	N.A.	N.A
Drug metabolism - cytochrome P450	1.8035964	none	GSTM3	69

Table C.2: KEGG Pathways significantly up- or down-regulated by light treatment in papillary fibroblasts (450 nm, $30\ J.cm^{-2}$) together with the NES (normalized enrichment score) and the names of the genes significantly expressed in the treated group compared to the control group. Pathway significance was evaluated on p-value ($p < 0.05$) and and false discovery rate ($FDR < 0.1$). Gene expression significance is evaluated on p-value ($p < 0.05$) (N=1, reticular and papillary, 3 replicates) (continued).

Pathway name	NES	Genes downregulated	Genes up-regulated	Number of gene
Metabolism of xenobiotics by cytochrome P450	2.0077324	none	GSTM3, AKR1C1, AKR7A2	74
Chemical carcinogenesis	1.8742994	none	GSTM3, AKR1C2	82
N-Glycan biosynthesis	1.591949	none	MAN1A1	49
Mucin type O-Glycan biosynthesis	1.7480844	GALNT3	GALNT11, GALNT14, GALNT10, C1GALT1	31
One carbon pool by folate	-1.7246779	MTHFD2, SHMT2, ALDH1L2	none	20
Glycine; serine and threonine metabolism	-1.7476225	SHMT2, PHGDH, PSAT1, PSPH, CBS	none	40
Butanoate metabolism	1.5420164	none	none	28
Nitrogen metabolism	1.5878055	none	GLUD2, CA12	17

Table C.3: KEGG Pathways significantly up- or down-regulated by light treatment in reticular fibroblasts (450 nm, $30\ J.cm^{-2}$) together with the NES (normalized enrichment score) and the names of the genes significantly expressed in the treated group compared to the control group. Pathway significance was evaluated on p-value ($p < 0.05$) and and false discovery rate ($FDR < 0.1$). Gene expression significance is evaluated on p-value ($p < 0.05$) (N=1, reticular and papillary, 3 replicates).

Pathway name	NES	Genes downregulated	Genes up-regulated	Number of gene
Cell cycle	-1.431511	CDKN2C, CDK1, CCNH, CDC16, BUB1, BUB1B, CHEK2	MAD1L1	124
Proteasome	-1.8041621	PSMA4, PSMB4	none	45
Spliceosome	-1.6148239	SNRPE,LSM5, SNRNP40,CWC15,MAGOH,HNRNPA1	CHERP ,SRSF7,SRSF10	134
Peroxisome	-1.6028103	PEX1, PEX2, PEX7, PEX12, SLC25A17, AGPS, HMGCL	none	83
Basal transcription factors	-1.7322046	TAF11, GTF2H3, CCNH	none	45
Ribosome biogenesis in eukaryotes	-1.6378033	N.A.	N.A.	N.A.
Ubiquitin mediated proteolysis	-1.5840052	RFWD2, RCHY1, MID1, CUL1, FBXO4, ERCC8, CUL5, ANAPC4, CDC16	AIRE	137
RNA transport	-1.5472972	RPP14, TRNT1, NUP54, MAGOH	EIF4G1	171
Protein export	-1.6788809	none	none	23
Aminoacyl-tRNA biosynthesis	-1.9460524	DARS2, SEPSECS, RARS2, WARS2	VARS	66

Table C.4: KEGG Pathways significantly up- or down-regulated by light treatment in reticular fibroblasts (450 nm, $30\ J.cm^{-2}$) together with the NES (normalized enrichment score) and the names of the genes significantly expressed in the treated group compared to the control group. Pathway significance was evaluated on p-value ($p < 0.05$) and and false discovery rate ($FDR < 0.1$). Gene expression significance is evaluated on p-value ($p < 0.05$) (N=1, reticular and papillary, 3 replicates) (continued).

Tryptophan metabolism	-1.4797724	ACAT2, ALDH9A1	OGDH, AANAT	40
Citrate cycle (TCA cycle)	-1.7040707	DLD, PDHA1	OGDH	30
Terpenoid backbone biosynthesis	-1.6759536	ACAT2, GGPS1, NUS1	none	22
Metabolism of xenobiotics by cytochrome P450	-1.5794929	GSTM3	none	74
Chemical carcinogenesis	-1.7272831	GSTM3	none	82
Drug metabolism - cytochrome P450	-1.8717248	GSTM3	none	69
Oxidative phosphorylation	-1.512209	NDUFS4, NDUFA10, NDUFB5, UQCRC2, UQCRHL, COX15, ATP5L, ATP6V1G2, PPA2	ATP4A	133
Ascorbate and aldarate metabolism	-1.4534084	ALDH9A1	none	27
Glyoxylate and dicarboxylate metabolism	-1.4279966	ACAT2, MUT, DLD	none	28
Histidine metabolism	-1.4961768	ALDH9A1	none	24
Pyruvate metabolism	-1.5581487	PDHA1, DLD, ALDH9A1, ME1, ACAT2	none	39

Table C.5: KEGG Pathways significantly up- or down-regulated by light treatment in reticular fibroblasts (450 nm, $30\ J.cm^{-2}$) together with the NES (normalized enrichment score) and the names of the genes significantly expressed in the treated group compared to the control group. Pathway significance was evaluated on p-value ($p < 0.05$) and and false discovery rate ($FDR < 0.1$). Gene expression significance is evaluated on p-value ($p < 0.05$) (N=1, reticular and papillary, 3 replicates) (finished).

Pathway name	NES	Genes downregulated	Genes up-regulated	Number of gene
Carbon metabolism	-1.5236957	N.A.	N.A.	N.A.
Propanoate metabolism	-1.7985165	DLD, ACADM, MUT, ALDH6A1, ACAT2	none	32
Valine; leucine and isoleucine degradation	-1.8624911	DLD, ACADM, MUT, ALDH6A1, ALDH9Q1, MCCC2, HMGCL, ACAT2	ACSF3	48
Mismatch repair	-1.5272224	MLH1	POLD1, LIG1	23
RNA degradation	-1.5478282	EXOSC1, EXOSC8, LSM5, PNPT1	TOB2	77
Nucleotide excision repair	-1.6528642	ERCC8, CCNH, GTF2H3	POLD1, LIG1	47
Pentose phosphate pathway	-1.4586552	RPE, PRPS2, PRPS1	none	30
Systemic lupus erythematosus	-1.9076029	HIST1H2AM, HIST2H2AB, HIST1H2BB, HIST1H2BL, HIST1H3I, HIST1H3G, HIST1H4A	none	133
Alcoholism	-1.5722377	HIST1H2AM, HIST2H2AB, HIST1H2BB, HIST1H2BL, HIST1H3I, HIST1H3G, HIST1H4A, ATF2, NRAS	HDAC4, SLC29A1	180

Table C.6: KEGG Pathways significantly up- or down-regulated by light treatment in papillary fibroblasts (450 nm, $2\ J.cm^{-2}$) together with the NES (normalized enrichment score) and the names of the genes significantly expressed in the treated group compared to the control group. Pathway significance was evaluated on p-value ($p < 0.05$) and and false discovery rate ($FDR < 0.1$). Gene expression significance is evaluated on p-value ($p < 0.05$) (N=1, reticular and papillary, 3 replicates).

Pathway name	NES	Genes downregulated	Genes up-regulated	Number of gene
Melanogenesis	-1.7159798	none	none	101
Regulation of lipolysis in adipocytes	-1.631497	none	none	54
Cell cycle	-1.6179968	none	none	124
Proteasome	1.6185344	none	none	45
Peroxisome	1.5190909	none	SOD2	83
Spliceosome	1.7316881	none	none	134
Adherens junction	-2.0047781	none	none	72
Axon guidance	-1.7177373	none	none	175
Cell adhesion molecules (CAMs)	-1.604016	none	none	145
Regulation of actin cytoskeleton	-1.5604889	none	none	212
Vascular smooth muscle contraction	-1.4751832	none	none	121
Tight junction	-1.4717782	none	none	170
Focal adhesion	-1.8413672	none	none	199
ECM-receptor interaction	-1.7703414	none	none	82
Thyroid hormone signaling pathway	-1.8591211	none	none	116
Aldosterone synthesis and secretion	-1.6161983	none	none	82

Table C.7: KEGG Pathways significantly up- or down-regulated by light treatment in papillary fibroblasts (450 nm, $2\ J.cm^{-2}$) together with the NES (normalized enrichment score) and the names of the genes significantly expressed in the treated group compared to the control group. Pathway significance was evaluated on p-value ($p < 0.05$) and and false discovery rate ($FDR < 0.1$). Gene expression significance is evaluated on p-value ($p < 0.05$) (N=1, reticular and papillary, 3 replicates) (continued).

Pathway name	NES	Genes downregulated	Genes up-regulated	Number of gene
Insulin secretion	-1.533535	none	none	85
Endocrine and other factor-regulated calcium reabsorption	-1.417587	none	none	47
Thyroid hormone synthesis	-1.4156275	none	none	74
Steroid hormone biosynthesis	1.8111371	none	none	58
Wnt signaling pathway	-1.7548352	none	none	143
Hippo signaling pathway	-1.7374191	none	none	154
PI3K-Akt signaling pathway	-1.6878659	FOXO3	none	342
Notch signaling pathway	-1.6730193	none	none	48
Estrogen signaling pathway	-1.616947	none	none	98
TGF-beta signaling pathway	-1.596677	NOG	none	84
Signaling pathways regulating pluripotency of stem cells	-1.5887636	none	none	139
AMPK signaling pathway	-1.5677165	PFKFB3, FOXO3	none	121
cAMP signaling pathway	-1.540972	none	none	198
FoxO signaling pathway	-1.5353276	FOXO3	SOD2	132
cGMP-PKG signaling pathway	-1.5240852	none	none	163

Table C.8: KEGG Pathways significantly up- or down-regulated by light treatment in papillary fibroblasts (450 nm, $2\ J.cm^{-2}$) together with the NES (normalized enrichment score) and the names of the genes significantly expressed in the treated group compared to the control group. Pathway significance was evaluated on p-value ($p < 0.05$) and and false discovery rate ($FDR < 0.1$). Gene expression significance is evaluated on p-value ($p < 0.05$) (N=1, reticular and papillary, 3 replicates) (finished).

Pathway name	NES	Genes downregulated	Genes up-regulated	Number of gene
MAPK signaling pathway	-1.5235144	none	none	255
ErbB signaling pathway	-1.4812877	none	none	86
HIF-1 signaling pathway	-1.4809254	PFKFB3	none	99
Hedgehog signaling pathway	-1.4734361	none	none	47
Calcium signaling pathway	-1.435459	none	none	182
Longevity regulating pathway	-1.4018744	FOXO3	SOD2	89
mRNA surveillance pathway	1.5294238	none	none	91
Metabolism of xenobiotics by cytochrome P450	1.77034	none	none	74
Nitrogen metabolism	1.6219934	none	none	17
Propanoate metabolism	1.6914045	none	none	32
Ribosome	1.7792321	N.A.	N.A.	N.A
Protein export	1.8716654	none	none	23
RNA transport	1.6351532	none	RPP14	171
Ribosome biogenesis in eukaryotes	1.6757627	none	none	106
Basal cell carcinoma	-1.7625054	none	none	55
Melanoma	-1.4373103	none	none	69

Table C.9: KEGG Pathways significantly up- or down-regulated by light treatment in reticular fibroblasts (450 nm, $2\ J.cm^{-2}$) together with the NES (normalized enrichment score) and the names of the genes significantly expressed in the treated group compared to the control group. Pathway significance was evaluated on p-value ($p < 0.05$) and and false discovery rate ($FDR < 0.1$). Gene expression significance is evaluated on p-value ($p < 0.05$) (N=1, reticular and papillary, 3 replicates).

Pathway name	NES	Genes downregulated	Genes up-regulated	Number of gene
Cell cycle	-1.7006239	RB1, RBL1, CDKN2C, CDK1, CDC25C, PLK1, CCNH, CDC16, CDC20, PTTG1, STAG1, RAD21, TTK, BUB1, BUB1B, CHEK2, ORC2	CDC25B, MAD1L1, SFN	124
DNA replication	-1.6504444	RPA1, POLA1, POLA2, PRIM1, POLD3, MCM2, MCM3, MCM4, MCM5, MCM6, RFC1, RFC3, RFC4, RFC5	LIG1	36
Aminoacyl-tRNA biosynthesis	-1.9557592	EPRS, GATB, DARS2, SEPSECS, LARS, LARS2, IARS, IARS2, RARS2, HARS, YARS2, WARS2	none	66
TGF-beta signaling pathway	-1.6935377	NOG, FST, BMP6, TGFB2, INHBB, ACVR2A, TGFBR1, BAMBI, SMAD9, SMURF2, ZFYVE9, ID4, RBL1, CUL1	MAPK3	84
Metabolism of xenobiotics by cytochrome P450	1.7880045	none	EPHX1, AKR1C1, ALDH3A1	74
Malaria	-1.807181	MET. TLR4, TGFB2, CCL2, IL8, COMP	CD81	49

Table C.10: KEGG Pathways significantly up- or down-regulated by light treatment in papillary fibroblasts (850 nm, $20\ J.cm^{-2}$) together with the NES (normalized enrichment score) and the names of the genes significantly expressed in the treated group compared to the control group. Pathway significance was evaluated on p-value ($p < 0.05$) and and false discovery rate ($FDR < 0.1$). Gene expression significance is evaluated on p-value ($p < 0.05$) (N=1, reticular and papillary, 3 replicates).

Pathway name	NES	Genes downregulated	Genes up-regulated	Number of gene
Melanogenesis	-1.7487755	none	none	49
Propanoate metabolism	1.9205828	none	none	32
Valine; leucine and isoleucine degradation	1.8318887	none	none	48
Butanoate metabolism	1.7215024	none	none	28
Fatty acid degradation	1.7076399	none	none	32
Tryptophan metabolism	1.6473422	none	none	40
Glutathione metabolism	1.6343609	none	none	54
Pyruvate metabolism	1.592411	none	none	39
Citrate cycle (TCA cycle)	1.5188315	none	none	30
Fatty acid metabolism	1.4998813	N.A.	N.A.	N.A
Adherens junction	-1.9479437	none	none	72
N-Glycan biosynthesis	1.7345755	none	none	49
Focal adhesion	-1.6740363	none	none	199
Axon guidance	-1.6382114	none	none	175
Regulation of actin cytoskeleton	-1.6561174	none	none	212
Glycosaminoglycan biosynthesis - CS/DS	-1.7292342	none	none	20
ECM-receptor interaction	-1.4643635	none	none	82
Metabolism of xenobiotics by cytochrome P450	1.9438053	none	none	74

Table C.11: KEGG Pathways significantly up- or down-regulated by light treatment in papillary fibroblasts (850 nm, $20\ J.cm^{-2}$) together with the NES (normalized enrichment score) and the names of the genes significantly expressed in the treated group compared to the control group. Pathway significance was evaluated on p-value ($p < 0.05$) and and false discovery rate ($FDR < 0.1$). Gene expression significance is evaluated on p-value ($p < 0.05$) (N=1, reticular and papillary, 3 replicates) (continued).

Pathway name	NES	Genes downregulated	Genes up-regulated	Number of gene
Drug metabolism - cytochrome P450	1.6840506	none	none	69
Chemical carcinogenesis	1.7395574	none	none	82
Spliceosome	1.7170328	none	none	134
Peroxisome	1.738403	none	none	83
Proteasome	1.7530085	none	none	45
Thyroid hormone signaling pathway	-1.7015197	none	none	116
Notch signaling pathway	-1.7043067	none	none	48
Arylhydrocarbon receptor (AhR) signaling pathway	-1.6766986	N.A.	N.A.	N.A.
Wnt signaling pathway	-1.7075477	none	none	143
ErbB signaling pathway	-1.7212892	none	none	86
Hippo signaling pathway	-1.6524384	none	none	154
HIF-1 signaling pathway	-1.6393592	PFKFB3	none	99
Estrogen signaling pathway	-1.763633	none	none	98
PI3K-Akt signaling pathway	-1.596584	none	none	342
Signaling pathways regulating pluripotency of stem cells	-1.5976858	none	none	139
cGMP-PKG signaling pathway	-1.6102675	none	none	163

Table C.12: KEGG Pathways significantly up- or down-regulated by light treatment in papillary fibroblasts (850 nm, $20\ J.cm^{-2}$) together with the NES (normalized enrichment score) and the names of the genes significantly expressed in the treated group compared to the control group. Pathway significance was evaluated on p-value ($p < 0.05$) and and false discovery rate ($FDR < 0.1$). Gene expression significance is evaluated on p-value ($p < 0.05$) (N=1, reticular and papillary, 3 replicates) (finished).

Pathway name	NES	Genes downregulated	Genes up-regulated	Number of gene
TGF-beta signaling pathway	-1.6048452	NOG	none	84
GnRH signaling pathway	-1.5702934	none	none	92
MAPK signaling pathway	-1.5728117	none	none	255
Rap1 signaling pathway	-1.5538113	none	none	210
AMPK signaling pathway	-1.5566193	PFKFB3	none	121
cAMP signaling pathway	-1.5439705	none	none	198
Insulin signaling pathway	-1.4865843	none	none	138
Longevity regulating pathway	-1.4551225	none	none	89
Insulin secretion	-1.7120755	none	none	85
Aldosterone synthesis and secretion	-1.6003517	none	none	82
Insulin resistance	-1.519534	none	none	107
Thyroid hormone synthesis	-1.4930233	none	none	74
Ribosome biogenesis in eukaryotes	1.6076086	none	none	106
Protein export	1.521781	none	none	23
RNA transport	1.4878073	none	none	171
Regulation of lipolysis in adipocytes	-1.9137777	none	none	54
Pentose and glucuronate interconversions	1.6787208	none	none	30
Basal cell carcinoma	-1.6900502	none	none	55
Terpenoid backbone biosynthesis	1.5370069	none	none	22

Table C.13: KEGG Pathways significantly up- or down-regulated by light treatment in reticular fibroblasts (850 nm, $20\ J.cm^{-2}$) together with the NES (normalized enrichment score) and the names of the genes significantly expressed in the treated group compared to the control group. Pathway significance was evaluated on p-value ($p < 0.05$) and and false discovery rate ($FDR < 0.1$). Gene expression significance is evaluated on p-value ($p < 0.05$) (N=1, reticular and papillary, 3 replicates).

Pathway name	NES	Genes downregulated	Genes up-regulated	Number of gene
Valine; leucine and isoleucine degradation	-2.0308387	DLD, MUT, ALDH6A1	none	48
Citrate cycle (TCA cycle)	-1.8056693	DLD	none	30
Propanoate metabolism	-1.7853854	DLD, MUT, ALDH6A1	none	32
Tryptophan metabolism	-1.7038528	none	none	40
Butanoate metabolism	-1.6805074	none	none	28
Carbon metabolism	-1.6347615	N.A.	N.A.	N.A.
Pyruvate metabolism	-1.634951	DLD, ME1	none	39
Fatty acid degradation	-1.5532509	none	none	32
Histidine metabolism	-1.4949332	none	none	24
Aminoacyl-tRNA biosynthesis	-1.7508003	none	none	66
Protein export	-1.6616352	none	none	23
Ribosome biogenesis in eukaryotes	-1.5341054	FCF1	none	106

Table C.14: KEGG Pathways significantly up- or down-regulated by light treatment in reticular fibroblasts (850 nm, $20\ J.cm^{-2}$) together with the NES (normalized enrichment score) and the names of the genes significantly expressed in the treated group compared to the control group. Pathway significance was evaluated on p-value ($p < 0.05$) and and false discovery rate ($FDR < 0.1$). Gene expression significance is evaluated on p-value ($p < 0.05$) (N=1, reticular and papillary, 3 replicates) (continued).

Pathway name	NES	Genes downregulated	Genes up-regulated	Number of gene
Proteasome	-1.8125454	PSMB4	none	45
Peroxisome	-1.8164659	AGPS, SOD2	none	83
Drug metabolism - cytochrome P450	-1.5608991	GSTM3	none	69
Chemical carcinogenesis	-1.7382302	GSTM3	none	82
Metabolism of xenobiotics by cytochrome P450	-1.7407138	GSTM3	none	74
Mucin type O-Glycan biosynthesis	-1.5217128	none	none	31
Terpenoid backbone biosynthesis	-1.64256	NUS1	none	22
Pentose and glucuronate interconversions	-1.5813133	none	none	30
Basal transcription factors	-1.564115	none	none	45

Chapter D: Publications and presentations that are derived from this project and thesis

Full-text publications:

a. C. Mignon et al. (2017b). “Photobiomodulation of human dermal fibroblasts in vitro: decisive role of cell culture conditions and treatment protocols on experimental outcome”. In: *Scientific Reports* 7.1, p. 2797. ISSN: 2045-2322. DOI: 10.1038/s41598-017-02802-0. URL: http://www.ncbi.nlm.nih.gov/pubmed/28584230http://www.pubmedcentral.nih.gov/articlerender.fcgi?artid=PMC5459822http://www.nature.com/articles/s41598-017-02802-0

b. C Mignon et al. (2016b). “Photobiomodulation devices for hair regrowth and wound healing: a therapy full of promise but a literature full of confusion”. In: *Exp Dermatol*. ISSN: 1600-0625. DOI: 10.1111/exd.13035. URL: https://www.ncbi.nlm.nih.gov/pubmed/27095546

c. C Mignon et al. (2016c). “Photobiomodulation of distinct lineages of human dermal fibroblasts: a rational approach towards the selection of effective light parameters for skin rejuvenation and wound healing”. In: *Proc. SPIE* 9695, pp. 969508–969516. DOI: 10.1117/12.2208574

d. C. Mignon et al. “Investigation of the origin of the variability of the values of

the skin layers optical properties for a more accurate prediction of the light propagation in the skin". In: *(in preparation)*

e. C. Mignon et al. "Reticular and papillary fibroblasts exhibit a differential response to visible and NIR light". In: *(in preparation)*

Abstracts in official journals and conference proceedings:

a. C. Mignon et al. (2017c). "The importance of the selection of optical parameters, cell culture conditions and treatment protocols in photobiomodulation in vitro: a multi-factorial analysis of the response of primary human dermal fibroblasts to visible and NIR light". In: *ASLMS San Diego 2017 (Travel grant)*

b. C. Mignon et al. (2017a). "Optical settings, cell culture conditions and treatment protocols all significantly impact on interpretation of photobiomodulation responses in primary human dermal fibroblasts". In: *BSID Manchester 2017*

c. C. Mignon et al. (2016a). "Impact of variability of the optical properties of skin layers on prediction of photon density using a Monte Carlo model." In: *Lasers in surgery and medicine*. 111 RIVER ST, HOBOKEN 07030-5774, NJ USA: Wiley-Blackwell, p. 48

d. C. Mignon et al. (2016d). "Visible light differentially influences distinct human dermal fibroblast lineages and may be exploitable for wound-healing therapy". In: *British Journal of Dermatology* 174.5, e72. ISSN: 0007-0963

e. C. Mignon et al. (2015b). “Light Parameters in Low-Level Light Therapy. A systematic literature review.” In: *Lasers in surgery and medicine*, ASLMS Kissimmee 2015

f. C. Mignon et al. (2015a). “A systematic approach to unravel how light impacts primary human dermal fibroblasts”. In: *Lasers in surgery and medicine*, ASLMS Kissimmee 2015